

*Microwave Electronics*

**MICROSTRIP-FED COMPACT DUAL BAND  
PLANAR ANTENNA**

*A thesis submitted by*

**MANOJ JOSEPH**

*in partial fulfillment of the requirements for the degree of*

**DOCTOR OF PHILOSOPHY**

*Under the guidance of*

**Prof. P. MOHANAN**



**DEPARTMENT OF ELECTRONICS  
FACULTY OF TECHNOLOGY  
COCHIN UNIVERSITY OF SCIENCE AND TECHNOLOGY  
COCHIN-22, INDIA**

**October 2010**



*Dedicated to the Almighty,  
my parents, teachers and dear ones*





**DEPARTMENT OF ELECTRONICS**  
**COCHIN UNIVERSITY OF SCIENCE AND TECHNOLOGY,**  
**KOCHI – 682 022**

---

**Dr. P. Mohanan**

Professor

Department of Electronics

0484 2576418

Cochin University of Science and Technology

mail: drmohan@cusat.ac.in

---

Ph:

E-

*18<sup>th</sup> October 2010*

## **Certificate**

This is to certify that this thesis entitled “**MICROSTRIP-FED COMPACT DUAL BAND PLANAR ANTENNA**” is a bonafide record of the research work carried out by Mr. Manoj Joseph under my supervision in the Department of Electronics, Cochin University of Science and Technology. The results embodied in this thesis or parts of it have not been presented for any other degree.

**Dr. P. Mohanan**  
(Supervising Teacher)

## **DECLARATION**

I hereby declare that the work presented in this thesis entitled “**MICROSTRIP-FED COMPACT DUAL BAND PLANAR ANTENNA**” is a bonafide record of the research work done by me under the supervision of Dr. P. Mohanan, Professor, Department of Electronics, Cochin University of Science and Technology, India and that no part thereof has been presented for the award of any other degree.

Cochin-22  
18<sup>th</sup> October 2010

**Manoj Joseph**  
Research Scholar  
Department of Electronics  
Cochin University of Science  
and Technology

## ACKNOWLEDGEMENT

*I would like to express my sincere gratitude to my supervising guide, Dr. Mohanan Pezhohil, Professor, Department of Electronics, Cochin University of Science and Technology, for his guidance, encouragement and the timely care that he rendered to me during my research period. The opportunities and exposure that he offered during the course of my research is invaluable to me. His profound view points and extraordinary motivation enlightened me to shape my traits and career. I really enjoyed the period of learning under him.*

*My sincere thanks to Dr. K.G. Nair, Director, Centre for Science in Society, Cochin University of Science and Technology and former Head, Department of Electronics, Cochin University of Science and Technology for transferring new informations through his precious advices and suggestions.*

*I am grateful to Prof. K. Vasudevan, Dean Faculty of Technology and former Head, Department of Electronics for his well-timed care in my research, valuable suggestions and constant encouragements to improve my work,*

*In this context let me also thank Prof. P.R.S. Pillai, Head of the Department of Electronics for his whole hearted support, constant encouragement, and for extending the facilities of Department of Electronics for my research.*

*A special and sincere acknowledgement goes to Dr. C. K. Aanandan, Professor, Department of Electronics, Cochin University of Science and Technology for his valuable suggestions and constant encouragement, which helped me very much to improve my research work,*

*My sincere thanks to Dr. Tessamma Thomas, Dr. James Kunien, Dr. M.H. Supriya, Mr. Cyriac M. Odakkal and all other faculty members of Department of Electronics for the help and assistance extended to me.*

*I thankfully bear in mind the sincere directions and inspiring words of Dr. K.K.Narayanan, Associate Professor, S.D.College, Alappuzha which directed me towards research.*

*I would like to acknowledge Dr.J.R.Sharma, General Manager, RRSC(west), NRSC/ISRO, Jodhpur for the support and care he provided for my research.*

*I express my sincere thanks to Dr. Rohith K. Raj for his valuable support and technical advice provided during my research. We worked as a team and that helps me to learn and attempt many tasks.*

*I remember with appreciation Dr. Suma M.N, and Dr. Deepu V about the supreme rapport, care and technical and scientific talks we shared together.*

*I remember with gratitude, Dr. Binu Paul, faculty, School of Engineering , CUSAT for her guidance and encouragement towards my research.*

*Special thanks to, Dr. Anupam R. Chandran, Dr. Shynu S.V, Dr. A.V. Praveen Kumar, Dr. Gijo Augustine, Dr. Lethakumary B, Dr. Mridula S, Dr. K. Francis Jacob, Dr. Sreedevi K, Menon for their whole hearted support, helps and above all the association with me.*

*I also would like to acknowledge Mr. Sujith Raman and Mr. Sarin V.P for their valuable suggestions and support.*

*I Wish to thank Mr. Gopikrishna M, Mrs Deepthi Das Krishna, Mr. Tony D, Mr. Sreejith, Mr. Dinesh R, Mr. Nijas, research scholars, Centre for Research in Electromagnetics and Antennas, Dept. of Electronics for the valuable suggestions and support extended to me.*

*I acknowledge Ms. Jitha B, Mrs. Bybi P.C, Mrs. Shameena V.A, Mrs. Nisha Nassar, Mrs. Laila D., Mrs. Sara Jacob for their constructive comments on my thesis*

*I would also like to thank the colleagues at Centre for Ocean Electronics (CUCENTOL), Microwave Tomography and Material Research Laboratory (MTMR) and Audio and Image Research Lab (AIRL), Department of Electronics, Cochin University of Science and Technology.*

*Special thanks to my colleagues at Regional Remote Sensing Centre, NRSC/ISRO, Jodhpur for their support and inspiration.*

*I wish to thank Kerala State Council for Science Technology and Environment (KSCSTE), Govt. of Kerala for financial assistance in the form of JRF and SRF.*

*My sincere thanks to all non teaching staff of Department of Electronics for their amicable relation, sincere cooperation and valuable helps.*

*I wish to place on record my gratitude to the great teachers, mentors, my intimate friends at all stages of my education.*

*My Grand mother, parents, sisters, uncles, aunts and cousins for their boundless love, care and their seamless effort, which gave me courage and stiffness to complete this work in this form.*

*Above all there is the god almighty whose blessings and kindness helped me a lot to tide over.*

***Manoj Joseph***

## **Preface**

Rapid developments in the communication industry lead towards the design of compact devices with multi-functionalities. Mobile phones are equipped with different services like GSM, DCS, Blue tooth, GPS, DVB-H etc. Since antenna being the key component of wireless gadgets, these demand an increasing need for compact, conformal antennas with multiband characteristics. Printed antennas are popular due to its conformal characteristics which allow easy integration with the planar circuit board. In most of the designs ground plane is the main hindrance for compactness. This leads towards the designs with finite ground plane. In this thesis printed monopole antenna with finite ground plane is analyzed and modified to a compact dual band dual strip antenna by adding another strip as an extension to the ground plane. The new configuration behaves as an asymmetric dipole for the new lower resonance and the fundamental resonance of the monopole is retained without much change in the frequency. The ground plane truncation has been studied and the ground plane edge between the strips has been effectively utilized to form a part of the asymmetric dipole. The required phase for the excitation of the dipole is facilitated by the microstrip line. This avoids the use of balun in the design and leads towards a simple dipole configuration. Thus the proposed configuration gives two wideband resonances; one due to the fundamental monopole mode and the other due to the asymmetric dipole mode. Since only ground plane edge is utilized, the rest of the ground plane can be used for integrating other circuit components. This will give an extra freedom for the antenna designer. For achieving further compactness the dual strip configuration has been folded and a new compact folded dual strip antenna has been designed. The main objectives covered in the thesis are

- Analysis of Microstrip-fed printed monopole antenna
- Feed offset analysis on a finite ground plane printed monopole antenna
- Analysis of printed monopole with additional strip on the ground plane
- Design and development of compact dual band dual strip antenna
- Investigations on the folding analysis of printed monopole antenna
- Design of dual band folded dual strip antenna

All these objectives are fulfilled and compact planar dual band antennas have been designed. Design equations were developed and validated for various personal communication applications.

.....❧.....



## CONTENTS

### *Chapter 1*

## **INTRODUCTION ..... 01 - 23**

<b>1.1 Introduction</b>	02
<b>1.2 A brief introduction to printed antennas</b>	03
1.2.1 Microstrip Antenna	03
1.2.2 Planar Inverted F Antenna	05
1.2.3 Printed monopoles	06
1.2.4 Printed dipoles	07
1.2.5 Metamaterial Antennas	09
<b>1.3 Overview of research in compact antennas</b>	10
1.3.1 Design challenges	11
1.3.1.1 Device specifications	11
1.3.1.2 Impedance bandwidth & Efficiency	12
1.3.2 Present state of art	12
<b>1.4 Printed dipoles for compact applications</b>	13
<b>1.5 Printed monopoles for compact applications</b>	14
<b>1.6 Motivation of the present research</b>	15
<b>1.7 Thesis organisation</b>	20
<b>1.8 References</b>	21

### *Chapter - 2*

## **LITERATURE REVIEW ..... 25 - 56**

<b>2.1 Introduction</b>	26
<b>2.2 Antennas for mobile/WLAN applications</b>	26
<b>2.3 Broad band /Multiband antennas</b>	32
<b>2.4 Printed monopoles and dipoles for compact applications</b>	37
<b>2.5 FDTD analysis</b>	42
<b>2.6 Conclusion</b>	45
<b>2.7 References</b>	45

### *Chapter - 3*

## **ANTENNA SIMULATION, FABRICATION AND MEASUREMENT TECHNIQUES ..... 57 - 89**

<b>3.1 Simulation Techniques</b>	
3.1.1 Finite Difference Time Domain Technique (FDTD)	59

3.1.1.1	Mathematical Formulation	60
3.1.1.2	Stability criteria	63
3.1.1.3	Numerical Dispersion	63
3.1.1.4	Absorbing Boundary Conditions	64
3.1.1.5	Lubbers feed model for fast FDTD convergence	67
3.1.1.7	General flow chart of FDTD algorithm	71
3.1.1.8	Return loss calculation	72
3.1.1.9	Radiation pattern calculation	73
3.1.2	Finite Element Method (FEM)	77
3.1.2.1	HFSS: 3D Electromagnetic simulator	79
<b>3.2</b>	<b>Fabrication method</b>	<b>80</b>
<b>3.3</b>	<b>Microwave substrates</b>	<b>81</b>
<b>3.4</b>	<b>Experimental setup</b>	<b>82</b>
3.4.1	HP 8510C Vector Network Analyzer	82
3.4.2	Anechoic Chamber	84
3.4.3	Turn table assembly for far field radiation pattern measurement	84
<b>3.5</b>	<b>Measurement procedure</b>	<b>85</b>
3.5.1	Return loss, Resonant frequency and Bandwidth	85
3.5.2	Far field radiation pattern	86
3.5.3	Antenna Gain	86
3.5.4	Antenna Efficiency	87
<b>3.6</b>	<b>References</b>	<b>87</b>

## *Chapter - 4*

# **DESIGN AND ANALYSIS OF COMPACT DUAL BAND DUAL STRIP ANTENNA ..... 91 – 149**

<b>4.1</b>	<b>Microstrip-fed printed monopole antenna</b>	<b>92</b>
4.1.1	Introduction	92
4.1.2	Reflection characteristics	93
4.1.3	Radiation characteristics	96
4.1.4	Gain and Efficiency	98
4.1.5	Effect of offset feed	98
4.1.5.1	Reflection characteristics	99
4.1.5.2	Surface current distribution	101
4.1.5.3	Radiation characteristics	103
4.1.6	Effect of monopole strip length ' $l_m$ '	105
4.1.7	Finite ground plane effects	106
4.1.7.1	Effect of ground plane Length, $L_g$	107
4.1.7.2	Effect of ground plane width $W_g$	109
<b>4.2</b>	<b>Compact printed antenna with modified ground plane</b>	<b>112</b>
4.2.1	Effect of adding additional strip on printed monopole configuration	113
4.2.1.1	Description of the problem	113

4.2.1.2	Reflection characteristics	115
4.2.1.3	Radiation characteristics	116
4.2.1.4	Gain and Efficiency	118
4.2.2	Feed offsetting to achieve compactness	118
4.2.3	Impact of additional strip	122
4.2.3.1	Reflection characteristics	123
4.2.3.2	Radiation Mechanism	126
4.2.3.3	Impact of coupling between the strips	126
4.2.3.4	Ground plane optimization	129
4.2.3.5	Impact of strip length $l_g$	133
4.2.3.6	Impact of monopole strip length ' $l_m$ '	134
4.2.3.7	Impact of strip widths	134
4.2.4	Important inferences	136
4.2.5	Effect of dielectric constant ( $\epsilon_r$ )	138
4.2.6	Effect of substrate height (h)	139
<b>4.3</b>	<b>Design procedure for a compact dual strip antenna</b>	<b>140</b>
<b>4.4</b>	<b>Design and analysis of dual band dual strip antenna for 1.8/2.4GHz bands.</b>	<b>142</b>
4.4.1	Introduction	142
4.4.2	Antenna design	142
4.4.3	Reflection characteristics	144
4.4.4	Electric field distribution	144
4.4.5	Radiation Characteristics	144
<b>4.5</b>	<b>Conclusion</b>	<b>148</b>
<b>4.6</b>	<b>References</b>	<b>149</b>

## *Chapter - 5*

### **DESIGN AND ANALYSIS OF COMPACT DUAL BAND FOLDED DUAL STRIP ANTENNA.....**

**151 - 194**

<b>5.1</b>	<b>Introduction</b>	<b>152</b>
<b>5.2</b>	<b>Double folded printed monopole</b>	<b>152</b>
5.2.1	FDTD modelling	153
5.2.2	Reflection characteristics	154
5.2.3	Radiation Pattern	156
5.2.4	$d_1$ variation /off setting	158
5.2.5	Ground plane study	162
5.2.5.1	Effect of ground plane width ' $W_g$ '	162
5.2.5.2	Effect of ground plane Length ' $L_g$ '	164
5.2.6	Effect of top loading	168
5.2.6.1	Variation of $l_1$	169
5.2.6.2	Variation of $l_2$	170
5.2.6.3	Variation of $l_3$	170

<b>5.3</b>	<b>Double folded dual strip antenna</b>	172
5.3.1	Reflection characteristics	173
5.3.2	Surface current distribution	174
5.3.3	Radiation pattern	176
5.3.4	Variation of spacing between the arms 's'	178
5.3.5	Impact of folded arm lengths	181
5.3.6	Effect of dielectric constant ( $\epsilon_r$ )	183
5.3.7	Effect of substrate thickness (h)	183
<b>5.4</b>	<b>Design procedure for a compact dual band folded dual strip antenna</b>	184
<b>5.5</b>	<b>Design and development of folded dual strip antenna for modern communication bands</b>	187
5.5.1	Design and development of dual band folded dual strip antenna for DCS/PCS/2.4GHz WLAN applications	187
5.5.1.1	Introduction	187
5.5.1.2	Antenna Structure and Design	187
5.5.1.3	Results and discussion	188
5.5.2.	Design and development of dual band folded dual strip antenna for GSM applications	192
<b>5.6</b>	<b>Conclusion</b>	193

## *Chapter 6*

### **CONCLUSION..... 195 - 202**

<b>6.1</b>	<b>Thesis Highlights</b>	196
<b>6.2</b>	<b>Inferences from the analysis of microstrip-fed printed monopole antenna</b>	197
<b>6.3</b>	<b>Inferences from compact dual band dual strip antenna</b>	198
<b>6.4</b>	<b>Salient features of compact dual band folded dual strip antenna</b>	199
<b>6.5</b>	<b>Comparison of Compact folded dual strip antenna, dual strip antenna and printed monopole antenna</b>	200
<b>6.6</b>	<b>Suggestions for future work</b>	201

## *Appendix -A*

### **A COMPACT DUAL BAND PLANAR BRANCHED MONOPOLE ANTENNA FOR DCS/2.4GHz WLAN APPLICATIONS ..... 203 - 211**

<b>1.</b>	<b>Introduction</b>	204
<b>2.</b>	<b>Antenna design</b>	204

3. Experimental results	207
4. Conclusion	211
5. References	211

*Appendix –B*

**COMPACT PLANAR MULTIBAND ANTENNA FOR  
GPS,DCS,2.4/5.8 GHz WLAN APPLICATIONS ..... 213 - 218**

1. Introduction	214
2. Antenna design	214
3. Results and discussion	216
4. Conclusion	218
5. References	218

**RESUME OF THE AUTHOR**

**LIST OF PUBLICATIONS OF THE AUTHOR**

**INDEX**

.....❧.....

# INTRODUCTION

---

<i>Contents</i>	<b>1.1 Introduction</b>
	<b>1.2 A brief introduction to printed antennas</b>
	<b>1.3 Overview of research in compact antennas</b>
	<b>1.4 Printed dipoles for compact applications</b>
	<b>1.5 Printed monopoles for compact applications</b>
	<b>1.6 Motivation of the present research</b>
	<b>1.7 Thesis organisation</b>
	<b>1.8 References</b>

---

This chapter gives an overview of printed antennas which finds application in compact electronic gadgets like mobile and WLAN systems. Challenges for the design of compact antenna are elaborately described. Different printed antennas are well explained with special emphasis on printed monopoles and dipoles. Various excitation methods and techniques for achieving multiband characteristics are discussed. The motivation of the research section well explains how a printed monopole configuration has been suitably modified to achieve dual resonance and compactness.

---

## **1.1 Introduction**

Communication industry made a revolutionary remark in this 21st century with the development of modern communication equipments having ultra compact size with multiprofile applications. Mobile phones are now equipped with multiple services such as Bluetooth, GPS, DVB-H etc and the compactness has been achieved without deteriorating the performance. Another remarkable development is wireless system for local area network including Wireless Local Area Network (WLAN) and Bluetooth. WLAN is able to provide mobility and quick connectivity with high data rate.

Antennas, becoming a key element in wireless communication devices undergone amazing developments especially in the direction of compactness. Antenna history starts with Hertz when he proved Maxwell's theoretical prediction of electromagnetic waves by the classical experiments in 1880s [1]. But the long distance communication using antennas was first realized by Marconi's transatlantic experiments in 1901. During these period our Indian scientist J.C.Bose also conducted experiments on high frequencies even in millimetre waves and developed first horn antenna, which he called a collecting funnel. World War II made some historic developments in antenna research, especially in centimetre wave antennas. Dipoles, loops, reflectors, horn radiators and lens antennas were introduced and the concept of antenna array were proposed [2]. But during the last two decades personal communication industry undergone a tremendous growth especially in mobile communications. Strong need for the integration of multiband, multi-purpose services to the mobile phones focuses the antenna research to compact multiband printed antennas.

In earlier devices wire antennas were used which protruded outside and make the device bulky. Research and developments in the printed

antenna designs allow antenna to be integrated to the printed circuit board of the communication device, thus allows compactness. Planar inverted antennas (PIFA), printed monopoles and printed dipoles are commonly being used for compact applications. But the demand for the integration of more and more services to the mobile phone while reducing its size has been a great challenge for the antenna designer.

## **1.2 A brief introduction to printed antennas**

In this modern communication age, mobile phones and other personal communication devices are becoming smaller and light weight. Printed antennas are well exploited in these compact applications because of its features like low profile, small size, conformal to the mounting host etc [3]. Printed antenna history started in 1953 with Deschamps when he first proposed microstrip antenna [4]. Almost all printed antennas are developed based on microstrip configuration or its modifications. In this section an attempt is made to briefly explain various popular printed antenna configurations starting from microstrip antenna to the newly reported metamaterial based printed antennas.

### **1.2.1 Microstrip Antenna**

Microstrip antenna consists of a radiating element or a patch printed on a grounded low loss dielectric substrate. Usually the ground plane is very large compared to the radiating patch. Radiating patch can be of any shape; but rectangular or circular are more popular. Substrate is of low loss dielectric material to enhance the radiation performance. Commonly used dielectric materials are FR4, RT Duroid, Alumina etc. Configuration of a typical rectangular microstrip antenna is shown in Fig.1.1.



Microstrip antenna can be excited using a microstrip line as shown in the Fig.1.1. Electromagnetic coupling, aperture coupling or coaxial feed can also be used for the excitation of microstrip antennas.

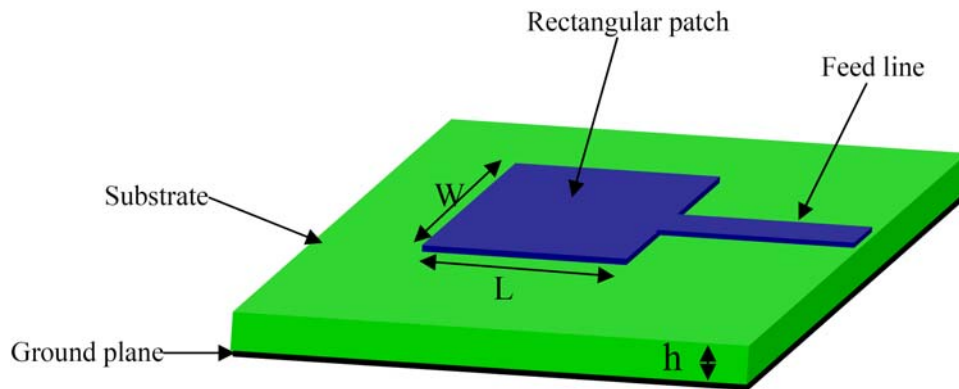


**Fig.1.1** Geometry of a rectangular microstrip antenna excited by microstrip line

Microstrip antenna geometry became popular because of its features like [5]

- Low volume, low profile and conformal configuration
- Low fabrication cost
- Easily integrated with microwave integrated circuits
- Feed lines and matching networks can be fabricated simultaneously along with the antenna structure.
- Any desired polarisation

Along with these advantages, microstrip antenna has some drawbacks, which limits its direct application in compact devices. They are

- Narrow bandwidth
- Limited half space radiation
- Large size, half wave length dimensions
- Comparatively large ground plane
- Poor end fire radiation

### 1.2.2 Planar Inverted F Antenna

The planar Inverted F Antenna (PIFA) consists of a top patch, ground plane, a feed wire and a shorting mechanism which short circuits the top patch to the ground as shown in Fig.1.2. The shorting mechanism makes it a quarter wave resonator, thus reduces the electrical length by 50% compared to a microstrip antenna[6]. Resonant frequency is mainly controlled by the length of the radiating patch. Bandwidth of the antenna can be enhanced by increasing the height, the width of the shorting plate and width of the radiating patch. [7]

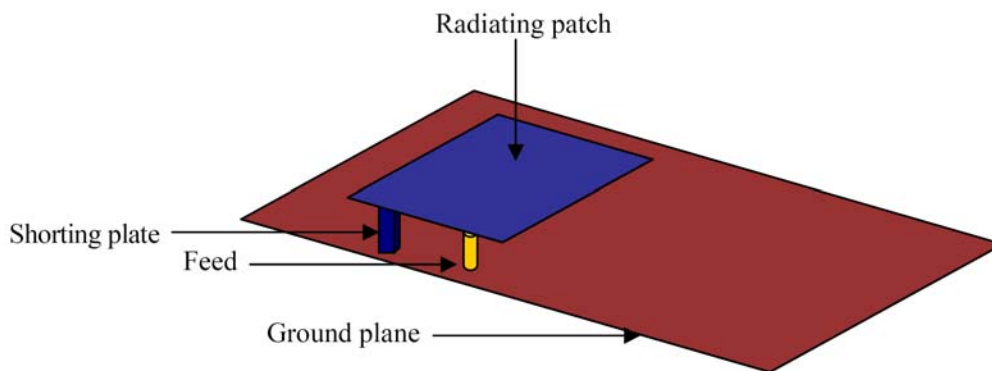


Fig.1.2 Geometry of a PIFA

The major features of the PIFA, which makes it a popular choice for compact applications, are highlighted below

- Reduced size
- Easily integrated on the housing of mobile phones
- Comparatively low backward radiation
- Ability to facilitate multiband operation

Planar inverted F antennas are widely used in mobile phones and laptops mainly due to the easiness to achieve multiband response with its conformal design.

### 1.2.3 Printed monopoles

Conventional quarter wave monopole when printed on a dielectric substrate act like a printed monopole. The radiating element can be a strip or a patch of any shape such as circular, rectangular etc. Fractal geometries are also being used for achieving wideband or multiband responses. The basic configuration of a conventional rectangular printed monopole antenna is shown in Fig.1.3.

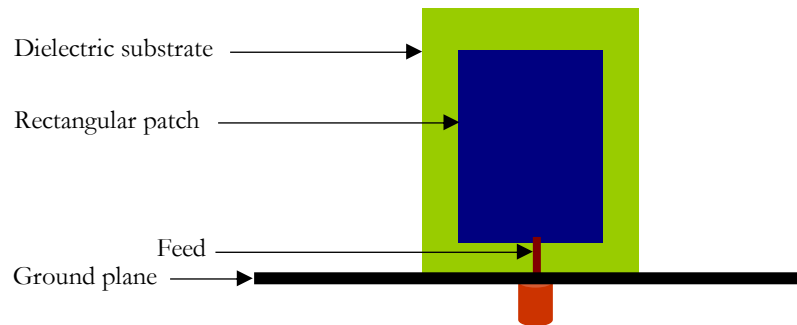


Fig.1.3 Geometry of a rectangular printed monopole antenna

But this configuration is not entirely planar because of the large ground plane. So for compact applications, microstrip fed or coplanar waveguide fed printed monopoles are preferred. Geometry of the microstrip fed and coplanar waveguide fed printed monopole antennas are shown in Fig.1.4. These printed monopole antennas offers low profile, conformal configuration, omni directional radiation coverage, wide bandwidth and simple design

It has been reported that by truncating the ground plane, bandwidth can be increased to a substantial level [8]. By properly optimising the ground plane dimension and offset space between the patch and the ground plane, ultra wideband response can be achieved [9].

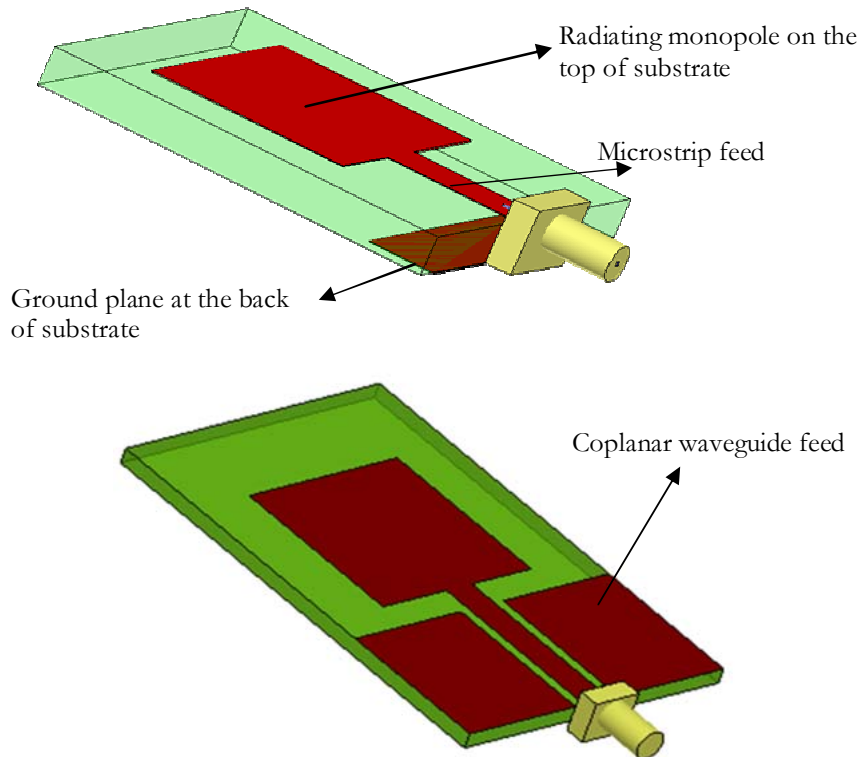


Fig.1.4 Geometry of (a) Microstrip fed monopole  
(b) Coplanar waveguide fed monopole

#### 1.2.4 Printed dipoles

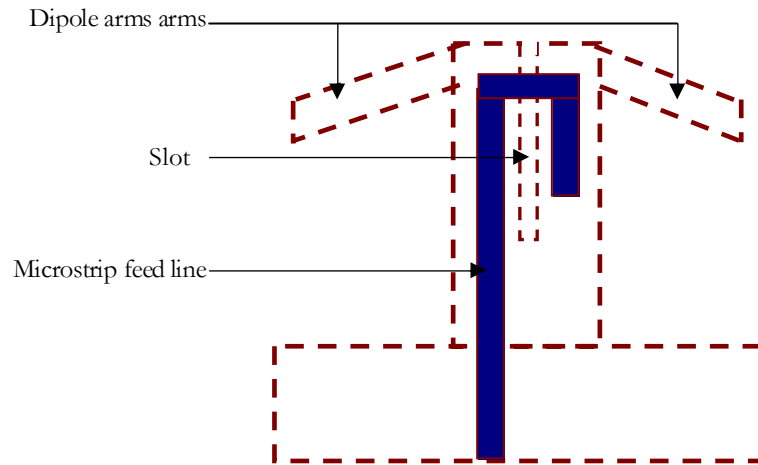
A printed version of the free space dipole is shown in Fig.1.5. As in the case of free space dipole, electric field is along the axis of the dipole.



Fig.1.5 Printed dipole configuration

The dipole is fed in such a way that a horizontal field distribution exists between the gap of the dipole arms and a balanced current distribution exists

on the dipole arms. So normally baluns are used when connected to an unbalanced coaxial transmission line. The first reported broadband printed dipole [10] with integrated balun is shown in fig.1.6.



**Fig.1.6 Geometry of a broadband printed dipole antenna**

This is a microstrip configuration, in which dipole arms are printed on the ground plane. A folded Microstrip line is used as the feed. Feed line and narrow slot on the ground plane are well designed to excite the horizontal electric field between the dipole arms.

A combination of coplanar waveguide (CPW) and coplanar strip line (CPS), with a printed balun is also being used to excite the printed dipoles [11]. This configuration is given in Fig.1.7.

Similar to the CPW-CPS configuration, a combination of Microstrip line (MSL) and parallel strip line (or bifilar line, BFL) is also reported in the literature for the excitation of printed dipole [12, 13]. Fig.1.8 illustrates the configuration of a printed dipole excited by MSL-BFL combination.

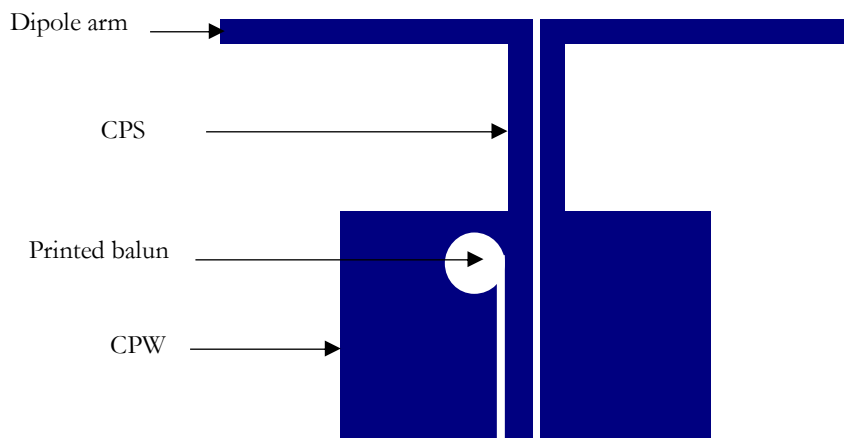


Fig.1.7 CPW fed CPS dipole antenna

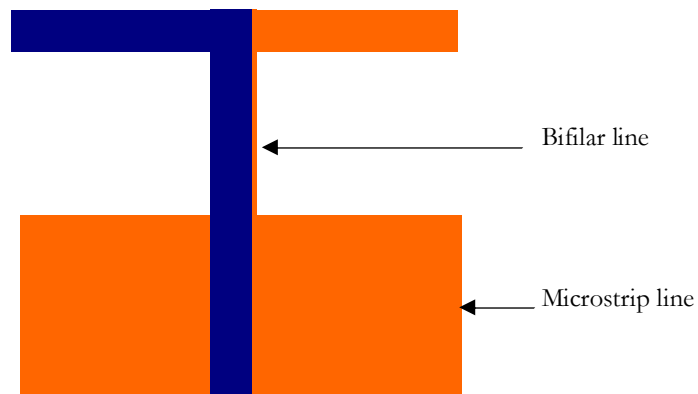


Fig.1.8 MSL-BFL fed printed dipole

### 1.2.5 Metamaterial Antennas

In 1968, the Russian scientist Vesalago proposed the concept of Negative refractive index materials or metamaterials [14]. According to him a medium with simultaneous negative permittivity and permeability could support backward wave propagation and exhibits negative refractive index. Later this concept has been proved by Smith et al[15]. Recently this concept has been well explored by the antenna designers for miniaturisation and bandwidth enhancement.

Configuration of a recently reported metamaterial based patch antenna is shown in Fig.1.9 [16]. In this a rectangular microstrip antenna,

having a combination of Double Negative (DNG) medium and normal Double Positive (DPS) medium as substrate is demonstrated. DNG medium consists of a  $40 \times 2$  DNG unit cells. Schematic illustration of a double negative (DNG) unit cell is shown in Fig.1.9.b. It employs split ring resonators and thin wires. Thin wires can produce effective negative permittivity in some frequency range and split ring resonators can produce negative permeability in a given frequency range. Thus by overlaying these two frequency ranges, a double negative or a negative refractive index performance can be achieved.

By using the combination of DPS-DNG medium it is claimed that resonant length has been decreased from  $0.5\lambda_d$  to  $0.2\lambda_d$ .

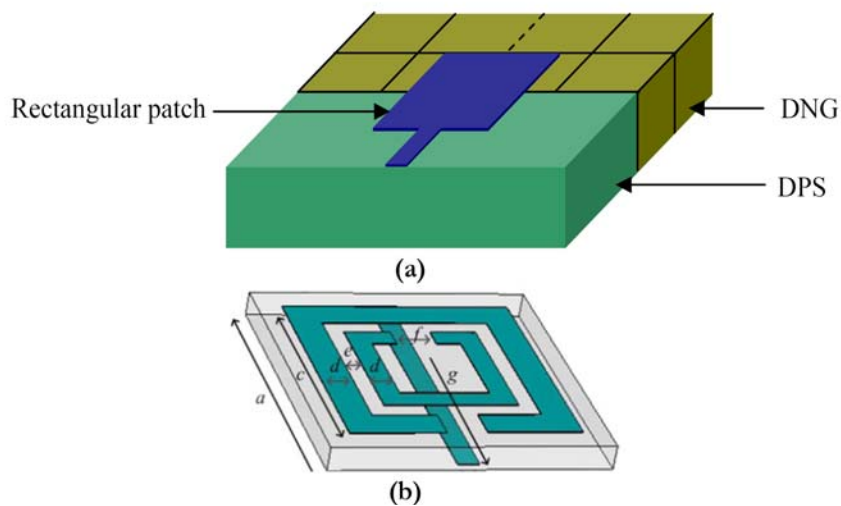


Fig.1.9 Configuration of a metamaterial based patch antenna  
(a) DNG-DPS patch antenna (b) DNG unit cell

### 1.3 Overview of research in compact antennas

Communication industry is going through a developmental era. Personal communication equipments, especially mobile phones became more popular and an essential device now a days. Evolution of mobile phone technology is unbelievable. When it was introduced, it was only a

communication equipment with one single band (GSM). Later more mobile standards have been integrated, thus giving triple band operations (900/1800/1900MHz). Around the same time, Bluetooth modules with a separate internal antenna and FM radio receivers using the earpiece cord as antenna, started to become standard features in phones. In about few years, mobile phones became a multiband, multifunction device. Another important feature is, along with multi-functionalities mobile phones became more compact and aesthetic in appearance. At present, mobile phones with additional facilities like Bluetooth, WLAN, GPS, and DVB-H are common in market. As the device became compact, space allotted for antenna also became less and this will be a real challenge for the antenna designer. Miniaturisation has direct impact on antenna performances like gain, efficiency and bandwidth.

### **1.3.1 Design challenges**

There are some critical aspects, to be considered for designing an antenna for a compact module. Some of these important aspects are mentioned below.

#### **1.3.1.1 Device specifications**

As the antenna performances deteriorate with size reduction, prime importance is given to the device size and allotted volume for the antenna element [17, 18]. As the thickness of the device decreases, the freedom for giving some heights between the radiating element and the ground plane also decrease. This has a huge adverse impact on the bandwidth and efficiency. All the compact communication modules are built around a multi-layered PCB and at least one of the layers of this PCB is completely metallized to act as a ground plane for the system. All currently used RF modules have unbalanced I/O ports with the ground plane as a reference terminal, implying that the antennas should also be implemented in an



unbalanced configuration [19]. Another crucial element is the device chassis; the metallized PCB layer along with metallic parts of the chassis forms the ground plane for many of the subcomponents in the device. So antenna designer cannot customise the chassis as per his requirement. But still chassis is also being used as a radiator along with the primary radiator and chassis dimensions have significant impact on antenna resonance.

### **1.3.1.2 Impedance bandwidth & Efficiency**

Normally almost all compact personal communication applications are in low frequency range, and require a reasonable bandwidth for the proper functioning. Mainly for GSM and DVB-H applications even device dimension is very less than the operating wavelength. So some meandering techniques or the use of high dielectric substrate is needed. This it self reduces the efficiency and bandwidth. So there exists a compromise between miniaturisation and performance. Another important hurdle is deriving multiband responses with optimum bandwidth, gain and polarisation. Usage of multiple antennas for this purpose is usually not preferred because of the unavailability of space, mutual coupling between the antennas etc. Normally for multiple services either multiband or wideband antennas are preferred.

### **1.3.2 Present state of art**

Initially mobile phones were introduced in the market with external antenna. This was a quarter wave monopole with metallic case of the phone as a ground plane. In the next stage down sizing of mobile terminals happened and metallic case has been replaced by plastic case. External antenna is replaced by compact internal antenna. But still the performance is not deteriorated much because of the effective usage of the conductive plate or metalised layer of the PCB inside the case. So the effective radiating surface increases. Different techniques are already been adopted in various

antenna configurations for achieving compactness. Mostly the ground plane of the antenna is the hindrance in miniaturisation. Planar inverted antennas are commonly used for these applications with metal shielding inside the phone as ground plane. When the device became compact, obviously ground plane dimensions reduces and the configuration behaves as asymmetrical dipole with ground plane as one of the arms. So ground plane also has to be considered as a primary source of radiation rather than a separate entity [21]. Research on this ground plane truncation has revealed some interesting results, such as wide bandwidth, nearly omnidirectional radiation pattern etc [22].

#### **1.4 Printed dipoles for compact applications**

The basic parameters of printed dipoles are already mentioned in section 1.2.4. This section highlights the different techniques adopted for achieving compactness and multiband behaviour in printed dipole configuration.

Most of the printed dipole antennas are based on the design developed by Edward and Rees in 1987[10]. Even though this configuration gives a wideband performance, dimension of the antenna is too large for a compact module. The major problem in the printed dipole configuration is the feeding. To excite a balanced current distribution in the dipole arms, baluns are required. The balun design is complicated and bandwidth of the antenna is limited by the balun. For the compact applications integrated printed circuit baluns are preferred.

Several modifications of the above configuration have been reported [23,24,25]. But most of them use complicated baluns with shorting pin, highly critical slots etc. These designs are having wide bandwidth, still because of large size and complicated designs; they are not well suited for compact applications. A coplanar waveguide fed coplanar strip dipole antenna with a wideband printed circuit balun is reported in [11]. This configuration is more popular in printed circuits because of the simple

balun. In another attempt, a combination of microstrip line and parallel strip line (bifilar line) is proposed to excite printed dipoles [12, 13].

Several methods have already been implemented in printed dipoles for achieving multiband performance. Dual band printed dipole antenna reported in [12] uses a combination of microstrip line and parallel strip line for feeding the dipole. For dual band operation a spur line was etched on the dipole arms. In [13] multiband operation was realised by the use of parasitic elements on the same plane of the dipole. Dual band is also achieved [24] by the use of a series fed printed dipoles. In another attempt dual band is achieved by etching slots on the dipole arms [25].

## 1.5 Printed monopoles for compact applications

The basic configurations of printed monopoles are explained in section 1.2.3. Normally printed monopoles are excited using microstrip line or coplanar line as mentioned in section 1.2.3. Printed version of the monopoles is well suitable for integration with other circuit elements on the printed circuit board. Printed monopoles with its inherent wide bandwidth, broad radiation coverage and moderate gain are suitable for modern communication equipments.

Microstrip fed printed monopole antenna reported in [20] shows wide impedance bandwidth with simple design. It has been also reported that impedance bandwidth of the antenna strongly depends on the ground plane size. For compact applications monopole antennas with truncated ground plane are preferred.

There are different attempts to achieve dual band /multiband behaviour in printed monopoles. The coplanar waveguide fed dual frequency antenna reported in [26] uses combination of two monopole strips connected in parallel to the feed point, to achieve dual resonance. In this paper it is also reported that ground plane dimensions shows significant impact on impedance bandwidth. The printed double T monopole antenna mentioned

in [27] uses two stacked T shaped monopoles for achieving dual resonance. In this case also the ground plane dimensions have significant impact on resonant frequency and bandwidth. It is also proposed that ground plane has to be considered as an integral part of the radiating structure.

## 1.6 Motivation of the present research

Modern communication devices are equipped with antennas printed on the circuit board itself for achieving compactness. Printed monopoles and dipoles are widely preferred because of wide bandwidth and omnidirectional radiation coverage. Microstrip fed printed monopole antenna shows wide impedance bandwidth as mentioned in [20]. It has been reported [8, 20] that impedance bandwidth of the microstrip fed printed monopole antenna strongly depends on ground plane dimensions.

Further on our analysis it has been observed that microstrip fed printed monopole antenna shows a second higher resonance with poor impedance matching, other than the expected resonance, when the ground plane length is large ( $>0.75\lambda_d$ ). Impedance matching for the second resonance can be improved by offsetting the feed towards the edge of the ground plane as shown in the Fig.1.10.

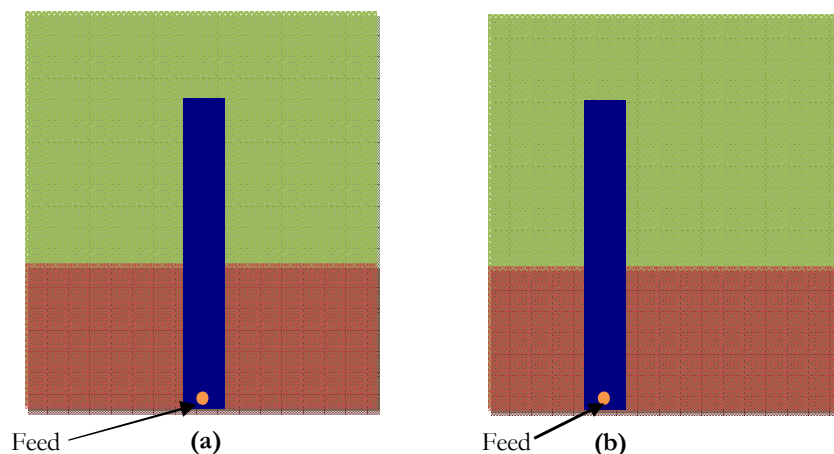


Fig.1.10 Microstrip-fed printed strip monopole antenna  
a. Symmetric b. Offset

A detailed investigation on the simulated surface current distribution shows that the first resonance is due to the monopole strip and the second resonance is due to the L shaped path(abc) including the ground plane as shown in Fig.1.11.

Reduction in ground plane length results in decrease of L shaped resonant length and the second resonance shifts towards the higher side. So in compact ground plane, even with feed offset, antenna shows only one resonance in the lower frequency range. Since the second resonance partly depends on the edge current on the ground plane as shown in Fig.1.11b, an attempt has been made to meander the current path (L-shaped) corresponds to the second resonance by adding another strip to the ground plane as an extension as shown in the Fig.1.12

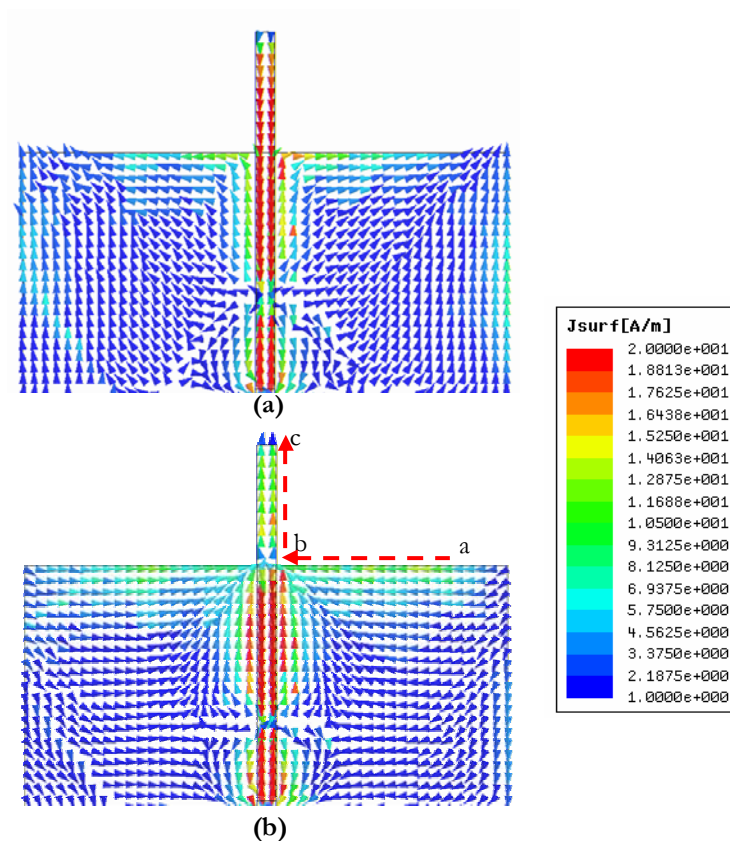


Fig.1.11 Surface current distribution  
 (a) First resonance (b) second resonance

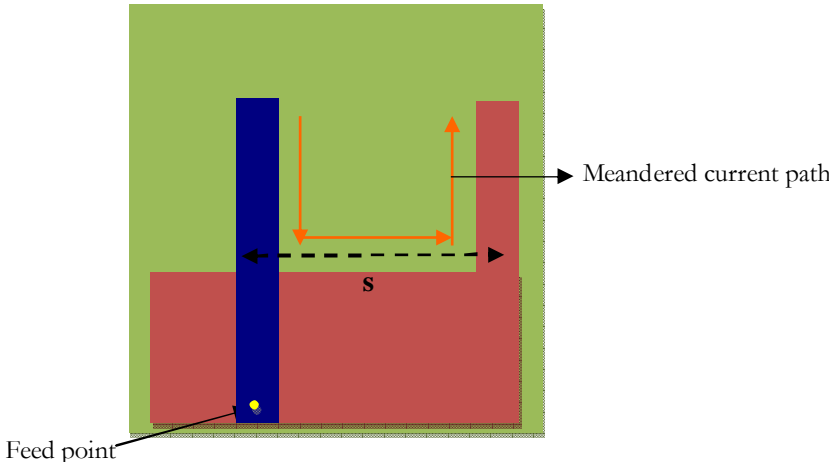


Fig. 1.12 Dual strip antenna

The simulated surface current distribution for this dual strip configuration is as shown in the Fig.1.13.

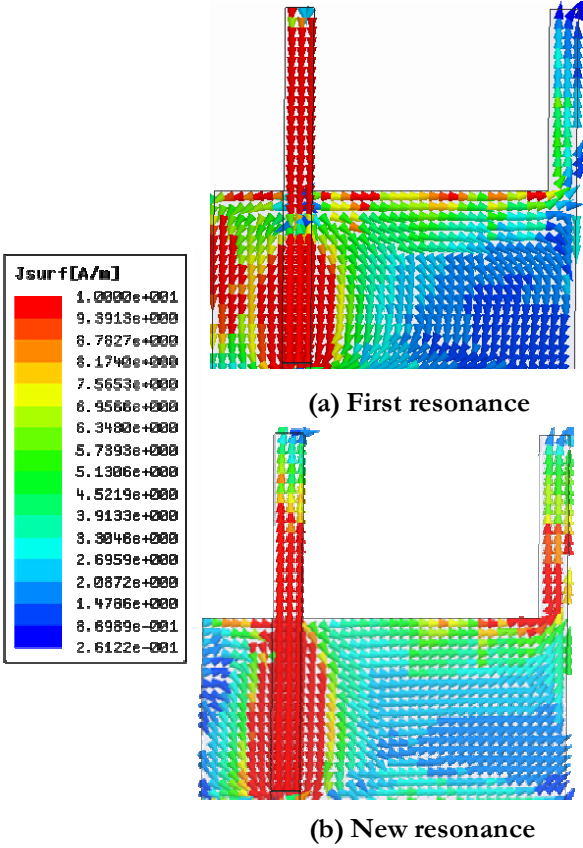


Fig.1.13 Surface current distribution for second resonance

After adding the additional strip, resonant length corresponding to the second resonance has been increased and the frequency has been shifted to the lower side. In this case as shown in Fig.1.13.b, the L shaped path becomes U shape with an 'I' and 'reflected L' as mentioned Fig.1.14. This path includes edge of the ground plane between the signal strip and ground strip. This configuration behaves as an asymmetrically fed dipole with one 'I' shaped strip on top of the substrate and an 'inverted L' shaped strip on bottom of the substrate. Electric field between the microstrip feed line tip and the ground plane excites the asymmetric fed dipole as shown in Fig.1.14. This is achieved by the current path of length 's' which is also acting as a balun. This avoids the use of balun in the design and leads towards a simple dipole configuration.

Currents on the vertical strips are in the same direction, which favours the radiation. For the first resonance current strength is maximum on the monopole strip as shown in the Fig.1.13a.

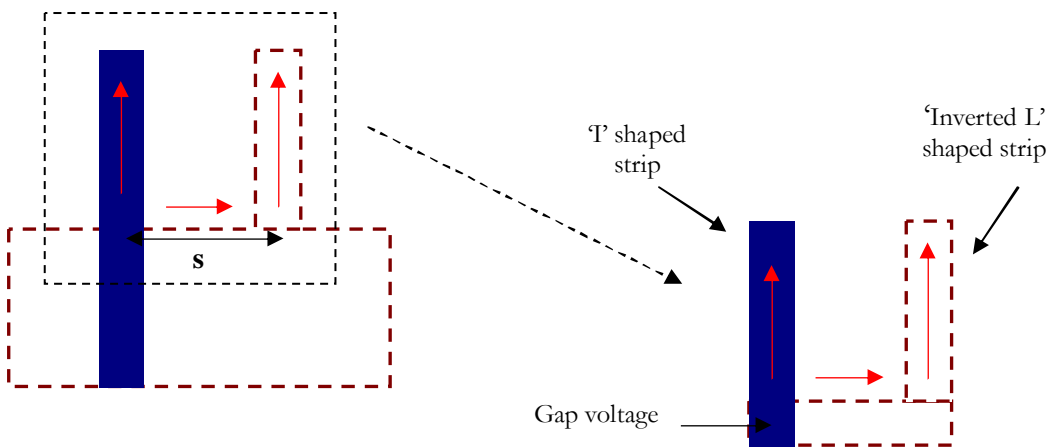


Fig.1.14 Equivalent model of asymmetric fed dipole

This concept has been well explored for the design of a compact dual band dual strip antenna. This technique gives two wide resonances with compact ground plane compared to the other techniques mentioned in

[26,27]. Another important point is for generating the additional resonance, only ground plane edge is utilised without disturbing the ground plane. This will give more freedom for the integration of antenna to the circuit board. In that case common ground plane of the circuit board can be used as the ground plane of the antenna. Since only the edge current on the ground plane is utilized for the resonance, placement of other components on the circuit board will not affect antenna performance.

For more compactness, electrical length is increased by meandering the signal strip and ground strip as shown in Fig.1.15. This folding analysis further reduces the dimensions of the antenna, including the ground plane. Thus a compact dual band antenna can be designed using the above mentioned concept.

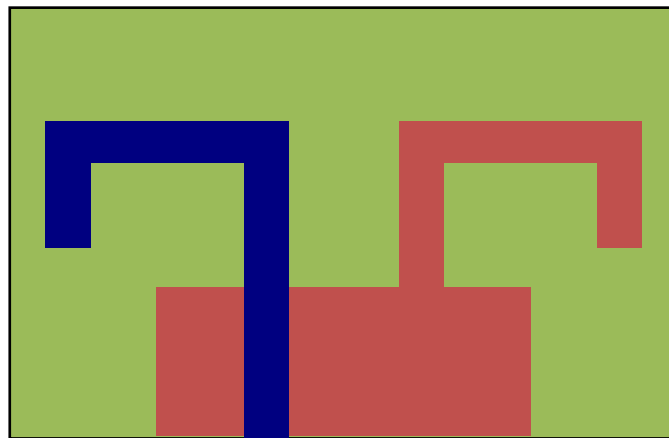


Fig.1.15 Compact folded dual band dual strip antenna

A detailed investigation on this concept has been well explained in the following chapters. Based on this a compact dual band dual strip antenna and compact folded dual strip antenna have been designed for mobile and WLAN applications.



## **1.7 Thesis organisation**

Chapter 1 describes an overview of compact antennas. The challenges in compact antenna design and present state of art in compact antenna research are summarised. It also explains the scope of printed monopoles and dipoles in compact applications. Motivation of the present research and objective of the thesis are illustrated at the end of the chapter.

Chapter 2 is the review of literature which was referred for the present work. A thorough review of compact antennas, antennas for mobile/WLAN applications, wide band and multiband techniques has been carried out. Multiband techniques adopted in various printed monopole and dipole configurations are refereed. Literature related to Finite Difference Time Domain (FDTD) and theoretical analysis using FDTD are also presented.

Chapter 3 gives a brief description of the measurement and simulation techniques used for the thesis work. This chapter also explains briefly the FDTD method which is used in the present thesis for the analysis of compact dual band antenna.

Chapter 4 illustrates the theoretical and experimental investigation on the resonance and radiation mechanism of the dual band dual strip antenna. Evolution of a dual band antenna from microstrip fed printed monopole configuration is well explained with the help of experiment and simulation. Effect of various antenna dimensions on antenna performances has been analysed by experiment and simulations. Based on that, design equations are derived. The design equations are validated for a dual band antenna for DCS/2.4GHz WLAN applications.

Chapter 5 explains the design of a compact dual band folded dual strip antenna based on the above concept. Effect of folding/top loading has been well studied. Design formula is also developed based on the experimental and simulation analysis. Using these design equations compact dual band

folded dual strip antennas for various applications such as GSM,DCS and WLAN have been designed and presented.

Chapter 6 gives the conclusion of the thesis. Scope of the work and future proposals are also described.

Appendix1 gives the design of a planar branched monopole antenna from a simple microstrip fed printed monopole antenna.

In Appendix2, A planar multiband printed antenna for GPS/DCS/PCS/WLAN applications are presented.

## 1.8 References

- [1]. A.D.Olver, Trends in antenna design over 100 years, 100 Years of radio, *IEEE conference*, pp 83-88, September 1995.
- [2]. Jack Ramsay Highlights of antenna history, *IEEE Antennas and Propagation Society Newsletter*, pp. 8-20, December 1981.
- [3]. T.S. Rappaport, Wireless Communications, Principles and Practice, *Prentice Hall, 1996*
- [4]. G.A. Deschamps, Microstrip Microwave Antennas, presented at the Third *USAF symposium on Antennas*, 1953
- [5]. Ramesh Garg et al., Microstrip antenna design handbook, *Artech House, London*.
- [6]. Kin- Lu Wong, Planar antennas for wireless communications, *Wiley interscience publications*.
- [7]. Design of Conformal Antennas for Telephone Handsets, *Thesis by Andrew James Causley, University of Queensland*.
- [8]. M.J.Ammann and M.John , Optimum design of the printed strip monopole, *IEEE Antennas and propagation Magazine*,Vol.47, No.6, pp 59-61,December 2005.
- [9]. K.S.Lim, M.Nagalingam and C.P.Tan, Design and construction of microstrip UWB antenna with time domain analysis, *Progress In Electromagnetics Research M*, Vol.3, pp153-164, 2008.

- [10]. Brian Edward and Daniel Rees, A broadband printed dipole with integrated Balun, *Microwave Journal*, Vol.5, pp339-344, 1987.
- [11]. K.Tilly, X.D.Wu and K.Chang, Coplanar waveguide fed coplanar strip dipole antenna, *Electron.Lett*,vol.30,pp176-177,1994.
- [12]. H.M.Chen, J.M.Chen, P.S.Cheng and Y.F.Lin, Feed for dual band printed dipole antenna, *Electron.Lett*, Vol.40, No.21, pp.176-177, 2004.
- [13]. Jean-Marie Floch and Hatem Rmili , Design of multiband printed dipole antennas using parasitic elements, *Microwave and Optical Technology Letters*,Vol.48 No.8, pp 1639-1645, August 2006.
- [14]. V. G. Veselago, The electrodynamics of substances with simultaneously negative values of permittivity and permeability, *Soviet Physics. Usp.*, Vol. 10, 509-514, 1968.
- [15]. D. R. Smith, W. J. Padilla, D. C. Vier, S. C. Nemat-Nasser, and S. Schultz, Composite medium with simultaneously negative permeability and permittivity, *Phys. Rev. Lett.*, Vol. 84, No. 18, pp.4184–4187, May 2000.
- [16]. M.-F. Wu, F.-Y. Meng, Q. Wu, J. Wu, L.-W. Li, Miniaturization of a Patch Antenna with Dispersive Double Negative Medium Substrates, *Asia Pacific Microwave Conference*, Vol.1, 2005.
- [17]. Compact integrated antennas, *Freescale Semiconductor*, Document No: AN2731, 2004.
- [18]. Hisashi Morishita, Yongho Kim, and Kyohei Fujimoto, Design Concept of Antennas for Small Mobile Terminals and the Future Perspective, *IEEE Antennas and Propagation Magazine*, Vol. 44, No. 5, pp 30-43, October 2002
- [19]. Peter Lindberg, Wideband Active and Passive Antenna Solutions for Handheld Terminals, *Thesis submitted to Uppsala university*.
- [20]. M. N. Suma, P. C. Bybi, P. Mohanan, A wideband printed monopole antenna for 2.4-GHz WLAN applications, *Microwave and Optical Technology Letters*, Vol. 48, No. 5 , pp. 871 – 873, Mar 2006
- [21]. Xiao-Peng Lu and Yan Li, Novel Broadband Printed dipole , *Microwave and Optical Technology Letters*, Vol. 48, No.10, pp. 1996-1998, October 2006

- [22]. Chun Yiu Chu and Milica Popovic, Printed dipole antenna for use in wireless networks: techniques for the design improvement, *IEEE Antennas and Propagation Society International Symposium*, Vol.3B, pp.285-288, 2005
- [23]. Anatoly P. Gorbachev and Vladimir M. Egorov, The dipole radiating integrated module: Experimental results, *IEEE Transactions on Antennas and propagation*, vol.55 No.11, pp 3085-3087, November 2007.
- [24]. Faton Tefiku and Craig A. Grimes, Design of broad-band and dual-band antennas comprised of serious-fed printed-strip dipole pairs, *IEEE Transactions on Antennas and propagation*, vol.48 No.6, pp 895-900, June 2000.
- [25]. Chih-Ming Su, Hong-Twu Chen and Kin-Lu Wong, Printed dual band dipole antenna with U-slotted arms for 2.4/5.2GHz WLAN operation, *Electron.Lett*, Vol.38, No.22, pp 1308-1309, October 2002.
- [26]. Horng-Dean Chen, and Hong-Twu Chen, A CPW-Fed Dual-Frequency Monopole Antenna, *IEEE Transactions on Antennas and propagation*, Vol. 52, No.4, pp 978-982 April 2004.
- [27]. Yen-Liang Kuo and Kin-Lu Wong, Printed Double-T Monopole Antenna for 2.4/5.2 GHz Dual-Band WLAN Operations, *IEEE Transactions on Antennas and propagation*, Vol. 51, No.9, pp 2187-2192, September 2003

.....✂.....

## **LITERATURE REVIEW**

---

<b>Contents</b>	<b>2.1 Introduction</b>
	<b>2.2 Antennas for mobile/WLAN applications</b>
	<b>2.3 Broad band/Multiband antennas</b>
	<b>2.4 Printed monopoles and dipoles for compact applications</b>
	<b>2.5 FDTD analysis</b>
	<b>2.6 Conclusion</b>
	<b>2.7 References</b>

---

This chapter gives a detailed review of different technologies and designs adopted by different researchers in the case of printed antennas for compact and multiband applications. Recent developments in antenna design for mobile and WLAN applications have been referred. Different techniques for broadband and multiband designs that have been reported recently are also highlighted. A number of papers on compact multiband printed monopoles and dipoles are reviewed here. A review of Finite Difference Time Domain (FDTD) techniques which have been employed for modeling the antennas in this thesis is also presented.

---

## 2.1 Introduction

Wireless communication industry had a tremendous development with the advent of mobile phones and Wireless LAN devices. Mobile phones and PDAs with multi functionalities and high level of compactness have been introduced in the market. Antennas, becoming a key element in wireless communication devices undergone amazing developments especially in the case of size and bandwidth.

This thesis highlights the development and analysis of a microstrip-fed dual band dual strip antenna and a compact dual band folded dual strip antenna. The proposed antennas are derived from the basic microstrip fed printed monopole configuration and have been proposed primarily for mobile and WLAN applications. The list of previous works on printed antennas which helps in the design are summarized in this chapter. A thorough review has been conducted on dual band and multiband antennas for mobile and WLAN applications. This chapter begins with the review of works related to the mobile and WLAN applications. Different techniques adopted for dual band/multiband operation and various works on printed monopoles and dipoles for multiband applications are also summarized here. In this thesis numerical analysis has been performed using FDTD technique. The most relevant contributions in this field are also presented here.

## 2.2 Antennas for mobile/WLAN applications

Wireless communications have progressed very rapidly in recent years, and many mobile units are becoming smaller and smaller. To meet the miniaturization requirement, compact antennas are required. Planar printed antennas have the attractive features of low profile, small size and conformability to mounting hosts. They are very promising candidates for satisfying the above applications. For this reason, compact and broadband design techniques for planar antennas have attracted much attention from

antenna researchers. Very recently, especially after the year 2000, many novel planar antenna designs to satisfy specific bandwidth specifications of present-day mobile cellular communication systems, including the global system for mobile communication (GSM: 890–960MHz), the digital communication system (DCS: 1710–1880MHz), the personal communication system (PCS: 1850–1990MHz), and the universal mobile telecommunication system (UMTS: 1920–2170MHz), have been developed and published in the open literature. Planar antennas are also very attractive for applications in communication devices for wireless local area network (WLAN) systems in the 2.4GHz (2400–2484MHz) and 5.2GHz (5150–5350MHz) bands. In this section some of the works related to the mobile and WLAN applications have been referred and discussed.

Jean Yea Jan *et al.* [1] proposed a microstrip fed dual band planar monopole antenna with shorted parasitic inverted L wire for 2.4/5.2/5.8 WLAN bands. In this design inverted L shaped monopole is the exciting element and which controls the higher frequency. Another shorted inverted L shaped parasitic strip etched nearer to the monopole controls the lower frequency.

Wong *et al.* [2] presented a low-Profile planar monopole antenna for multiband operation of mobile handsets. The proposed antenna has a planar rectangular radiating patch in which a folded slit is inserted at the patch's bottom edge. The folded slit separates the rectangular patch into two sub patches, one smaller inner sub patch encircled by the larger outer one. The proposed antenna is then operated with the inner sub-patch resonating as a quarter-wavelength structure and the outer one resonating as both a quarter-wavelength and a half-wavelength structure.

A Multiband Folded Planar Monopole Antenna has been proposed for mobile Handset by Shun-Yun Lin [3]. This paper introduces a folded planar

monopole antenna, which has a very low profile of about one twentieth of the wavelength of the lowest operating frequency. The effect is achieved by using a bended rectangular radiating patch and an inverted L-shaped ground plane.

In another attempt Ching Yuan Chiu *et al.* [4] proposed a shorted, folded planar monopole antenna for dual-band mobile phone. The antenna is fabricated from stamping a single metal plate, which is then folded onto a foam base. The antenna has two separate branches of different sizes: the larger one supports a longer resonant path (path1) for generating a lower mode for GSM operation, while the smaller one provides a shorter resonant path (path2) for generating a higher mode for DCS operation.

Jan and Kuo [5] discussed a CPW-fed wideband planar monopole antenna with a symmetrically slope ground plane. Antenna has an impedance bandwidth of 1162 MHz extends from 1700MHz to 2862 MHz, which covers DCS, PCS and Bluetooth bands. In this case wideband operations can be controlled by choosing the slope angle of the symmetrical ground plane.

Liu and Hsu [6] proposed a Dual-band CPW-fed Y-shaped monopole antenna for PCS&WLAN application. In this paper a rectangular notch is introduced to expand the impedance bandwidth of a dual-band planar monopole antenna. The antenna is fed by a CPW line and resembles the shape of the letter 'Y'. Antenna exhibits 14.4% and 34.1% bandwidths for the lower (1.95GHz) and upper (5.45GHz) bands which covers PCS and WLAN bands.

Yacouba Coulibaly *et al.* [7] presented a broadband CPW fed printed monopole antenna. This configuration comprise of a coplanar waveguide fed monopole antenna with two parasitic strips placed symmetrically on both sides of the monopole. The two parasitic strips adds capacitive coupling and hence improves the impedance bandwidth to 47% with center frequency 2.35GHz.



Cho *et al.* [8] proposed a PIFA configuration for 2.4/5GHz applications. This configuration offers 110MHz bandwidth in Bluetooth band and 900MHz in WLAN band.

Hao Chun Tung *et al.* [9] proposed a printed dual band monopole antenna for 2.4/5.2GHz WLAN access point. The trident monopole antenna comprises a central arm for the 2.4 GHz band (2.4–2.484GHz) operation and two side arms for the 5.2 GHz band (5.15–5.35GHz) operation.

A Compact Dual Band Planar Branched Monopole Antenna has been proposed by Suma *et al.* [10] for DCS/2.4GHz WLAN Application. The two resonant modes of the proposed antenna are associated with various lengths of the monopoles, in which a longer arm contributes for the lower resonant frequency and a shorter arm for higher resonant frequency.

Raj *et al.* [11] discussed a compact dual band coplanar antenna for WLAN application. The antenna comprises of a rectangular center strip and two lateral strips printed on a dielectric substrate and excited using a  $50\Omega$  microstrip transmission line. The lower resonant frequency of the antenna is due to a “U” shaped resonant path on the center strip and the upper resonant frequency is obtained due to the width of the center strip, corresponding to a half wavelength variation in substrate.

Jeun-Wen Wu *et al.* [12] proposed a planar meander-line antenna consisting of three branched strips for very-low-profile GSM/DCS/PCS/WLAN triple-band operation of mobile phones. The branch strips are designed to operate as quarter-wavelength structures at 900 and 1800 MHz, respectively, and covering GSM/DCS/PCS and WLAN bands.

Yong Sun Shin *et al.* [13] developed a broadband interior planar monopole type antenna for hand set applications. The antenna is suitable to be built-in within the housing of a mobile phone. In order to achieve the

broad bandwidth, the feed which is connected between the microstrip line and antenna is a trapezoidal shape with a tilted angle. By adjusting the width of the bottom and top side of a trapezoidal feed, the broad bandwidth can be achieved.

Shao Lun Chien *et al.* [14] proposed a Planar Inverted-F Antenna with a Hollow Shorting Cylinder for Internal Mobile Phone Antenna applications.

Fa Shian Chang *et al.* [15] presented a Folded Meandered-Patch Monopole Antenna for Triple-Band Operation. The proposed antenna is suitable for applications in mobile phones for GSM, DCS and PCS triple-band operations.

An internal GSM/DCS antenna backed by a step-shaped ground plane for a PDA Phone was proposed by K.L. Wong *et al.* [16]. The antenna has two radiating strips designed to operate at about 900 and 1800MHz for GSM/DCS operation, and is backed by a step-shaped ground plane.

Zi Dong Liu *et al.* [17] presented a dual frequency planar inverted-F antenna which operates at 0.9GHz and 1.8GHz bands. In this paper two configurations of dual band antennas are proposed. The antenna with two input ports and single-port are described. The two port antenna consists of two separate radiating elements with the rectangular radiating element for 1.8 GHz and the L-shaped radiating element for 0.9 GHz.

Raj *et al.* [18] presented a compact planar multiband antenna for GPS, DCS, 2.4/5.8 GHz WLAN applications. Antenna has two longer arms on either side separated by a short middle element. A simple  $50\Omega$  probe is used to excite the antenna. A metallic patch is embedded on the bottom side of the substrate, which acts as a reflector and controls the impedance matching.

Deepu *et al.* [19] presented a compact uniplanar antenna for WLAN applications. The dual-band antenna is obtained by modifying one of the

lateral strips of a slot line, thereby producing two different current paths. The antenna resonates with two bands from 2.2 to 2.52 GHz and from 5 to 10 GHz with good matching, good radiation characteristics and moderate gain.

Deepti Das Krishna *et al.* [20] proposed an ultra-wideband slot antenna for wireless USB dongle applications. The design comprises a near-rectangular slot fed by a coplanar waveguide printed on a PCB of width 20 mm. The proposed design has a large bandwidth covering the 3.1-10.6 GHz UWB band and omnidirectional radiation patterns.

Bybi *et al.* [21] presented a quasi-omnidirectional antenna for modern wireless communication gadgets. The antenna has been derived from the conventional CPW by embedding a modified short, which results in an appreciable improvement in the impedance bandwidth while retaining an almost omnidirectional radiation behavior.

A compact dual band planar antenna has been proposed by Gijo Augustin *et al.* [22]. It is a Finite Ground CPW fed, dual-band monopole configuration. The dual-band operation is achieved by loading the flared monopole antenna with a “V”-shaped sleeve.

A dual wide-band CPW-fed modified Koch fractal printed slot antenna, suitable for WLAN and WiMAX operations is proposed by Krishna *et al.* [23]. Here the operating frequency of a triangular slot antenna is lowered by the Koch iteration technique resulting in a compact antenna. Koch fractal slot antenna has an impedance bandwidth from 2.38-3.95GHz and 4.95–6.05GHz covering 2.4/5.2/5.8GHz WLAN bands and the 2.5/3.5/5.5 GHz WiMAX bands.

Deepu *et al.* [24] presented an ACS fed printed F-shaped uniplanar antenna for dual band WLAN applications. Asymmetric coplanar strip is used as the feed for this uniplanar configuration.

A wide band printed microstrip antenna has been proposed for Wireless communications by Sarin *et al.* [25]. This is an electromagnetically coupled strip loaded slotted broad band microstrip antenna having 38% impedance bandwidth.

### 2.3 Broad band /Multiband antennas

In this section some of the works related to broadband and multiband antennas are presented.

George *et al.* [26] presented a single-feed dual frequency compact microstrip antenna with a shorting pin. This new antenna configuration gives a large variation in frequency ratio of the two operating frequencies, without increasing the overall size of the antenna.

Liu [27] proposed a CPW-fed notched planar monopole antenna for multiband operations using a genetic algorithm. By introducing a suitable notch to a rectangular CPW-fed patch, the desired multi-frequency resonant modes and broad impedance bandwidths can be obtained.

Kundukulam et al [28] presented a dual-frequency antenna arrived from a compact microstrip antenna by loading a pair of narrow slots close to its radiating edges. The two frequencies have parallel polarization planes and similar radiation characteristics.

Puente *et al.* [29] proposed a fractal multiband antenna based on sierpinski gasket. In this the self-similarity properties of the antenna's fractal shape has been utilized for achieving the multiband behavior.

Aanandan *et al.* [30] presented a broad band gap coupled microstrip antenna for broad band operation using parasitic elements. The antenna is compact and produces less distortion in the radiation pattern.

The closed form expression for calculating the impedance bandwidth of a wide band printed dipole is proposed by S. Dey *et al.* [31]

Mridula *et al.* [32] reported a broadband rectangular microstrip antenna utilizing an electromagnetically coupled L-strip feed. Experimental study shows a 2:1 VSWR bandwidth of  $\sim 10\%$  and excellent cross-polarization performance with a radiation coverage almost as same as that of the rectangular microstrip antenna fed by conventional methods.

An electromagnetically coupled T-shaped microstrip feed to enhance the impedance bandwidth of a rectangular microstrip antenna has been proposed by Lethakumary *et al.* [33].

Manju Paulson *et al.* [34] described an arrow-shaped microstrip antenna with a pair of narrow slots embedded near the non-radiating edges to provide wide impedance bandwidth.

Lethakumary *et al.* [35] introduced a hook shaped feeding technique for bandwidth enhancement of a rectangular microstrip antenna. This antenna offers an impedance bandwidth of 22% without degrading the efficiency.

Jacob *et al.* [36] proposed the development of a compact microstrip-fed, branched monopole antenna for ultra wide band (UWB) applications. By suitably embedding branches on the top edge of the strip monopole, UWB response can be easily achieved by merging different resonances.

Suma *et al.* [37] proposed a planar monopole antenna suitable for broadband wireless communication. With the use of a truncated ground plane, the proposed printed monopole antenna offers nearly 60% 2:1 VSWR bandwidth and good radiation characteristics for the frequencies across the operating band. The antenna can be easily integrated into wireless circuitry and is convenient for application in laptop computers.

A novel modified T shaped planar monopole antenna has been proposed for multiband operation by Sheng Bing Chen *et al.* in [38]. In this paper, a T-shaped planar monopole antenna in that two asymmetric

horizontal strips are used as additional resonators to produce the lower and upper resonant modes are proposed. As a result, a dual-band antenna for covering 2.4 and 5-GHz wireless local area network (WLAN) bands is implemented. In order to cover simultaneously the DCS, PCS, and UMTS bands, the right horizontal strip has been widened and introduced an L-shaped notch in the right horizontal strip.

Nepa *et al.* presented a Multiband PIFA for WLAN Mobile Terminals [39]. The multiband behaviour is obtained by combining a trapezoidal feed plate with two different resonance paths in the radiating structure.

Rong Lin Le *et al.* [40] proposed a broadband planar antenna for GPS, DCS-1800, IMT-2000, and WLAN Applications. The planar antenna consists of an S-strip and a T-strip, which are separately printed on the two sides of a thin substrate. The antenna size is only 18 mm X 7.2 mm X 0.254 mm. The bandwidth of the planar antenna is enhanced by the mutual coupling between the S-strip and the T-strip.

A Printed double S-shaped monopole antenna has been proposed by W.C. Liu *et al.* for wideband and multiband operation [41]. In this design, to expand the antenna bandwidth, three meandered strips of different shapes, connected and fed by a  $50\Omega$  microstrip line are used.

Shameena *et al.* proposed a Compact ultra-wideband planar serrated antenna with notch band ON-OFF control [42]. The UWB response is achieved by a microstrip fed staircase patch with an identical inverted ground plane. The notch band is switched ON or OFF by integrating a pin diode across a  $\lambda/2$  inverted 'U' slot embedded in the patch.

Best [43] presented a multiband conical monopole antenna. The conical monopole exhibits broader impedance bandwidth and improved radiation pattern performance.

Hayes *et al.* [44] presented a novel triple-band antenna that consists of a driven meander-line element and two parasitic coupled elements. The geometrical configuration, size, and proximity of the driven and parasitic elements materialized the desired multiband operation.

Sanz Izquierdo *et al.* [45] introduced a novel multiband PIFA. The antenna uses a novel technique to incorporate an extra band. The additional band is incorporated by using a parasitic element in the plane of the ground that is excited by coupling from the surrounding finite-sized ground plane.

Design of miniature multiband monopole antenna with application to ground-based and vehicular communication systems was presented by Werner *et al.* [46]. The multiband response was achieved by placing a fixed number of thin stubs at strategic locations along the antenna. A robust genetic algorithm technique was introduced to determine the optimal lengths and locations of the stubs.

Heejun Yoon *et al.* [47] presented the design of a multiband internal antenna for mobile handset applications. Two antenna elements are formed on top and bottom of the common substrate and connected by metallic pin to obtain the multi band characteristics.

Deepukumar *et al.* [48] proposed a new dual port microstrip antenna geometry for dual frequency operation. The structure consists of the intersection of two circles of the same radius with their centers displaced by a small fraction of the wavelength. This antenna provides wide impedance bandwidth and excellent isolation between its ports.

Zhi Ning Chen *et al.* [49] proposed a broadband monopole antenna. A parasitic planar thin conductive element is placed in parallel with the monopole, and electromagnetically coupled to the monopole.

The design of a short-circuited triangular patch antenna with broadband operation has been proposed by J.S. Row *et al.* [50]. By placing two shorting walls at the opposite edges of a tip-truncated triangular patch antenna with a V-shaped slot, two resonant modes can be excited simultaneously and they can be coupled together to achieve the broadband operation.

A novel compact antenna operating at GSM, DCS, PCS and IMT2000 bands has been presented by Peng Sun *et al.* [51]. With a loosely coupled ground branch, the antenna covers all 2G and 3G wireless communication bands.

Wen Chung Liu *et al.* [52] presented a coplanar waveguide (CPW)-fed monopole antenna with dual folded strips for the radio frequency identification (RFID) application. The proposed antenna has a very compact size including ground plane.

Deepu *et al.* [53] presented a slot line fed dipole antenna with a parasitic element for wide band applications. The presented antenna offers a 2:1 VSWR bandwidth from 1.66 to 2.71 GHz with a gain better than 6.5 dBi. The parasitic element improves the bandwidth and gain of the antenna.

Gopikrishna *et al.* [54] proposed a compact semi-elliptic monopole slot antenna for UWB Systems. The antenna features a coplanar waveguide signal strip terminated with a semi-elliptic stub and a modified ground plane to achieve wide bandwidth from 2.85-20 GHz.

A Compact asymmetric coplanar strip fed antenna has been proposed for wideband application by Laila *et al.* [55]. In this configuration wide bandwidth is obtained by merging three resonances at 1.85GHz, 3.18GHz and 4.4GHz.

A Compact Asymmetric Coplanar Strip Fed Monopole Antenna has been proposed by Deepu *et al.* [56] for Multiband Applications. The antenna



exhibits three resonances around 1.8, 2.4, and 5.6 GHz. The multiband characteristic of the antenna is due to the various meandered current paths excited in the radiating structure. The antenna has an overall dimension of only 28 X30 mm<sup>2</sup>.

Shynu *et al.* [57] presented a varactor controlled dual frequency reconfigurable microstrip antenna capable of achieving tunable frequency ratios in the range 1.1 to 1.37. Varactor diodes integrated with the arms of the hexagonal slot and embedded in the square patch are used to tune the operating frequencies by applying reverse-bias voltage. The design has the advantage of size reduction up to 73.21% and 49.86% for the two resonant frequencies, respectively, as compared to standard rectangular patches. The antenna offers good bandwidth of 5.74% and 5.36% for the two operating frequencies.

Row and Wu [58] proposed a wideband square patch antenna. The antenna has a square patch that is shorted to the ground plane through two shorting walls and is excited by a top-loaded coaxial feed centered below the square patch. The antenna shows a 50% impedance bandwidth and a stable monopole-like conical radiation pattern.

## 2.4 Printed monopoles and dipoles for compact applications

Printed monopoles and dipoles are widely used in the case of compact applications due to the simplicity in design and optimum reflection and radiation performances. In this section some of the most relevant work on printed monopoles and dipoles, which highlight the dual band/multiband techniques, have been discussed.

Hornng Dean Chen *et al.* [59] proposed a CPW-Fed Dual-Frequency Monopole Antenna. The proposed antenna consists of two monopoles printed on a FR4 dielectric substrate and excited by a 50Ω CPW transmission line. The two monopoles are centered and connected at the end

of the CPW feed line. The two operating modes of the proposed antenna are associated with various lengths of two monopoles, in which the longer monopole works for the first resonant mode and the shorter monopole works for the second mode. Moreover, by increasing the width of the longer monopole, a broadband dual-frequency operation is demonstrated.

A Dual Band CPW-Fed Printed T-Shaped Planar Antenna has been proposed by Qiu *et al.* [60]. The proposed antenna comprised of two horizontal arms of different lengths and an L-shaped shorted strip, which connects between the vertical arm and the ground plane. It has been reported that the short-circuiting L-shaped element is the key component responsible for the two separate resonant modes. It introduces additional inductance to compensate for the large capacitance contributed from the area between the designed antenna and the ground plane, thus helping to generate two different resonant modes at 1.8GHz and 2.4GHz respectively.

Jung *et al.* [61] proposed a Wideband monopole antenna for various mobile communication applications. This design is basically a microstrip fed printed monopole configuration, which consists of a radiating patch with two L-shaped notches and stubs at the lower corners with a truncated ground plane. A wideband characteristic of the proposed antenna is easily achieved by cutting two L-shaped notches and attaching two stubs to the radiating patch. The L-shaped notches of suitable dimensions improve impedance matching performance at middle frequencies within the bandwidth of interest. To achieve good impedance matching at higher frequencies, two stubs are appended to the radiating patch.

Chung *et al.* [62] introduced a Wideband CPW-fed monopole antenna with parasitic elements and slots. The antenna operates over 3.1 to 11 GHz for the return loss of less than -10 dB. The geometry consists of a rectangular monopole with parallel slots excited by a CPW line. Two

parasitic strips are etched symmetrically on either side of the monopole. The wideband characteristic is achieved by utilizing the electromagnetic coupling effects of two parasitic elements. Three narrow slots also provide additional impedance matching capability. In addition, a gap between parasitic elements and ground planes is also an important parameter to control the impedance bandwidth.

Amman and John [63] have presented an optimum design for the printed strip monopole. In this paper a microstrip fed printed monopole antenna has been studied and effect of ground plane dimensions on impedance bandwidth and radiation pattern have been investigated. It is reported that the impedance bandwidth of the printed monopole was strongly dependant on the ground plane dimensions.

Y. F. Lin *et al.* [64] proposed a microstrip fed dual band monopole antenna. The antenna consists of two strip monopoles printed on the same side of an electrically thin dielectric substrate, and fed by a microstrip feed line with an open-circuited tuning stub. The proposed antenna is designed to have dual-band operation suitable for applications in DCS and WLAN bands. The lengths of the antenna's larger and smaller strips can easily control the lower and upper operating frequencies, respectively. Antenna shows 2:1 VSWR bandwidth of 12.4% in DCS band and 8.9% in WLAN band.

Ultra-wideband performance is achieved in Planar CPW-fed sleeve monopole antenna by Chen *et al.* [65]. Antenna shows bandwidth from 2.43 to 8.16GHz. Antenna consists of a monopole and two sleeves, and is printed on an FR4 microwave substrate. The monopole is centrally placed at the end of the signal strip of the CPW feed line. The two sleeves are the extension of the ground planes of the CPW feed line. The lower-edge frequency of impedance bandwidth is determined by the monopole length  $L$ . The upper-edge frequency of impedance bandwidth is controlled by the sleeve length,

the spacing and the dimensions of the CPW feed line. Hence, with the selection of proper dimensions of the  $50\Omega$  CPW feed line and adjusting the sleeve length and the spacing, good impedance match across a very wide operating bandwidth can be achieved.

Michael Johnson and Yahya Rahmat Samii [66] proposed a broadband tab monopole antenna with a 2:1 VSWR bandwidth of more than 50%. The tab monopole consists of a sub-wavelength tapered radiating element fed by a coplanar waveguide with ground plane.

Liu [67] proposed a wideband dual-frequency double inverted-L CPW-fed monopole antenna for WLAN application. The antenna comprises a planar patch element with a sided L-shaped slit to become a double inverted-L monopole and is capable of generating two separate resonant modes with good impedance match. Antenna shows -10dB impedance bandwidths of 7.3% and 35.1% at the resonant frequencies of 2.48 and 5.22GHz, respectively.

Yang and Yan [68] proposed a Dualband Printed Monopole Antenna for WLAN applications. The microstrip fed printed monopole consists of a P shaped radiating element. Antenna is resonating at 2.45 GHz with a -10 dB impedance bandwidth of 360 MHz (2.28–2.64 GHz) and at 5.8 GHz with an impedance bandwidth of 1.45 GHz (4.92–6.37GHz).

Brian Edward and Daniel Rees [69] proposed a broadband printed dipole with integrated balun. It is of microstrip configuration, in which dipole arms are printed on the ground plane. A folded Microstrip line is used as the feed. Feed line and narrow slot on the ground plane is well designed to excite the horizontal electric field between the dipole arms.

Tilly *et al.* [70] proposed a printed dipole antenna excited using a combination of coplanar waveguide (CPW) and coplanar strip line (CPS), with a printed balun.

Kihun Chang *et al.* [71] proposed a Wideband Dual Frequency Printed Dipole Antenna using a parasitic element. This antenna is fed by a broadband radial stub balun with a transition, which converts microstrip line into CPS (Co-Planar Stripline). Antenna shows dual-resonance at 1.8 GHz and 2.1 GHz and has an operating bandwidth of 860 MHz for VSWR 2:1.

Jean Marie Floch and Hatem Rmili [72] proposed multiband printed dipole antennas using parasitic elements. Three different antenna designs were studied in this paper, one is the elementary dipole, and another two are dipoles with single and double parasitic elements which give double and triple resonances respectively.

A low cost microstrip fed dual frequency dipole antenna has been proposed by Young Ho Suh and Kai Chang [73]. In this design a microstrip line is used to excite the shorter dipole and the longer dipole is placed nearer to it. Antenna shows resonances at 2.4GHz and 5.2GHz with 2:1 VSWR bandwidths of 18.75% and 7.7% respectively.

Chih Ming Su *et al.* [74] proposed a printed dual band dipole antenna with U-slotted arms for 2.4/5.2GHz WLAN applications. The dipole arms are designed for 2.4GHz and the embedded U-shaped slots forms a second dipole antenna with smaller length and generates higher resonant mode at 5.2GHz band.

Chen *et al.* [75] proposed a dual band printed dipole antenna for 2.4/5.2GHz WLAN applications. A combination of microstrip line and parallel strip line is used to excite the dipole antenna. For achieving the higher resonance a spur line is etched on the dipole arms. Antenna shows impedance bandwidths of 9.3% and 5.1% for the lower and higher bands respectively.

Sujith *et al.* [76] proposed a compact dual-band modified T-shaped CPW-fed monopole antenna. The antenna has resonances at 1.77 and 5.54

GHz with a wide band from 1.47–1.97 GHz and from 5.13–6.48 GHz with an impedance bandwidth of 34% and 26%, respectively. Antenna shows an average gain of 3 dBi in lower band and 3.5 dBi in higher band with an average efficiency of 90%

Lee *et al.* [77] proposed a Wideband Planar Monopole Antennas with Dual Band-Notched Characteristics. The proposed antenna consists of a wideband planar monopole antenna and the multiple U,  $\cap$  and inverted L-shaped slots, producing band-notched characteristics.

Chang *et al.* [78] presented a CPW-fed U type Monopole Antenna for UWB applications.. The antenna consists of two components; finite width ground plane and U type-loaded. A 50ohms CPW transmission line is used to excite the antenna. Antenna shows a peak gain of 2.9dBi.

## 2.5 FDTD analysis

The Finite-Difference Time-Domain (FDTD) method is arguably the most popular numerical method in electromagnetics. Although the FDTD method has existed for nearly 40 years, its popularity continues to grow as computing costs continue to decline. Furthermore, extensions and enhancements to the method are continually being published, which further broaden its appeal. Most relevant papers concerning the FDTD computation of printed antenna problems are referred in this section.

The Finite-Difference Time-Domain (FDTD) method, as first proposed by Yee [79] in 1966, is a simple and elegant way to discretize the differential form of Maxwell's equations. Yee used an electric field grid, which was offset both spatially and temporally from a magnetic-field grid, to update the present fields throughout the computational domain, in terms of the past fields.

The original Yee FDTD algorithm is second-order accurate in both space and time. Numerical-dispersion and grid-anisotropy errors can be kept

small by having a sufficient number of grid spaces per wavelength. Taflove [80] was among the first to rigorously analyze these errors. Taflove [81] was also the first to present the correct stability criteria for the original orthogonal-grid Yee algorithm.

Sheen *et al.* [82] described application of 3D FDTD method for the analysis of microstrip antenna and other microstrip circuits. In order to model open-region problems, an absorbing boundary condition (ABC) is often used to truncate the computational domain. There are two different types of ABCs, differential ABC and material based ABC. Mur [83] has proposed differential ABC called Mur's ABC. The most relevant advance in material-based ABCs was put forward by Berenger [84]. His ABC, termed the Perfectly-Matched-Layer (PML) absorbing boundary condition, appears to yield a major improvement in the reduction of boundary reflections, compared to any ABC proposed previously.

Reineix and Jecko [85] were the first to apply the FDTD method to the analysis of microstrip antennas. In 1992, Leveque *et al.* [86] modeled frequency-dispersive microstrip antennas, while Wu *et al.* [87] used the FDTD method to accurately measure the reflection coefficient of various microstrip-patch configurations.

Uehara and Kagoshima [88] presented an analysis of the mutual coupling between two microstrip antennas, while Oonishi *et al.* [89] and Kashiwa *et al.* [90] used one of the conformal FDTD approaches to analyze microstrip antennas on a curved surface.

In 1994, Qian *et al.* [91] used the FDTD method to design twin-slot antennas. Recently, Reineix *et al.* [92, 93, and 94] have expanded their FDTD analysis to include the input impedance of micro strips with slots, to obtain the radar cross section of microstrip-patch antennas, and to model the radiation from microstrip patches with a ferrite substrate.

In 1992, Luebbers *et al.* [95] and Chen *et al.* [96] analyzed a monopole antenna on a conducting or dielectric box using FDTD. Toftgird *et al.* [97] calculated the effect of the presence of a person on the radiation from such antennas. In 1994, Jensen and Rahmat Samii [98] presented results for the input impedance and gain of monopole, PIFA, and loop antennas on hand-held transceivers.

The interaction of a hand held antenna and a human were also studied by Jensen and Rahmat Samii [99]. Also in 1994, Chen and Wang [100] calculated the currents induced in the human head with a dipole-antenna from a cellular phone. Martens *et al.* [101] have studied the capability of the finite difference time domain (FDTD) method to predict the interaction between the human body and the electromagnetic field generated by a cordless telephone.

Analysis of CPW-fed folded-slot and multiple-slot antennas on thin substrates were carried out using FDTD method by Huan Shang Tsai and York [102]. Kar and Wahid [103] described the FDTD analysis of dual-feed microstrip patch antennas. Dey *et al.* [104] proposed conformal FDTD analysis technique for modeling cylindrical DRs. FDTD analysis of radiation pattern of antenna on truncated ground plane was investigated by Yamamoto *et al.* [105].

The 3-D FDTD design analysis of a 2.4-GHz polarization-diversity printed dipole antenna with integrated balun and polarization-switching circuit for WLAN and wireless communication applications was carried out by Huey Ru Chuang *et al.* [106]. Pattern reconfigurable leaky-wave antenna analysis using FDTD method was introduced by Shaoqiu Xiao *et al.* [107]. FDTD analysis of printed dipole antenna with balun has been presented by Michishita *et al.* [108].



## 2.6 Conclusion

A detailed review has been carried out on dual band and multiband techniques, antennas for mobile and WLAN applications and FDTD modeling of planar antennas. Different methods for achieving compactness and dual band/multiband performance has been refereed for designing compact dual band antenna in the thesis.

## 2.7 References

- [1]. Jen Yea Jan and Liang Chih Tseng, Small Planar Monopole Antenna With a Shorted Parasitic Inverted-L Wire for Wireless Communications in the 2.4, 5.2, and 5.8-GHz Bands, *IEEE Transactions on Antennas and Propagation*, Vol. 52, No. 7, pp.1903-1905, July 2004.
- [2]. Kin Lu Wong, Gwo Yun Lee, and Tzung Wern Chiou, A Low-Profile Planar Monopole Antenna for Multiband Operation of Mobile Handsets, *IEEE Transactions on Antennas and Propagation*, Vol. 51, No. 1, pp.121-125, January 2003.
- [3]. Shun Yun Lin, Multiband Folded Planar Monopole Antenna for Mobile Handset, *IEEE Transactions on Antennas and Propagation*, Vol. 52, No. 7, pp. 1790-1794, July 2004
- [4]. Ching Yuan Chiu, Pey Ling Teng and Kin Lu Wong, Shorted, folded planar monopole antenna for dual-band mobile phone, *IEE Electronics Letters*, Vol. 39 No. 18, pp.1301 - 1302, September 2003.
- [5]. J.Y. Jan and T.M. Kuo, CPW-fed wideband planar monopole antenna for operations in DCS, PCS, 3G, and Bluetooth bands, *IEE Electronics Letters*, Vol. 41 No. 18, pp.991-993, September 2005.
- [6]. W.C. Liu and C.F. Hsu, Dual-band CPW-fed Y-shaped monopole antenna for PCS/WLAN applications, *IEE Electronics Letters*, Vol. 41 No., pp. 390-391, March 2005.
- [7]. Yacouba Coulibaly, Tayeb A. Dendini, Larbi talbi and Abdel R. Sebak, A new single layer broadband cpw fed printed monopole antenna for wireless applications, *IEEE CCECE*, Niagra Falls, Vol.3, pp-1541 - 1544, May 2004.

- [8]. Y.J.Cho, Y.S.Shin and S.O. Park, Internal PIFA for 2.4/5GHz WLAN applications, *IEE Electronics Letters*, Vol.42, No.1,pp. 8-10, January 2006.
- [9]. Hao Chun Tung, Shyh Tirng Fang and Kin Lu Wong, Printed Dual-Band Monopole Antenna for 2.4/5.2 GHz WLAN Access Point, *Microwave and Optical Technology Letters*, Vol. 35, No. 4, pp. 286-288, November 2002.
- [10]. M.N. Suma, Rohith K Raj, Manoj Joseph, P.C. Bybi and P. Mohanan, A Compact Dual Band Planar Branched Monopole Antenna for DCS/2.4GHz WLAN Applications, *IEEE Microwave and Wireless Components Letters*, Vol. 16, No.5, pp. 275-277, May 2006.
- [11]. Rohith K. Raj, Manoj Joseph, K. Vasudevan, C. K. Aanandan and P. Mohanan A New Compact Microstrip-fed Dual-band Coplanar Antenna for WLAN applications, *IEEE Transactions on Antennas and Propagation*, Vol.54, No.12, pp. 3755-3762, December 2006.
- [12]. Jeun Wen Wu, Chun Ren Lin, Jui Han Lu, A planar meander-line antenna for triple-band operation of mobile, *Microwave and optical technology letters*, Vol. 41, No. 5, pp. 380 - 386, Apr 2004
- [13]. Yong Sun Shin, Seong Ook Park, and Manjai Lee, A Broadband Interior Antenna of Planar Monopole Type in Handsets, *IEEE Antennas and Wireless Propagation Letters*, Vol. 4, pp. 9-12, 2005.
- [14]. Shao Lun Chien, Hong Twu Chen, Chih Ming Su, Fu Ren Hsiao and Kin Lu Wong, Planar Inverted-F Antenna with a Hollow Shorting Cylinder for Internal Mobile Phone Antenna, *IEEE Antennas and propagation International symposium*, Vol.2, pp. 1947-1950, 2004.
- [15]. Fa Shian Chang, Wen Kuan Su and Kin Lu Wong, Folded Meandered-Patch Monopole Antenna for Triple-Band Operation, *IEEE Antennas and Propagation International symposium*, Vol.1, pp. 278-281, 2003.
- [16]. Kin Lu Wong and Chun Lin, Internal GSM/DCS Antenna Backed by a Step-Shaped Ground Plane for a PDA Phone, *IEEE Transactions on Antennas and Propagation*, Vol. 54, No. 8, pp. 2408-2410, August 2006.
- [17]. Zi Dong Liu, Peter S. Hall, and David Wake, Dual-Frequency Planar Inverted-F Antenna, *IEEE Transactions on Antennas and Propagation*, Vol. 45, No. 10, pp. 1451-1458, October 1997.

- [18]. Rohith K Raj, Manoj Joseph, B. Paul and P. Mohanan, Compact planar multiband antenna for GPS, DCS, 2.4/5.8 GHz WLAN applications, *IEE Electronics Letters*, Vol.41, No.6, pp. 290-291, March 2005.
- [19]. V. Deepu, , Rohith K Raj, Manoj Joseph, M.N. Suma, K. Vasudevan, C.K. Aanandan and P. Mohanan, Compact uniplanar antenna for WLAN applications, *IEE Electronics Letters*, Vol.43, No.2, pp.70-72, January 2007.
- [20]. D.D. Krishna, M. Gopikrishna, C.K. Aanandan, P. Mohanan and K. Vasudevan, Ultra-wideband slot antenna for wireless USB dongle applications , *IEE Electronics Letters*, Vol. 44 No. 18, pp. 1057-1058, August 2008.
- [21]. P. C. Bybi, Gijo Augustin, B. Jitha, C. K. Aanandan, K. Vasudevan and P. Mohanan, A Quasi-Omnidirectional Antenna for Modern Wireless Communication Gadgets, *IEEE Antennas and wireless propagation letters*, Vol. 7, pp-505-508, 2008
- [22]. Gijo Augustin, P.C Bybi, V.P. Sarin, P. Mohanan, C.K Aanandan and K. Vasudevan, A compact dual band planar antenna for DCS-1900/PCS/PHS, WCDMA/IMT-2000 and WLAN applications, *IEEE Antennas and wireless propagation letters*, Vol. 7, pp- 108-111, January, 2008.
- [23]. D.D. Krishna, M. Gopikrishna, C. K. Anandan, P. Mohanan, and K. Vasudevan, CPW-Fed Koch Fractal Slot Antenna for WLAN/WiMAX Applications, *IEEE Antennas and wireless propagation letters*, Vol.7, pp-389-392, 2008.
- [24]. V. Deepu, R. Sujith, S. Mridula, C. K. Aanandan, K.Vasudevan, P. Mohanan, ACS fed printed F-shaped uniplanar antenna for dual band WLAN applications, *Microwave and Optical Technology Letters*, Vol. 51, No. 8, pp. 1852 – 1856, May 2009.
- [25]. V.P. Sarin, Nisha Nassar, V. Deepu, C.K Aanandan, P. Mohanan and K. Vasudevan, Wide band printed microstrip antenna for Wireless communications, *IEEE Antennas and wireless propagation letters*, Vol. 8, pp. 779-781, 2009.
- [26]. J. George, K. Vasudevan, P. Mohanan and K.G. Nair, Dual frequency miniature microstrip antenna, , *IEE Electronics Letters*, Vol. 34, No. 12, pp. 1168-1170, June 1998.

- [27]. W.C. Liu, Design of a CPW-fed notched planar monopole antenna for multiband operations using a genetic algorithm, *IEE Proc. Microw. Antennas Propag.*, Vol. 152, No. 4, pp.273-277, August 2005.
- [28]. O. Sona, Kundukulam, Manju Paulson, C. K. Aanandan and P. Mohanan, Slot-loaded compact microstrip antenna for dual-frequency operation, *Microwave and Optical Technology Letters*, Vol. 31, No. 5 , pp. 379 – 381, October 2001.
- [29]. C. Puente, J. Romeu, R. Pous, X. Garcia and F. Benitez, Fractal multiband antenna based on the Sierpinski gasket, *IEE Electronics Letters*, Vol. 32, No.1 pp 1-2, January 1996.
- [30]. C. K. Aanandan, P. Mohanan and K. G. Nair, Broad band gap coupled microstrip antenna, *IEEE Transactionas on Antennas and Propagation*, Vol. 38, No. 10, pp. 1581-1586, October 1990.
- [31]. S. Dey, C.K. Aanandan, P. Mohanan and K.G. Nair, Analysis of cavity backed printed dipoles, *IEE Electronics Letters*, Vol. 30 No. 3, pp. 173-174, February 1994.
- [32]. S. Mridula, Sreedevi K. Menon, B. Lethakumary, Binu Paul, C. K. Aanandan and P. Mohanan, Planar L-strip fed broadband microstrip antenna, *Microwave and Optical Technology Letters*, Vol. 34, No. 2, pp. 115 – 117, June 2002.
- [33]. B. Lethakumary, Sreedevi K. Menon, C. K. Aanandan and P. Mohanan, A wideband rectangular microstrip antenna using an asymmetric T-shaped feed, *Microwave and Optical Technology Letters*, Vol. 37, No. 1 , pp. 31-32, February 2003.
- [34]. Manju Paulson, O. Sona, Kundukulam, C. K. Aanandan, P. Mohanan and K. Vasudevan, Compact microstrip slot antenna for broadband operation, *Microwave and Optical Technology Letters*, Vol. 37, No. 4 , pp. 248 -250, March 2003.
- [35]. B. Lethakumary, Sreedevi K. Menon, Priya Francis, C. K. Aanandan, K. Vasudevan and P. Mohanan, Wideband microstrip antenna using hook-shaped feed, *Microwave and Optical Technology Letters*, Vol. 44, No. 2 , pp. 169 - 171, Decenber 2004.

- 
- [36]. K. Francis Jacob, M. N. Suma, Rohith K. Raj, Manoj Joseph and P. Mohanan Planar branched monopole antenna for UWB applications, *Microwave and Optical Technology Letters*, Vol. 49, No. 1 , pp. 45 – 47, November 2006.
- [37]. M. N. Suma, P. C. Bybi and P. Mohanan, A wideband printed monopole antenna for 2.4-GHz WLAN applications, *Microwave and Optical Technology Letters*, Vol. 48, No. 5 , pp. 871-873, March 2006.
- [38]. Sheng Bing Chen, Yong Chang Jiao, Wei Wang and Fu-Shun Zhang, Modified T-Shaped Planar Monopole Antennas for Multiband Operation, *IEEE Transactions on Microwave Theory and Techniques*, Vol. 54, No. 8, pp 3267-3270, August 2006.
- [39]. P. Nepa, G. Manara, A. A. Serra, and G. Nenna, Multiband PIFA for WLAN Mobile Terminals, *IEEE Antennas and Wireless Propagation Letters*, Vol. 4, pp 349-350, 2005.
- [40]. RongLin Li, Bo Pan, Joy Laskar and Manos M. Tentzeris, A Compact Broadband Planar Antenna for GPS, DCS-1800, IMT-2000 and WLAN Applications, *IEEE Antennas and Wireless Propagation Letters*, Vol. 6, pp 25-27, 2007.
- [41]. W.C. Liu, W.R. Chen and C.M. Wu, Printed double S-shaped monopole antenna for wideband and multiband operation of wireless communications, *IEE Proc. Microw. Antennas Propag.*, Vol. 151, No. 6, pp 473-476, December 2004.
- [42]. V.A. Shameena, M.N. Suma, Rohith K. Raj, P.C. Bybi and P. Mohanan, Compact ultra-wideband planar serrated antenna with notch band ON/OFF control, *IEE Electronics Letters*, Vol. 42, No. 23, pp.1323-1324, November 2006.
- [43]. S.R. Best, A multi-band conical monopole antenna derived from a modified Sierpinski gasket, *Antennas and Wireless Propagation*, Vol. 2, No. 1, pp. 205 - 207, 2003.
- [44]. M. Ali, G.J. Hayes, Huan-Sheng Hwang and R.A. Sadler, Design of a multiband internal antenna for third generation mobile phone handsets, *IEEE Transactions on Antennas and Propagation*, Vol. 51, No. 7, pp. 1452 -1461, July 2003

- [45]. B. Sanz Izquierdo, J .Batchelor and R. Langley, Multiband printed PIFA antenna with ground plane capacitive resonator, *IEE Electronics Letters*, Vol. 40, No.22, pp. 1391 - 1392, October 2004.
- [46]. Werner P.L and D.H. Werner, Design synthesis of miniature multiband monopole antennas with application to ground-based and vehicular communication systems, *IEEE Antennas and Wireless Propagation Letters*, Vol. 4, pp. 104 – 106, 2005.
- [47]. Heejun Yoon, Harackiewicz F.J Rhyu, H Myun-Joo Park and Byungje Lee, Internal antenna for multiband mobile handset applications, *Antennas and Propagation Society International Symposium*, Vol. 1, pp. 463-466, pp. 3-8, July 2005.
- [48]. M. Deepukumar, J. George, C.K. Aanandan, P. Mohanan and K.G. Nair, Broadband dual frequency microstrip antenna, *IEE Electronics Letters*, Vol. 32 No. 17, pp. 1531-1532, August 1996.
- [49]. Zhi Ning Chen, Y. W. M. Chia, Broadband monopole antenna with parasitic planar element, *Microwave and Optical Technology Letters*, Vol. 27, No. 3, pp. 209 – 210, September 2000.
- [50]. Row J.S, Yen Yu Liou, Broadband short-circuited triangular patch antenna, *IEEE Transactions on Antennas and Propagation*, Vol. 54, No. 7, pp. 2137 - 2141, July 2006.
- [51]. Peng Sun and Zhenghe Feng, Compact planar monopole antenna with ground branch for GSM/DCS/PCS/IMT2000 operation, *Microwave and Optical Technology Letters*, Vol. 48, No. 4, pp. 719 – 721, February 2006.
- [52]. Wen Chung Liu, Ping Chi Kao, Compact CPW-fed dual folded-strip monopole antenna for 5.8-GHz RFID application, *Microwave and Optical Technology Letters*, Vol. 48, No. 8, pp. 1614 -1615, May 2006.
- [53]. V. Deepu, S. Mridula, R. Sujith and P. Mohanan, Slot Line Fed Dipole Antenna For Wide Band Applications, *Microwave and Optical Technology Letters*, Vol. 51, No. 3, pp.826 - 830, January 2009.
- [54]. M. Gopikrishna, D.D. Krishna, C.K. Anandan, P. Mohanan and K. Vasudevan, Design of a Compact Semi-Elliptic Monopole Slot Antenna for UWB Systems, *IEEE Transactions on Antennas and Propagation*, Vol. 57, No. 6, pp.1834 -1837, June 2009.

- [55]. D. Laila, V. Deepu, R. Sujith, P. Mohanan, C.K. Aanandan and K. Vasudevan, Compact asymmetric coplanar strip fed antenna for wide band applications, *Microwave and Optical Technology Letters*, Vol.51, No.5, pp.1170 -1172 , May 2009
- [56]. Deepu V, Rohith K. Raj, Manoj Joseph, M.N. Suma and P. Mohanan, Compact Asymmetric Coplanar Strip Fed Monopole Antenna for Multiband Applications, *IEEE Transactions on Antennas and Propagation*, Vol. 55, No. 8, pp.2351-2357, August 2007.
- [57]. S. V. Shynu, Gijo Augustin, C. K. Aanandan, P. Mohanan and K. Vasudevan, Development of a varactor controlled dual frequency reconfigurable microstrip antenna, *Microwave and Optical Technology Letters*, Vol. 46, No. 4, pp. 375-377, August 2005.
- [58]. J.S. Row and S.W. Wu, Monopolar square patch antennas with wideband operation, *IEE Electronics Letters*, Vol. 42, No. 3, pp. 139-140, February 2006.
- [59]. Horng Dean Chen and Hong Twu Chen, CPW-Fed Dual-Frequency Monopole Antenna, *IEEE Transactions on Antennas and Propagation*, Vol. 52, No. 4, pp 978-982, April 2004.
- [60]. X. N. Qiu, H. M. Chiu and A. S. Mohan, Dual Band CPW-Fed Printed T-Shaped Planar Antenna, *IEEE International Symposium on Microwave, Antenna, Propagation and EMC Technologies for Wireless Communications Proceedings*, pp 176-179, 2005.
- [61]. J. Jung, K. Seol, W. Choi and J. Choi , Wideband monopole antenna for various mobile communication applications, *IEE Electronics Letters*, Vol. 41 No. 24, pp.1313-1314, November 2005.
- [62]. K. Chung, T. Yun and J. Choi, Wideband CPW-fed monopole antenna with parasitic elements and slots, *IEE Electronics Letters*, Vol. 40 No. 17, August 2004.
- [63]. M.J. Amman and M. John, Optimum design of the printed strip monopole, *IEEE Antennas and Propagation Magazine*, Vol.47, No.6, pp 59-61, December 2005.
- [64]. Y.F. Lin, H.M. Chen and K.L. Wong, Parametric study of dual-band operation in a microstrip-fed uniplanar monopole antenna, *IEE Proc. Microw. Antennas Propag.*, Vol. 150, No. 6, pp.411-414, December 2003.

- [65]. H.D. Chen, H.M. Chen and W.S. Chen, Planar CPW-fed sleeve monopole antenna for ultra-wideband operation, *IEE Proc. Microw. Antennas Propag.*, Vol. 152, No. 6, pp. 491-494, December 2005.
- [66]. J. Michael Johnson and Yahya Rahmat Samii, The Tab Monopole, *IEEE Transactions on Antennas and Propagation*, Vol.45, No.1, pp. 187-188, January 1997.
- [67]. W. C. Liu, Wideband dual-frequency double inverted-L CPW-fed monopole antenna for WLAN application, *IEE Proc. Microw. Antennas Propag.*, Vol. 152, No. 6, pp. 505-510, December 2005.
- [68]. Hanhua Yang and Shu Yan, Design of a Dual band Printed Monopole Antenna for WLAN applications, *4th International Conference Wireless Communications, Networking and Mobile Computing*, pp. 1-3, 2008.
- [69]. Brian Edward and Daniel Rees, A broadband printed dipole with integrated Balun, *Microwave Journal*, Vol.5, pp. 339-344, 1987.
- [70]. K. Tilly, X.D. Wu and K. Chang, Coplanar waveguide fed coplanar strip dipole antenna, *IEE Electronics Letters*, Vol.30, No.3, pp.176-177, February 1994.
- [71]. Kihun Chang, Hyunrak Kim, Kwang Sun Hwang, Sung Hun Sim, Seok Jin Yoon, and Young Joong Yoon, A Wideband Dual Frequency Printed Dipole Antenna Using a Parasitic Element, *IEEE Topical Conference on Wireless Communication Technology*, pp. 343-344, 2003.
- [72]. Jean Marie Floc'h and Hatem Rmili, Design of multiband printed dipole antennas using parasitic elements, *Microwave and Optical Technology Letters*, Vol. 48, No. 8, pp. 1639-1645, August 2006.
- [73]. Young Ho Suh and Kai Chang, Low cost microstrip-fed dual frequency printed dipole antenna for wireless communications, *IEE Electronics Letters*, Vol. 36, No. 14, pp. 1177-1179, July 2000.
- [74]. Printed dual-band dipole antenna with U-slotted arms for 2.4/5.2GHz WLAN operation, *IEE Electronics Letters*, Vol.38, No.22, pp.1308-1309, August 2002.
- [75]. Chih Ming Su, Hong Twu Chen and K.L. Wong H.M. Chen, J.M Chen, P.S. Cheng and Y.F. Lin, Feed for dual band printed dipole antenna, *IEE Electronics Letters*, Vol.40, No.21, October 2004.



- 
- [76]. R. Sujith, V. Deepu, D. Laila, C.K. Aanandan, K. Vasudevan and P. Mohanan, A Compact Dual-Band Modified T-shaped CPW-Fed Monopole Antenna, *Microwave and Optical Technology Letters*, Vol. 51, No. 4, pp. April 2009.
- [77]. W. S. Lee, D. Z. Kim, K. J. Kim, and J. W. Yu, Wideband Planar Monopole Antennas with Dual Band-Notched Characteristics, *IEEE Transactions on Microwave Theory Tech.*, Vol.54, No.6, pp.2800-2806, June 2006.
- [78]. D. C. Chang, M. Y. Lin, and C. H. Lin, A CPW-fed U type Monopole Antenna for UWB Applications, *Proc. IEEE Antennas and Propagation Society Int. Symposium*, Vol.5, pp. 512-515, July 2005.
- [79]. K. S. Yee, Numerical solution of initial boundary value problems involving Maxwell's equations in isotropic media, *IEEE Transactions on Antennas and Propagation*, Vol.14, No.4, pp. 302-307, 1966.
- [80]. Taflove, Review of the formulation and applications of the finite-difference time-domain method for numerical modeling of electromagnetic wave interactions with arbitrary structures, *Wave Motion*, Vol.10, No.6, pp. 547-582, 1988.
- [81]. A. Taflove and M. E. Brodwin, Numerical solution of steady state electromagnetic scattering problems using the time-dependent Maxwell's equations, *IEEE Transactions on Microwave Theory and Techniques*, Vol.23, No.8, pp. 623-630, 1975.
- [82]. D.M. Sheen, Sami, M. Ali, D. Mohamed, Abouzahra and Jin Au Kong, Application of the 3D FDTD method to the analysis of planar microstrip circuits, *IEEE Transactions on Microwave Theory and Techniques*, Vol. 38, No. 7, pp. 849-857, July 1990.
- [83]. G. Mur, Absorbing boundary conditions for the finite-difference approximation of the time-domain electromagnetic-field equations, *IEEE Transactions on Electromagnetic Compatibility*, Vol. 23, No. 4, pp. 377-382, 1981.
- [84]. J. P. Berenger, A perfectly matched layer for the absorption of electromagnetics waves, *Journal of Computational Physics*, Vol.114, No.2, pp. 185-200, 1994.

- [85]. Reineix and B. Jecko, Analysis of microstrip patch antennas using finite difference time domain method, *IEEE Transactions on Antennas and Propagation*, Vol.37, No.11, pp. 1361-1369, 1989.
- [86]. P. Leveque, A. Reineix, and B. Jecko, Modelling dielectric losses in microstrip patch antennas: Application of FDTD method, *IEEE Electronics Letters*, Vol. 28, No.6, pp. 539-540, 1992.
- [87]. C. Wu, K. L. Wu, Z. Q. Bi, and J. Litva, Accurate characterization of planar printed antennas using finite-difference time domain method, *IEEE Transactions on Antennas and Propagation*, Vol.40, No.5, pp. 526-533, 1992.
- [88]. K. Uehara and K. Kagoshima, FDTD method analysis of mutual coupling between microstrip antennas, *IEICE Transactions on Communication*, Vol.76, No.7, pp.762-764, 1993.
- [89]. T. Oonishi, T. Kashiwa, and I. Fukai, Analysis of microstrip antennas on a curved surface using the conformal grids FD-TD method, *Electronics and Communications in Japan*, Vol. 1, pp. 73-81, 1993.
- [90]. T. Kashiwa, T. Onishi, and I. Fukai, Analysis of microstrip antennas on a curved surface using the conformal grids FD-TD method, *IEEE Transactions on Antennas and Propagation*, Vol.42, No.3, pp. 423-427, 1994
- [91]. Y. Qian, S. Iwata, and E. Yamashita, Optimal design of an offset-fed, twin-slot antenna element for millimeter-wave imaging arrays, *IEEE Microwave and Guided Wave Letters*, Vol.4, No.7, pp. 232-234, 1994.
- [92]. A. Reineix and B. Jecko, A time domain theoretical method for the analysis of microstrip antennas composed by slots, *Annales des Telecommunications*, Vol. 48, pp. 29-34, January 1993.
- [93]. A. Reineix, J. Paillol, and B. Jecko, FDTD method applied to the study of radar cross section of microstrip patch antennas, *Annales des Telecommunications*, Vol. 48, pp. 589-593, November 1993.
- [94]. A. Reineix, C. Melon, T. Monediere, and F. Jecko, The FDTD method applied to the study of microstrip patch antennas with a biased ferrite substrate, *Annales des Telecommunications*, Vol.49, pp. 137-142, 1994.

- 
- [95]. R. Luebbers, L. Chen, T. Uno, and S. Adachi, FDTD calculation of radiation patterns, impedance, and gain for a monopole antenna on a conducting box, *IEEE Transactions on Antennas and Propagation*, Vol.40, No.12, pp.1577-1583, 1992.
- [96]. L. Chen, T. Uno, S. Adachi, and R. J. Luebbers, FDTD analysis of a monopole antenna mounted on a conducting box covered with a layer of dielectric, *IEICE Transactions on Communications*, Vol.76, No.12, pp. 1583-1586, 1993.
- [97]. Toftgird, S. N. Hornsleth and J. B. Andersen, Effects on portable antennas of the presence of a person, *IEEE Transactions on Antennas and Propagation*, Vol. 41, No.6, pp, 739-746, 1993.
- [98]. M. A. Jensen and Y. Rahmat Samii, Performance analysis of antennas for hand-held transceivers using FDTD, *IEEE Transactions on Antennas and Propagation*, Vol. 42, No.8, pp.1106-1113, 1994.
- [99]. M. A. Jensen and Y. Rahmat Samii, EM interaction of handset antennas and a human in personal communications, *Proceedings of the IEEE*, Vol. 83, No.1, pp. 7-17, 1995.
- [100]. H. Y. Chen and H. H. Wang, Current and SAR induced in a human head model by electromagnetic fields irradiated from a cellular phone, *IEEE Transactions on Microwave Theory Techniques*, Vol.42, No.12, pp. 2249-2254, 1994.
- [101]. L. Martens, J. De Moerloose, D. De Zutter, J. De Poorter, and C. De Wagter, Calculation of the electromagnetic fields induced in the head of an operator of a cordless telephone, *Radio Science*, Vol.30, No.1, pp. 283-290, 1995.
- [102]. Huan-Shang Tsai and R.A. York, FDTD analysis of CPW-fed folded-slot and multiple-slot antennas on thin substrates, *IEEE Transactions on Antennas and Propagation*, Vol. 44, No.2, pp. 217 - 226, February 1996.
- [103]. M. Kar and P.F Wahid, The FDTD analysis of a microstrip patch antenna with dual feed lines, *Proc. IEEE southeast conference*, pp.84-96,1998.

- [104]. Supriyo Dey and Raj Mittra, A conformal Finite Difference Time Domain technique for modeling cylindrical dielectric resonators, *IEEE Trans. Microwave Theory and Tech.*, Vol. 47, No. 9, pp.1737-1739, September 1999.
- [105]. D. Yamamoto, H. Arai, FDTD analysis of radiation pattern of antenna on truncated ground plane, *Microwave Conference Asia-Pacific*, pp. 378 - 381, December 2000.
- [106]. Huey Ru Chuang and Liang Chen Kuo, 3-D FDTD Design Analysis of a 2.4-GHz Polarization-Diversity Printed Dipole Antenna With Integrated Balun and Polarization-Switching Circuit for WLAN and Wireless Communication Applications, *IEEE Transactions On Microwave Theory And Techniques*, Vol. 51, No. 2, pp.374-381, February 2003.
- [107]. Shaoqiu Xiao, Zhenhai Shao, M. Fujise and Bing Zhong Wang, Pattern reconfigurable leaky-wave antenna design by FDTD method and Floquet's Theorem, *IEEE Transactions on Antennas and Propagation*, Vol. 53, No.5, pp. 1845-1848, May 2005.
- [108]. Naobumi Michishita, Hiroyuki Arai, Masayuki Nakano, Toshio Satoh and Tohru Matsuoka, FDTD analysis for printed dipole antenna with balun, *Microwave conference Asia-Pacific*, pp.739-742, December 2000.

.....❧.....

# **ANTENNA SIMULATION, FABRICATION AND MEASUREMENT TECHNIQUES**

---

<b>Contents</b>	<b>3.1 Simulation Techniques</b>
	<b>3.2 Fabrication method</b>
	<b>3.3 Microwave substrates</b>
	<b>3.4 Experimental setup</b>
	<b>3.5 Measurement procedure</b>
	<b>3.6 References</b>

---

In this chapter antenna simulation, fabrication and measurement techniques are presented. Simulation of the antenna has been carried out using in-house developed Matlab based Finite Difference Time Domain Technique (FDTD). Parametric analysis has been conducted using FEM based HFSS. Photolithographic technique is used for the fabrication of the antenna. Experimental set up used for the measurement of different antenna parameters is also discussed.

---

### 3.1 Simulation Techniques

powerful computer resources. Scientists and engineers use different techniques for solving field problems. Most common techniques are either analytical or numerical. Exact analytical solutions are always the preferred method to a given problem, if possible. However, for most of the electromagnetic problems, exact solutions are more complicated and we have to depend on numerical solutions. Numerical solution of EM problems started in the mid-1960s with the availability of modern high-speed digital computers. Since then, considerable effort has been spent on solving practical, complex EM-related problems for which closed form analytical solutions are either intractable or do not exist. The numerical approach has the advantage of allowing the actual work to be carried out by operators without the knowledge of higher mathematics or physics.

Differential equation solutions such as Finite difference (FDM) and Finite Element (FEM) methods are the easiest techniques to implement but result in large sparse matrices. Integral equation solutions employing Method of Moments (MoM) involves more detailed mathematical formulation, and for complex problem, can lead to complex matrices. Time domain numerical solution has gained attention as modeling technique and solution to the problem can be obtained either Fourier transforming the time domain results or directly implementing finite difference time stepping algorithm. Application of these techniques to antenna analysis yields design flexibility and a physical insight to the actual radiation phenomenon and operating principles that could help the design and its enhancement.

In this thesis, simulation has been carried out using in-house developed MATLAB based FDTD code and FEM based HFSS package. A brief description of both of these techniques are summarised in the following sections.

### **3.1.1 Finite Difference Time Domain Technique (FDTD)**

Finite Difference Time Domain (FDTD) is a Computational ElectroMagnetic (CEM) technique that directly solves the differential form of Maxwell's equations, the curl equations, in the time domain using a discretized space-time grid. Compared to an integral equation solution of Maxwell's equations, such as Method of Moments, FDTD does not lead to a system of linear equations defined over the entire problem space. FDTD also has the benefits of well-understood error sources, impulse and nonlinear behavior that is treated naturally, enhanced visualization of the wave interactions, and a systematic approach that does not require reformulations of integral equations for each new structure. Finite Difference Time Domain (FDTD) method was introduced by Yee [1] in 1966 for solving Maxwell's curl equations directly in the time domain on a space grid. The algorithm was based on a central difference solution of Maxwell's equations with spatially staggered electric and magnetic fields placed alternatively at each time steps in a leap-frog algorithm. This method has been implemented by Teflove in 1975 for the solution of complex inhomogeneous problems.

The FDTD has been used by many investigators, because it has the following advantages over other techniques:

- From the mathematical point of view, it is a direct implementation of Maxwell's curl equations.
- Broadband frequency response can be easily predicted since the analysis is carried out in the time domain.

- Arbitrary, irregular geometries, wires of any thickness can be easily modeled,
- It is capable of analyzing structures having different types of materials
- Time histories of electric and magnetic fields throughout the entire simulation domain are available
- Impedance, radiation pattern are easily obtainable
- Lumped loads can be easily included in the model

### 3.1.1.1 Mathematical Formulation

Formulation of the FDTD method begins by considering the differential form of Maxwell’s two curl equations which govern the propagation of fields in the structures. For simplicity, the media is assumed to be uniform, isotropic, homogeneous and lossless.

With these assumptions, Maxwell’s equations can be written as,

$$\mu \frac{\partial H}{\partial t} = -\nabla \times E \dots\dots\dots(1)$$

$$\varepsilon \frac{\partial E}{\partial t} = \nabla \times H \dots\dots\dots(2)$$

In order to find an approximate solution to these set of equations, the problem is discretized over a finite three dimensional computational domain with appropriate boundary conditions enforced on the source, conductors, and mesh walls. The divergence equations are automatically satisfied by the FDTD method.

To obtain discrete approximations to these continuous partial differential equations the centered difference approximation is used on both time and space. For convenience, the six field locations are considered to be interleaved



in space as shown in Fig. 3.1 which is a drawing of the FDTD unit cell. The entire computational domain is obtained by stacking these Yee cubes into a larger rectangular volume. The x, y and z dimensions of the unit cell are  $\Delta x$ ,  $\Delta y$  and  $\Delta z$ , respectively. The advantages of this field arrangement are that centered differences are realized in the calculation of each field component and the continuity of tangential field components is automatically satisfied.

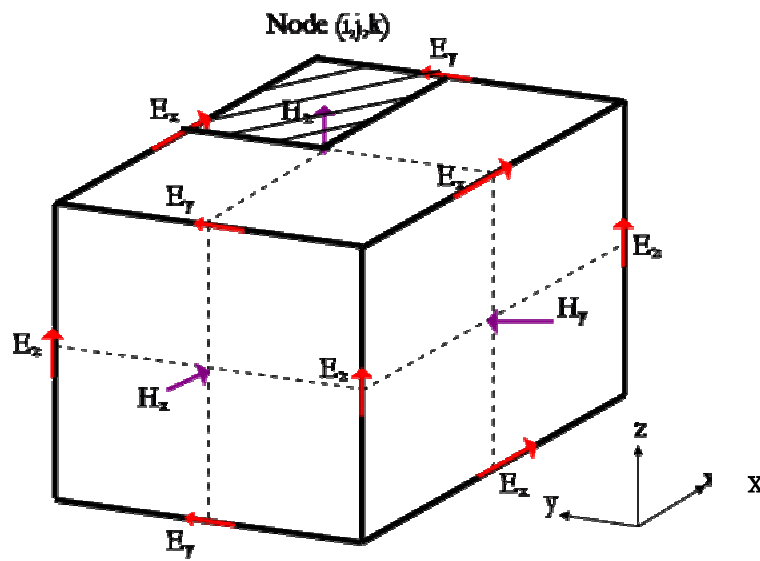


**Fig. 3.1** Yee Cell using in FDTD with Electric and Magnetic field components

Because there are only six unique field components within the unit cell, the six field components touching the shaded upper eighth of the unit cell in Fig. 3.1 are considered to be a unit node with subscript indices  $i$ ,  $j$ , and  $k$  corresponding to the node numbers in the  $x$ ,  $y$  and  $z$  directions.

The notation implicitly assumes the  $\pm 1/2$  space indices and thus simplifies the notation, rendering the formulas directly implementable on the computer.

The time steps are indicated with the superscript  $n$ . Using this field component arrangement and the centered difference approximation, the explicit finite difference approximations to (1) and (2) are

$$H_{x,i,j,k}^{n+1/2} = H_{x,i,j,k}^{n-1/2} + \frac{\Delta t}{\mu\Delta z} (E_{y,i,j,k}^n - E_{y,i,j,k-1}^n) - \frac{\Delta t}{\mu\Delta y} (E_{z,i,j,k}^n - E_{z,i,j-1,k}^n) \dots\dots\dots(3)$$

$$H_{y,i,j,k}^{n+1/2} = H_{y,i,j,k}^{n-1/2} + \frac{\Delta t}{\mu\Delta x} (E_{z,i,j,k}^n - E_{z,i-1,j,k}^n) - \frac{\Delta t}{\mu\Delta z} (E_{x,i,j,k}^n - E_{x,i,j,k-1}^n) \dots\dots\dots(4)$$

$$H_{z,i,j,k}^{n+1/2} = H_{z,i,j,k}^{n-1/2} + \frac{\Delta t}{\mu\Delta y} (E_{x,i,j,k}^n - E_{x,i,j-1,k}^n) - \frac{\Delta t}{\mu\Delta x} (E_{y,i,j,k}^n - E_{y,i-1,j,k}^n) \dots\dots\dots(5)$$

$$E_{x,i,j,k}^{n+1} = E_{x,i,j,k}^n + \frac{\Delta t}{\epsilon\Delta y} (H_{z,i,j+1,k}^{n+1/2} - H_{z,i,j,k}^{n+1/2}) - \frac{\Delta t}{\epsilon\Delta z} (H_{y,i,j,k+1}^{n+1/2} - H_{y,i,j,k}^{n+1/2}) \dots\dots\dots(6)$$

$$E_{y,i,j,k}^{n+1} = E_{y,i,j,k}^n + \frac{\Delta t}{\epsilon\Delta z} (H_{x,i,j,k+1}^{n+1/2} - H_{x,i,j,k}^{n+1/2}) - \frac{\Delta t}{\epsilon\Delta x} (H_{z,i+1,j,k}^{n+1/2} - H_{z,i,j,k}^{n+1/2}) \dots\dots\dots(7)$$

$$E_{z,i,j,k}^{n+1} = E_{z,i,j,k}^n + \frac{\Delta t}{\epsilon\Delta x} (H_{y,i+1,j,k}^{n+1/2} - H_{y,i,j,k}^{n+1/2}) - \frac{\Delta t}{\epsilon\Delta y} (H_{x,i,j+1,k}^{n+1/2} - H_{x,i,j,k}^{n+1/2}) \dots\dots\dots(8)$$

The half time steps indicate that E and H are alternately calculated in order to achieve centered differences for the time derivatives. In these equations, the permittivity and the permeability are set to the appropriate values, depending on the location of each field component. For the dielectric-air interface the average of the two permittivities ( $\epsilon_{r+1}$ )/2 is used [2].

The discretization in space and time and the calculation methodology of E and H granted the name leap frog algorithm to this method (Fig 3.2).

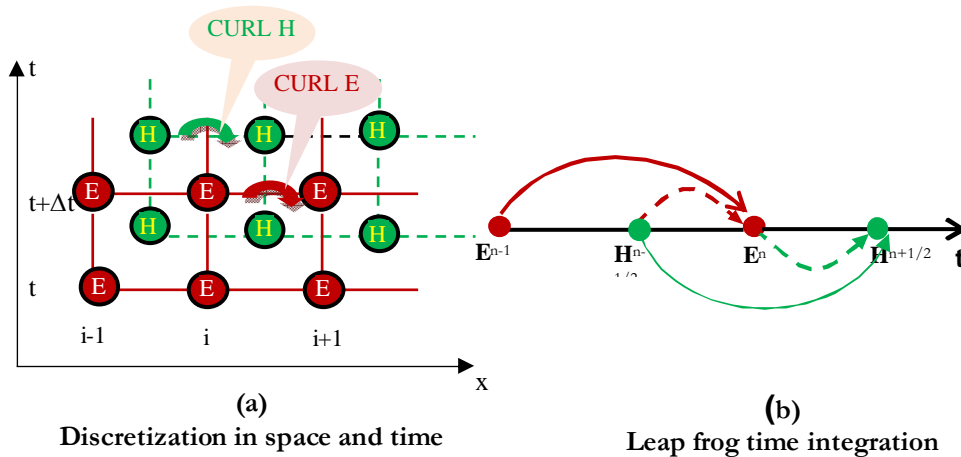


Fig.3.2 Central differencing with Leapfrog method

### 3.1.1.2 Stability criteria

The Finite Difference Time Domain requires the time increment  $\Delta t$  to have a specific upper bound relative to the space increments  $\Delta x$ ,  $\Delta y$  and  $\Delta z$ . This bound is necessary to avoid numerical instability that can cause the computed results to increase spuriously without limit as time marching continues. The cause for numerical instability is the finite difference implementation of the derivative. The final expression for the upper bound on  $\Delta t$  can be written as,

$$\Delta t \leq \frac{1}{V_{\max}} \frac{1}{\sqrt{1/\Delta x^2 + 1/\Delta y^2 + 1/\Delta z^2}} \dots\dots\dots (9)$$

Where  $V_{\max}$  is the maximum phase velocity of the signal in the problem being considered. Typically  $V_{\max}$  will be the velocity of light in free space unless the entire volume is filled with dielectric. These equations will allow the approximate solution of E and H in the volume of the computational domain or mesh. In practice, the maximum value of  $\Delta t$  used is about 90% of the value given by above equation.

### 3.1.1.3 Numerical Dispersion

Dispersion is defined as the variation of the phase constant of the propagating wave with frequency. The discretization of Maxwell's equations in space and time causes dispersion of the simulated wave in an otherwise dispersion-free structure. That is the phase velocity of the wave in an FDTD grid can differ from the analytical value. This dispersion is called numerical dispersion. The amount of dispersion depends on the wavelength, the direction of propagation in the grid, and the discretization size. Numerical dispersion can be reduced to any degree that is desired if one uses a fine enough FDTD mesh.

### 3.1.1.4 Absorbing Boundary Conditions

A large number of electromagnetic problems have associated open space regions, where the spatial domain is unbounded in one or more directions. The solution of such a problem in this form will require an unlimited amount of computer resources. To avoid this, the domain must be truncated with minimum error. For this, the domain can be divided into two regions: the interior region and the exterior region as shown in Fig. 3.3.

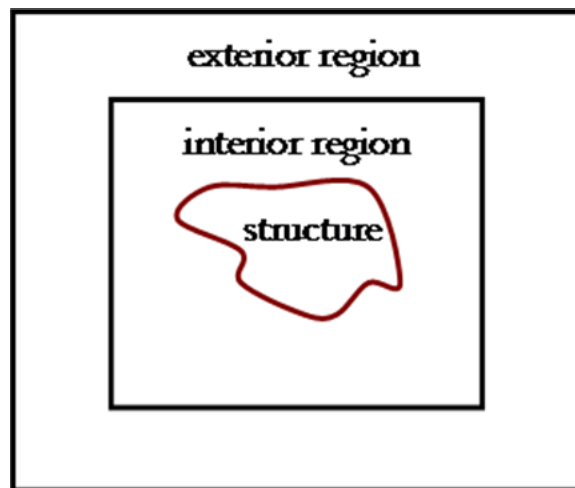


Fig. 3.3 Truncation of the domain by the exterior region in FDTD algorithm

The interior region must be large enough to enclose the structure of interest. The exterior region simulates the infinite space. The FDTD algorithm is applied in the interior region. It simulates wave propagation in the forward and backward directions. However, only the propagation in the interior region is desired with minimum space without reflection from the truncated boundary. These reflections must be suppressed to an acceptable level so that the FDTD solution is valid for all time steps.

Two options are available to simulate the open region surrounding the problem physical space.

1. Terminate the interior region with equivalent currents on the surface of the interior region and use the Green's function to simulate the fields in the exterior region
2. Simulate the exterior region with absorbing boundary conditions to minimize reflections from the truncation of the mesh.

Simulation of the open region with the help of equivalent currents yields a solution whereby the radiation condition is satisfied exactly. But the values of fields on the surface enclosing the interior region are needed, for which CPU time and storage requirement increases rapidly with the surface size. On the other hand, the absorbing boundary concept truncates the computation domain and reduces the computational time and storage space. The absorbing boundary condition (ABC) can be simulated in a number of ways. These are classified as analytical (or differential) ABC and material ABC. The material ABC is realized from the physical absorption of the incident signal by means of a lossy medium [3], whereas analytical ABC is simulated by approximating the wave equation on the boundary [4].

### ***Mur's first order ABC***

Mur's first order ABC is the simple and optimal analytical ABC. In the thesis it is used as the boundary condition. Analysis of Mur's first-order ABC is based on the work of Enquist and Majda [4] and the optimal implementation given by Mur [5]. It provides satisfactory absorption for a great variety of problems and is extremely simple to implement. Mur's first order ABC looks back one step in time and one cell into the space location. An arbitrary wave can be expanded in terms of a spectrum of plane waves. If a plane wave is incident normally on a planar surface, and if the surface is perfectly absorbing, there will be no reflected wave. For the x normal wall the one dimensional wave equation can be written as

$$\left( \frac{\partial}{\partial x} - \frac{1}{c} \frac{\partial}{\partial t} \right) E_{\tan} = 0. \dots\dots\dots (10)$$

By imposing above equation on a wave normally incident on planar surface, absorbing condition for a normal incident wave with out reflection can be obtained as

$$\frac{\partial E(x,t)}{\partial x} = \frac{1}{c} \frac{\partial E(x,t)}{\partial t} \dots\dots\dots (11)$$

Where  $x=\Delta x/2$ ,  $t=(n+1/2) \Delta t$

For updating of the electric field at

$$x = \Delta x/2, t = (n + 1/2)\Delta t$$

In finite-difference form it can be written as follows:

$$\frac{E_1^{n+1/2} - E_0^{n+1/2}}{\Delta x} = \frac{1}{c} \frac{E_{1/2}^{n+1} - E_{1/2}^n}{\Delta t} \dots\dots\dots (12)$$

In this form, the finite-difference approximation is accurate to the second order in  $\Delta x$  and  $\Delta t$ . But the values at the half grid points and half time steps are not available, and can be averaged as

$$E_m^{n+1/2} = \frac{E_m^{n+1} + E_m^n}{2} \dots\dots\dots (13)$$

$$E_{m+1/2}^n = \frac{E_{m+1}^n + E_m^n}{2} \dots\dots\dots (14)$$

The equations 10, 11 and 12 yields an explicit finite difference equation

$$E_0^{n+1} = E_1^n + \left( \frac{c\Delta t - \Delta x}{c\Delta t + \Delta x} \right) (E_1^{n+1} - E_0^n) \dots\dots\dots (15)$$

Where  $E_0$  represents the tangential electric field component on the mesh wall and  $E_1$  represents the tangential electric field component on node inside of the mesh wall. Similar expressions are obtained for the other absorbing boundaries by using the corresponding fields for each wall. But while implementing the Mur's first order boundary conditions for truncated ground plane in printed monopole antennas the boundary walls should be far enough from the radiating element to ensure the normal incidence at the boundary walls. For the oblique incidence case the wave will be reflected from the boundary walls.

#### **3.1.1.5 Lubbers feed model for fast FDTD convergence**

With the transient excitation in FDTD, impedance and scattering parameters over a wide frequency band can be calculated. One difficulty with FDTD is that for some applications, few thousands of time steps may be required for the transient fields to decay. This difficulty is common in the case of circuits having very high quality factor. One method to reduce the time steps required is to apply signal processing methods to predict the voltages and currents at later times from the results computed for early times. Instead of making FDTD calculations for the full number of time steps required for transients to dissipate, one might make actual FDTD calculations for some fraction of this total number of time steps, and use these results to predict those for the later times [6].

Applying the various prediction methods adds additional complexity to the FDTD calculation process. The prediction methods are complicated, and may require care and skill by the user to obtain accurate results. Most of the methods described require the user to determine the order of the prediction process, related to the number of terms of whatever expansion function is used to approximate the FDTD time signal. A poor choice for the order of the prediction model can result in large precision errors.

Another simple approach is to include a source resistance in the excitation signal source [7]. This can considerably reduce the large time steps required for the simulation. The source resistance value which is equal to the characteristic impedance of the system is usually employed.

### ***Resistive source model***

FDTD transient calculations are often excited by a hard voltage source, whose internal source resistance is zero ohms. These sources are very easy to implement in an FDTD code. The electric field at the mesh edge where the source is located is determined by some function of time rather than by the FDTD update equations. A common choice is a Gaussian pulse, but other functions may also be used. The Gaussian pulse is significantly greater than zero amplitude for only a very short fraction of the total computation time, especially for resonant geometries such as many antennas and micro strip circuits.

Once the pulse amplitude drops the source voltage becomes essentially zero, the source effectively becoming a short circuit. Thus, any reflections from the antenna or circuit which return to the source are totally reflected. The only way the energy introduced into the calculation space can be dissipated is through radiation or by absorption by lossy media or lumped loads. For resonant structures, there are frequencies for which this radiation or absorption process requires a relatively long time to dissipate the excitation energy. Using a source with an internal resistance to excite the FDTD calculation provides an additional loss mechanism for the calculations.

Consider that it is desired to excite an FDTD calculation with a voltage source that corresponds to an electric field  $E$  in the  $z$  direction at a certain mesh location  $i_s\Delta x, j_s\Delta y, k_s\Delta z$ , described using the usual Yee notation. The corresponding equivalent circuit for a voltage source which includes an internal source resistance  $R_s$  is illustrated in Fig. 3.4. If the source



resistance  $R_s$  is set to zero then the usual FDTD electric field at the source location is simply given by

$$E_s^n(i_s, j_s, k_s) = \frac{V_s(n\Delta t)}{\Delta z} \dots\dots\dots (16)$$

$V_s$  is any function of time, often a Gaussian pulse.

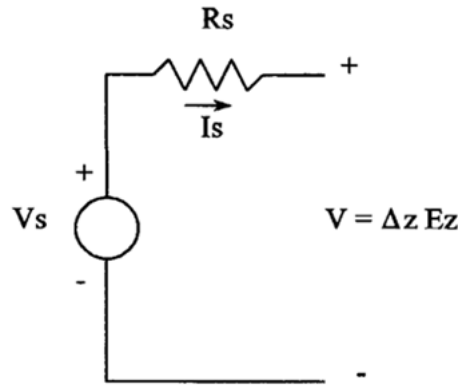


**Fig.3.4 FDTD source with source resistance  $R_s$ .**

However, with the source resistance included, the calculation of the source field  $E_s^n(i_s, j_s, k_s)$  at each time step is complicated slightly. To determine the terminal voltage  $V$  of Fig. 3.4 and, thus, the FDTD electric source field  $E_s^n(i_s, j_s, k_s)$ , the current through the source must be determined. This can be done by Ampere’s circuital law, taking the line integral of the magnetic field around the electric field source location. The current through the source is then given by,

$$I_s^{n-1/2} = (H_x^{n-1/2}(i_s, j_{s-1}, k_s) - H_x^{n-1/2}(i_s, j_s, k_s))\Delta x + (H_y^{n-1/2}(i_s, j_s, k_s) - H_y^{n-1/2}(i_{s-1}, j_s, k_s))\Delta y \dots\dots\dots (17)$$

so that by applying Ohm’s law to the circuit of Fig. 3.4, the electric source field is given by

$$E_s^n(i_s, j_s, k_s) = \frac{V_s(n\Delta t)}{\Delta z} + \frac{I_s^{n-1/2} R_s}{\Delta z} \dots\dots\dots (18)$$

If  $R_s=0$ , in this equation, then the usual hard-voltage source results. The value of the internal resistance does not appear to be critical. A reasonable choice for  $R_s$  is to use the value of the characteristic impedance of the transmission line.

### ***Staircase transition for microstrip line feed***

The antenna discussed in thesis uses a microstrip line as the feed. The microstrip excitation presented in the thesis is implemented by using Luebber's [7] approach of stair cased FDTD mesh transition from electric field sources location to the full width of the microstrip transmission line. In order to model the microstrip line, the substrate thickness is discretized as more than one Yee cell. The excitation field is to be applied to the cell between the top PEC of the strip line and the PEC ground plane. In order to obtain a gap feed model, a staircased mesh transition as shown in the fig. 3.5 is used in FDTD.

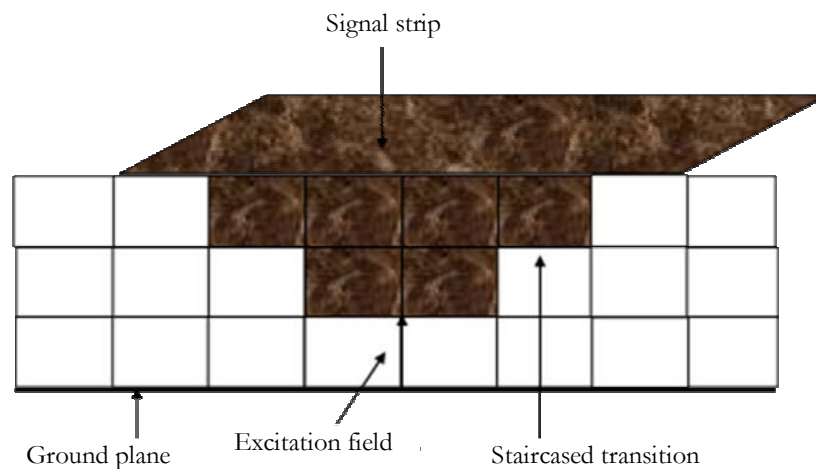


**Fig. 3.5 FDTD Staircase feed model for microstrip line in FDTD**

In the figure the darkened portions are treated as PEC. This stair cased configuration results a gap model between the top patch and ground plane. The excitation field is shown as arrow in the figure. The stair case model transition from the electric field feed to the microstrip line at the top is used to provide a relatively smooth connection from the feed location to the microstrip.

### ***Excitation functions***

A variety of excitation functions such as Gaussian pulse, sinusoidal, sine modulated by a Gaussian can be used to excite a system in FDTD computation. Gaussian pulse and sinusoidal functions are used in the thesis to analyze the problem. Gaussian pulse excitation gives a broadband response of the problem. But sinusoidal function needs a single frequency response, and thus a frequency sweep has to be used for broadband frequency response.

#### ***Gaussian pulse function***

A Gaussian pulse can be expressed as,  $E(t) = e^{-(t-t_0)^2/T^2}$

Where 't' is the present instant, 't<sub>0</sub>' is the time at which the amplitude is maximum (unity) and 'T' determines the pulse width. The parameter T is very significant in the FDTD simulation. Because the pulse width determines the frequency up to which the simulation is accurate. When the pulse width is narrow, broad band simulation can be attained.

#### ***Sine function***

Sinusoidal excitations are important while computing the E/H field values for a particular frequency (f) of interest. A function of the following form is termed as sine function  $E(t) = E_0 \text{Sin}(2\pi ft)$

Where 'E<sub>0</sub>' determines the peak amplitude (usually unity), 't' is the present instant of time.

#### **3.1.1.7 General flow chart of FDTD algorithm**

The MATLAB based computer codes were developed to study the resonant behavior of the microstrip-fed printed monopole antenna, dual strip antenna and folded dual strip antenna. The general flow chart for the program to calculate the return loss characteristics is shown in Fig. 3.6.

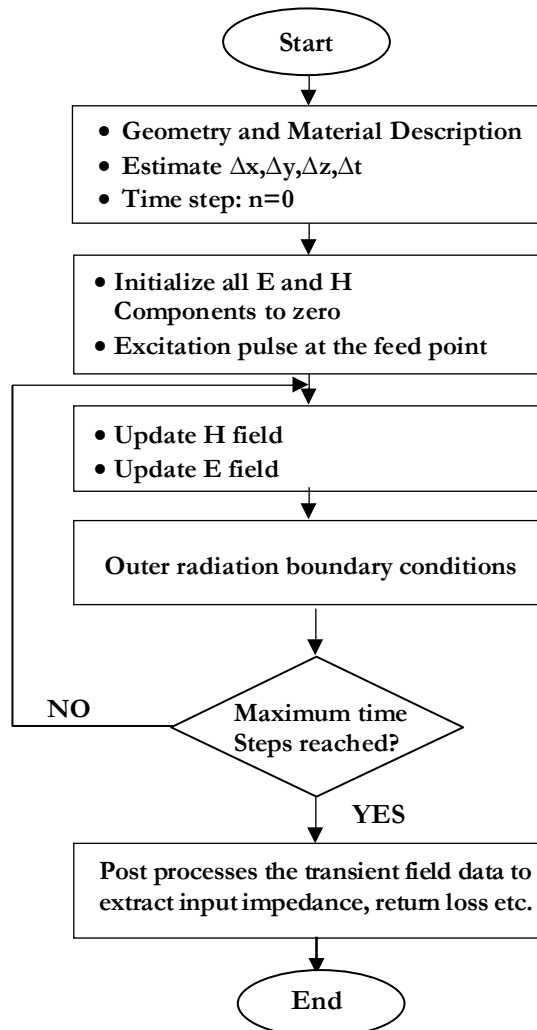


Fig.3.6 Flow chart for the computation of return loss

### 3.1.1.8 Return loss calculation

The voltage at the input port location is computed from the  $E_z$  field components at the feed point over the entire simulation time interval. The current at the feed point is calculated from the H field values around the feed point using Ampere's circuital law. The input impedance of the antenna is computed as

$$Z_{in}(\omega) = \frac{FFT(V^n, P)}{FFT(I^{n-1}, P)} \dots\dots\dots (19)$$

Where P is the suitable Zero padding used for taking FFT,  $V^n = E_z^n * \Delta z$  and  $I^{n-1}$  is given by equation (17)

Since microstrip line is modeled using Leubber’s staircase approach, the internal impedance of source resistance  $R_s$  is taken as the characteristic impedance ( $Z_0$ ) of microstrip line.

Reflection coefficient is given as  $\Gamma(\omega) = \frac{Z_{in} - Z_0}{Z_{in} + Z_0} \dots\dots\dots (20)$

Return loss in dB,  $S_{11} = 20\log_{10} \Gamma(\omega) \dots\dots\dots (20)$

The return loss computed in the above process is processed for extracting the fundamental resonant frequency and 2:1 VSWR bandwidth corresponding to the -10 dB return loss.

**3.1.1.9 Radiation pattern calculation**

To extract the radiation pattern at the resonant frequency a sinusoidal source is used as the excitation source. Initially using the Gaussian pulse the resonant frequency of the antenna is extracted and thus obtained resonant frequency  $f_r$  is used for FDTD run for pattern computation. The source voltage for pattern computation is given by

$$V(n\Delta t) = \sin(2\pi f_r n\Delta t)$$

A near field transformation surface layer is selected just above the printed monopole layer as the transformation layer for field computations. The surface S is chosen to be in the near field of radiating monopole with proper dimensions to ensure that tangential E field components are negligible outside this boundary. Usually a rectangular surface as shown in Fig.3.7 is chosen for the easy implementation of near to far field transformation algorithm.

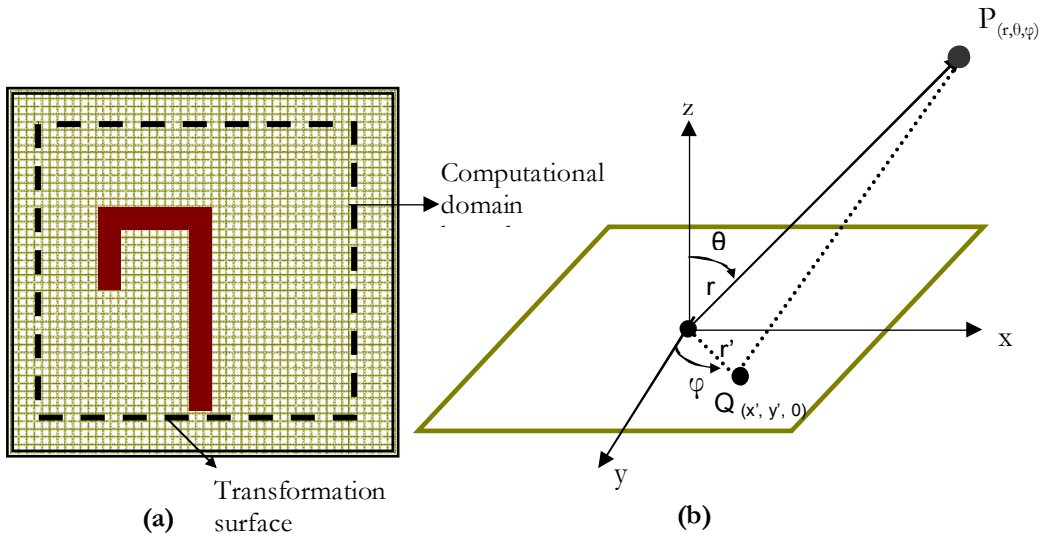


**Fig 3.7 Radiation pattern computation using FDTD.**  
 (a) Near field transformation surface  
 (b) Spatial point Q in near field and far field point P.

The tangential near field electric and magnetic field vectors on this surface are sampled and converted to equivalent surface currents.

$$\bar{J}_s = \hat{a}_n \times \bar{H}_A \dots\dots\dots (21)$$

$$\bar{M}_s = \bar{E}_A \times \hat{a}_n \dots\dots\dots (22)$$

Where  $\hat{a}_n$  is the unit outward normal from the transformation surface. The far field at any point outside this transformation surface is computed from the electric and magnetic vector potential derived from the surface current equivalence principle. The far field E field vectors tangential to the direction of propagation is given by

$$E_\theta = -\mu \frac{\partial A_\theta}{\partial t} - \frac{1}{c} \frac{\partial F_\phi}{\partial t} \dots\dots\dots (23)$$

$$E_\phi = -\mu \frac{\partial A_\phi}{\partial t} + \frac{1}{c} \frac{\partial F_\theta}{\partial t} \dots\dots\dots (24)$$

where A and F represents magnetic and electric vector potentials and  $\theta$  and  $\phi$  denotes the coordinates in the spherical coordinate system. Suppressing the  $e^{j\omega t}$  variation [8] the electric field in the free space can be written as

$$E(r, \theta, \phi) = j\omega\eta_0 (F_\theta \vec{a}_\phi - F_\phi \vec{a}_\theta) \dots\dots\dots (25)$$

$E_\theta$  and  $E_\phi$  are derived by transforming into spherical coordinate system as

$$E_\theta = j\omega\eta_0 (F_x \sin(\phi) - F_y \cos(\phi)) \dots\dots\dots (26)$$

$$E_\phi = j\omega\eta_0 \cos(\theta)(F_x \cos(\phi) + F_y \sin(\phi)) \dots\dots\dots (27)$$

Following assumptions are made for the near to far field transformation

- The antenna radiates into the  $z > 0$  and  $z < 0$  region from the aperture in the  $z = 0$  plane
- $r$  is in the far field i.e ( $r \gg (x'^2 + y'^2)^{1/2}$ ) &  $k_0 r \gg 1$
- Transformation surface dimensions are proper so that tangential electric fields are negligible outside the transformation aperture boundary.

Eqn 25 now becomes

$$E = j \exp(-jkr) / (\lambda \cdot r) \bullet \left( \begin{array}{l} \left( \cos(\theta)(f_x \cos(\phi) + f_y \sin(\phi)) \vec{a}_\phi \right) \\ - \left( f_x \sin(\phi) - f_y \cos(\phi) \right) \vec{a}_\theta \end{array} \right) \dots\dots\dots (28)$$

Where

$$f_* = \iint_S E_*(x', y', 0) \bullet \exp(jk(x' \sin(\theta) \cos(\phi) + y' \sin(\theta) \sin(\phi))) \bullet dx' dy'$$

The E field components  $E_*(x', y', 0)$  can be computed by the technique proposed by Zimmerman et.al [9] as

$$E_{*(x', y', z'=0)} = (1/N) \sum_{n=1}^N E_*(n) \bullet \exp(j2\pi n/N) \dots\dots\dots (29)$$

Where  $E(n)$  correspond to the corresponding tangential electric field components  $E_x^n$  and  $E_y^n$  sampled at the point on the transformation surface point  $Q(x',y',0)$  at the  $n^{\text{th}}$  time step.  $N$  corresponding to time steps for one period of sinusoidal excitation frequency. From the  $E_\theta$  and  $E_\phi$  values obtained using the above computation the E-plane and H-plane pattern can be derived. A complete flow chart illustrating the radiation pattern computation algorithm is illustrated in the Fig 3.8

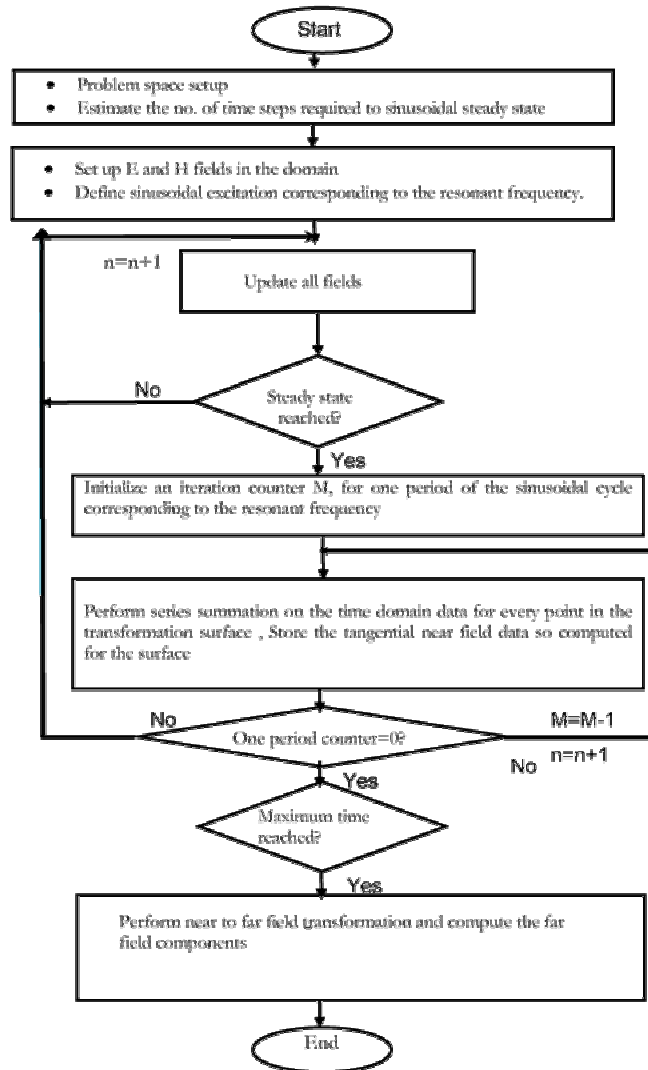


Fig.3.8 Flow chart for the computation of return loss



### **3.1.2 Finite Element Method (FEM)**

The Finite Element Method (FEM) is a well developed and used method for solving differential equations in electromagnetics. The greatest advantage of this method is its ability to describe complex geometry. This quality comes out of FEM using an unstructured grid (mesh), which typically consists of triangles in 2D and tetrahedron in 3D, to model the object. The unstructured nature of the time domain version of FEM gives a clear advantage over numerical computational methods in modeling complex antenna geometries. The main concept of the finite element method is based on subdividing the geometrical domain of a boundary-value problem into smaller sub-domains, called finite elements, and expressing the governing differential equation along with the associated boundary conditions as a set of linear equations that can be solved computationally using linear algebra techniques.

The finite element analysis of any problem involves basically four steps [10]:

- discretizing the solution region into a finite number of sub regions or elements,
- deriving governing equations for a typical element,
- assembling of all elements in the solution region, and
- solving the system of equations.

The main idea behind the FEM [11,12] is to solve Boundary Value Problems (BVP) governed by a differential equation and a set of boundary conditions. The representation of the domain is split into smaller sub-domains called the finite elements. The distribution of the primary unknown quantity inside an element is interpolated based on the values at the nodes, provided nodal elements are used, or the values at the edges, in case vector

elements are used. The interpolation or shape functions must be a complete set of polynomials.

The accuracy of the solution depends, among other factors, on the order of these polynomials, which may be linear, quadratic, or higher order. The numerical solution corresponds to the values of the primary unknown quantity at the nodes or the edges of the discretized domain. The solution is obtained after solving a system of linear equations. To form such a linear system of equations, the governing differential equation and associated boundary conditions must first be converted to an integro-differential formulation either by minimizing a functional or using a weighted residual method such as the Galerkin approach. This integro-differential formulation is applied to a single element and with the use of proper weight and interpolation functions the respective element equations are obtained. The assembly of all elements results in a global matrix system that represents the entire domain of the BVP.

There are two methods that are widely used to obtain the finite element equations: the variational method and the weighted-residual method.

The variational approach requires construction of a functional which represents the energy associated with the BVP at hand. A functional is a function expressed in an integral form and has arguments that are functions themselves. A stable or stationary solution to a BVP can be obtained by minimizing or maximizing the governing functional. Such a solution corresponds to either a minimum point, a maximum point, or a saddle point. In the vicinity of such a point, the numerical solution is stable meaning that it is rather insensitive to small variations of dependent parameters. This translates to a smaller numerical error compared to a solution that corresponds to any other point.

The second method is a weighted-residual method widely known as the Galerkin method. This method begins by forming a residual directly from the partial differential equation that is associated with the BVP under study. Simply stated, this method does not require the use of a functional. The residual is formed by transferring all terms of the partial differential equation on one side. This residual is then multiplied by a weight function and integrated over the domain of a single element. This is the reason why the method is termed as weighted-residual method. The Galerkin approach is simple and starts directly from the governing differential equation.

### **3.1.2.1 HFSS: 3D Electromagnetic simulator**

HFSS utilizes a 3D full-wave Finite Element Method (FEM) to compute the electrical behavior of high-frequency and high-speed components [13]. With HFSS one can extract the parameters such as S, Y, and Z, visualize 3D electromagnetic fields (near- and far-field), and optimize design performance. An important and useful feature of this simulation engine is the availability of different kinds of port schemes. It provides lumped port, wave port, incident wave scheme etc. The accurate simulation of microstrip lines can be done using lumped port.

In this thesis some parts of the investigations are done using HFSS. The optimization algorithm available with HFSS is very useful for antenna engineers to optimize the dimensions very accurately. There are many kinds of boundary schemes available in HFSS. Radiation boundary and PML boundary are the important and widely used in this work.

The first step in simulating a system in HFSS is to define the geometry of the system by giving the material properties and boundaries for 3D or 2D elements available in HFSS window. The suitable port excitation scheme is then given. A radiation boundary filled with air is then defined surrounding the structure to be simulated. Now, the simulation engine can be invoked by

giving the proper frequency of operations and the number of frequency points. Finally the simulation results such as scattering parameters, current distributions and far field radiation pattern can be displayed. The vector as well as scalar representation of E, H and J values of the device under simulation gives a good insight into the structure under analysis.

### 3.2 Fabrication method

Antennas are fabricated using standard photolithographic technique. Photolithographic method gives good accuracy for the etched patterns. This is very critical when the frequency of operation of the device is in higher microwave bands. The step by step process for the fabrication is very simple and illustrated in Fig. 3.9.

The computer aided design of the geometry is initially made and a negative mask of the geometry to be generated is printed on a butter paper. A double sided copper clad lamination of suitable dimension required for the antenna is cleaned very well and dried. Any dust or impurities on it will produce small discontinuity on the copper traces etched on the substrate. This will shift the resonant frequency from the predicted values, especially when the operating frequency is very high. Now, the negative photo resist material is applied on copper surfaces. It is then exposed to ultra violet radiation through the mask. The layer of photo-resist material in the exposed portions hardens. Now the board is immersed in developer solution for few minutes. The hardened portions will not be washed out by the developer solution. The board is then dipped in the dye solution in order to clearly view the hardened photo-resist portions on the copper coating.

The unwanted copper traces exposes after the developing phase is to be etched off to get the required antenna geometry on the substrate. Ferric Chloride ( $\text{FeCl}_3$ ) solution is used for this purpose.  $\text{FeCl}_3$  dissolves the copper parts except underneath the hardened photo resist layer after few minutes.

The laminate is then washed with water and cleaned using acetone to remove the hardened photoresist.

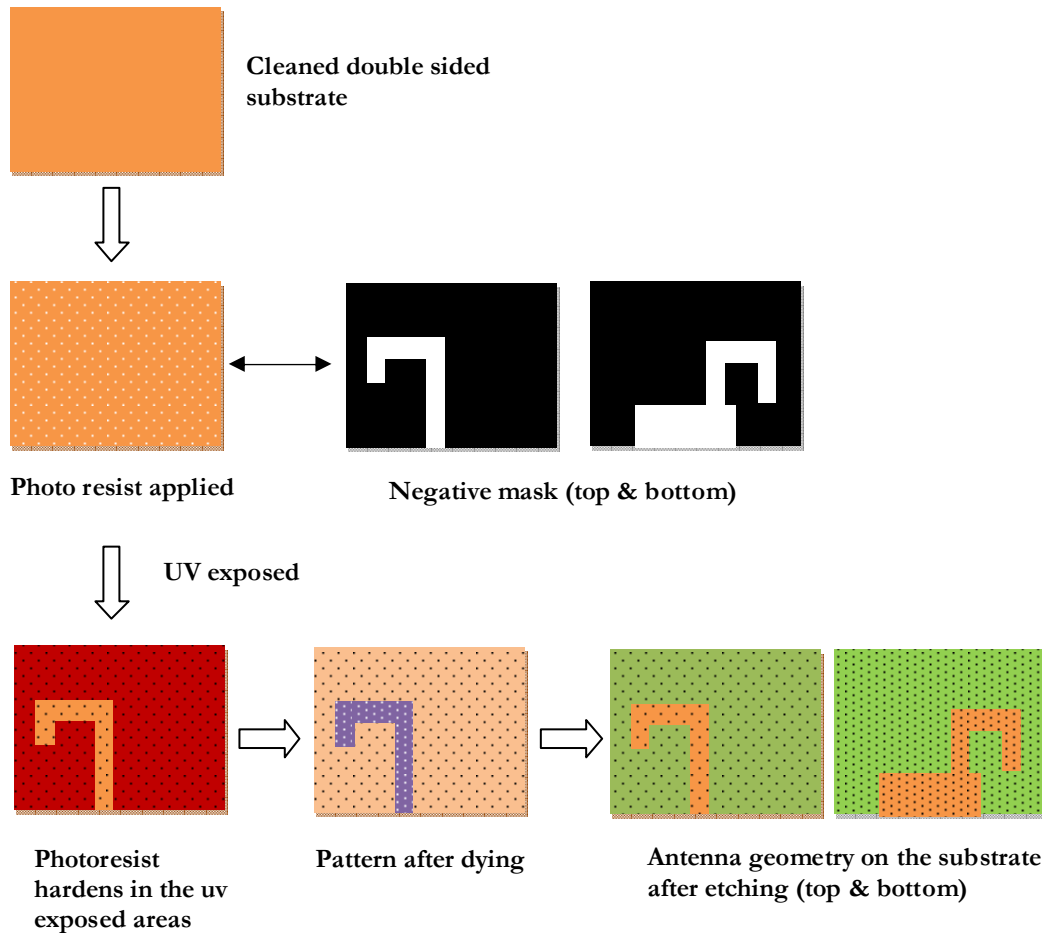


Fig.3.9 Step by step procedure involved in the photolithographic technique.

### 3.3 Microwave substrates

Selection of substrates in microwave circuits is very important. Low loss substrates are very important at microwave bands. As frequency of operation increases, the loss tangent of the material used for substrates slightly increases, which in turn adversely affect the efficiency of the antenna. The power handling capability of the antenna depends on the substrate materials also. Certain substrate materials cannot withstand high

power. A variety of substrate materials are available in the market. Flexible substrate materials are also available, so that the antenna can be mounted on curved surfaces. The selection of dielectric constant of the substrate depends on the application of the antenna and the radiation characteristics specifications. It is worth noting that surface waves will be excited in high dielectric constant substrates. This will generate spurious radiations in unwanted directions from the antenna. Dielectric constant and loss tangent of the material are measured using cavity perturbation technique.

### 3.4 Experimental setup

Antenna characteristics such as return loss, radiation pattern and gain are measured using the HP8510C and associated setup. The indigenously developed CREMA SOFT is used for the automatic measurement of the radiation properties using HP 8510C Network analyzer. The important systems used for the antenna characterization are Vector network Analyzer, Anechoic Chamber, Automated turn table etc.

#### 3.4.1 HP 8510C Vector Network Analyzer

This is a sophisticated Vector Network Analyzer (VNA) from Hewlett Packard with time domain and frequency domain operation capability [14]. The microprocessor based system can measure two port network parameters such as  $s_{11}$ ,  $s_{12}$ ,  $s_{21}$  and  $s_{22}$  very accurately. The in built signal processing algorithms of the network analyzer process the transmit and receive data and finally displays the measured values in many plot formats. The schematic of the VNA is shown in Fig. 3.10.

The network analyzer consists of a microwave generator, S parameter test set, signal processor and the display unit as illustrated in Fig. 3.10. The synthesized sweep generator HP83651B uses an open loop YIG tuned element to generate the RF stimulus. It can synthesize frequencies from

10MHz to 50GHz. The frequencies can be set in step mode or ramp mode depending on the required measurement accuracy.

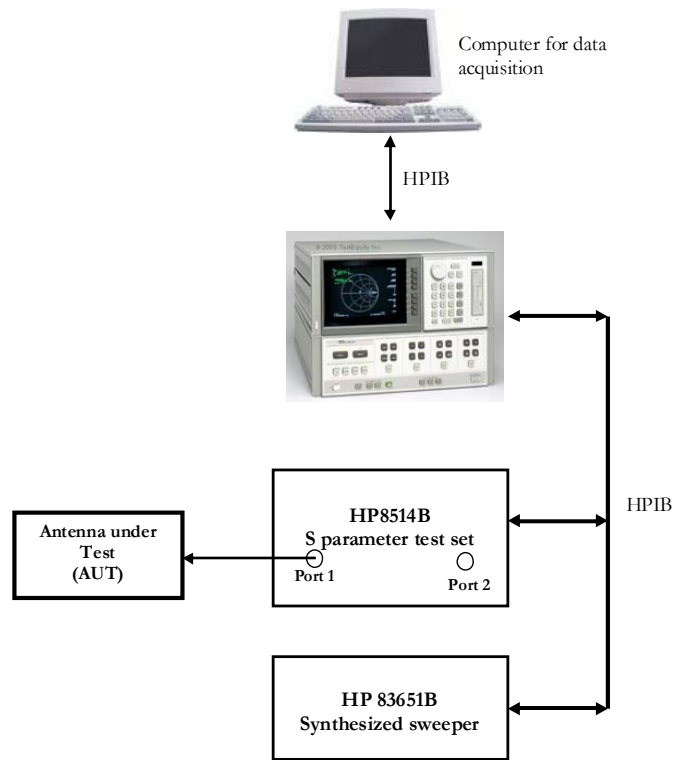


**Fig. 3.10** Schematic diagram of the HP8510C vector network analyzer setup used for the characterization of the antennas

The antenna under test (AUT) is connected to the port of the S-parameter test set HP8514B and the forward and reflected power at the measurement point is separated and down converted to 20MHz using frequency down converter. It is again down converted to lower frequency and processed in the HP8510C processing unit. All the systems discussed above are interconnected using HPIB bus. A computer interfaced to the system is used for coordinating the whole operation remotely. Measurement data can be saved on a storage medium.

### 3.4.2 Anechoic Chamber

The anechoic chamber provides a 'quiet zone', free from all types of EM reflections. All the antenna characterizations are done in an Anechoic chamber to avoid reflections from nearby objects. It is a very big room compared to the wave length of operation, consists of microwave absorbers [15] fixed on the walls, roof and the floor to avoid the EM reflections. A photograph of the anechoic chamber used for the study is shown in Fig. 3.11 below.

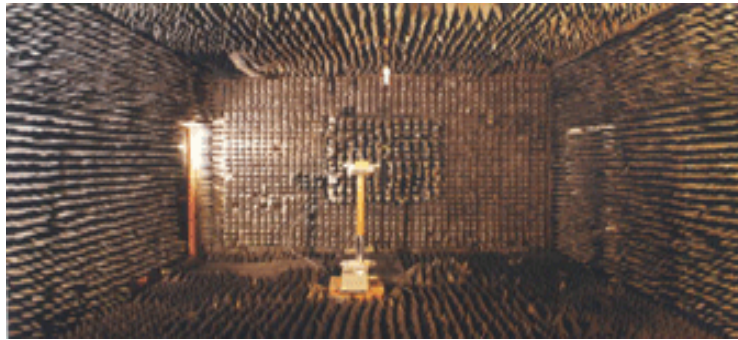


Fig. 3.11 Photograph of the anechoic chamber used for the antenna measurements

The absorbers fixed on the walls are highly lossy at microwave frequencies. They have tapered shapes to achieve good impedance matching for the microwave power impinges upon it. The chamber is made free from the surrounding EM interferences by covering all the walls and the roof with aluminium sheet.

### 3.4.3 Turn table assembly for far field radiation pattern measurement

The turn table assembly consists of a stepper motor driven rotating platform for mounting the Antenna Under Test (AUT). The in-house developed microcontroller based antenna positioner STIC 310C is used for radiation pattern measurement. The main lobe tracking for gain measurement and radiation pattern measurement is done using this setup. A standard wideband horn (1-18GHz) is used as receiving antenna for



radiation pattern measurements. The in-house developed automation software '*Crema Soft*' coordinates all the measurements.

### **3.5 Measurement procedure**

The experimental procedures followed to determine the antenna characteristics are discussed below. The network analyzer in real practice is connected to large cables and connectors. The connectors and cables will have its own losses. Thus the instrument should be calibrated with known standards of open, short and matched loads to get accurate scattering parameters. There are many calibration procedures available in the network analyzer. Single port, full two port and TRL calibration methods are usually used. The two port passive or active device scattering parameters can be accurately measured using TRL calibration method. Return loss, VSWR and input impedance can be characterized using single port calibration method.

#### **3.5.1 Return loss, Resonant frequency and Bandwidth**

The return loss characteristic of the antenna is obtained by connecting the antenna to any one of the network analyzer port and operating the VNA in  $S_{11}/S_{22}$  mode. The calibration of the port cable is done for the frequency range of interest using the standard open, short and matched load. The device under test is now connected to one end of the calibrated port cable. The frequency vs reflection parameter ( $S_{11}/S_{22}$ ) is then stored on a computer using the '*Crema Soft*'.

The frequency for which the return loss value is minimum is taken as resonant frequency of the antenna. The range of frequencies for which the return loss value is within the -10dB points is usually treated as the bandwidth of the antenna. The antenna bandwidth is usually expressed as percentage of bandwidth, which is defined as,

$$\% \text{ Bandwidth} = \frac{\text{bandwidth}}{\text{centrefrequency}} * 100$$

At -10dB points the VSWR is ~2. The above bandwidth is sometimes referred to as 2:1 VSWR bandwidth.

### 3.5.2 Far field radiation pattern

The measurement of far field radiation pattern is conducted in an anechoic chamber. The AUT is placed in the quiet zone of the chamber on a turn table and connected to one port of the network analyzer. A wideband horn is used as a transmitter and connected to the other port of the network analyzer. The turn table is controlled by a STIC positioner controller. The automated radiation pattern measurement process is coordinated by the '*Crema Soft*'.

In order to measure the radiation pattern, the network analyzer is kept in  $S_{21}/S_{12}$  mode with the frequency range within the -10dB return loss bandwidth. The antenna is boresighted manually. The number of frequency points is set according to the convenience. The start angle, stop angle and step angle of the positioner is also configured in the '*Crema Soft*'. Now the THRU calibration is performed for the frequency band specified and saved in the CAL set. Suitable gate parameters are provided in the time domain to avoid unwanted reflections if any. The *Crema Soft* will automatically perform the radiation pattern measurement and store it as a text file

### 3.5.3 Antenna Gain

The gain of the antenna under test is measured in the bore sight direction. The gain transfer method using a standard gain antenna is employed to determine the absolute gain of the AUT [16,17]. The experimental setup is similar to the radiation pattern measurement setup. An antenna with known gain is first placed in the antenna positioner and bore sighted. A THRU calibration is done for the frequency range of interest. Standard antenna is then replaced by the AUT and the change in  $S_{21}$  is noted. Note that the AUT should be aligned so that the gain in the main

beam direction is measured. This is the relative gain of the antenna with respect to the reference antenna. The absolute gain of the antenna is obtained by adding this relative gain to the original gain of the standard antenna.

### **3.5.4 Antenna Efficiency**

Conventional antenna radiation efficiency measurement techniques, such as the Wheeler cap, are generally narrowband and, thus, well suited for resonant antennas [18,19]. The method involves making only two input resistance measurement of antenna under test: one with conducting cap enclosing the antenna and one without. For the Wheeler cap, a conducting cylindrical box is used whose radius is radius of the antenna and which completely encloses the test antenna. Input impedance of the test antenna is measured with and without the cap using NWA. Since the test antenna behaves like a series resonant RLC circuit near resonance the efficiency is calculated by the following expression:

$$\text{Efficiency, } \eta = \frac{R_{no\_cap} - R_{cap}}{R_{no\_cap}}$$

Where,  $R_{no\_cap}$  denotes the input resistance without the cap and  $R_{cap}$  is the resistance with the cap.

## **3.6 References**

- [1]. K. S. Yee, Numerical solution of initial boundary value problems involving Maxwell's equations in isotropic media, *IEEE Transactions on Antennas and Propagation*, Vol.14, No. 3, pp. 302-307, 1966.
- [2]. X. Zhang and K. K. Mei, Time domain finite difference approach to the calculation of the frequency dependent characteristics of microstrip discontinuities, *IEEE Trans. Microwave Theory Tech.*, Vol. 36, pp. 1775-1787, Dec. 1988.

- [3]. Hallond, R, and J. W. Williams, Total field versus scattered field finite difference codes: A comparative Assessment, *IEEE Transactions on Nuclear Science*, Vol. 30, No.6, pp. 4583-4588, 1983.
- [4]. Enquist and Majada, Absorbing Boundary Conditions for the Numerical simulation of waves, *Mathematics of Computation*, Vol. 31, pp. 629-651, 1977.
- [5]. Mur G, Absorbing boundary conditions for the Finite Difference Approximation of the Time domain Electromagnetic field equations, *IEEE Trans. Electromagn. Compat.*, Vol .EMC-23, pp. 377-382, Nov. 1981
- [6]. V. Jandhyala, E. Michielssen, and R. Mittra, FDTD signal extrapolation using the forward-backward autoregressive model, *IEEE Microwave and Guide Wave Letters*, Vol. 4, pp. 163-165, June 1994.
- [7]. R.J Leubbers and H.S Langdon., A simple feed Model that reduces Time steps Needed for FDTD Antenna and Microstrip Calculations, *IEEE Trans. Antennas and Propogat.*, Vol.44,No.7, pp.1000-1005, July 1996.
- [8]. R.J Leubbers,Karl s Kunz,Micheal Schneider and Forrest Hunsberger., A finite difference time Domain near zone to far zone transformation, *IEEE Trans. Antennas and Propogat.*, Vol.39,pp429-433,April 1991.
- [9]. Martin L Zimmerman and Richard Q Lee, Use of FDTD method in the design of microstrip antenna arrays, *Int.Journal of Microwave and Millimeter wave Comp. aided Engg.*, Vol.4, No.1,pp 58-66,1994.
- [10]. M.N.O. Sadiku, A simple introduction to finite element analysis of electromagnetic problems, *IEEE Trans. Educ.*, Vol.32, No.2, pp.85-93, May 1989.
- [11]. Anastasis C. Polycarpous, Introduction to the Finite Element Method in Electromagnetics, Morgan & Claypool, USA,2006.
- [12]. Joao pedro a. Bastos and Nelson Sadowski , Electromagnetic modeling by finite element methods, Marcel Dekker,2003
- [13]. HFSS User's manual, version 10, Ansoft Corporation, July 2005
- [14]. HP8510C Network Analyzer operating and programming manual, Hewlett Packard, 1988.

- [15]. E. J. Zachariah, K. Vasudevan, P. A. Praveen Kumar, P. Mohanan and K. G. Nair Design, Development and Performance Evaluation of an Anechoic Chamber for Microwave Antennas Studies, *Indian Journal of Radio and Space Physics*, Vo. 13, pp. 29-31, February 1984.
- [16]. C. A. Balanis, *Antenna Theory: Analysis and Design*, Second Edition, John Wiley & Sons Inc. 1982
- [17]. John D. Kraus, *Antennas* Mc. Graw Hill International, second edition, 1988
- [18]. H.A Wheeler, The Radiansphere around a small antenna, *Proc. IRE*, pp 1325-1331, August 1959.
- [19]. Hosung Choo; Rogers, R.; Hao Ling; On the Wheeler cap measurement of the efficiency of microstrip antennas, *IEEE Transactions on Antennas and Propagat.*, Vol. 53, Issue 7, pp.2328 – 2332, July 2005.

.....❧.....

## **DESIGN AND ANALYSIS OF COMPACT DUAL BAND DUAL STRIP ANTENNA**

---

<b>Contents</b>	<b>4.1 Microstrip – fed printed monopole antenna</b>
	<b>4.2 Compact printed antenna with modified ground plane</b>
	<b>4.3 Design procedure for a compact dual strip antenna</b>
	<b>4.4 Design and analysis of dual band dual strip antenna for 1.8/2.4 GHz bands</b>
	<b>4.5 Conclusion</b>
	<b>4.6 References</b>

---

---

This chapter deals with the design and analysis of a compact dual band dual strip antenna. A microstrip-fed printed monopole antenna has been analysed. The effect of ground plane dimensions and feed offset on the radiation characteristics has been studied in detail. Finite ground plane has been effectively utilized to excite a new resonance near the fundamental mode by introducing another extended strip from the ground plane, without affecting the compactness. Design equations are derived based on the experimental and simulation analysis. The equations are validated for a compact dual band dual strip antenna operating in 1.8/2.4GHz band for DCS and WLAN applications.

---

## 4.1 Microstrip-fed printed monopole antenna

### 4.1.1 Introduction

The monopole antenna is attractive for communication due to simple design, wide bandwidth and nearly omnidirectional radiation coverage. A conventional monopole antenna is a wire of  $\lambda/4$  (quarter wave monopole) length above a large ground plane. It is well understood that impedance bandwidth can be improved by increasing the wire diameter. In many cases for achieving good impedance bandwidth and moderate gain, wire element can be replaced by flat square plate or circular disc. Several geometries like square, triangle and circle are used. But monopole antennas with linear configuration are the simplest and widely preferred one. The main handicap of a conventional monopole antenna is its large ground plane. In conventional monopole antenna design, radiating element is perpendicular to the ground plane, thus makes the system too bulky for compact applications. In present scenario compactness is the major concern. To comply with this, low profile printed monopole antennas are preferred. In the case of printed monopoles a strip or a flat plate is printed on a dielectric substrate for compactness. In microstrip-fed printed monopole antenna configuration, ground plane and the radiating element are placed parallel to each other and printed on either side of the substrate. This configuration gives a low profile, conformal design and the antenna can be easily integrated with the printed circuit board. Planar monopole antennas can be easily optimized to provide wide impedance bandwidth with acceptable radiation performances.

A simple microstrip-fed printed strip monopole configuration is shown in Fig.4.1. In the figure a  $50\Omega$  microstrip line of width 'w' and a strip monopole of length ' $l_m$ ' are printed on a dielectric substrate of dielectric constant  $\epsilon_r$  and height 'h'. Strip monopole is having a length  $l_m = 0.25\lambda_d$  and width same as that of a  $50\Omega$  microstrip line. A ground plane having a length,

$L_g = 1\lambda_d$  and width  $W_g = 0.5\lambda_d$  is printed on the other side of the substrate.

Where  $\lambda_d = \lambda/\sqrt{\epsilon_{eff}}$ ,  $\epsilon_{eff} = \frac{\epsilon_r + 1}{2}$  and  $\lambda$  is the free space wavelength

corresponding to the resonant frequency. FR4 substrate of thickness  $h=1.6\text{mm}$ , dielectric constant,  $\epsilon_r=4.4$  and loss tangent,  $\tan\delta=0.02$  is used as the substrate. Ground plane dimensions are selected as per the specifications given in [1]

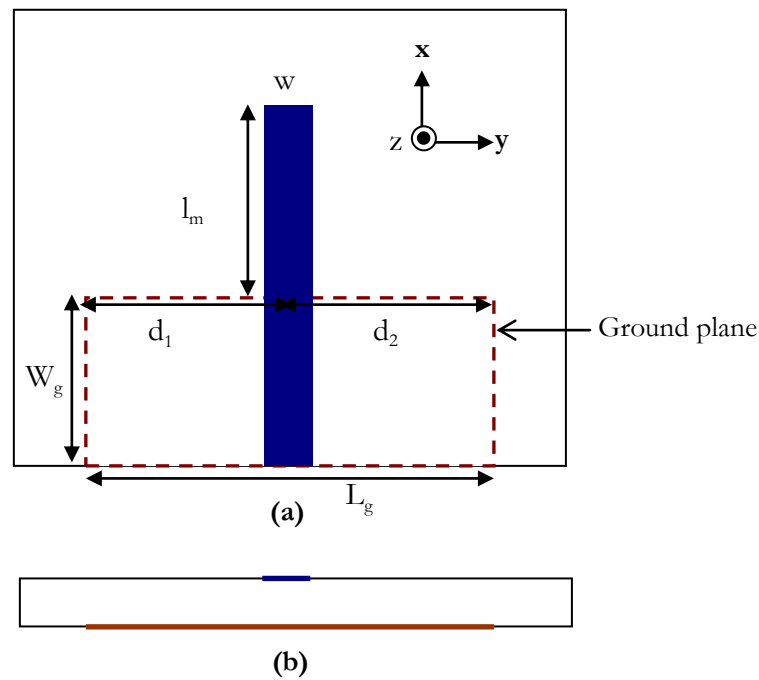


**Fig.4.1. Microstrip-fed printed strip monopole antenna**  
 $(L_g = 1\lambda_d, W_g = 0.5\lambda_d, d_1=d_2= 0.5\lambda_d, l_m= 0.25\lambda_d)$   
 (a) Top view (b) side view

#### 4.1.2 Reflection characteristics

Return loss characteristics of the above configuration is illustrated in Fig.4.2a. Antenna shows resonance at 2.5GHz with 20% bandwidth. From the return loss characteristics it is clear that there is a resonance at 3.2GHz which is poorly matched. This may be due to the effect of ground plane. The



first resonance is obviously due to the  $\lambda/4$  monopole strip ( $l_m=0.25\lambda_d$ ). Prime focus of this section is to find out the resonant length corresponding to the second resonance. Smith chart showing the impedance variation for the two resonant frequencies is given in Fig.4.2b. Input impedance at 2.5GHz is  $42.15-j10.35\Omega$ ; where as at 3.2GHz, it is  $22.05-j0.3\Omega$ . For the second resonance real part of the impedance is very low and hence it is not matched. If this real part of the impedance is increased, matching can be improved. This can be achieved only by understanding the resonance behaviour in the antenna. To understand the resonance behaviour of the antenna, the current distribution in the antenna at the two resonant frequencies are required.

The simulated surface current distributions for the resonant frequencies are shown in Fig.4.3. Simulation has been carried out using Ansoft HFSS. From the Fig.4.3.a, it is clear that there is a quarter wave current variation along the monopole strip length corresponding to the first resonance. Current distribution is similar to that of a quarter wave monopole as expected and not much variation along the ground plane. Current flow is opposite on the ground plane edges on either side of the monopole strip. But for the second resonance there exists equal current distribution on both the strip and the ground plane edge as shown in the fig.4.3.b. From the current distribution it can be inferred that, second resonance may be due to the 'L' shaped path 'a-b-c' which may act as an asymmetric dipole, including the ground plane. Since the feeding is given symmetrically with respect to the ground plane, the two L shaped paths ('L' (abc) and 'reflected L' (a'b'c')) will create same electrical length and gives resonance at 3.2GHz. For confirming the resonant length corresponding to second resonance further analysis has been carried out by offsetting feed positions and varying ground plane dimensions. This is discussed in section 4.1.5.

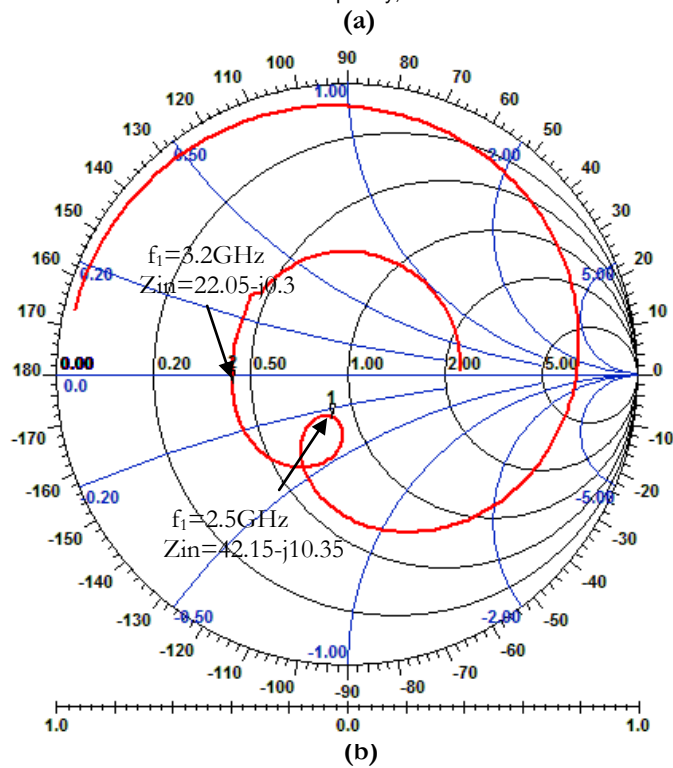
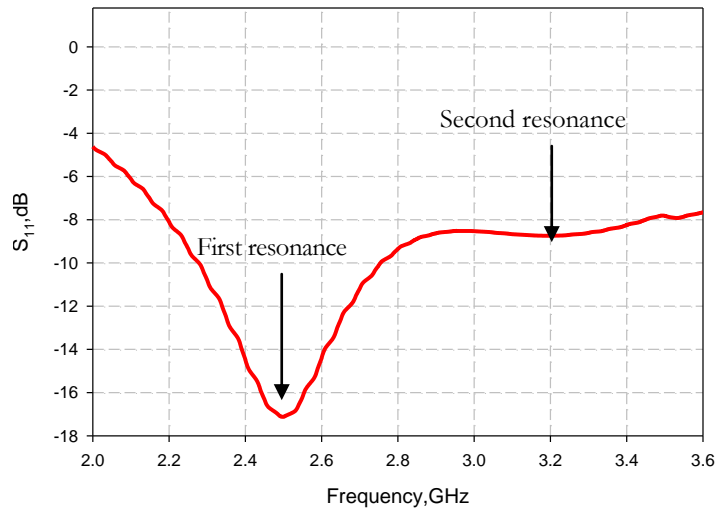


Fig.4.2(a) Reflection characteristics of the Microstrip-fed printed strip monopole antenna  
 (b). Smith chart for the Microstrip-fed printed strip monopole antenna  
 ( $L_g = 76\text{mm}$ ,  $W_g = 38\text{mm}$ ,  $d_1=d_2=38\text{mm}$ ,  $l_m=19\text{mm}$ ,  $w = 3\text{mm}$ ,  $\epsilon_r=4.4$ ,  $h=1.6\text{mm}$ )

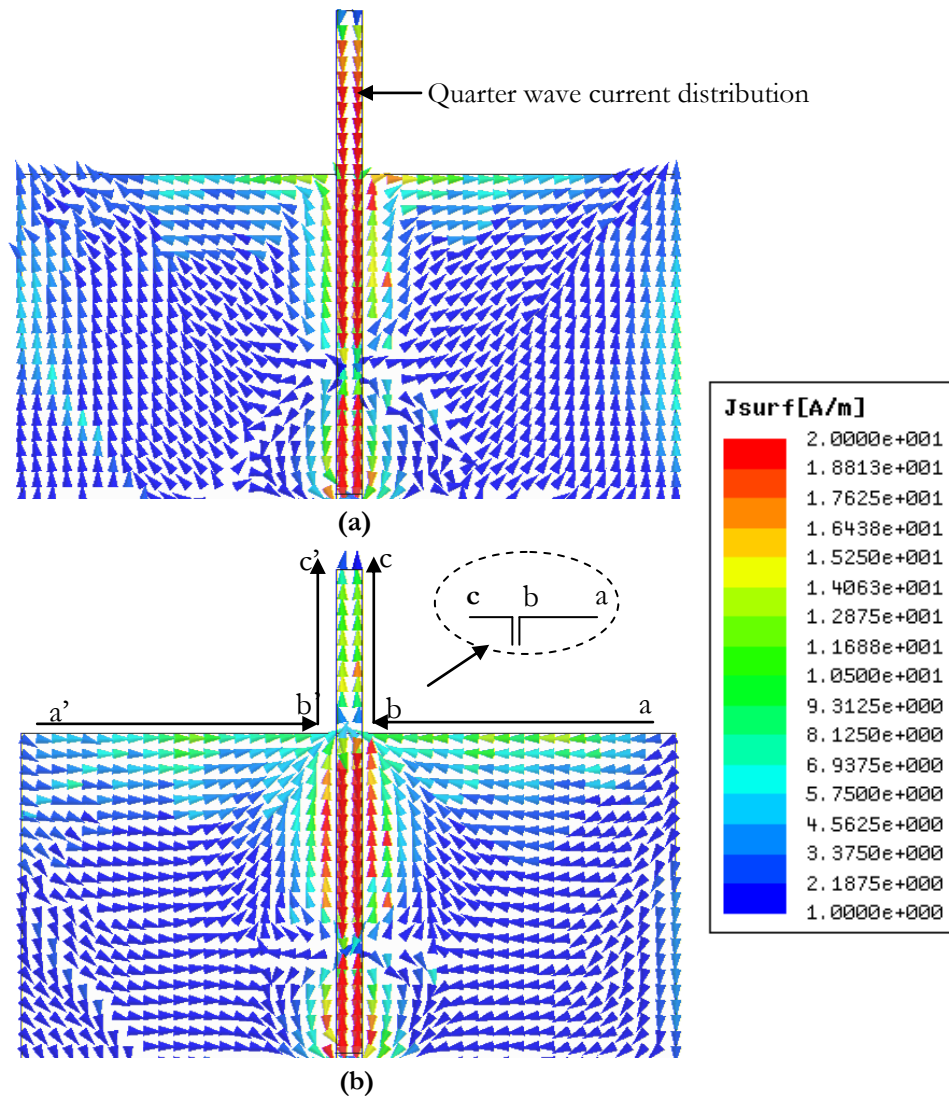


Fig.4.3 Surface current distribution  
 (a)2.5GHz (b) 3.2GHz  
 ( $L_g = 76\text{mm}$ ,  $W_g = 38\text{mm}$ ,  $d_1=d_2=38\text{mm}$ ,  $l_m=19\text{mm}$ ,  $w = 3\text{mm}$   
 $\epsilon_r=4.4$ ,  $h = 1.6\text{mm}$ )

### 4.1.3 Radiation characteristics

Measured radiation pattern of the microstrip-fed printed monopole antenna at 2.5GHz is shown in Fig.4.4. Antenna is linearly polarized along x direction with a cross polar level better than -20dB along the bore sight direction. The two principal plane patterns (E-plane and H-plane) measured

in xz plane and yz plane are given in the figure for discussion. The radiation pattern is nearly omnidirectional with figure of eight in the E- plane. Half power beam width along the E-plane pattern is  $65^\circ$  where as H-plane pattern is nearly non directional. The simulated 3D pattern is shown in figure 4.4.c. A nearly doughnut shaped radiation pattern is observed.

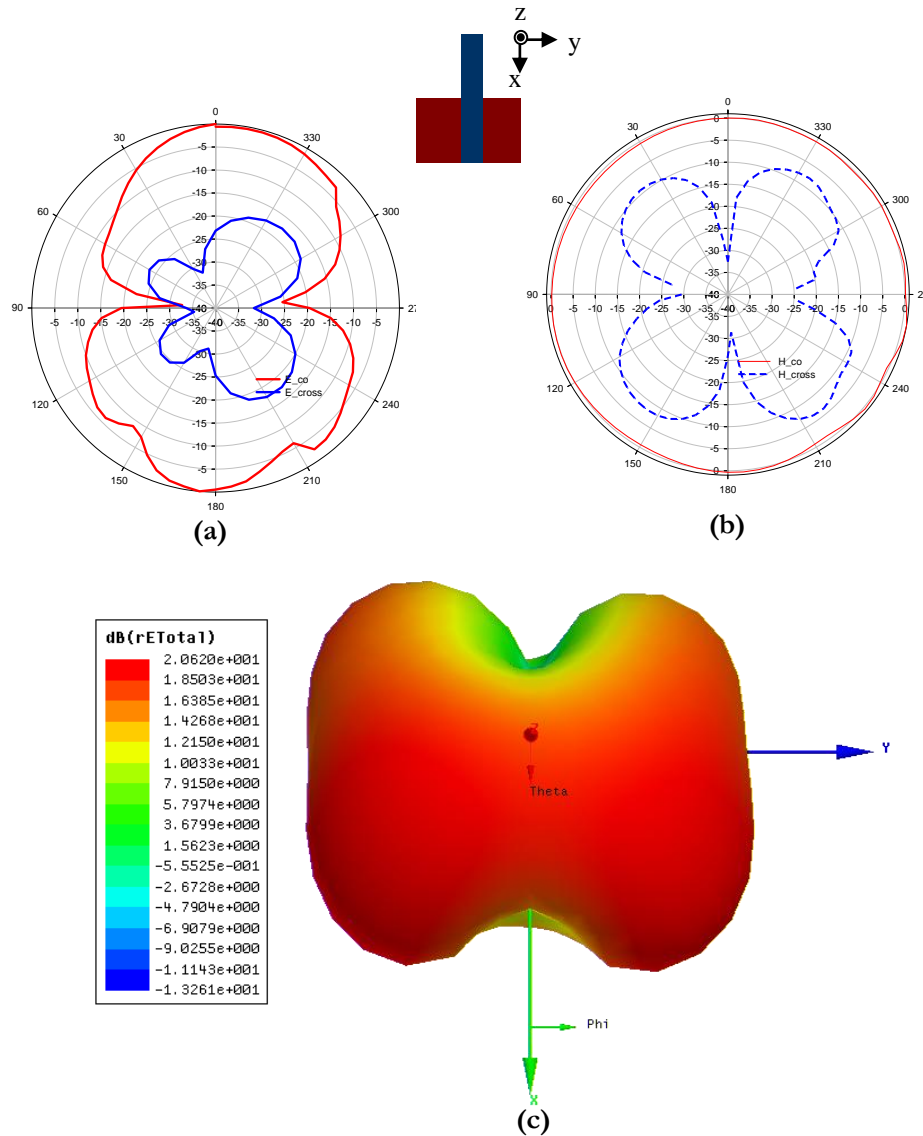
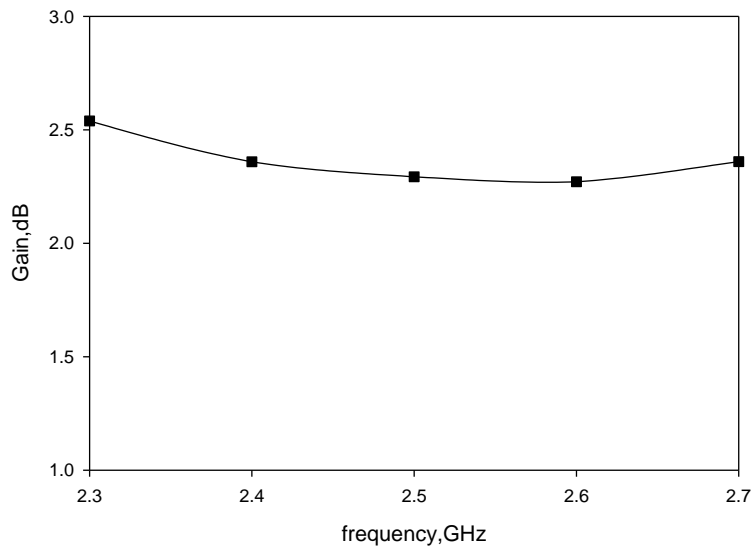


Fig.4.4 Radiation pattern of the microstrip-fed printed monopole  
 (a) E plane (b) H plane (c) 3D pattern  
 $(L_g = 76\text{mm}, W_g = 38\text{mm}, l_m = 19\text{mm}, w = 3\text{mm}, \epsilon_r = 4.4, h = 1.6\text{mm})$

#### 4.1.4 Gain and Efficiency

Gain of the microstrip fed printed monopole antenna measured in the operating band is shown in Fig.4.5. Antenna shows an average gain of 2.36dBi in the band. Efficiency of the antenna computed at the resonant frequency is 86%. So we can say that this printed monopole antenna is offering moderate gain and efficiency at the fundamental mode.



**Fig.4.5 Gain of the microstrip-fed printed monopole antenna**  
 $(L_g = 76\text{mm}, W_g = 38\text{mm}, l_m = 19\text{mm}, w = 3\text{mm}, \epsilon_r = 4.4, h = 1.6\text{mm})$

#### 4.1.5 Effect of offset feed

A detailed investigation has been carried out to find out the effect of offset feed on resonant frequencies and impedance bandwidth. Initially the microstrip feed line and the monopole strip are placed symmetric with respect to the ground plane ( $d_1 = d_2 = 0.5\lambda_d$ ) as shown in Fig 4.1. In the present analysis  $d_1$  has been varied as shown in Fig.4.6 to give an offset feed. Feed offset analysis is carried out by keeping the length  $d_1 + d_2 = \lambda_d$ . If the second resonance is due to the L and reflected L shaped path, three resonances can be produced. This is narrated in the next sections.

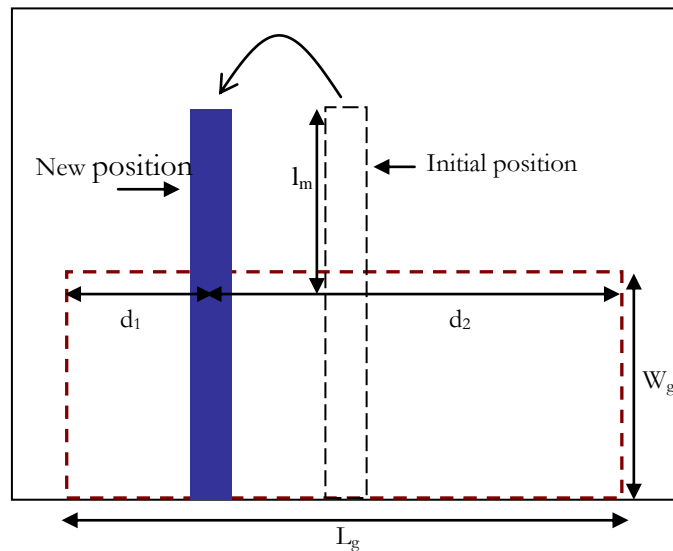
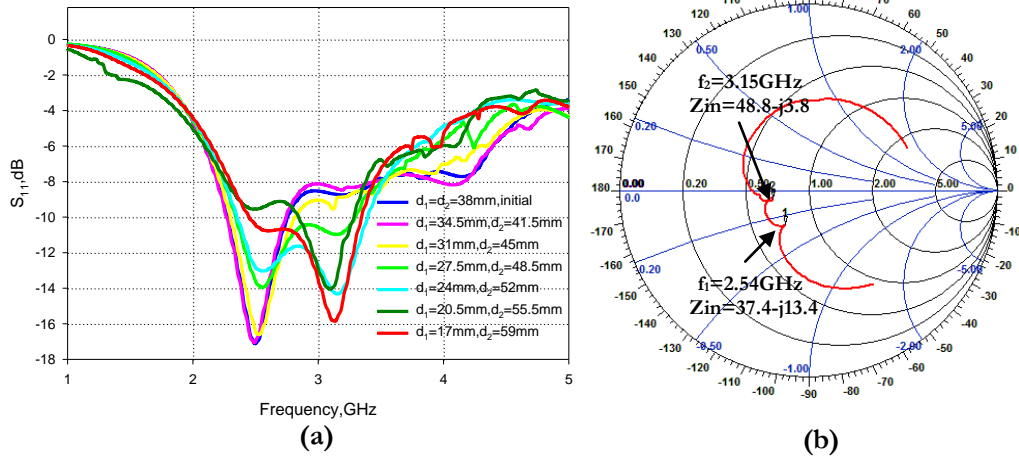


Fig.4.6 Feed offsetting on microstrip-fed printed monopole

#### 4.1.5.1 Reflection characteristics

The reflections characteristics corresponding to different feed positions are shown in Fig 4.7a. Offsetting the feed with respect to the centre, the first resonance remains almost constant. But the second resonance is slightly affected and the resonant frequency is decreased with better impedance matching. In the case of second resonance, variation in  $d_1$  results in a change in feed position along the L shaped resonant path and hence varies the input impedance. Smith chart showing the input impedance variation for  $d_1=24\text{mm}=0.33\lambda_d$  is given in fig.4.7b. Due to the feed offset, real part of the input impedance corresponding to the second resonance increases as shown in the smith chart. Slight decrease in the resonant frequency is due to the increase in the L shaped resonant length. For the first resonance, input impedance decreases due to the offset. Variation of real and imaginary part of the input impedance with respect to the feed offset is plotted in Fig.4.8a and 4.8b. It is clear that for the lower resonance as real part of the input impedance decreases due to the feed offset, impedance matching reduces. But for the second resonance, real part of the input impedance increases and

imaginary part shifts towards the inductive side and hence impedance matching improves.



**Fig.4.7** (a) Reflection characteristics for different feed positions  
 (b) Smith chart for feed offset  $d_1=24\text{mm}$ ,  $d_2=52\text{mm}$   
 ( $L_g = 76\text{mm}$ ,  $W_g = 38\text{mm}$ ,  $l_m=19\text{mm}$ ,  $w = 3\text{mm}$ ,  $\epsilon_r = 4.4$ ,  $h=1.6\text{mm}$ )

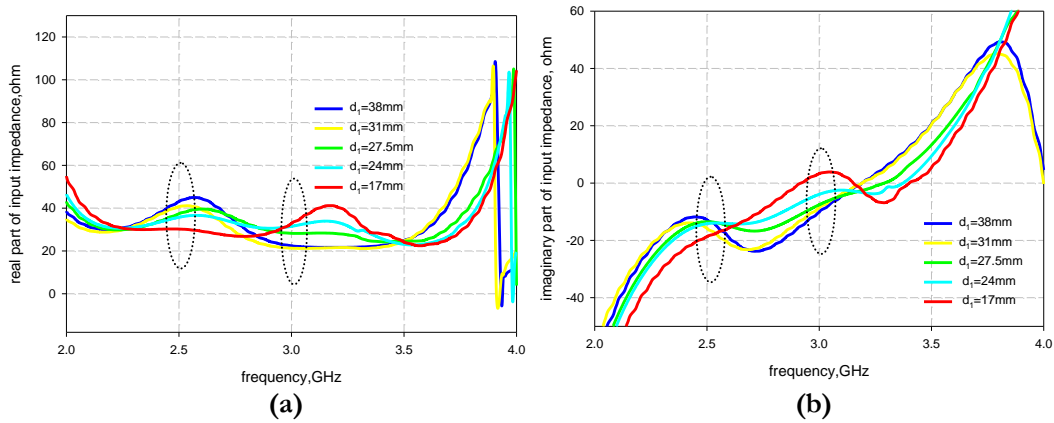


**Fig.4.8** Input impedance variation for various feed offsets  
 ( $L_g = 76\text{mm}$ ,  $W_g = 38\text{mm}$ ,  $l_m=19\text{mm}$ ,  $w = 3\text{mm}$ ,  $\epsilon_r = 4.4$ ,  $h=1.6\text{mm}$ )  
 (a) Real part (b) Imaginary part

By suitably optimizing the feed offset position the two resonances can be merged to form a wide impedance response with nearly similar radiation performances.

Variation of percentage bandwidth for different feed offset positions is plotted in Fig.4.9. For the initial configuration, i.e. for printed monopole with feed line placed symmetric with respect to the ground plane, a 20% bandwidth has been observed. This is explicitly due to the first resonant mode. As the feed position varies, the impedance matching corresponding to the second resonance improves and both the resonances merge together to give a wideband response as shown in Fig.4.7a. A maximum bandwidth of 36% is achieved for  $d_1=0.33\lambda_{d1}$ , where  $\lambda_{d1}=\lambda/\sqrt{\epsilon_{eff}}$ , as explained earlier and  $\lambda_1$  is the wavelength for the lower resonance. For further change in offset  $d_1$ , bandwidth reduces drastically.

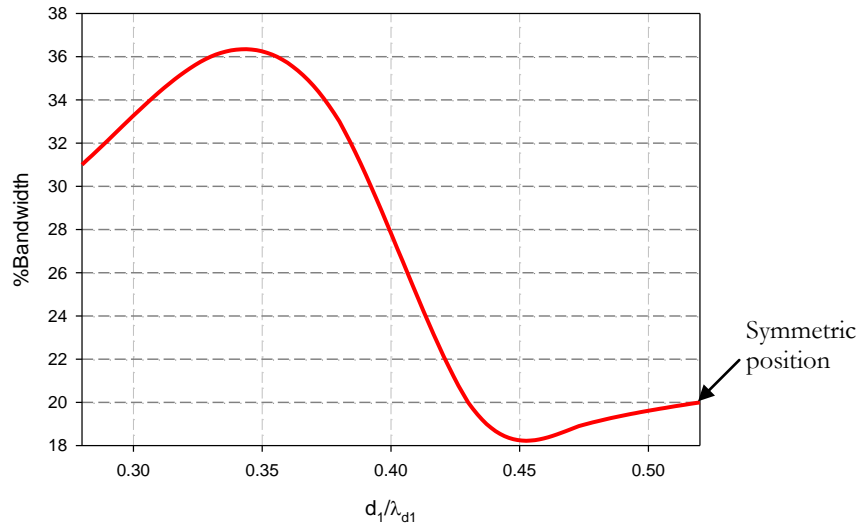


**Fig.4.9. Bandwidth versus feed offset**

( $L_g = 76\text{mm}$ ,  $W_g = 38\text{mm}$ ,  $l_m=19\text{mm}$ ,  $w = 3\text{mm}$ ,  $\epsilon_r = 4.4$ ,  $h=1.6\text{mm}$ )

#### 4.1.5.2 Surface current distribution

The simulated surface current distribution for the offset fed printed monopole antenna at 2.54GHz with an offset distance of  $d_1=0.33\lambda_{d1}$  is given in Fig.4.10a. In this case a quarter wave current variation is observed along the monopole strip ' $l_m$ '. It is also noted that asymmetry in the configuration causes an asymmetric current flow on the ground plane. This current distribution can induce a tilt in the radiation pattern.



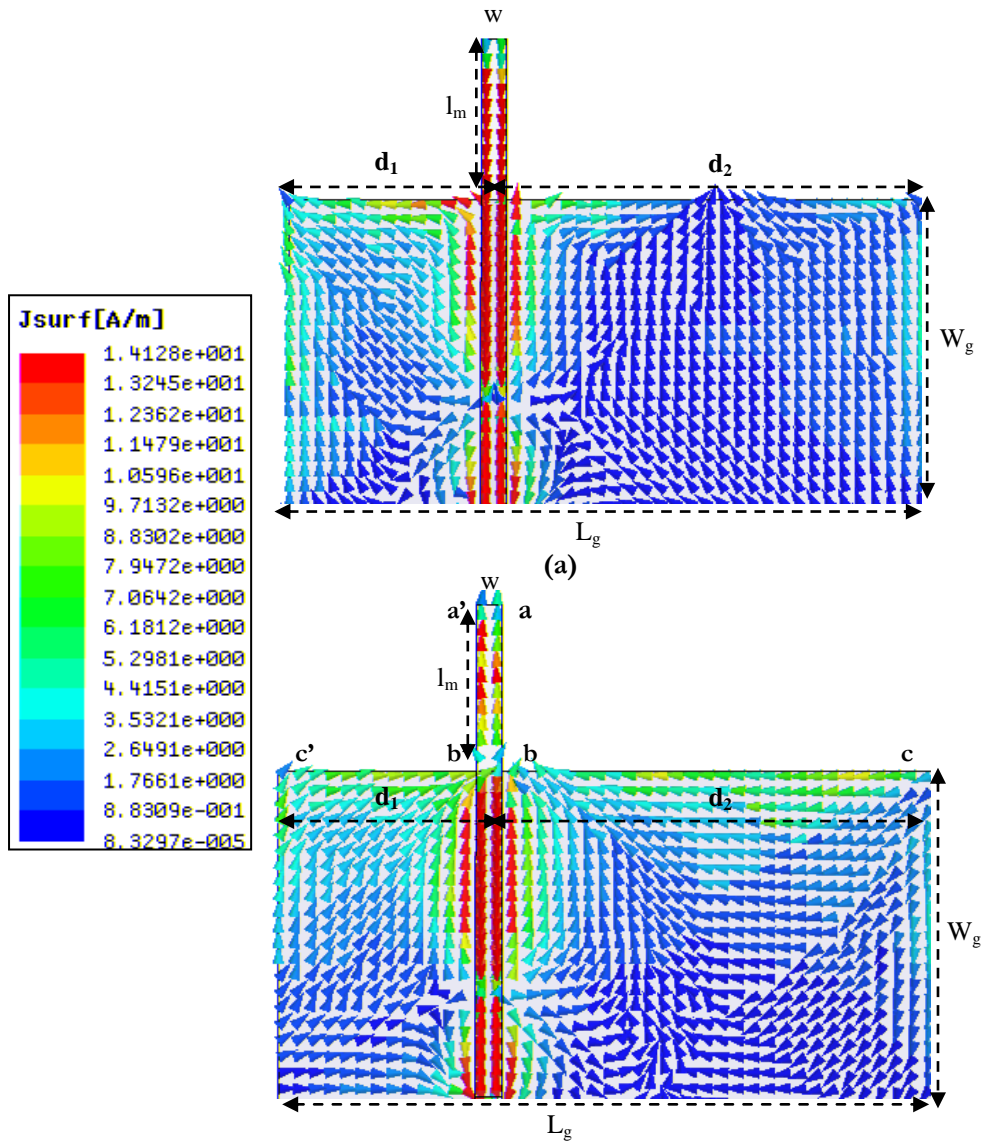


Fig.4.10 Simulated Surface current distribution  
 ( $L_g = 76\text{mm}$ ,  $W_g = 38\text{mm}$ ,  $l_m = 19\text{mm}$ ,  $w = 3\text{mm}$ ,  $d_1 = 24\text{mm}$ ,  
 $d_2 = 52\text{mm}$ ,  $\epsilon_r = 4.4$ ,  $h = 1.6\text{mm}$ ) (a) 2.54GHz (b) 3.16GHz

The surface current distribution corresponding to the second resonance 3.16GHz is illustrated in Fig.4.10b. There is equal variation along the monopole strip  $l_m$  and ground edge, which constitutes L shaped path. The L shaped current path which constitutes the resonance is clearly seen in the figure.

The resonance corresponding to the ‘reflected L’ shaped path (a’b’c’) will be in the higher side and not matched. Increase in  $d_1$  may improve the matching for this. This is discussed in section 4.1.7.

#### 4.1.5.3 Radiation characteristics

Radiation characteristic of the feed offset configuration having maximum bandwidth ( $d_1=0.33\lambda_{d1}$ ) is shown in Fig.4.11.

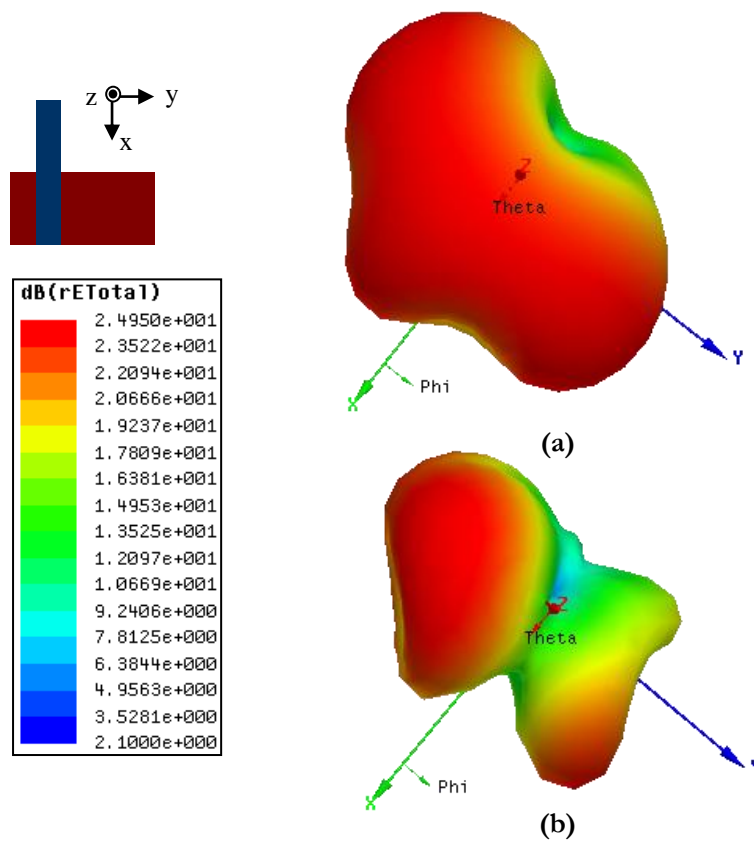


**Fig.4.11 Simulated 3D radiation pattern**

( $L_g = 76\text{mm}$ ,  $W_g = 38\text{mm}$ ,  $l_m=19\text{mm}$ ,  $w = 3\text{mm}$ ,  $d_1=24\text{mm}$ ,  $d_2=52\text{mm}$   $\epsilon_r =4.4$ ,  $h=1.6\text{mm}$ ) (a) 2.54GHz (b) 3.16GHz

Radiation pattern is highly distorted due to the asymmetry in the configuration. Asymmetry in the structure induces an asymmetric

current flow on the ground plane as shown in Fig.4.10. In the case of lower resonance current strength is more on monopole strip ' $l_m$ '. But still a slight change in the radiation pattern is observed which is due to the asymmetric horizontal current flow on the ground plane as shown in the Fig4.10a. In the case of printed monopole with symmetric feed, the field excited due to the equal and opposite current distribution on either side of the ground plane cancels at the far field and hence a symmetric pattern was observed.

For the higher resonance, which is due to the asymmetric dipole mode, the tilt in the radiation pattern is due to the L shaped current path which is highly asymmetric as shown in Fig.4.10b. It is also noted that for dipoles (even though length greater than half wave) with symmetric feed, radiation pattern due to travelling wave current distribution is symmetric about the axis as compared to the standing wave pattern. So this will not cause any disturbance to the net radiation pattern. But for dipoles (of length greater than half wavelength) with asymmetric feed, the radiation pattern due to travelling wave current distribution on the antenna is no longer symmetric about the axis and its effect on the resultant pattern become more pronounced. This will cause a tilt in the radiation pattern [2]. For the present case this tilt along with the asymmetry due to the configuration gives a distortion in the radiation pattern for the higher resonance.

For confirming the resonances, a detailed investigation has been carried out by varying the monopole strip length and the variations in resonant frequencies have been analyzed. Parametric analysis has been conducted on printed monopole strip with an offset of  $d_1=0.33\lambda_{d1}$  for which good impedance bandwidth has been recorded.

#### **4.1.6 Effect of monopole strip length ' $l_m$ '**

Reflection characteristics obtained for various monopole strip lengths ( $l_m$ ) is given in Fig.4.12. It is observed that as the strip length ' $l_m$ ' increases both the higher and lower frequencies decreases. Fig.4.13 shows the variation of resonant frequencies with respect to strip length ' $l_m$ '. Variation is more for first resonance than the second and found to be inversely proportional to the frequency. This again confirms that first resonance is primarily due to the length of the strip. Second resonance also shows variation with respect to change in strip length ' $l_m$ '. This is due to the variation in 'L' shaped path which constitutes the resonant length for the second resonance. Another important observation is the variation in input impedance corresponding to the second resonance. The strip length ' $l_m$ ' and the ground plane edge length  $d_2$  constitute an asymmetric dipole. This is responsible for the second resonance as mentioned earlier. The reduction in ' $l_m$ ' varies the length of the dipole and also the asymmetric feed position on the dipole hence varies the impedance matching. Variation of second resonance with respect to strip length, gives the preliminary proof for the second resonance. As the quarter wave current variation corresponding to the first resonance on the monopole strip varies with strip length, the first resonance changes. Since the strip length ' $l_m$ ' shares the part of the L-shaped current path for the second resonance, second frequency is also affected by ' $l_m$ '. Thus the influence of L shaped path including the ground plane need to be investigated.

Even though feed offset improves matching and enhance the impedance bandwidth, the large ground plane required for this configuration is the main hindrance for using this configuration for compact applications. So the effect of ground plane dimensions on antenna performances have to be analyzed. A detailed study on finite ground plane effect of offset fed printed monopole antenna is discussed in next section.

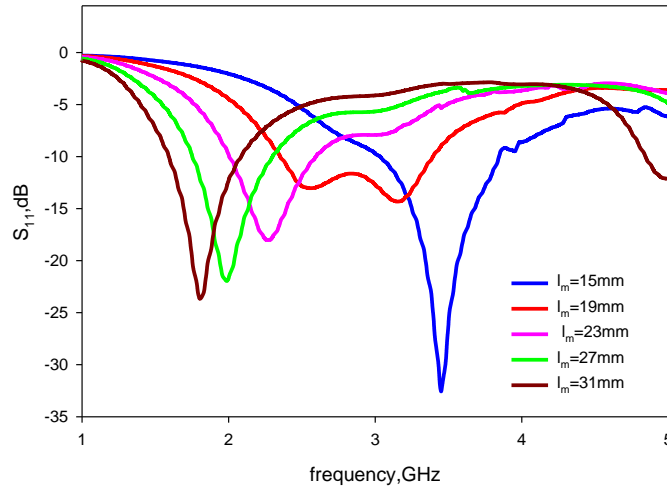


**Fig.4.12 Reflection characteristics for various strip lengths ( $l_m$ )**  
 ( $L_g = 76\text{mm}$ ,  $W_g = 38\text{mm}$ ,  $d_1=24\text{mm}$ ,  $\epsilon_r = 4.4$ ,  $h=1.6\text{mm}$ )

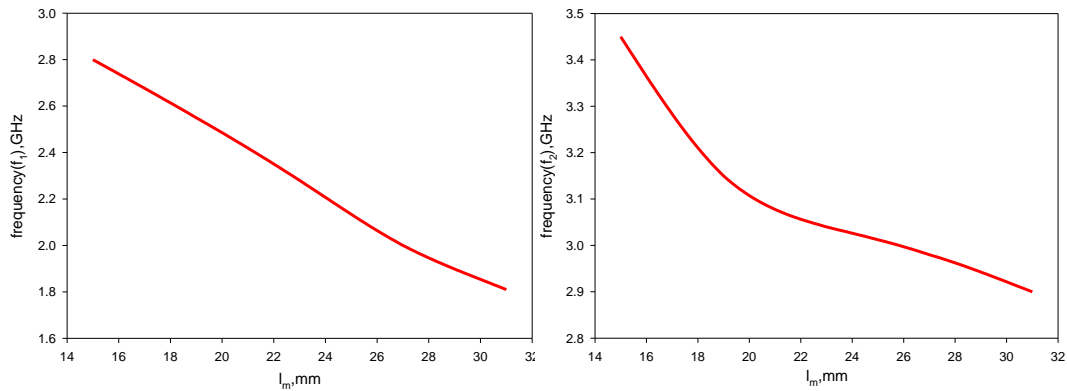


**Fig.4.13. Variation of resonant frequencies with monopole strip ‘ $l_m$ ’**  
 ( $L_g = 76\text{mm}$ ,  $W_g = 38\text{mm}$ ,  $d_1=24\text{mm}$ ,  $d_2=52\text{mm}$ ,  $w = 3\text{mm}$ ,  $\epsilon_r = 4.4$ ,  $h=1.6\text{mm}$ )

#### 4.1.7 Finite ground plane effects

Since the surface current on ground plane edge has significant impact on higher resonance, ground plane dimensions need to be studied. A rigorous analysis has been carried out by varying the ground plane length and width. The main objective of this analysis is to find out the role of ground plane dimensions on two modes. So the investigations have been carried out on

printed monopole configuration with a feed offset  $d_1=0.33\lambda_{d1}$ , which has got maximum bandwidth from the previous analysis.

#### 4.1.7.1 Effect of ground plane Length, $L_g$

##### *Effect of $d_2$*

In this case ground plane length  $L_g$  is varied by tailoring the parameter  $d_2$  and the change in resonant frequencies are analysed for various  $d_2$  values keeping  $d_1$  constant. Reflection characteristics obtained for different ground plane lengths are given in Fig4.14.

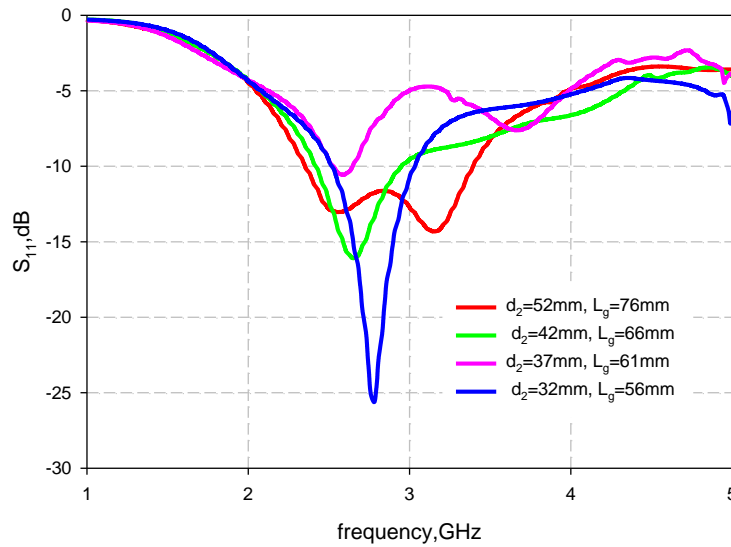


Fig.4.14 Reflections characteristics for various ground plane lengths ( $W_g = 38$ mm,  $l_m=19$ mm,  $d_1=24$ mm,  $\epsilon_r =4.4$ ,  $h=1.6$ mm)

Variation of the first resonant frequency with respect to ground plane length  $L_g$  is given in Fig.4.15a. The variation study shows that even though, first resonance is primarily due to the monopole strip, ground plane dimensions have significant impact on the impedance. For  $L_g > 0.8\lambda_{d1}$ , where  $\lambda_{d1}$  is the dielectric wavelength corresponding to the first resonance, resonant frequency remains almost constant. But for small  $L_g$  values resonant frequency increases considerably.

Variation of second resonance with respect to ground length  $L_g$  is given in Fig.4.15b. Here also as the ground plane length  $L_g$  increases second resonance decreases. Since the L shaped current path reduces as  $d_2$  decreases, effective resonant length decreases and frequency increases. This study again reassures the impact of L shaped path on the second resonance. Another important observation is as  $L_g$  decreases and reaches below  $0.75\lambda_{d1}$ , higher resonance shifts towards higher end with poor matching as shown in Fig.4.14. Thus printed monopoles with ground plane length  $<0.75\lambda_{d1}$  will give only single resonance with good impedance matching even with feed offset.

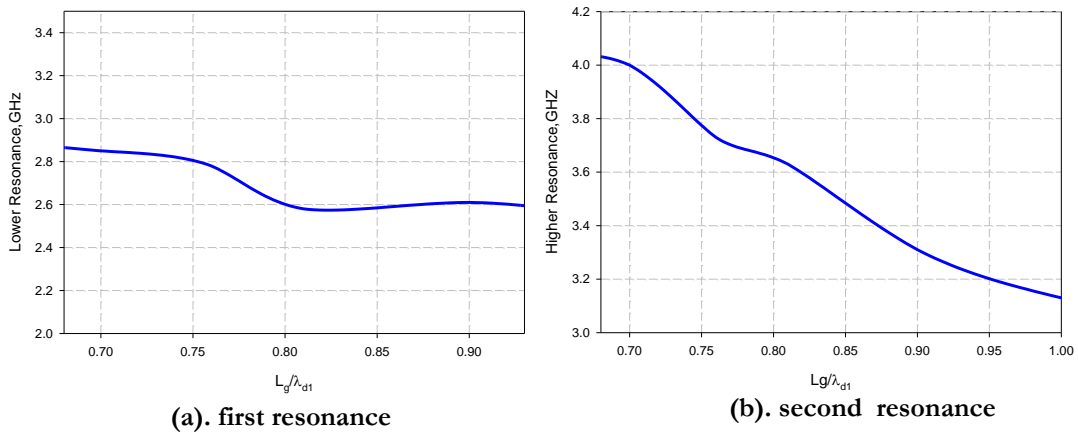


Fig.4.15 Variation of resonance frequency with groundplane length  $L_g$   
 $(W_g = 38\text{mm}, l_m = 19\text{mm}, w = 3\text{mm}, d_1 = 24\text{mm}, \epsilon_r = 4.4, h = 1.6\text{mm})$

### *Effect of $d_1$*

Variation of resonant frequencies with respect to  $d_1$ , by changing the total ground plane length  $L_g$  is analysed. In this case  $d_2$  is kept constant. The reflection characteristics obtained is shown in Fig.4.16. As  $d_1$  increases, resonant length for the 'reflected L' shaped path increases and this gives a third higher resonance as shown in the figure. But as  $d_1$  increases, ground plane dimension increases and antenna loses its compactness. So for further analysis  $d_1 = 0.33\lambda_{d1}$  which is the optimized case for the two lower resonances is used.

From the above studies, it is concluded that ground plane length affects the resonances and impedance matching. But the variation is more for compact dimensions. For a large ground plane with offset feed, three resonances can be produced.

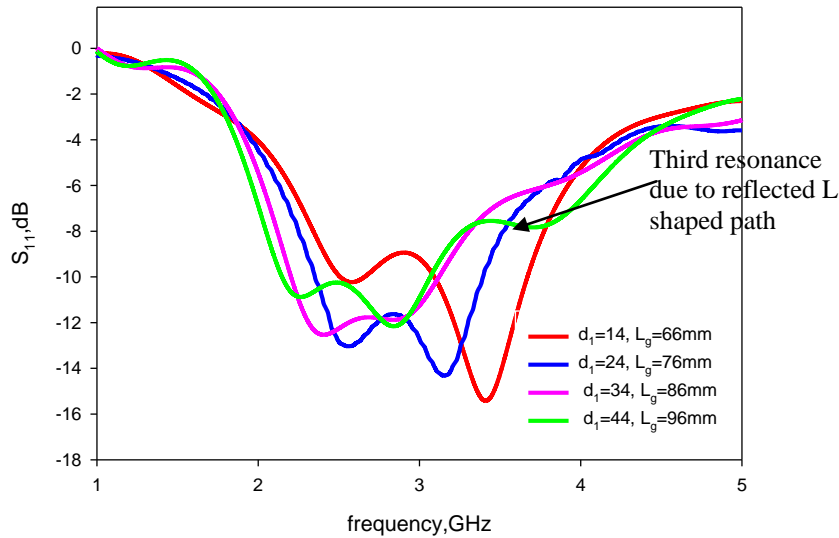


Fig.4.16. Reflection characteristics of the antenna with different  $d_1$   
 ( $W_g = 38\text{mm}$ ,  $l_m = 19\text{mm}$ ,  $w = 3\text{mm}$ ,  $d_2 = 52\text{mm}$ ,  $\epsilon_r = 4.4$ ,  $h = 1.6\text{mm}$ )

#### 4.1.7.2 Effect of ground plane width $W_g$

Impact of ground plane width  $W_g$  on antenna performances has been analyzed and reflection characteristics obtained after the investigation are illustrated in Fig.4.17. As  $W_g$  varies, there is not much significant change in both the resonant frequencies. Where as impedance bandwidth varies considerably. Variation in ground plane width has no direct impact on resonant length and hence less effect on resonant frequency. As ground plane width  $W_g$  increases the two resonances merges and hence bandwidth is increased.

Impedance bandwidth versus ground plane width  $W_g$  is plotted in Fig.4.18. Maximum bandwidth of 39% is observed for  $W_g = 0.5\lambda_{d1}$ . For further



increase in width  $W_g$ , bandwidth decreases. This variation is similar to that reported in [1] for the case of symmetric printed monopole.

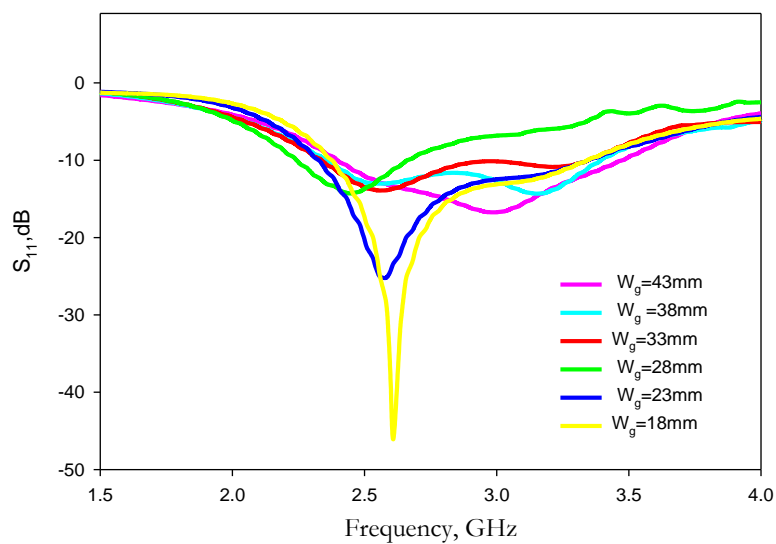


Fig.4.17. Variation of resonant frequencies with ground plane width  $W_g$  ( $L_g = 76\text{mm}$ ,  $l_m = 19\text{mm}$ ,  $w = 3\text{mm}$ ,  $d_1 = 24\text{mm}$ ,  $\epsilon_r = 4.4$ ,  $h = 1.6\text{mm}$ )

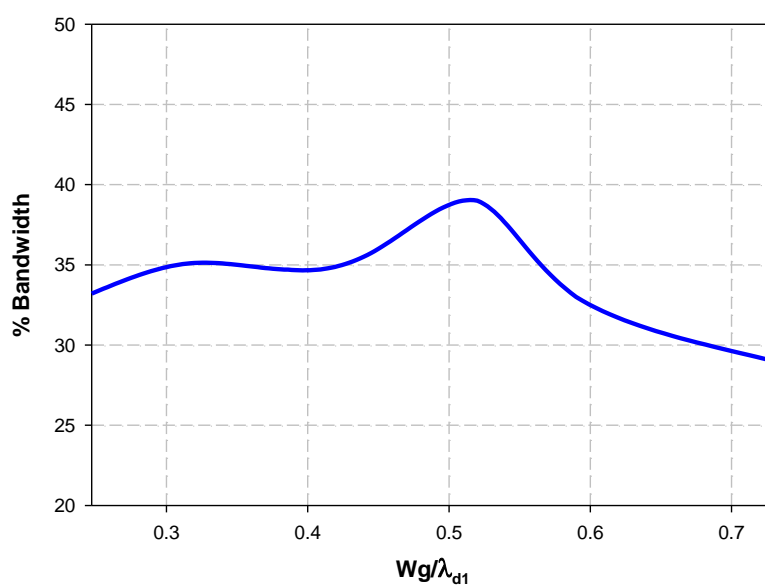


Fig.4.18 Bandwidth variation for different ground plane widths ( $L_g = 76\text{mm}$ ,  $l_m = 19\text{mm}$ ,  $w = 3\text{mm}$ ,  $d_1 = 24\text{mm}$ ,  $\epsilon_r = 4.4$ ,  $h = 1.6\text{mm}$ )

## Conclusion

In this section a microstrip-fed printed monopole antenna is thoroughly analyzed. The main inferences obtained from the experimental and simulation studies are described below.

- ♣ A printed monopole having a length of  $0.25\lambda_d$  with a ground plane dimensions  $\lambda_d \times 0.5\lambda_d$  will give two resonances. One is primarily due to monopole strip and the other is due to the L shaped path which includes both the monopole strip and the ground plane length ( $d_2$ )
- ♣ Impedance bandwidth for both the above resonances can be properly matched by offsetting the microstrip feed line.
- ♣ While offsetting the feed line there exist three resonant paths; one due to monopole strip, second due to the L shaped current path and the third one due to reflected L shaped path. Matching for the third resonance corresponding to reflected L shaped path is poor and it is at the higher end. So in the present study first two modes are considered for analysis.
- ♣ Even though offset feeding improves matching and gives good impedance bandwidth, high asymmetry in the configuration gives highly distorted radiation pattern.
- ♣ Ground plane truncation has significant impact on resonant frequencies and bandwidth. Ground plane width ( $W_g$ ) has very little influence on resonant frequencies but strong impact on bandwidths. Maximum bandwidth is observed for a width  $W_g$  of  $0.5\lambda_d$
- ♣ Ground plane length ( $L_g$ ) affects both the resonances and the variation is predominant for second resonance. This again confirms L shaped resonant path for second resonance. Variation of the first

resonance is more if ground plane length  $L_g$  is less than  $0.8\lambda_d$ . For a very finite  $L_g$ , matching for second resonance is poor and the antenna exhibits good performance only in first mode.

- ♣ Since truncated ground plane has significant impact on resonant frequencies, a suitable modification on the ground plane to enhance the current path will result in two distinct resonances.
- ♣ These resonances can be fine-tuned to lower resonant bands without compromising the compactness.

In the next section the ground plane is modified to excite a lower resonance by adding another strip. Ground plane modification not only lowers the resonant frequency but reduces the antenna dimension.

## 4.2 Compact printed antenna with modified ground plane

The microstrip fed printed monopole antenna with offset feed gives two distinct resonances as discussed in the previous section. But the main drawbacks for the present design are the large size and highly distorted radiation pattern due to the asymmetry in the configuration. For compact applications, ground plane of the printed monopole should be small so as to reduce the total antenna dimensions. But the analysis carried out in the previous section concludes that as the ground plane dimension becomes finite the second resonance shifts towards higher frequency range with poor matching. So for a compact ground plane, antenna shows only single resonance with good impedance match. Since the ground plane length controls the second resonance, resonant frequency can be lowered by modifying the ground plane without affecting the compactness. Etching an additional strip as an extension to the ground plane, parallel to the signal strip is an effective solution to lower the frequency without affecting the compactness. So keeping compactness as the primary concern a detailed investigation has been carried out on

microstrip-fed printed monopole configuration by adding an additional strip to the ground plane and described in this section. For the initial analysis the monopole configuration having compact dimensions  $0.5\lambda_d \times 0.25\lambda_d$  is chosen. The proposed configuration after adding the strip is shown in Fig.4.19.

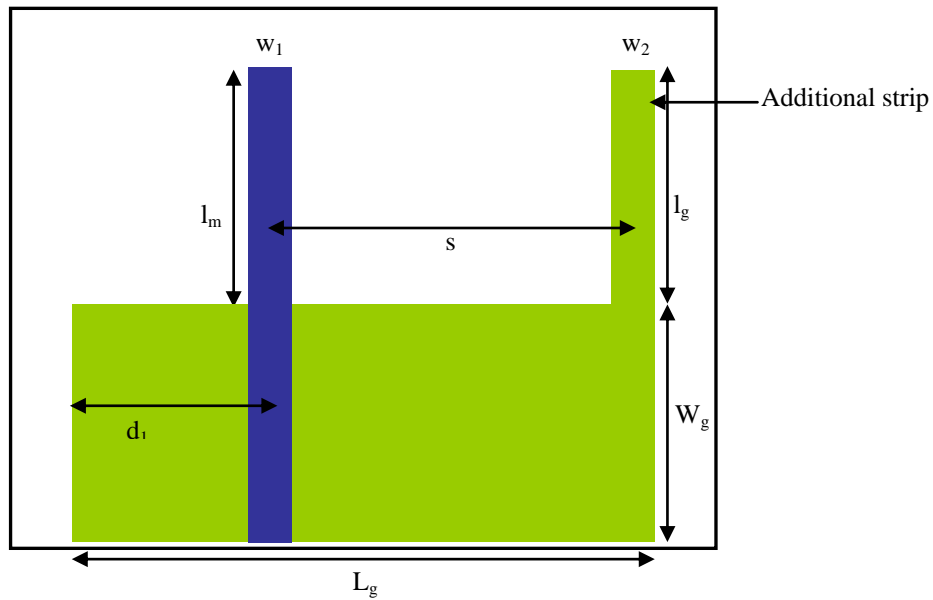


Fig.4.19. Microstrip- fed printed monopole with additional strip

#### 4.2.1 Effect of adding additional strip on printed monopole configuration

##### 4.2.1.1 Description of the problem

Main objective of this analysis is to derive a compact dual band antenna from the printed monopole configuration. As mentioned in the previous section, on a finite ground plane, the printed monopole gives only first mode in lower frequency range. So an attempt has been made to obtain another lower resonance in finite ground plane. For this a printed monopole with a finite ground plane dimension,  $0.5 \lambda_d \times 0.25 \lambda_d$  is chosen as a primary structure.

The compact monopole configuration which is used as the primary design for the analysis is shown in Fig.4.20. The proposed configuration has been analyzed using FDTD technique. MATLAB based in-house codes were developed for simulation of the antenna.

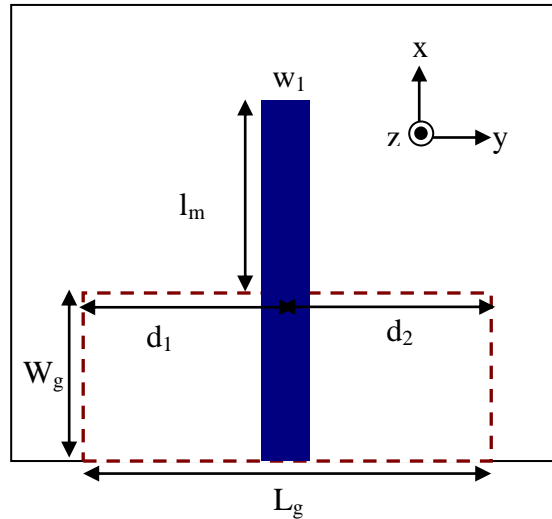
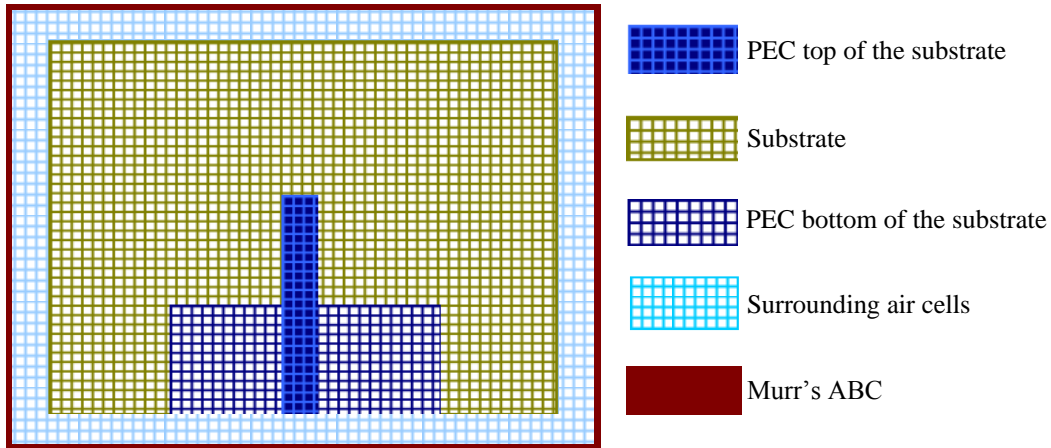


Fig.4.20. Microstrip-fed printed strip monopole antenna  
( $L_g = 0.5\lambda_d$ ,  $W_g = 0.25\lambda_d$ ,  $d_1=d_2= 0.25 \lambda_d$  ,  $l_m = 0.25\lambda_d$ ,  $w_1=3\text{mm}$ )

The length of the monopole ' $l_m$ ' is kept as 19mm and the ground plane dimensions are  $L_g=38\text{mm}$  and  $W_g=19\text{mm}$ . FR4 substrate of dielectric constant,  $\epsilon_r= 4.4$  and height,  $h=1.6\text{mm}$  is used for fabricating the antenna.

Two dimensional view of the FDTD computation domain is shown in Fig.4.21. The computational domain is divided into Yee cells of dimension  $\Delta x=\Delta y=0.5\text{mm}$  and  $\Delta z=0.4\text{mm}$ . Since substrate thickness is 1.6mm, 4 cells will exactly match substrate thickness. 15 cells on each of the 6 sides are used to model air cells. Substrate is modelled by a computational volume of  $96\Delta x*100\Delta y*4\Delta z$ . Thus the total computation domain is discretized into  $126\Delta x*130\Delta y*34\Delta z$  cells. Luebber's feed model is employed to excite the microstrip line feed of the antenna and a Gaussian pulse is used as the

source of excitation. Time step used for the computation is 0.95ps. The Gaussian half-width is  $T = 20\text{ps}$  and the time delay  $t_0$  is set to be  $3T$ .



**Fig.4.21.** 2D view of FDTD computation domain of microstrip line fed printed monopole antenna

#### **4.2.1.2 Reflection characteristics**

The computed and measured reflection characteristics of the above configuration are illustrated in Fig.4.22. Antenna shows resonance at 2.76GHz with a bandwidth of 19%. As explained in the previous section this resonance is primarily due to the monopole strip. Since the ground plane used is finite the second resonance corresponds to the L-shaped path shifts towards higher end of the spectrum.

The resultant electric field distribution computed one cell above the top layer of the dielectric substrate using FDTD technique at the resonant frequency is given in Fig.4.23b. A quarter wave variation of the electric field is observed on the monopole strip. The computed time domain response of the  $E_z$  component at the feed point is depicted in Fig. 4.23a. It is observed that the voltage is at steady state after 4000 time steps. So for all computations 5000 time steps is taken.

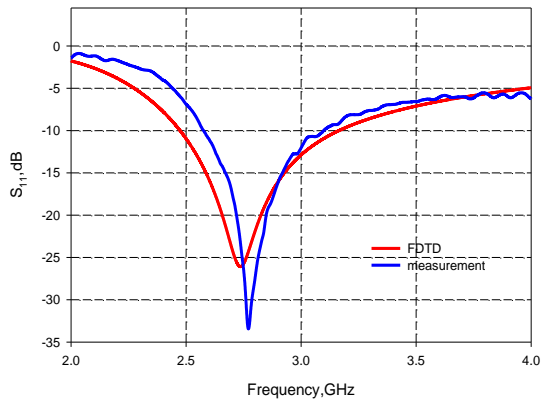


**Fig.4.22.** Reflection characteristics of the microstrip-fed printed monopole ( $L_g = 38\text{mm}$ ,  $W_g = 19\text{mm}$ ,  $l_m = 19\text{mm}$ ,  $d_1 = d_2 = 19\text{mm}$ ,  $w_1 = 3\text{mm}$ )

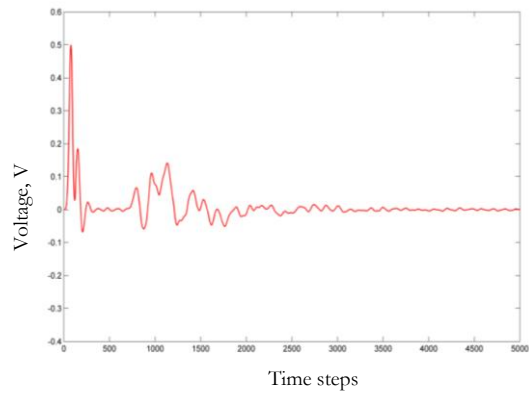


**Fig.4.23a.** Computed time domain characteristics at the feed point ( $L_g = 38\text{mm}$ ,  $W_g = 19\text{mm}$ ,  $l_m = 19\text{mm}$ ,  $d_1 = d_2 = 19\text{mm}$ ,  $w_1 = 3\text{mm}$ )

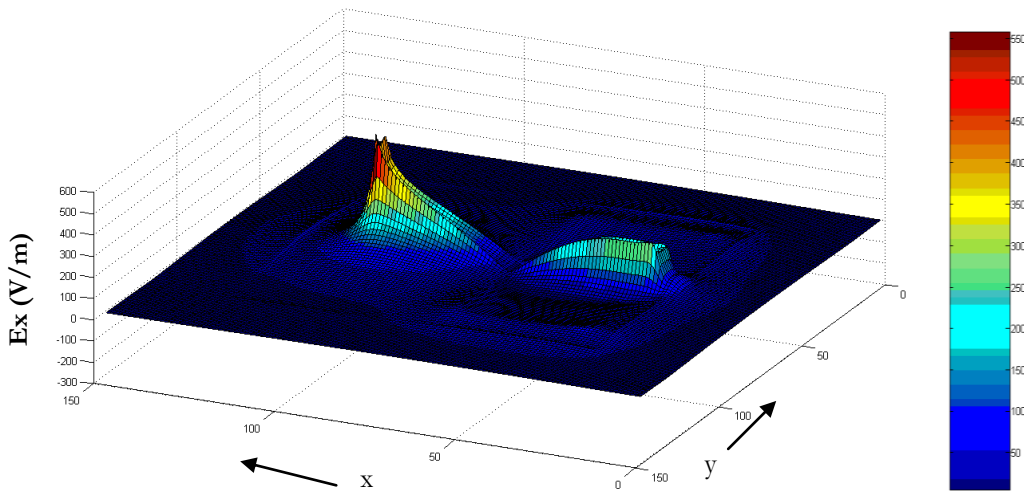


**Fig.4.23b** The resultant E-field computed using FDTD, one cell above the substrate at 2.76GHz after 5000 time steps

#### 4.2.1.3 Radiation characteristics

The measured and computed radiation patterns of the antenna at the resonant frequency are shown in Fig.4.24. The radiation pattern is similar to that of a half wave dipole with a null along the axial direction.

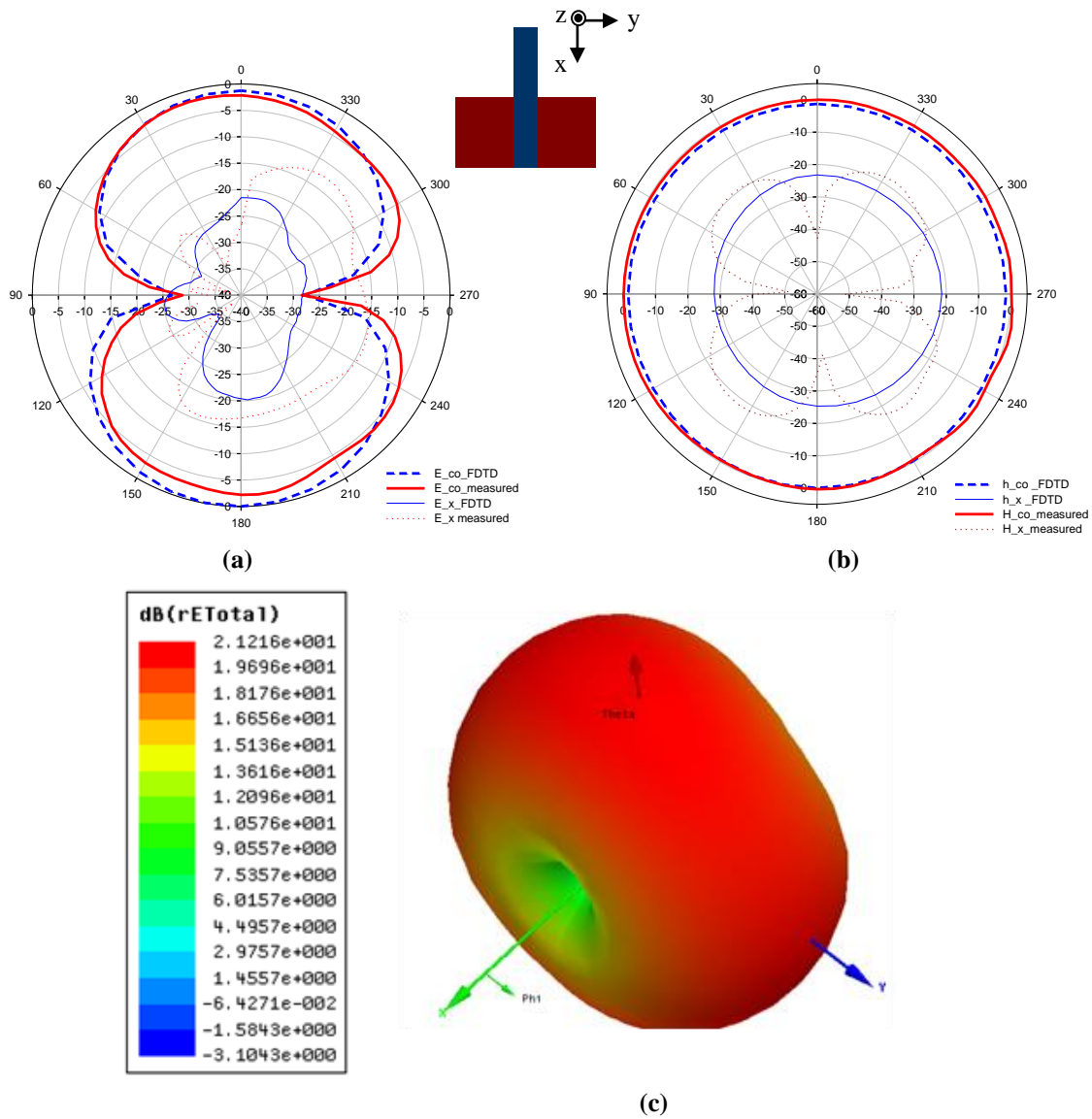


Fig.4.24 Radiation pattern of the microstrip - fed printed monopole ( $L_g = 38\text{mm}$ ,  $W_g = 19\text{mm}$ ,  $l_m = 19\text{mm}$ ,  $d_1 = d_2 = 19\text{mm}$ ,  $w_1 = 3\text{mm}$ )  
 (a) E plane (b) H plane (c) 3D pattern

Antenna is linearly polarized along x-direction. Fig. 4.24(a) and (b) shows two principal plane patterns, in which E-plane pattern is figure of eight with a half power beam width of  $80^\circ$ . H-plane pattern is non directional. Cross polarization is better than  $-20\text{dB}$ . This again confirms that



for the fundamental mode radiation from the ground plane edge is negligible and the primary radiator is the monopole strip.

The three dimensional simulated radiation pattern obtained from HFSS is given in Fig.4.24c. Radiation pattern is similar to a toroid along x axis.

#### 4.2.1.4. Gain and Efficiency

Gain of the antenna is measured using gain transfer method and is shown in Fig.4.25. Antenna shows an average gain of 2.24dBi in the band. Computed efficiency of the antenna at the resonant frequency is 93%. So compared to the earlier antenna, the efficiency is slightly increased.

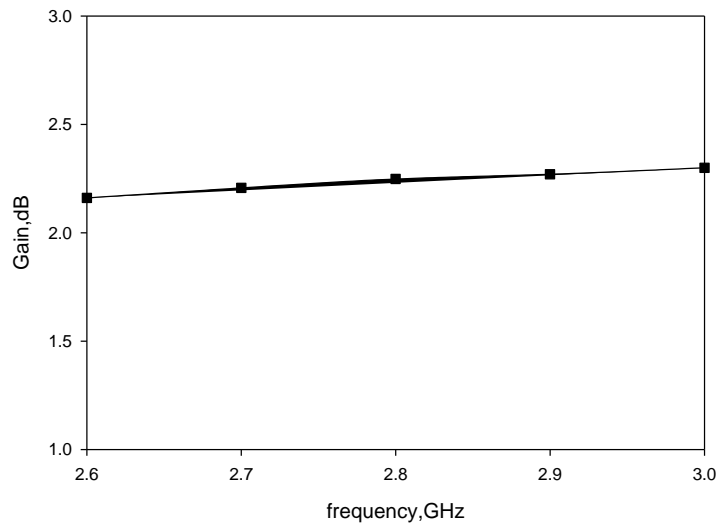


Fig.4.25 Gain of the printed monopole antenna with finite ground plane ( $L_g = 38\text{mm}$ ,  $W_g = 19\text{mm}$ ,  $l_m = 19\text{mm}$ ,  $d_1 = d_2 = 19\text{mm}$ ,  $w_1 = 3\text{mm}$ )

#### 4.2.2. Feed offsetting to achieve compactness

The present printed monopole configuration studied in the previous section resonates at 2.76GHz with a 2:1 VSWR bandwidth of 460MHz. The main objective of this section is to achieve a lower resonance without losing the compactness as mentioned in the previous section. So the ground plane

has to be modified by extending another strip from the ground plane as mentioned in Fig.4.19.

Resonant length corresponding to the new resonance can be increased by keeping the separation between the monopole strips at the maximum. Feed line offset study carried out in the previous section also reveals that feed offsetting can improve the impedance bandwidth. For achieving good impedance bandwidth along with compactness, the feed offset distance 'd<sub>1</sub>' has been varied as did in the previous section and the corresponding reflection characteristics are plotted in Fig.4.26.

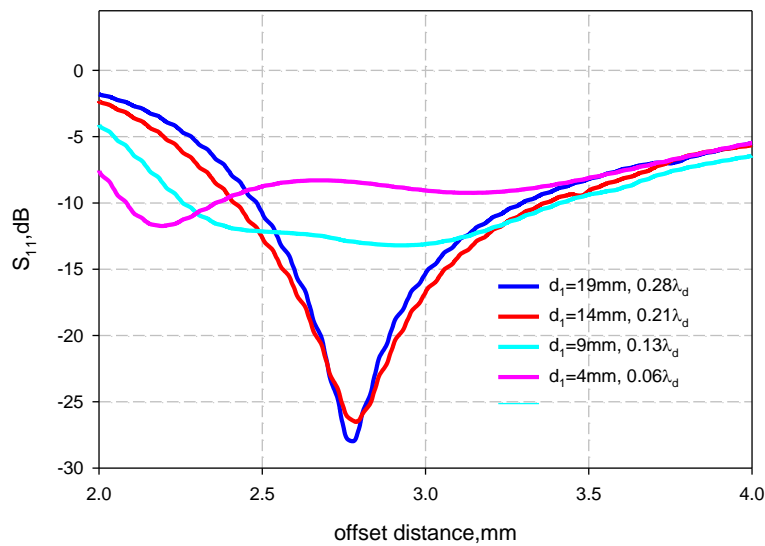


Fig.4.26. Reflection characteristics for various feed offset positions ( $L_g = 38\text{mm}$ ,  $W_g = 19\text{mm}$ ,  $l_m = 19\text{mm}$   $w_1 = 3\text{mm}$ )

Maximum bandwidth is achieved for an offset distance  $d_1 = 0.13\lambda_d$ , where  $\lambda_d$  is the effective wavelength in the substrate corresponds to the first resonance. Here the wideband response is due to the merging of the two resonances, one due to the fundamental mode and the other due to the L-shaped path including the ground plane as concluded from the previous section. Due to the feed offsetting, L shaped path corresponding to the second resonance is increased and resonance shifts toward the lower

frequency side. This structure offers a 40% bandwidth by merging 2.5GHz and 3GHz respectively. For further decrease in  $d_1$  impedance matching becomes poor since the feed line shifts towards the edge of the ground plane.

### Radiation pattern

The 3D radiation patterns of the compact offset fed printed monopole antenna simulated at the two resonant frequencies are given in Fig.4.27. Fig 4.27a shows the 3D pattern at 2.5GHz. Compared to the symmetric monopole, beam is tilted by an angle of  $30^\circ$  in the azimuth plane. Where as for 3GHz, beam has been shifted by an angle of  $20^\circ$  in the azimuth plane. Due to the asymmetry in the geometry, there exists an asymmetric current flow on the ground plane which modifies the radiation pattern. The resultant pattern is tilted compared to the normal printed monopole.

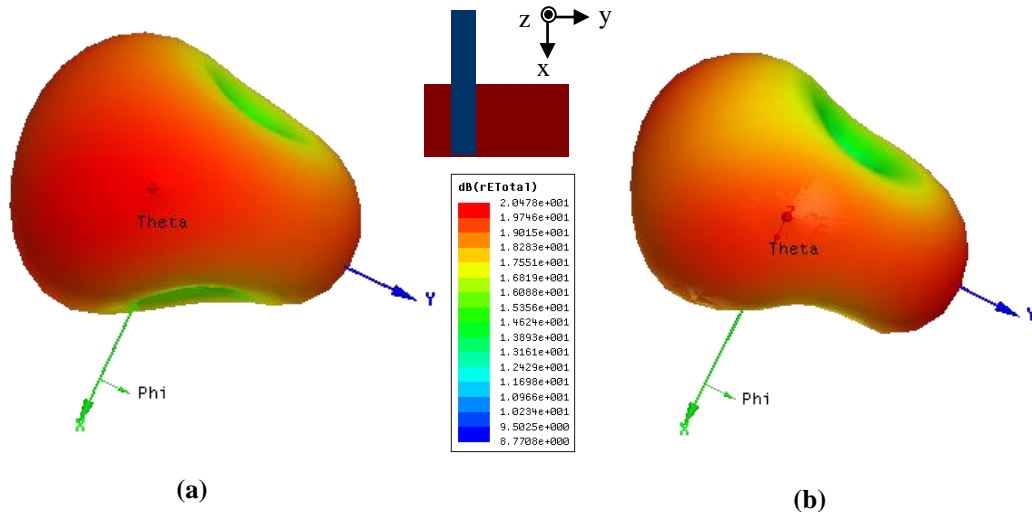


**Fig.4.27 3D Radiation pattern**  
 $(L_g = 38\text{mm}, W_g = 19\text{mm}, l_m = 19\text{mm}, w_1 = 3\text{mm}, d_1 = 9\text{mm})$   
 (a) 2.5GHz (b) 3GHz

Two dimensional patterns measured along the xz plane and yz plane for the two resonant frequencies are shown in Fig.4.28. The cross polar level is high in both the operating bands due to the radiation from the ground plane.

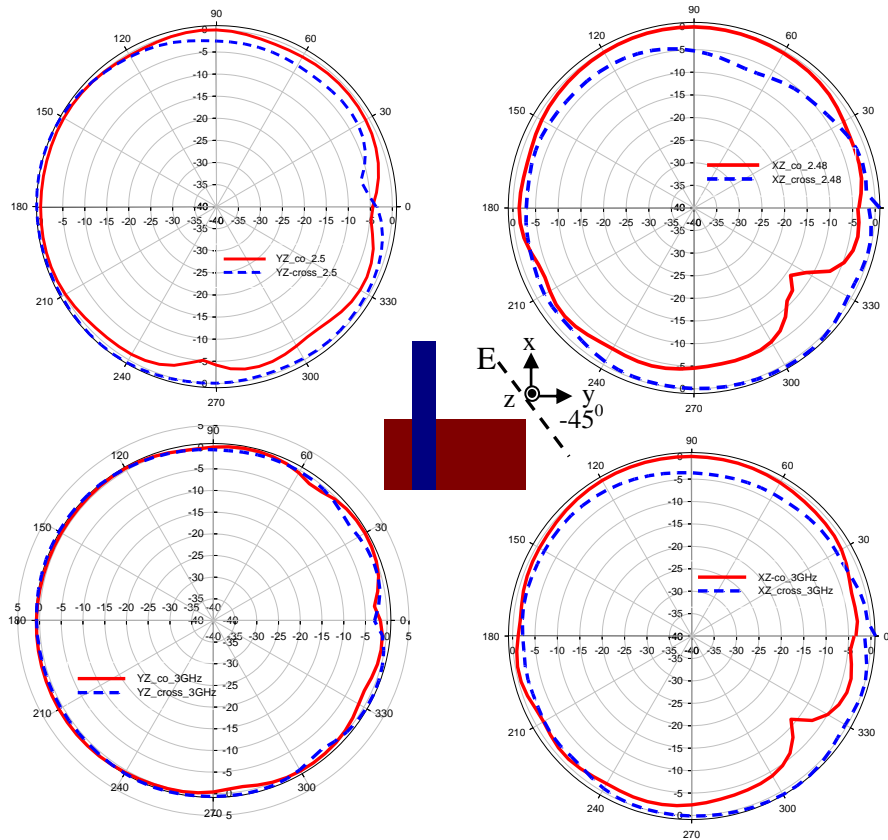


Fig.4.28 2D radiation patterns  
( $L_g = 38\text{mm}$ ,  $W_g = 19\text{mm}$ ,  $l_m = 19\text{mm}$ ,  $d_1 = 9\text{mm}$ )

Polarization vector of the antenna is tilted by an angle of  $-45^\circ$  with respect to the y axis for both the bands. X-polarised and Y-polarised components show almost equal intensity along the maximum beam direction. Where as the electric field measured at  $-45^\circ$  shows an increment of 3dB compared to the horizontal and vertical component. Due to the offset in feeding, the Y component of the electric field (due to the ground plane) also dominates and the resultant  $\mathbf{E}$  vector has been tilted by an angle of  $-45^\circ$ .

### Gain and Efficiency

Antenna shows 2.13dBi gain with an efficiency of 90% at the lower resonant frequency (2.5GHz). Where as the gain and efficiency at the higher resonant frequency (3GHz) are 2.32dBi and 87% respectively.

### 4.2.3 Impact of additional strip

A 3mm strip of length  $l_g$  same as that of the monopole strip is added at the bottom surface of the substrate as an extension from the ground plane as shown in Fig.4.19. From the feed offset analysis conducted in the earlier section it is found that  $d_1=0.13\lambda_{d1}$  is the optimum and hence taken for the present analysis. The strip  $l_g$  is placed at a spacing  $s=27.5\text{mm}$  from the centre of the first strip; which is the maximum possible distance from the first strip. Maximum distance is selected so as to increase the resonant length corresponding to the second resonance and to avoid the coupling effect from the signal strip ( $l_m$ ). Coupling between the signal strip and the ground strip ( $l_g$ ) can adversely affect the resonance and radiation from both the strips. A detailed investigation on the coupling effect is carried out in section 4.2.3.3.

#### 4.2.3.1 Reflection characteristics

Measured and simulated reflection characteristics after adding strip ' $l_g$ ' is given in Fig. 4.29.

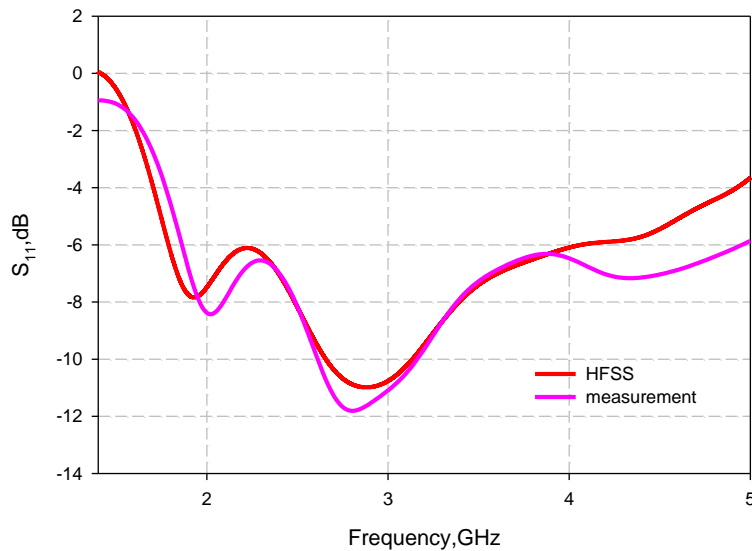
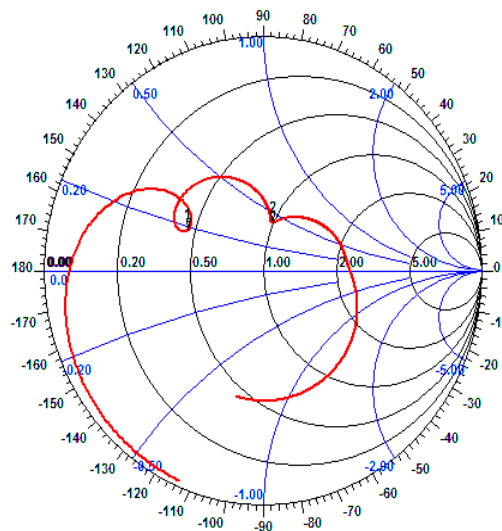


Fig.4.29 Reflection characteristics with additional strip  $l_g$   
 $(L_g = 38\text{mm}, W_g = 19\text{mm}, l_m = 19\text{mm}, l_g = 19\text{mm}, w_1 = w_2 = 3\text{mm},$   
 $d_1 = 9\text{mm}, s = 27.5\text{mm})$

After adding strip  $l_g$ , the higher resonance in the offset fed monopole is shifted to the lower side. Antenna shows a lower resonance at 2GHz. The fundamental resonance at 2.5GHz is shifted towards 2.82GHz. The resonance at 3GHz, which was due to the L shaped path, has been shifted to 2GHz. Now the L shaped resonant path becomes U shaped, and which is  $0.68\lambda_{d1}$  in length. Where  $\lambda_{d1}$  is the wavelength in the substrate corresponding to 2GHz. Impedance matching is poor at the lower band. So this mode is not matched. Smith chart showing the input impedance for both the resonances is given in Fig.4.30.

The coupling between the signal strip and the ground strip can be properly tuned to achieve good impedance match. Effect of coupling between the signal strip and ground strip is analyzed in the following section.



**Fig.4.30** Smith chart for the printed monopole with additional strip  $l_g$  ( $L_g = 38\text{mm}$ ,  $W_g = 19\text{mm}$ ,  $l_m = 19\text{mm}$ ,  $l_g = 19\text{mm}$ ,  $w_1 = w_2 = 3\text{mm}$ ,  $d_1 = 9\text{mm}$ ,  $s = 27.5\text{mm}$ )

#### **4.2.3.2. Radiation Mechanism**

The simulated surface current distributions for both the resonances are shown in Fig.4.31. For the higher resonance (2.82GHz), surface current density

is more on the signal strip than on the ground plane and ground strip. This clearly indicates that ground strip has very little impact on the second resonance which is primarily due to the monopole strip on top of the substrate. However, the ground strip ( $l_g$ ) slightly affects the radiation pattern at the higher resonance. The variation in  $l_g$  can change the coupling between the strips and hence may vary the impedance match and slightly the resonant frequency. This is discussed in the section 4.2.3.5.

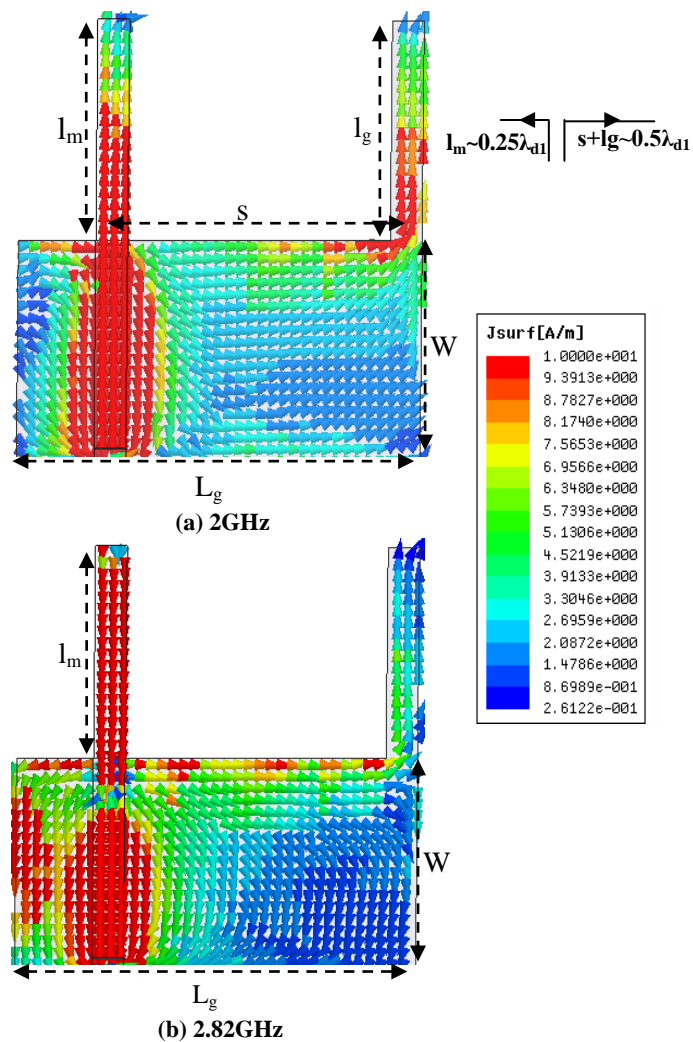


Fig.4.31 Simulated surface current distribution  
 $(L_g = 38\text{mm}, W_g = 19\text{mm}, l_m = 19\text{mm}, l_g = 19\text{mm}, w_1 = w_2 = 3\text{mm},$   
 $d_1 = 9\text{mm}, s = 27.5\text{mm})$

But for the lower resonance there exist a significant current distribution on both the strips as well as on the ground plane between the strips as shown in Fig.4.31a. In this case the resonant length ( $l_m+s+l_g$ ) is nearly  $0.68\lambda_{d1}$  and the current distribution clearly shows this mode on the structure. From the current distribution it can be inferred that for the lower resonance, antenna behaves as shown in Fig.4.32.

This configuration behaves as an asymmetrically fed dipole with one 'I' shaped strip on top of the substrate and an 'inverted L' shaped strip on bottom of the substrate. The electric field at the tip of the microstrip line can be modelled as the excitation source (gap voltage) for the asymmetric dipole as shown in the figure. Currents on the vertical strips are in the same direction, which favours the radiation. This is achieved by the current path of length 's' which is also acting as a balun. This avoids the use of balun in the design and leads towards a simple dipole configuration.

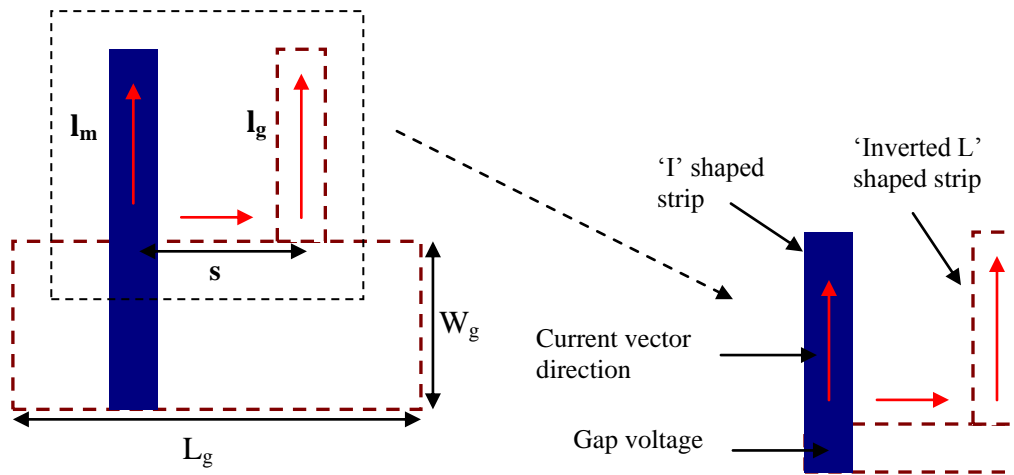


Fig.4.32. Equivalent model of asymmetric fed dipole

### Radiation pattern

The simulated 3D pattern at lower (2GHz) and higher resonances (2.82GHz) are given in Fig.4.33. For both the bands, beam of the antenna is



tilted by an angle of  $+30^\circ$  in the azimuth plane ( $\phi=+30^\circ$ ). The antenna is polarized along the x axis for both the resonances.

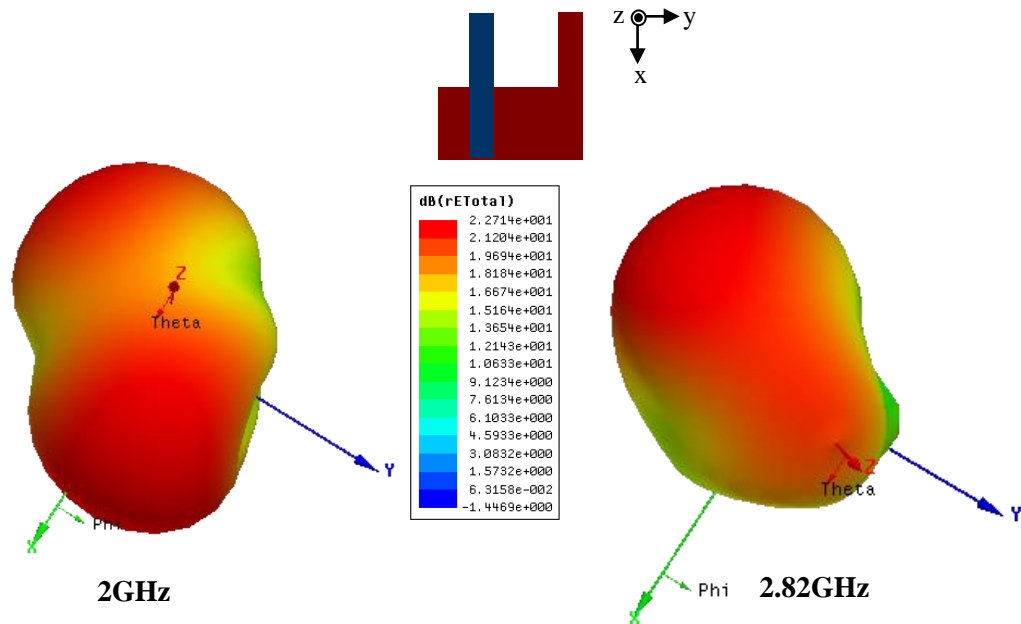


Fig.4.33. 3D radiation pattern  
 $(L_g = 38\text{mm}, W_g = 19\text{mm}, l_m = 19\text{mm}, l_g = 19\text{mm}, w_1 = w_2 = 3\text{mm}, s = 27.5\text{mm}, d_1 = 9\text{mm})$

#### 4.2.3.3 Impact of coupling between the strips

The important parameter which affects the impedance match in this case is the coupling between the signal strip ( $l_m$ ) and the newly added strip on the ground plane ( $l_g$ ). This coupling effect can be studied by varying the spacing 's' between the strips.

The detailed analysis has been carried out by varying the spacing 's' from  $s=27.5\text{mm}$  (the present position) to  $s=0$  by keeping all the other parameters constant. The reflection characteristics are plotted in Fig.4.34. As the spacing 's' decreases lower resonance shifts towards the higher side of the spectrum where as the higher resonance remains almost stable. As the spacing 's' decreases, the 'U' shaped resonant path corresponding to the lower resonance also decreases and the resonant frequency increases. But for very

small values of 's' (<10.5mm) matching is very poor for both the frequencies. For small spacing, the capacitive coupling between the signal strip on top of the substrate and the strip on the ground plane is high. When s=0, the two strips are placed just like a bifilar line and the configuration acts like an open transmission line. In this case radiation will be very poor and it cannot be used as an antenna.

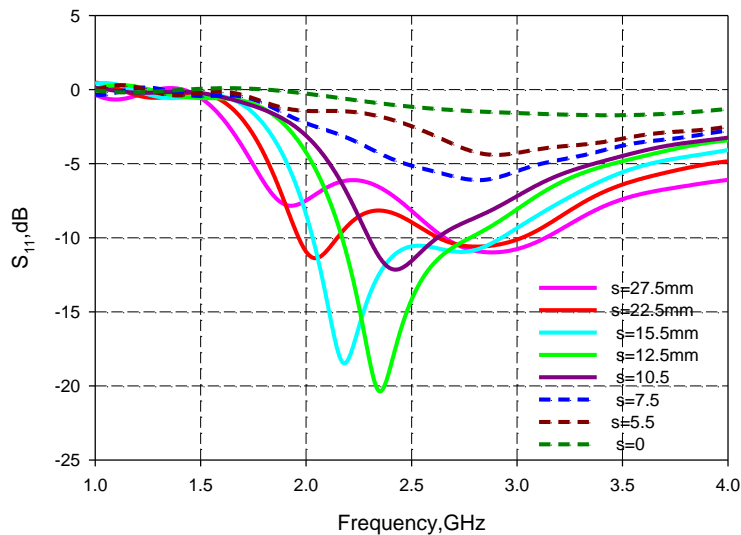


**Fig.4.34. Reflection characteristics for different spacing 's'**  
 ( $L_g = 38\text{mm}$ ,  $W_g = 19\text{mm}$ ,  $l_m = 19\text{mm}$ ,  $w_1 = w_2 = 3\text{mm}$ ,  $l_g = 19\text{mm}$ ,  $d_1 = 9\text{mm}$ )

The input impedance variation for different spacing s is shown in Fig.4.35. As spacing decreases, imaginary part of the input impedance for the higher resonance becomes less inductive. This is due to the capacitive coupling between the strips and hence loses the impedance matching. Whereas for the lower resonance impedance became more inductive. Real part of the impedance increases with decreases in spacing for the lower resonance.

The normalised resonant length ('U' shaped path= $l_m+s+l_g$ ) plotted against spacing 's' is given in Fig.4.36. It is clear that  $U/\lambda_{d1}$  remains almost constant throughout 's' variation. Where  $U=l_m+s+l_g$  and  $\lambda_{d1}$  is the wavelength in the

substrate corresponding to the first resonance. This confirms the resonant length for the first resonance. Average length of ‘U’ shaped path is  $\sim 0.65\lambda_{d1}$ .

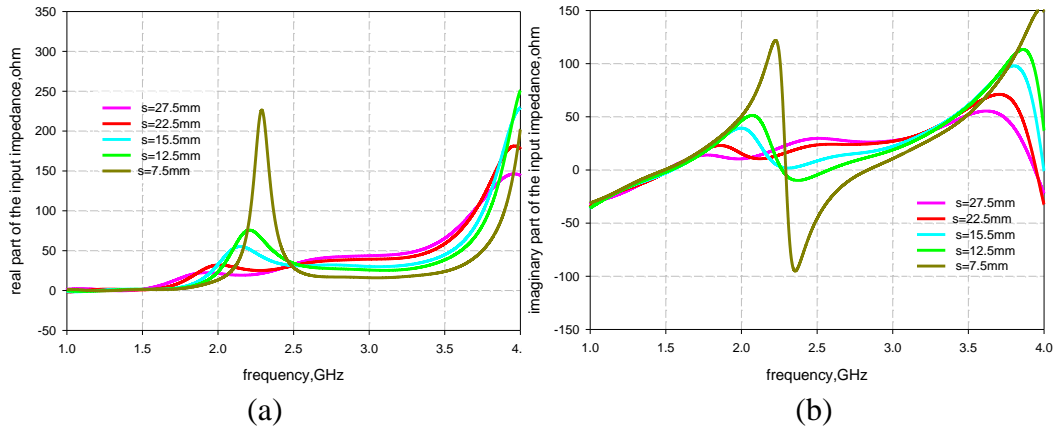


**Fig.4.35. Input impedance variation for different spacing's'**  
 $(L_g = 38\text{mm}, W_g = 19\text{mm}, l_m = 19\text{mm}, l_g = 19\text{mm}, w_1 = w_2 = 3\text{mm}, d_1 = 9\text{mm})$   
 (a) Real part (b) Imaginary part

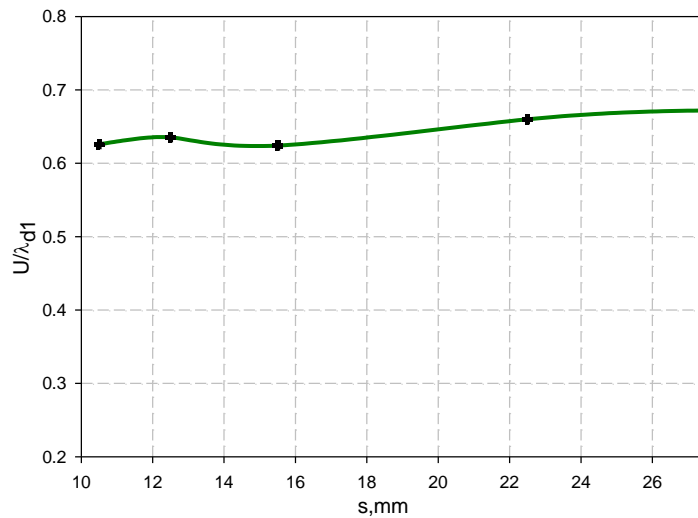


**Fig.4.36. Resonant length variation for different spacing (s)**  
 $(L_g = 38\text{mm}, W_g = 19\text{mm}, l_g = 19\text{mm}, l_m = 19\text{mm}, w_1 = w_2 = 3\text{mm}, d_1 = 9\text{mm})$

The optimized value of spacing ‘s’ for maximum bandwidth is  $0.17\lambda_{d1}$ . The measured and simulated reflection characteristic for this case is shown in Fig.4.37. In this case antenna resonates with a 2:1 VSWR bandwidth of 34.6%.

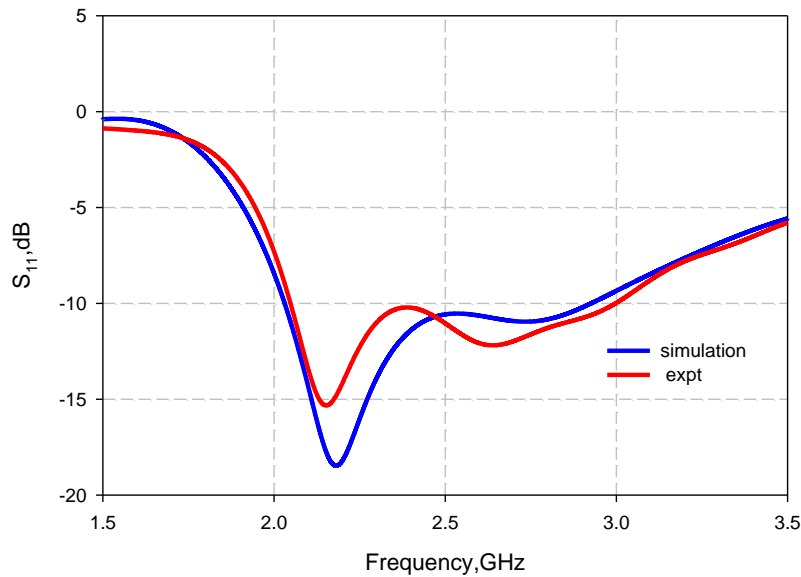
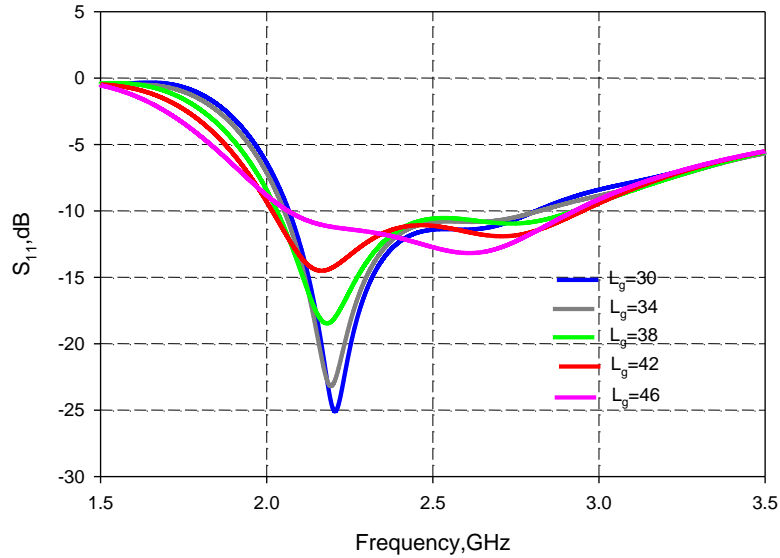


Fig.4.37. Reflection characteristics corresponding to optimized spacing,  $s=15.5\text{mm}$   
 $(L_g = 38\text{mm}, W_g = 19\text{mm}, l_m = 19\text{mm}, l_g = 19\text{mm}, w_1 = w_2 = 3\text{mm}, d_1 = 9\text{mm})$

#### 4.2.3.4. Ground plane optimization

Finite ground plane effect has been studied in section 4.1.7 for the case of microstrip-fed printed monopole and it has been observed that resonant frequency due to the monopole strip also vary with respect to the variation of ground plane length. It is also found that ground plane width affects the bandwidth.

In this section impact of ground plane dimensions on both the resonant frequencies of the dual strip antenna is analysed. The analysis has been carried out on dual strip configuration with optimized spacing ' $s$ '= $0.17\lambda_{d1}$ . This configuration resonates at 2.16GHz and 2.74GHz with a wide impedance bandwidth of 35%. In the earlier section ' $d_1$ ' is optimized as  $0.13\lambda_d$  beyond that feed line shows spurious radiations. So in the observation given below  $L_g$  is varied by keeping ' $d_1$ ' and ' $s$ ' as constant.



**Fig.4.38.** Reflection characteristics for different  $L_g$   
 ( $W_g = 19\text{mm}$ ,  $l_m = 19\text{mm}$ ,  $l_g = 19\text{mm}$ ,  $w_1 = w_2 = 3\text{mm}$ ,  
 $s = 15.5\text{mm}$ ,  $d_1 = 9\text{mm}$ )

The reflection characteristics obtained is given in Fig.4.38. It is observed that as  $L_g$  varies both the resonances remains almost constant. The variation in  $L_g$  will not affect the 'U' shaped current path and hence no variation for lower resonance.

The 2:1 VSWR bandwidth shows considerable variation with respect to  $L_g$ . Variations of percentage bandwidth for different  $L_g$  values are summarized in Table4.1. Bandwidth increases as  $L_g$  increases and reaches a maximum of 36% at  $L_g = 42\text{mm}$ . Variation of percentage bandwidth against normalised  $L_g$  is given in Fig.4.39. There is an optimum dimension for  $L_g$  for good impedance bandwidth. Keeping compactness as one of the important criteria,  $L_g = 38\text{mm}$ , which is equal to  $0.55\lambda_{d2}$  for which antenna shows 35% bandwidth can be taken as the optimum ground plane length. Where  $\lambda_{d2}$  is the wavelength in the substrate corresponds to the higher resonance.

**Table.4.1 Variation of percentage bandwidth with respect to  $L_g$**   
 ( $W_g = 19\text{mm}$ ,  $l_m = 19\text{mm}$ ,  $l_g = 19\text{mm}$ ,  $w_1 = w_2 = 3\text{mm}$ ,  $s = 15.5\text{mm}$ ,  $d_1 = 9\text{mm}$ )

Ground plane Length, $L_g$ (mm)	Percentage Bandwidth
28	30.5
30	30.6
32	30.2
34	31.3
36	33.7
38	35
42	36
46	35
50	29.5
54	29.3

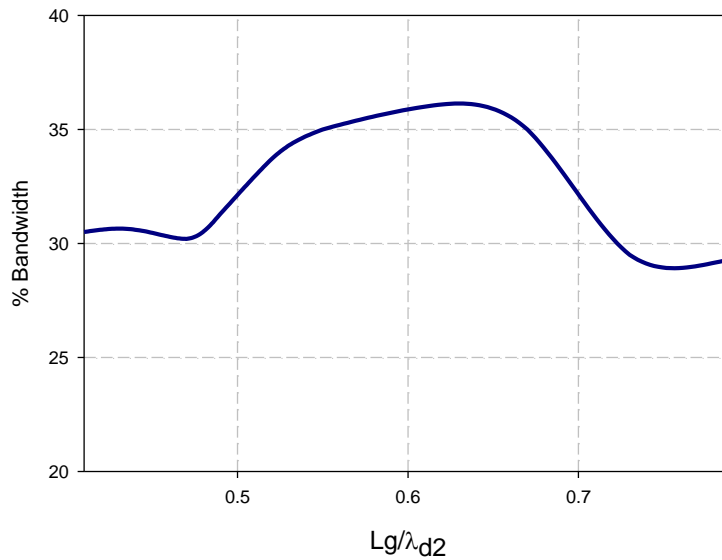


**Fig.4.39 Variation of percentage bandwidth with respect to  $L_g/\lambda_{d2}$**

After optimizing the ground plane length  $L_g$  for better impedance bandwidth, analysis has been carried out to optimize the ground plane width  $W_g$  for better performance. Dual strip antenna with optimized spacing and ground plane length  $L_g$  is taken for the analysis. Ground width  $W_g$  has been studied by keeping the length of the monopole strip and ground strip equal to 19mm.

Reflection characteristics obtained for different  $W_g$  values are plotted in Fig.4.40. As  $W_g$  increases there is a slight shift in the resonant frequencies. The two resonances merged together to give a wideband as shown in the figure. Variation of percentage bandwidth with ground plane width  $W_g$  is summarized in Table.4.2. As  $W_g$  increases, percentage bandwidth also increases. For  $W_g=19\text{mm}$  which corresponds to a length of  $0.28\lambda_{d2}$ , 35% bandwidth is observed. Where  $\lambda_{d2}$  is the wavelength in the substrate corresponding to higher resonance.

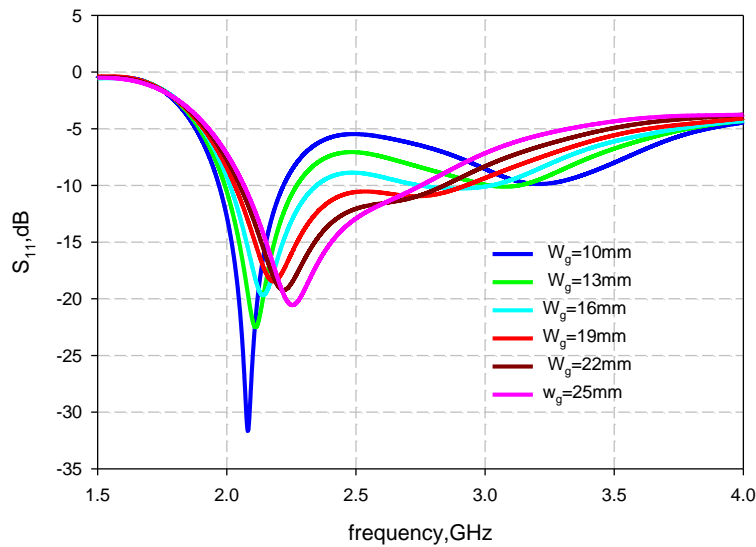


Fig. 4.40. Reflection characteristics for different  $W_g$   
 ( $L_g = 38\text{mm}$ ,  $l_m = 19\text{mm}$ ,  $l_g = 19\text{mm}$ ,  $w_1 = w_2 = 3\text{mm}$ ,  $s = 15.5\text{mm}$ ,  $d_1 = 9\text{mm}$ )

Table.4.2. Variation of percentage bandwidth with respect to  $W_g$   
 ( $L_g = 38\text{mm}$ ,  $l_m = 19\text{mm}$ ,  $l_g = 19\text{mm}$ ,  $w_1 = w_2 = 3\text{mm}$ ,  $s = 15.5\text{mm}$ ,  $d_1 = 9\text{mm}$ )

Ground plane Width, $W_g$ (mm)		Percentage Bandwidth	
$W_g$ (mm)	$W_g/\lambda_{d2}$	First band	Second band
10	0.18	12	No matching
13	0.22	13.2	5.4
16	0.25	15	11
19	0.28	35, merged together	
22	0.32	32, merged together	
25	0.34	28, merged together	

#### 4.2.3.5 Impact of strip length $l_g$

The previous analysis concludes that the spacing between the strips is the decisive parameter to achieve good impedance bandwidth. Now the effect of strip lengths on resonant frequency has to be found out to confirm the resonance and to formulate design equations. In this section the role of ground strip length ' $l_g$ ' on resonant frequencies is studied. The analysis has been carried out on dual strip antenna configuration with optimized spacing  $s=0.17\lambda_{d1}$  and  $L_g=0.55\lambda_{d2}$ ,  $W_g=0.28\lambda_{d2}$ ,  $d_1=0.13\lambda_{d2}$ .

Variation of resonant frequencies with respect to ' $l_g$ ' is summarized in Table 4.3. It is shown that as  $l_g$  increases, first resonance decreases almost linearly. Where as there is not much change for the second resonance. This again confirms the conclusions derived from the analysis of the offset fed printed monopole antenna. Since ' $l_g$ ' is one of the important parameter which forms the 'U' shaped current path corresponding to the lower resonance, the reduction in lower resonance with increase in  $l_g$  is as expected. From the analysis it is clear that  $U/\lambda_{d1}$  remain constant for  $l_g$  variation. This gives a strong indication that lower resonance can be controlled by strip length ' $l_g$ '. The variation in higher resonance is less compared to the lower resonance. As  $l_g$  varies, the coupling between the monopole strip  $l_m$  and  $l_g$  varies. This changes the input impedance for the higher resonance and a slight variation in the resonant frequency is observed.

**Table 4.3. Effect of strip length ' $l_g$ ' on resonant frequencies  
( $L_g=38\text{mm}$ ,  $W_g=19\text{mm}$ ,  $s=15.5$ ,  $l_m=19\text{mm}$ ,  $d_1 = 9\text{mm}$ )**

Length of ground strip $l_g$ (mm)			Lower resonance $f_1$ (GHz)	Higher resonance $f_2$ (GHz)
$l_g$ (mm)	$l_g/\lambda_{d2}$	$U/\lambda_{d1}$		
13	0.2	0.62	2.4	2.82
16	0.24	0.63	2.3	2.77
19	0.28	0.63	2.16	2.74
22	0.33	0.63	2.05	2.74
25	0.36	0.63	1.93	2.65
28	0.41	0.62	1.82	2.69
31	0.45	0.62	1.73	2.66

\*  $U=l_m+s+l_g$



### 4.2.3.6 Impact of monopole strip length ' $l_m$ '

Analysis carried out on the microstrip fed printed monopole antenna explained in section 4.1 concludes the role of monopole strip length ' $l_m$ ' on first resonant frequency. But in the case of dual strip antenna, monopole strip length ' $l_m$ ' has two roles. A quarter wave variations for the current density provides the second resonance. Moreover, ' $l_m$ ' is another important component of the 'U' shaped current path which leads to the lower resonance.

Variation of resonant frequencies with respect to ' $l_m$ ' is given in Table 4.4.

Table.4.4 Effect of strip length ' $l_m$ ' on resonant frequencies  
( $L_g=38\text{mm}$ ,  $W_g=19\text{mm}$ ,  $s=15.5$ ,  $l_g=28\text{mm}$ ,  $d_1 = 9\text{mm}$ )

Length of monopole strip			Lower resonance $f_1$ (GHz)	Higher resonance $f_2$ (GHz)
$l_m$ (mm)	$l_m/\lambda_{d2}$	$U/\lambda_{d1}$		
13	0.25	0.57	1.88	3.56
16	0.27	0.59	1.86	3.11
19	0.27	0.6	1.82	2.69
20	0.27	0.61	1.81	2.49
22	0.27	0.63	1.78	2.26
25	0.29	0.63	1.72	2.14
* $U=l_m+s+l_g$				

As expected both the frequencies are affected by the variation in ' $l_m$ '. When ' $l_m$ ' is increased both the frequencies are decreased. From the analysis it is clear that  $l_m/\lambda_{d2}$  is almost constant. This indicates ' $l_m$ ' as the major resonant length for the higher resonance. It is also noted that  $U/\lambda_{d1}$  is constant for  $l_m$  variation. This confirms the resonant length for the lower resonance.

### 4.2.3.7 Impact of strip widths

In this section analysis is carried out to find out the impact of monopole strip width ( $w_1$ ) and ground strip width ( $w_2$ ) on resonant frequencies and bandwidth. The monopole strip is directly connected to the

50Ω microstrip line. So for studying the impact of  $w_1$ , width of the microstrip line (for  $Z_0=50\Omega$ ) and  $w_2$  are kept at 3mm. Width of the monopole strip has been varied as shown in the Fig.4.41. Reflection characteristics are also shown in Fig.4.41. As  $w_1$  increases both the resonant frequencies remains constant. But the impedance matching corresponding to the higher resonance (due to the monopole) decreases.

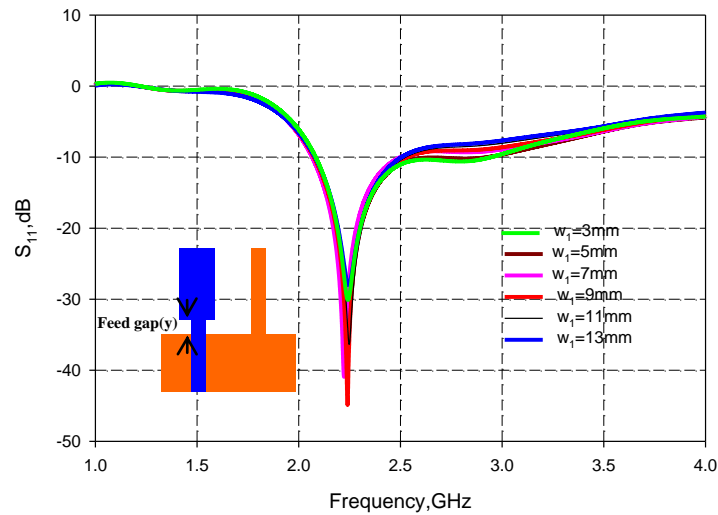


**Fig.4.41. Effect of monopole strip width,  $w_1$**   
 ( $L_g = 38\text{mm}$ ,  $W_g = 19\text{mm}$ ,  $l_m = 19\text{mm}$ ,  $l_g = 19\text{mm}$ ,  $w_2 = 3\text{mm}$ ,  
 $s = 15.5\text{mm}$ ,  $d_1 = 9\text{mm}$ )

Impedance bandwidth can be improved by varying the feed gap between the monopole strip and the ground plane as reported [4]. At present feed gap distance was selected as  $y=0\text{mm}$ . But for a simple design width  $w_1$  can be kept same as that of the microstrip line.

Impact of  $w_2$  has been analysed by keeping  $w_1$  constant at 3mm same as that of the microstrip line. The reflection characteristics obtained after varying  $w_2$  is shown in Fig.4.42. A slight increase in the lower resonant frequency is observed. This is because as  $w_2$  increases, the effective spacing between the strips and hence the total U shaped resonant length decreases.

Impedance matching improves with increase in width  $w_2$  for both the resonances.

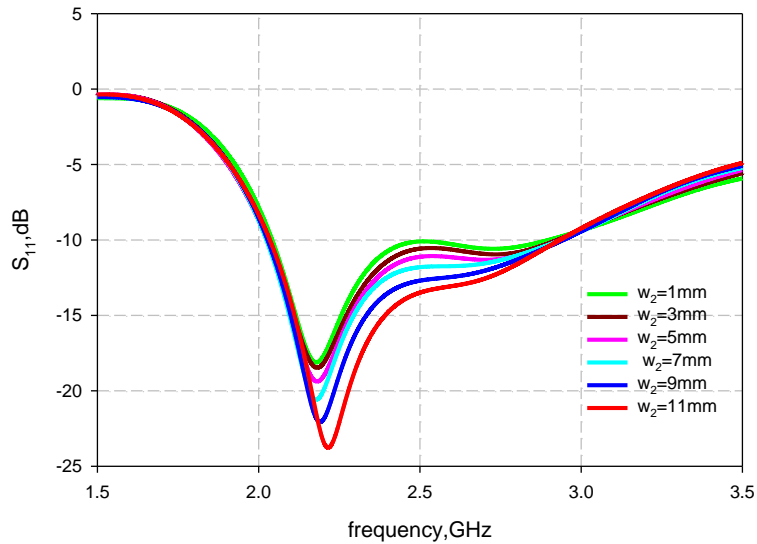


Fig.4.42. Effect of ground strip width,  $w_2$   
 $(L_g = 38\text{mm}, W_g = 19\text{mm}, l_m = 19\text{mm}, l_g = 19\text{mm}, w_1 = 3\text{mm},$   
 $s = 15.5\text{mm}, d_1 = 9\text{mm})$

From the above analysis it is concluded that increase in strip width affects the impedance bandwidth. Also further increase in strip width increases the lower resonance since it affects the U shaped resonant length. Hence for the further studies, widths of the strips are kept same as that of the microstrip line.

#### 4.2.4 Important inferences

In the above section compact printed monopole antenna has been modified by adding another strip to the ground plane as an extension. Important conjectures obtained in this analysis are listed below.

- ♣ Printed monopole antenna with compact ground plane ( $0.5\lambda_d \times 0.25\lambda_d$ ) shows only single resonance in the 1-6GHz operating band. The second resonance, due to the L shaped path has been shifted to the higher side due to reduction in ground plane dimension.

- ♣ Adding another strip to the ground plane lowers the second resonance due to the 'L' shaped path. Addition of another strip to the ground plane constitute a curved 'U' shaped current path which is responsible for the lower resonance and this is happening when 'U' length is  $0.68\lambda_{d1}$ .
- ♣ The spacing between the strips is the crucial parameter which controls the matching and to some extent the resonant frequency. There is an optimum spacing ( $0.17\lambda_{d1}$ ) for which antenna shows good impedance bandwidth for both the higher and lower bands.
- ♣ Variation in signal strip length ' $l_m$ ' affects both the resonant frequencies since it affects both the monopole resonant length and the meandered length ( $U=l_m+s+l_g$ ) for the lower resonance.
- ♣ Variation of ground strip length ' $l_g$ ' changes the lower resonance considerably. But the higher resonance remains almost unchanged.
- ♣ Increase in strip width increases the bandwidth. But for simple design, widths of the strips are kept same as microstrip line width.
- ♣ Variation in ground plane length  $L_g$ , does not affect the resonances significantly.
- ♣ Ground plane width  $W_g$  affects the impedance bandwidth for both the bands.
- ♣ In the case of lower resonance, the three important parameters which control the resonant frequency are monopole strip length ' $l_m$ ', ground strip length ' $l_g$ ' and spacing between the strips ' $s$ '. Even though the spacing ' $s$ ' is a part of the resonant length, more

variation in resonant frequency is observed with respect to the signal strip lengths. The lower resonant frequency can be easily tuned by varying  $l_g$  without much affecting the higher resonance because the total 'U' shaped path remains constant in our study.

#### 4.2.5 Effect of dielectric constant ( $\epsilon_r$ )

This section deals with the effect of dielectric constant on the dual strip antenna. Analysis has been carried out by varying the substrate dielectric constant from 2.2 to 6. A typical variation of  $S_{11}$  is shown in the Fig.4.43. For each dielectric constant, microstrip feed line has been redesigned for  $50\Omega$  and the corresponding width has been kept for the monopole and ground strip. As the dielectric constant increases both the resonant frequencies decreases as expected. Impedance matching corresponds to the lower resonance (due to the U shaped path) improves with increase in dielectric constant. But the matching corresponds to the monopole strip deteriorates as the dielectric constant decreases.

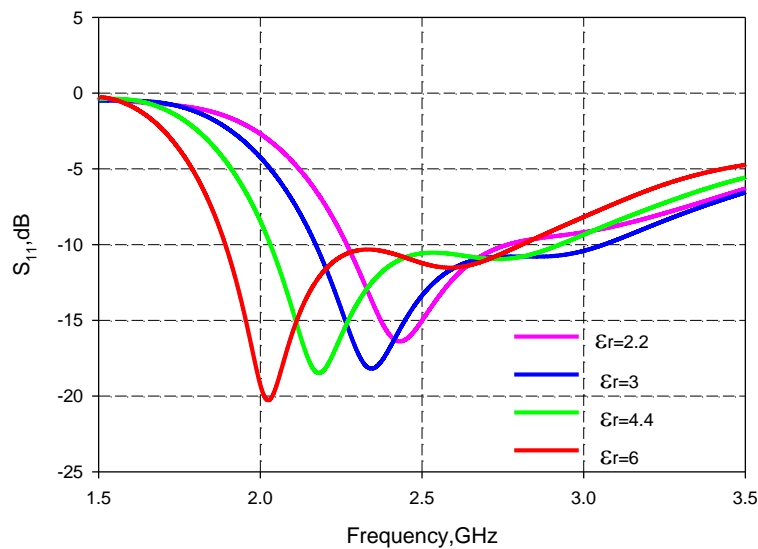
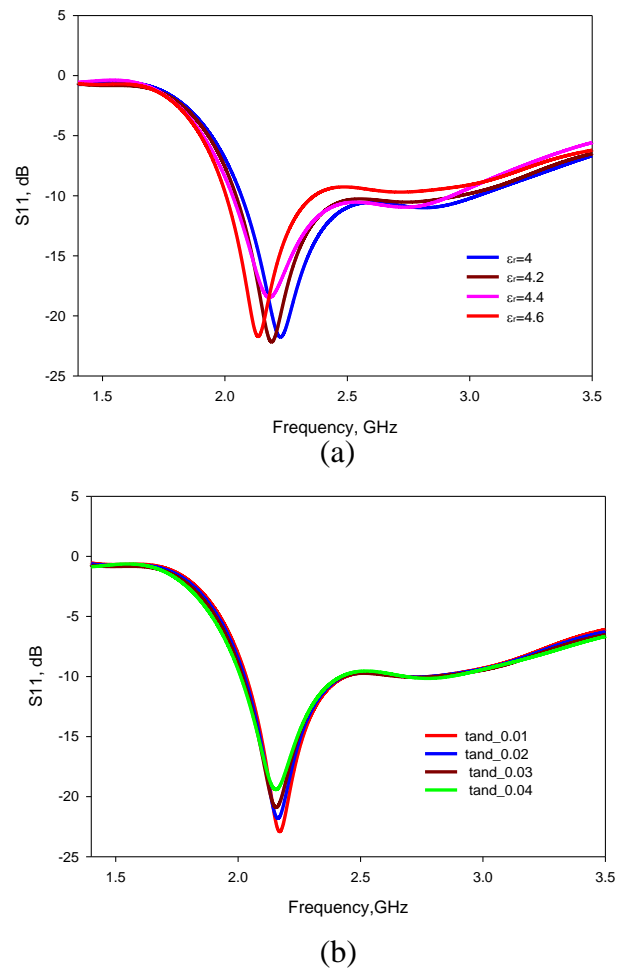


Fig.4.43. Effect of dielectric constant  
( $L_g=38\text{mm}$ ,  $W_g=19\text{mm}$ ,  $s=15.5\text{mm}$ ,  $l_m=19\text{mm}$ ,  $l_g=19\text{mm}$ ,  $d_i=9\text{mm}$ )

Sensitivity study has been carried out on FR4 substrate by varying dielectric constant from 4 to 4.6 and loss tangent from 0.01 to 0.04. The results are shown in Fig.4.43 b. For a 13% variation in dielectric constant,  $\pm 4\%$  variation is observed for lower resonant frequency and  $\pm 4.5\%$  is observed for higher resonant frequency. Variation on loss tangent affects the impedance matching and bandwidth. As the  $\tan\delta$  increases bandwidth also increases for both the resonances.



**Fig.4.43b. Sensitivity study on FR4 substrate**  
**(a) Dielectric constant variation (b) loss tangent variation**

**( $L_g=38\text{mm}$ ,  $W_g=19\text{mm}$ ,  $s=15.5\text{mm}$ ,  $l_m=19\text{mm}$ ,  $l_g=19\text{mm}$ ,  $d_1=9\text{mm}$ )**

#### 4.2.6 Effect of substrate thickness (h)

Impact of dielectric thickness on antenna performance has been studied by varying the thickness of the substrate from 1mm to 3mm. In this case also feed line has been designed for different substrate thickness. Width of the monopole strip and the ground strip is kept as same as  $50\Omega$  microstrip line width. As the dielectric thickness increases, lower resonance decreases with good impedance bandwidth. Matching is improved due to less coupling between the ground edge and the signal strip. The substrate thickness study gives a conclusion that the lower resonance highly depends on 'h' and hence the resonant length should be taken as  $l_m+h+s+l_g$ . The decrease in resonant frequency is due to the increase in resonant length as mentioned. In the case of higher resonance, as h increases matching becomes poor as shown in the Fig.4.44. This is due to the variation in the capacitive coupling between the strips.

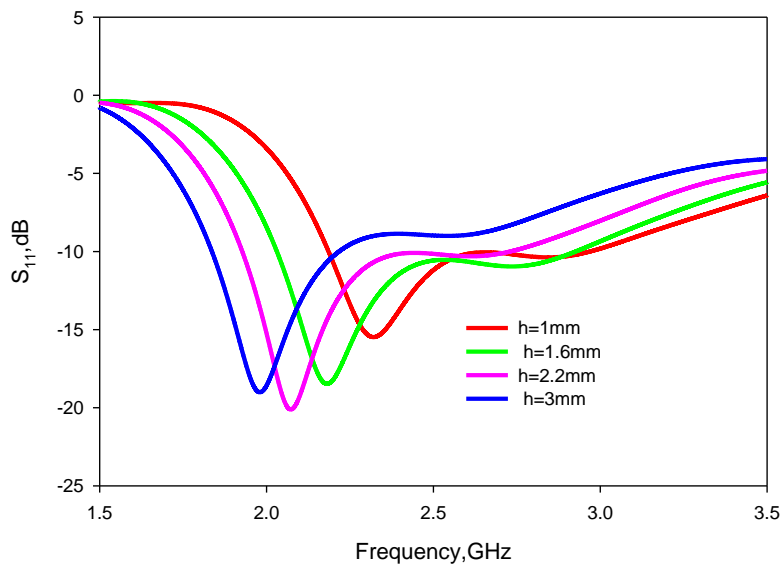


Fig.4.44. Effect of substrate thickness, h

$L_g=38\text{mm}, W_g=19\text{mm}, \epsilon_r, s=15.5\text{mm}, l_m=19\text{mm}, l_g=19\text{mm}, d_i=9\text{mm}$ )

### 4.3 Design procedure for a compact dual strip antenna

The detailed analysis carried out in the previous sections leads towards the design of a compact dual strip antenna. It has been well investigated that a compact dual band antenna can be derived from the printed monopole configuration by extending another strip from the ground plane. This section explains the design procedure for the design of dual strip antenna, based on the analysis carried out in the previous sections. While deriving the design equations, prime importance is given to the compactness.

In this dual band antenna design, the second resonance  $f_2$  (higher) is the fundamental mode of the printed monopole and the lower resonance  $f_1$  is the new mode which is due to the meandered path generated by adding the additional strip on the ground plane. The ground plane dimensions ( $L_g, W_g$ ), monopole strip length ( $l_m$ ) and the feed offset ( $d_1$ ) have to be designed for the second resonance ( $f_2$ ). The spacing 's' and the ground strip length ( $l_g$ ) have to be designed for the lower resonance ( $f_1$ ). The step by step design procedures are listed below.

Step1:- Select a substrate material with dielectric constant  $\epsilon_r$  and height h.

Step2:- Find out the width of a  $50\Omega$  microstrip feed line on the above substrate using the standard formula [3]. Keep same widths for signal strip as well as ground strip for design simplicity.

Step3. Calculate the effective dielectric constant using the equation

$$\epsilon_{eff} = \frac{\epsilon_r + 1}{2} \dots\dots\dots (4.1)$$

where  $\epsilon_r$  is the relative dielectric constant of the substrate.



Step4:- find out ground plane dimensions based on the given formulas

$$Lg = \frac{0.467c}{f_2 \sqrt{\epsilon_{eff}}} \dots\dots\dots (4.2)$$

$$Wg = \frac{0.24c}{f_2 \sqrt{\epsilon_{eff}}} \dots\dots\dots (4.3)$$

where c is the velocity of light and f<sub>2</sub> is the required higher resonant frequency.

Step5:- find out signal strip length corresponding to the higher frequency f<sub>2</sub> based on the equation,

$$l_m = \frac{0.32c}{f_2 \sqrt{\epsilon_{eff}}} - \frac{(h-1.6)}{0.4} \dots\dots\dots (4.4)$$

Step6:- find out the feed offset position from the ground plane edge d<sub>1</sub> as

$$d_1 = \frac{0.18c}{f_2 \sqrt{\epsilon_{eff}}} \dots\dots\dots (4.5)$$

Step7: find out the length of strip2 for the lower resonance f<sub>1</sub> as,

$$l_s = \frac{0.287c}{f_1 \sqrt{\epsilon_{eff}}} - \frac{(h-1.6)}{0.2} \dots\dots\dots (4.6)$$

Step8:- Calculate the spacing between the strips based on the equation,

$$s = \frac{0.129c}{f_1 \sqrt{\epsilon_{eff}}} \dots\dots\dots (4.7)$$

The constants in the above equations are derived from exhaustive parametric analysis.

The above design equations are valid only for a frequency ratio of  $1 \leq f_2/f_1 \leq 2$ . Since the design equations are focussed towards a compact design, for a large frequency ratio, the optimised ground plane length may not be sufficient to confine the spacing 's'. Large frequency ratio introduces high level of asymmetry in the configuration and also reduces the impedance match.

#### **4.4 Design and analysis of dual band dual strip antenna for 1.8/2.4GHz bands.**

##### **4.4.1 Introduction**

The design of dual band dual strip antenna from the printed monopole configuration have been discussed in the previous section. In this section the design equations have been validated by designing the antenna for 1.8GHz and 2.4GHz bands. These two bands are selected due to its industrial applications in Digital Communication System (DCS) and WLAN. The newly designed antenna has a dimension of 35mm x 47mm x 1.6mm on a FR4 substrate of dielectric constant  $\epsilon_r = 4.4$  and offers good radiation and wide return loss characteristics in the desired bands. Details of the antenna design and experimental results are discussed. Finite difference time domain analysis has been carried out to validate the design equations. The results are compared with HFSS simulation also.

##### **4.4.2 Antenna design**

Modified microstrip-fed printed monopole antenna etched on FR4 substrate of relative dielectric constant  $\epsilon_r = 4.4$  and height  $h=1.6\text{mm}$  is illustrated in Fig.4.45. Dimensions of the antenna for the designed frequencies are as given below. Ground plane dimensions are  $L_g=35\text{mm}$  and  $W_g=18\text{mm}$ , monopole strip length  $l_m=24\text{mm}$  and ground strip length  $l_g=29\text{mm}$ . Width of the strips are kept at 3mm. Spacing  $s=13\text{mm}$  and offset distance  $d_1=13.5\text{mm}$ .

Photographs of the fabricated antenna are shown in Fig. 4.46.

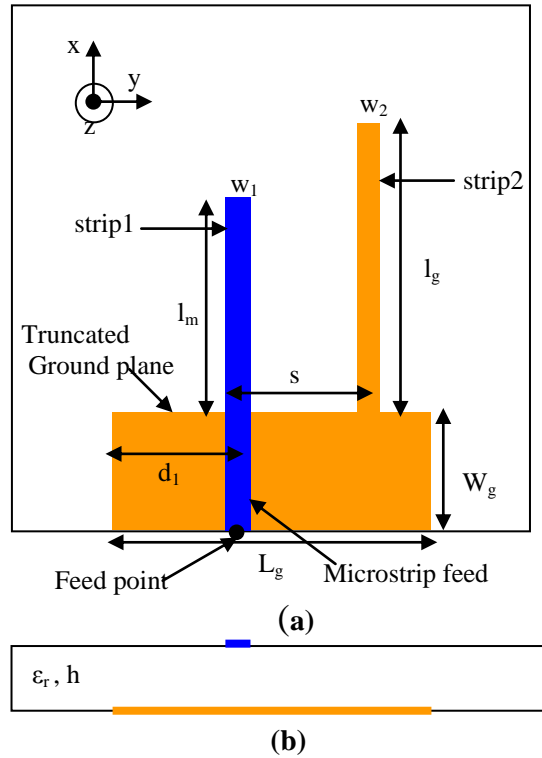
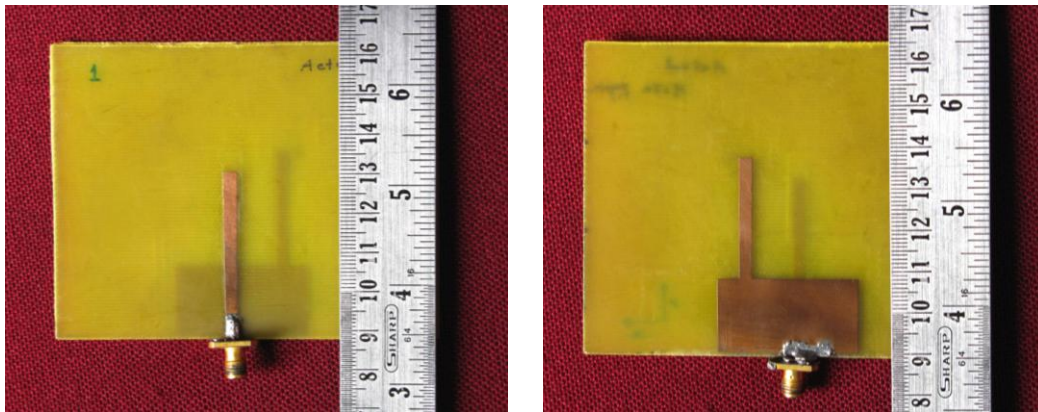


Fig. 4.45 Geometry of the proposed antenna  
 (a) Top view (b) Side view  
 $(L_g=35\text{ mm}, W_g=18\text{ mm}, l_m=24\text{ mm}, l_g=29\text{ mm}, d_1=13.5\text{ mm}, s=13\text{ mm}, w=3\text{ mm}, h=1.6\text{ mm}, \epsilon_r=4.4)$



(a) (b)  
 Fig.4.46 Photographs of the dual band dual strip antenna designed for 1.8/2.4GHz applications  
 (a) Top view (b) Bottom view

### 4.4.3 Reflection characteristics

The measured and simulated return loss characteristics of the dual strip antenna are shown in Fig.4.47.

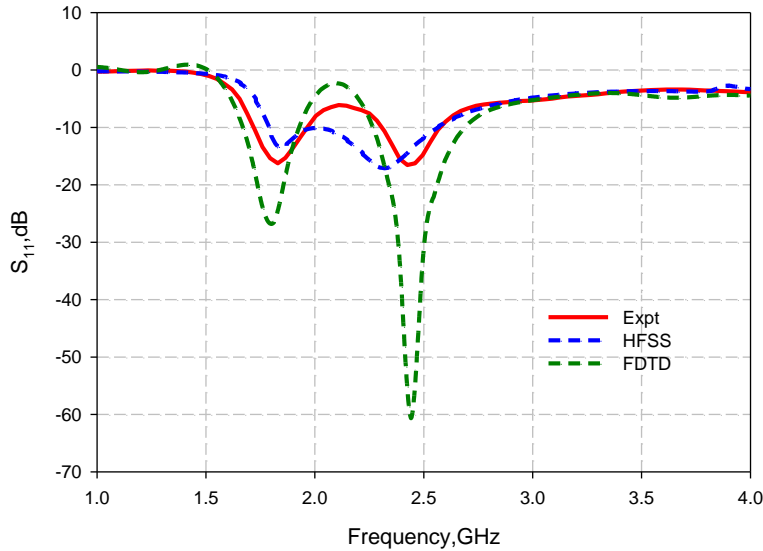


Fig.4.47 Reflection characteristics

( $L_g=35$  mm,  $W_g=18$ mm,  $l_m=24$ mm,  $l_g=29$ mm,  $d_1=13.5$ mm,  $s=13$  mm,  $w=3$ mm,  $h=1.6$  mm,  $\epsilon_r = 4.4$ )

Antenna exhibits resonances at 1.81GHz and 2.44GHz with 2:1 VSWR bandwidths of 10.8% and 9.8% respectively. The lower resonant band extending from 1729MHz to 1926MHz (197MHz) is wide enough to cover DCS and the higher resonant band from 2324 MHz to 2565MHz (241 MHz) covers the 2.4GHz WLAN.

### 4.4.4 Electric field distribution

FDTD computed electric field distributions at the resonant frequencies are given in Fig.4.48. Ex field computed one cell above the dielectric substrate at 1.8GHz is shown in Fig.4.48a. For the clear interpretation bottom view is given. The U shaped mode is clear in the figure. It is also clear that electric field radiating from both the strips are in same phase, which favours the radiation. For 2.4GHz there is a quarter wave variation along the monopole strip as shown in Fig.4.48b.

Field strength from the ground strip is very less compared to the monopole strip.

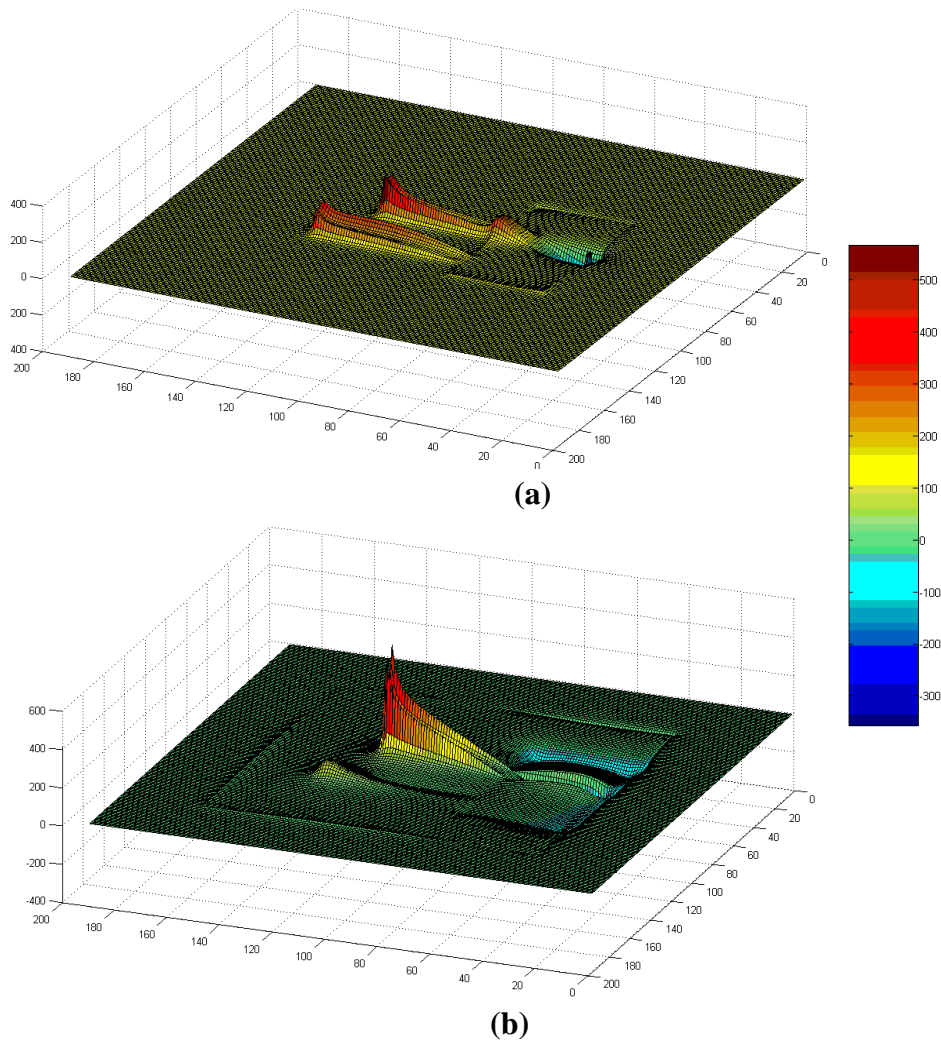


**Fig.4.48** Bottom view of the Electric field distribution  
(a) 1.8GHz (b) 2.4GHz  
( $L_g=35$  mm,  $W_g=18$ mm,  $l_m=24$ mm,  $l_g=29$ mm,  $d_1=13.5$ mm,  
 $s=13$  mm,  $w=3$ mm,  $h=1.6$  mm,  $\epsilon_r = 4.4$ )

#### 4.4.5 Radiation Characteristics

##### Radiation pattern:

Radiation patterns measured at the resonant frequencies are shown in Fig.4.49. Beam maximum is tilted by  $45^\circ$  in the azimuth plane.

Fig.4.49a,b shows the simulated 3D patterns of the antenna at the resonant frequencies. The normalized radiation patterns in the two principal planes, measured at the center frequencies of the respective bands are shown in Fig.4.49c and d. The 2D patterns have been measured at  $\phi = 45^\circ$  plane. It is observed that both the operating bands are linearly polarized along x axis with good radiation coverage. H plane patterns are broad with half power beam width of  $\sim 120^\circ$  for both the operating frequencies. Where as E plane pattern shows a half power beam width of  $\sim 83^\circ$  for both frequencies. In the case of 2.4 GHz a null is observed in the third quadrant due to the presence of ground strip  $l_g$  which acts as a reflector for the higher resonance and blocks the radiation towards back side. This increases the gain of the antenna compared to a printed monopole. From both the principal plane patterns, it is clear that antenna exhibits minimum radiation in one quadrant and fairly good coverage over the other quadrants, suggesting its usefulness in mobile telephone handsets. Radiation patterns at other frequencies in the respective bands are similar to those shown in Fig.4.49.

Antenna shows linear polarisation along X – direction for both the bands. Gain of the antenna measured in the two operating bands is shown in Fig.4.50. Antenna has an average gain of 2.3dBi in the DCS band and 3.6dBi in the WLAN band. Increase in gain at higher band (monopole mode) compared to earlier printed monopole is due to the presence of ground strip ' $l_g$ ' as a reflector. It is also clear from the radiation pattern that beam width of the antenna is less in both the planes compared to a printed monopole. The computed efficiency at the lower and higher resonant frequencies are 83% and 85% respectively.

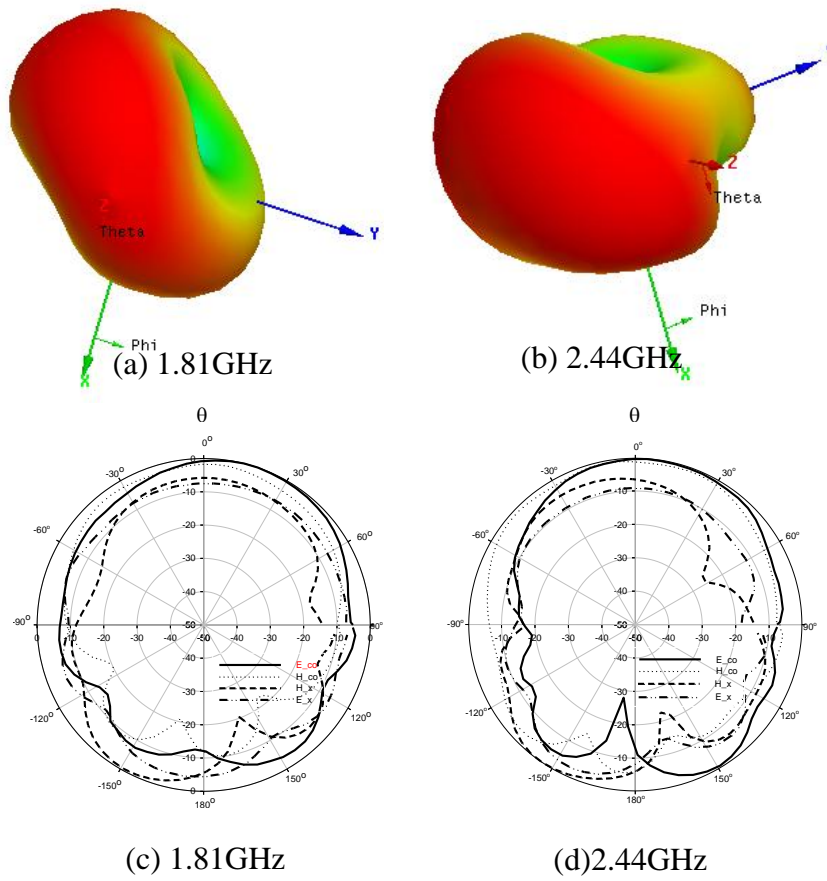


Fig.4.49 3D and 2D radiation patterns of the dual band antenna  
 $L_g=35$  mm,  $W_g=18$ mm,  $l_m=24$ mm,  $l_g=29$ mm,  $d_1=13.5$ mm,  
 $s=13$  mm,  $w=3$ mm,  $h=1.6$  mm,  $\epsilon_r = 4.4$

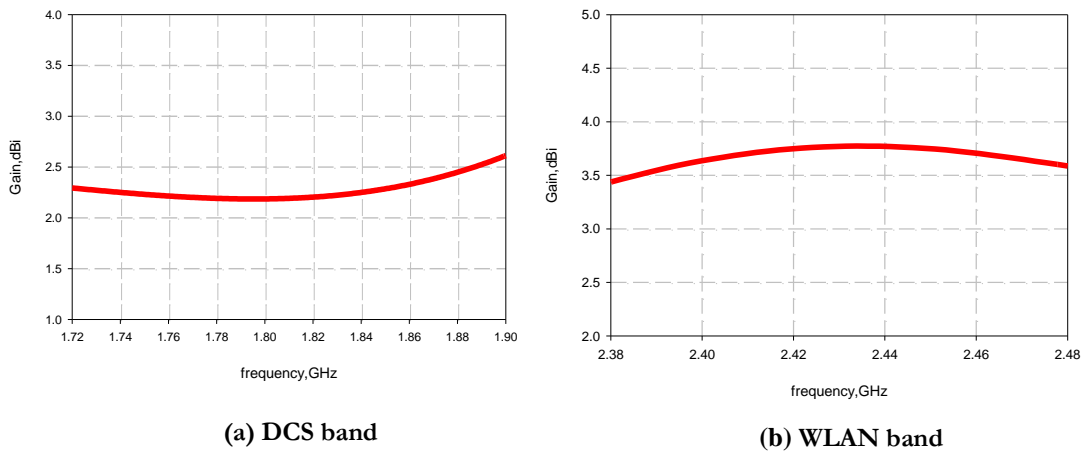


Fig.4.50 Gain of the dual band antenna  
 $L_g=35$  mm,  $W_g=18$ mm,  $l_m=24$ mm,  $l_g=29$ mm,  $d_1=13.5$ mm,  
 $s=13$  mm,  $w=3$ mm,  $h=1.6$  mm,  $\epsilon_r = 4.4$

The design equations are validated on other substrates with different  $\epsilon_r$  and thickness (h). Parameters of the designed antenna on different commercially available substrates are given in Table 4.5.

**Table 4.5 Design parameters on different substrates**

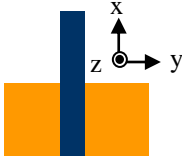
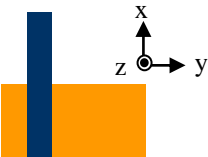
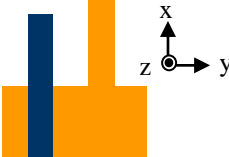
Substrate	Substrate Parameters		Antenna Parametrs(mm)							Designed frequencies (GHz)		Results obtained (GHz)	
	$\epsilon_r$	h(mm)	w	$l_m$	$l_g$	$L_g$	$W_g$	$d_1$	s	$f_1$	$f_2$	$f_1$	$f_2$
FR4 Epoxy	4.4	1.6	3	24	29	35	18	13.5	13	1.8	2.4	1.81	2.44
Rogers RO3006	6.15	1.28	1.8	21	26	31	16	12	11	1.8	2.4	1.8	2.32
Rogers 6010LM	10.2	0.635	0.6	18.5	25	24	12	9	9	1.8	2.4	1.85	2.48

#### 4.5 Conclusion

Evolution of a compact dual band dual strip antenna from a microstrip fed printed monopole antenna has been well explained in this chapter. Experimental and numerical analysis has been carried out to study the effect of various antenna parameters on antenna performances. Design equations were derived for the design of the compact dual strip antenna. Based on the design formulas, an antenna resonating at 1.8/2.4GHz bands suitable for DCS/WLAN applications has been designed and analysed. Design equations are validated on commercially available substrates with different  $\epsilon_r$  and h. The important findings of the analysis are summarized in Table 4.6.



Table 4.6. Comparison of Printed monopole antenna and Compact dual strip antenna

Parameters	Microstrip fed printed monopole antenna	Offset fed printed monopole antenna		Compact Dual strip Antenna	
Configuration					
Antenna Parameters (mm)	$L_g=38, W_g=19, l_m=19, l_g=29, d_1=d_2=19, w=3$	$L_g=38, W_g=19, l_m=19, d_1=9, w=3$		$L_g=35, W_g=18, l_m=24, l_g=29, d_1=13.5, s=13, w=3$	
Substrate parameters	$h=1.6\text{mm}, \epsilon_r = 4.4$	$h=1.6\text{mm}, \epsilon_r = 4.4$		$h=1.6\text{mm}, \epsilon_r = 4.4$	
Resonant frequency(GHz)	$f_2= 2.76$	$f_1=3$	$f_2=2.5$	$f_1=1.81$	$f_2=2.44$
Bandwidth(%)	19	40 merged		10.8	9.8
Radiation pattern	Doughnut like pattern, symmetric	Tilted by $20^\circ$ in the azimuth plane	Tilted by $30^\circ$ in the azimuth plane	Tilted by $45^\circ$ in the azimuth plane	Tilted by $45^\circ$ in the azimuth plane
Beam width	$80^\circ$ in E-plane omni directional in H-plane	$110^\circ$ in E-plane, $160^\circ$ in H-plane	$110^\circ$ in E-plane, $160^\circ$ in H-plane	$83^\circ$ in E-plane, $120^\circ$ in H-plane	$83^\circ$ in E-plane, $120^\circ$ in H-plane
Gain (dBi)	2.24	2.32	2.13	2.3	3.6
Efficiency (%)	93	87	90	83	85
Polarization	Linear along x	Linear $-45^\circ$ with respect to y	Linear $-45^\circ$ with respect to y	Linear, along x	Linear, along x

#### 4.6 References

- [1]. M.J. Amman and M. John, Optimum design of the printed strip monopole, *IEEE Antennas and Propagation Magazine*, Vol.47, No.6, pp 59-61, December 2005.
- [2]. E.C.Jordan, K.G.Balmain, *Electromagnetic waves and radiating systems*, Prentice-Hall India.
- [3]. Ramesh Garg et al., *Microstrip antenna design handbook*, Artech House, London.
- [4]. M.J. Amman , Impedance bandwidth of the square planar monopole, *Microwave and Optical Technology Letters*, Vol.24, No.3, pp 185-187, February 2000.

.....□□.....

## **DESIGN AND ANALYSIS OF COMPACT DUAL BAND FOLDED DUAL STRIP ANTENNA**

---

<b>Contents</b>	<b>5.1 Introduction</b>
	<b>5.2 Double folded printed monopole</b>
	<b>5.3 Double folded dual strip antenna</b>
	<b>5.4 Design procedure for a compact dual band folded dual strip antenna</b>
	<b>5.5 Design and development of folded dual strip antenna for modern communication bands</b>
	<b>5.6 Conclusion</b>

---

This chapter explains the design and analysis of compact dual band folded dual strip antenna. The present configuration is a modified version of the dual strip antenna mentioned in chapter4. In the previous chapter it has been well proved that extending an additional strip to the ground plane with a suitable spacing from the monopole strip can give two wide resonances. In this chapter the same configuration has been folded for achieving compactness. The effect of folding on antenna performances has been well studied by conducting various analysis. Design equations have been derived for the compact folded dual strip antenna and validated by designing the antenna for modern communications bands.

---

## 5.1 Introduction

Design of a compact dual band dual strip antenna from a microstrip fed printed monopole antenna has been explained in chapter 4. The lower resonance has been achieved by adding an additional strip as an extension to the ground plane. Even though the present configuration gives two wide resonances, the size of the antenna is still bigger compared to the ultra modern communication devices and radiation pattern shows a tilt in both the bands. So in this chapter an attempt has been made to achieve compactness as well as to correct the tilt in the radiation pattern. Double folding the strips towards ground plane, keeping the resonant length constant is an effective way to achieve compactness. But folding the strips towards ground plane changes the input impedance. Folding the monopole is equivalent as top loading. So initially top loading effects of printed monopole are studied.

For the detailed understanding of the effect of folding on antenna performances, study has been carried out on printed monopole with double folding (or top loaded monopole). Effect of loading, loading positions, ground plane dimensions on folding etc were well studied. Later another folded strip was added as an extension to the ground plane at a spacing of 's' from the folded monopole strip and the impact of spacing 's' has been analysed.

## 5.2 Double folded printed monopole

In this section the microstrip fed printed monopole antenna has been folded and analysed. The monopole strip length and ground plane dimensions have been kept same as the DCS/WLAN applications mentioned in chapter 4. In the present analysis the monopole strip has been placed symmetric to the ground plane as shown in the Fig.5.1a.

The microstrip fed printed monopole antenna has been fabricated on a FR4 substrate of dielectric constant  $\epsilon_r = 4.4$  and height  $h=1.6\text{mm}$ . Ground

plane dimensions and monopole strip length are chosen as  $L_g=35\text{mm}$ ,  $W_g=18\text{mm}$  and  $l_m=24\text{mm}$  respectively. All the above values are as per the design equations explained in the previous chapter.

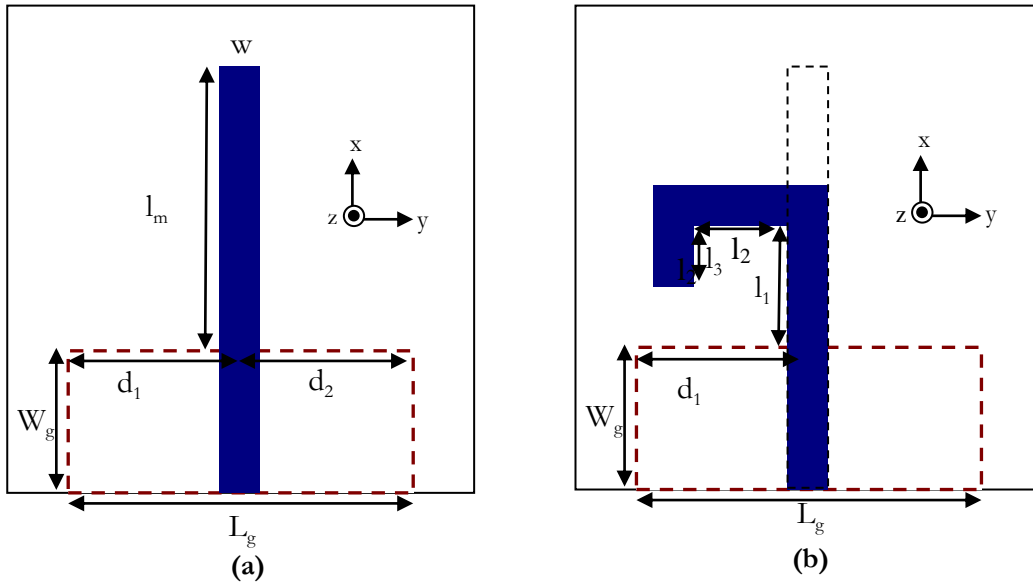


**Fig.5.1 Microstrip-fed printed strip monopole antenna**  
 $(L_g = 35\text{mm}, W_g = 18\text{mm}, l_m = 24\text{mm}, w = 3\text{mm}, d_1=d_2=17.5\text{mm})$

The present microstrip fed printed monopole antenna with the above mentioned dimensions has been folded as shown in Fig. 5.1 b. So in the folded monopole the total length ' $l_m$ ' is as  $l_1+l_2+l_3$  as shown in the figure. Initially the lengths have been selected as  $l_1=11\text{mm}$ ,  $l_2=10\text{mm}$  and  $l_3=3\text{mm}$ . The impact of different folding dimensions has been analysed in section 5.2.6.

### 5.2.1 FDTD modelling

Two dimensional view of the FDTD computation domain is given in Fig.5.2. The computational domain is divided into Yee cells of dimension  $\Delta x=\Delta y=0.5\text{mm}$  and  $\Delta z=0.4\text{mm}$ . 15 cells are used to model air cells on each of the six sides. Substrate is modelled by a computational volume of  $84\Delta x*126\Delta y*4\Delta z$ . Thus the total computation domain is discretized into

114 $\Delta x$ \*156 $\Delta y$ \*34 $\Delta z$  cells. Luebber's feed model is employed to excite the microstrip line feed of the antenna and a Gaussian pulse is used as the source of excitation. Mur's first order ABC is used as the boundary condition. Time step used for the computation is 0.95ps. The Gaussian half-width is  $T = 20$  ps, and the time delay  $t_0$  is set to be  $3T$ .

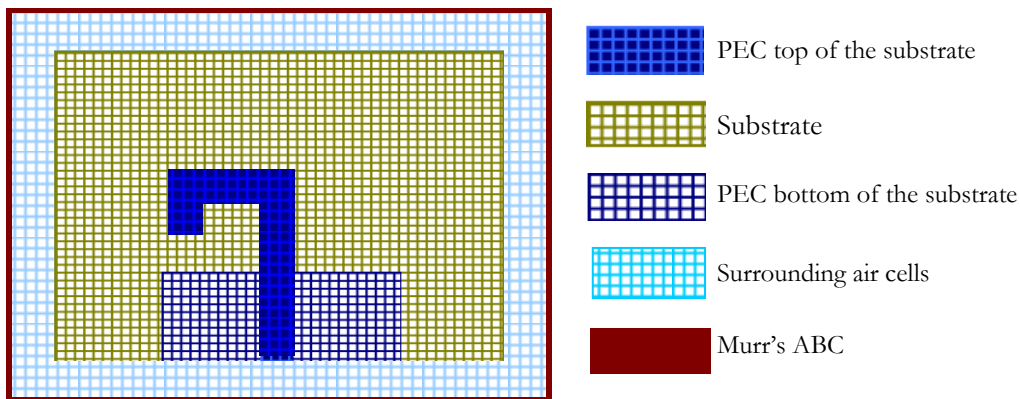


Fig.5.2. 2D view of FDTD computation domain of microstrip line fed folded monopole antenna

## 5.2.2 Reflection characteristics

Fig. 5.3 shows the reflection characteristics of the printed monopole antenna with and without folding. Monopole without folding shows resonance at 2.34GHz with good impedance matching. In this case antenna shows a wide resonance with 19% bandwidth from 2.15GHz to 2.55GHz as shown in the figure. With folding, antenna exhibits nearly same resonance (2.31GHz), but with poor impedance match as shown in Fig.5.3. The FDTD computed results are also shown in the figure. In this case also it is clear that folded monopole is having poor impedance bandwidth compared to the printed monopole without folding.

Fig.5.4 shows the impedance variations in both the cases. In the case of printed monopole without folding, the input impedance at the resonant frequency (2.34GHz) is  $48+j0.5\Omega$ . Where as in the case of folding it is increased to  $67.35-j45\Omega$  and the reactance became capacitive and antenna shows poor

impedance match. While folding, the signal strip becomes parallel and so close to the ground plane which in turn increases the coupling between the strip and the ground plane and hence the impedance became capacitive.

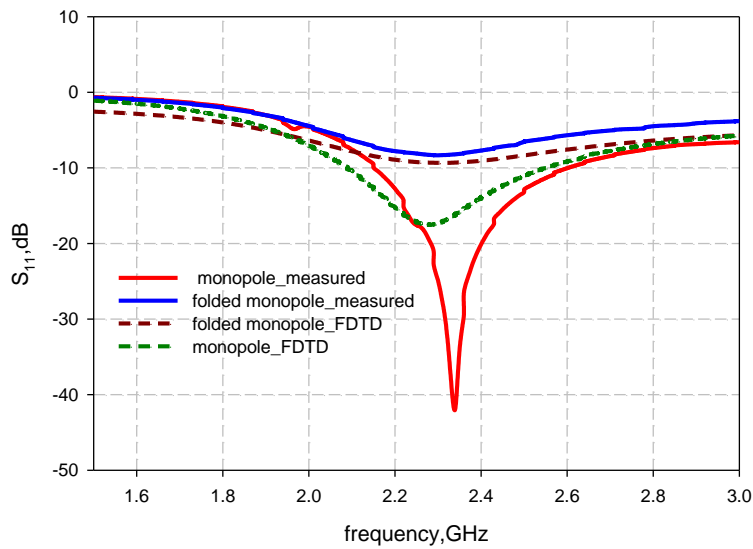


Fig.5.3 Reflection characteristics of printed monopole and folded monopole ( $L_g = 35\text{mm}$ ,  $W_g = 18\text{mm}$ ,  $l_m = 24\text{mm}$ ,  $w = 3\text{mm}$ ,  $l_1 = 11\text{mm}$ ,  $l_2 = 10\text{mm}$ ,  $l_3 = 3\text{mm}$ )

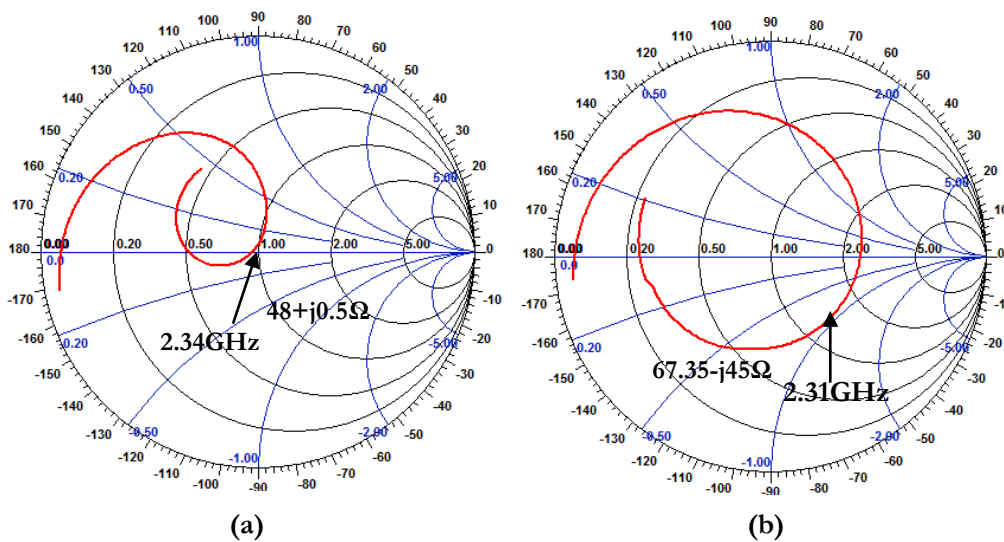


Fig.5.4 Impedance variation for printed monopole and folded monopole ( $L_g = 35\text{mm}$ ,  $W_g = 18\text{mm}$ ,  $l_m = 24\text{mm}$ ,  $l_1 = 11\text{mm}$ ,  $w = 3\text{mm}$ ,  $l_2 = 10\text{mm}$ ,  $l_3 = 3\text{mm}$ )  
 (a) Printed monopole (b) Folded monopole

### 5.2.3 Radiation Pattern

The 3D radiation plot obtained from HFSS for both the printed monopole and the folded monopole are illustrated in Fig.5.5.

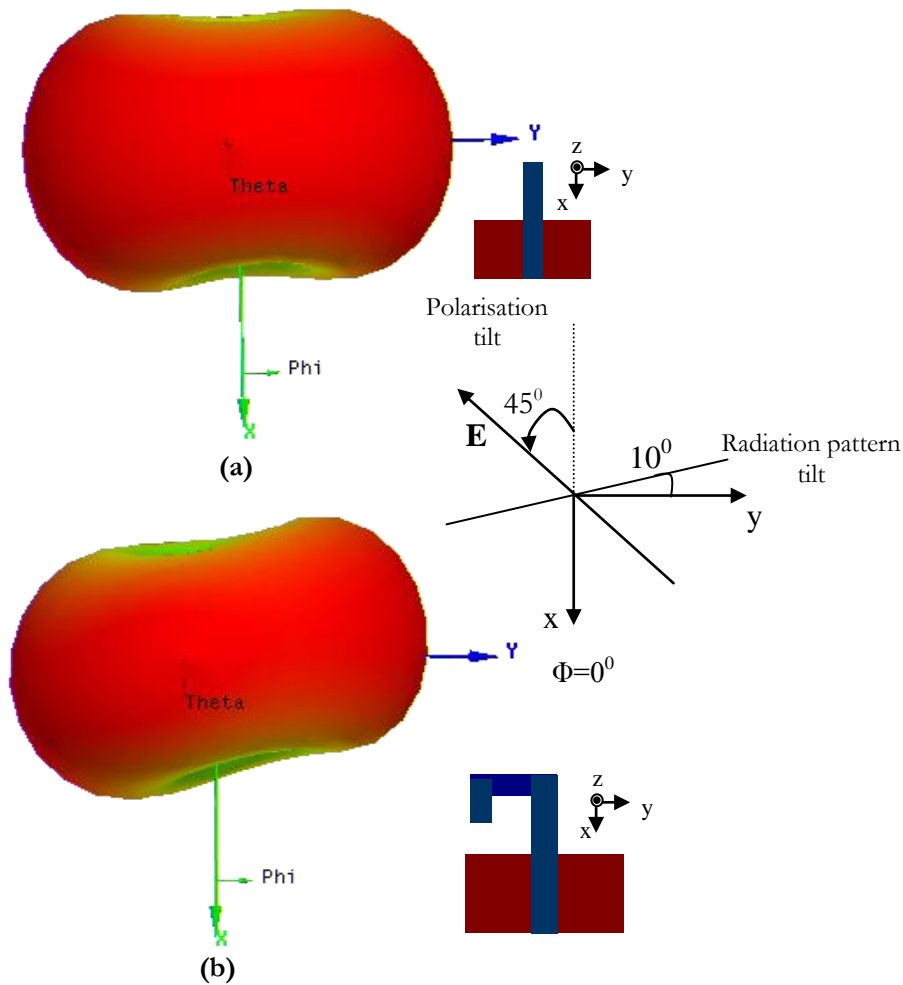
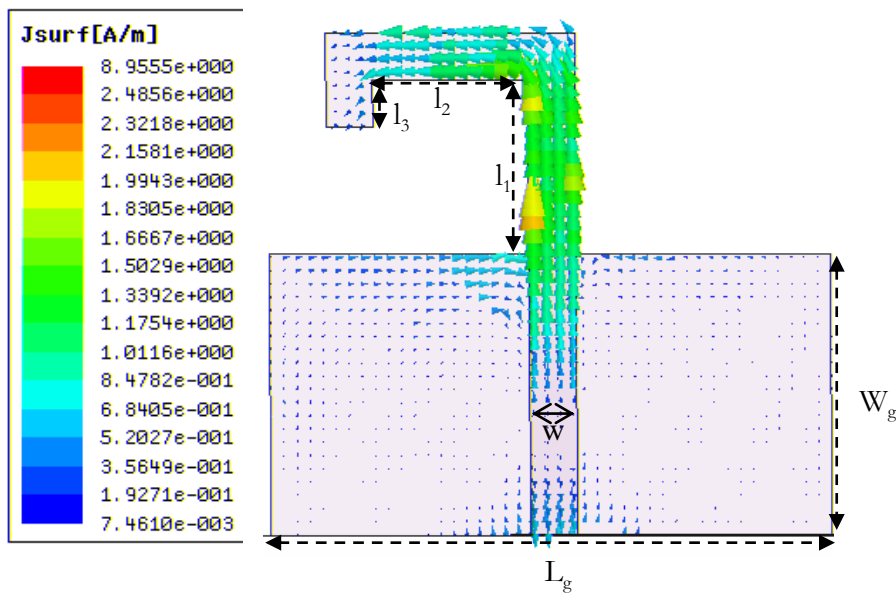


Fig.5.5. 3D radiation patterns for printed monopole and folded monopole  
 $(L_g = 35\text{mm}, W_g = 18\text{mm}, l_m = 24\text{mm}, l_1 = 11\text{mm}, w = 3\text{mm}, l_2 = 10\text{mm}, l_3 = 3\text{mm})$   
 (a) Printed monopole (b) Folded monopole

In the case of printed monopole antenna without folding, radiation pattern is doughnut shaped as shown in Fig.5.5.a. Radiation pattern is symmetric with respect to the x-axis. The measured average gain of the antenna is 2.1dBi. Antenna is linearly polarized along x-axis with an efficiency of 93%.

In the case of folded monopole, the radiation pattern is tilted by an angle of  $10^\circ$  in azimuth plane compared to the printed monopole as shown in Fig5.5.b.

The simulated surface current distribution corresponding to the resonant frequency of the folded monopole antenna is shown in Fig.5.6. A quarter wave current distribution is obtained on the folded arm surface. Surface current distribution on the ground edge on either side of the monopole strip is feeble and of opposite direction. The slight tilt in radiation pattern compared to the printed monopole is due to equal radiation from both the horizontal and vertical strips of the folded arm.



**Fig.5.6. Simulated surface current distribution at the resonant frequency ( $L_g = 35\text{mm}$ ,  $W_g = 18\text{mm}$ ,  $l_1 = 11\text{mm}$ ,  $w = 3\text{mm}$ ,  $l_2 = 10\text{mm}$ ,  $l_3 = 3\text{mm}$ )**

Polarization of the antenna is linear along  $-45^\circ$  with respect to y axis. Measured gain of the antenna at the resonant frequency is 1.74dBi with an efficiency of 80%. The reduction in the gain and efficiency may be due to the impedance mismatch with folding. The computed radiation efficiency at the resonant frequency is 89%.



### 5.2.4 $d_1$ variation /offsetting

For obtaining good impedance match an investigation is carried out by changing the offset distance  $d_1$ . In the initial configuration offset distance was  $0.22\lambda_d$ , where  $\lambda_d$  is the wavelength in the substrate corresponding to the resonant frequency. In the analysis  $d_1$  has been varied by keeping all the other parameters constant, and the reflection characteristics obtained for different cases are plotted in Fig.5.7. As  $d_1$  decreases, impedance match is improved as shown in the figure. This is because the signal strip moves outward and there will be less coupling between the folded strip and the ground plane. A slight decrease in the resonant frequency is also observed. It is also noted that there is a tendency for another resonance at 3GHz as the feed is moved to the edge. This resonance is similar to that observed in the case of printed monopole with offset feed discussed in chapter 4.

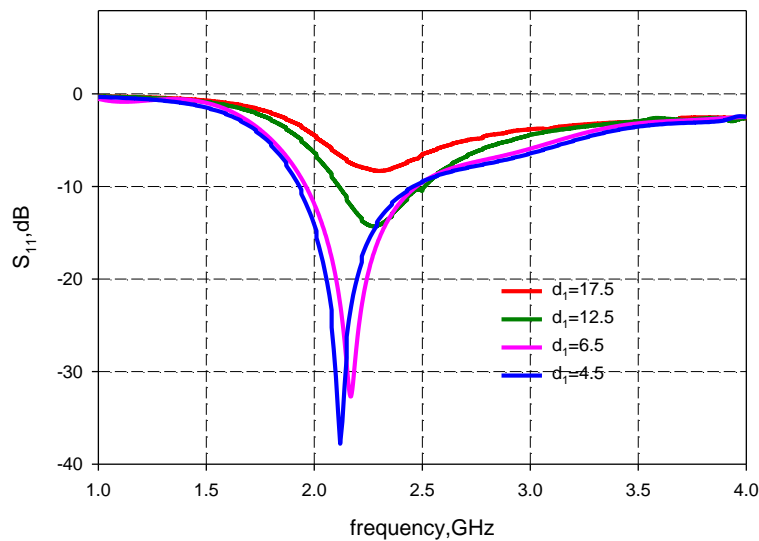


Fig.5.7. Reflection characteristics of folded monopole with offset feeding ( $L_g = 35\text{mm}$ ,  $W_g = 18\text{mm}$ ,  $w = 3\text{mm}$ ,  $l_1 = 11\text{mm}$ ,  $l_2 = 10\text{mm}$ ,  $l_3 = 3\text{mm}$ )

Variation of percentage bandwidth with respect to  $d_1/\lambda_d$  is given in Fig.5.8. Maximum bandwidth is observed for  $d_1 = 0.08\lambda_d$ . In this case, antenna resonates at 2.16GHz with 24% bandwidth.

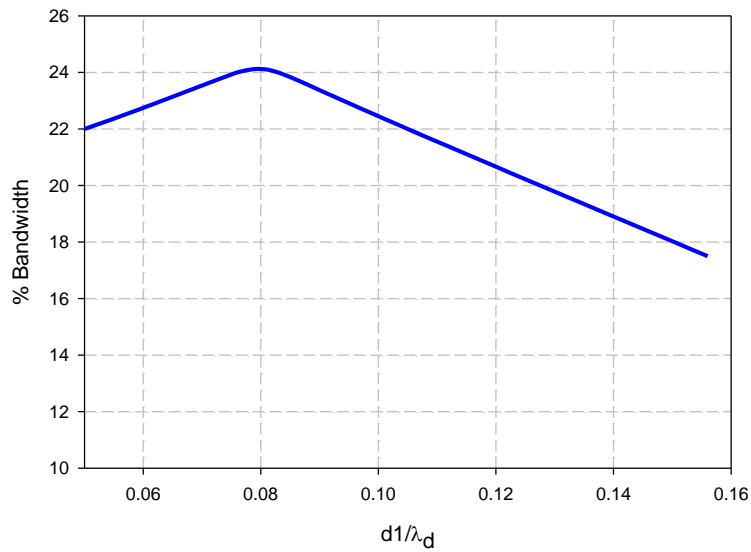


Fig.5.8 Variation of percentage bandwidth with respect to offset ( $L_g = 35\text{mm}$ ,  $W_g = 18\text{mm}$ ,  $l_1 = 11\text{mm}$ ,  $w = 3\text{mm}$ ,  $l_2 = 10\text{mm}$ ,  $l_3 = 3\text{mm}$ )

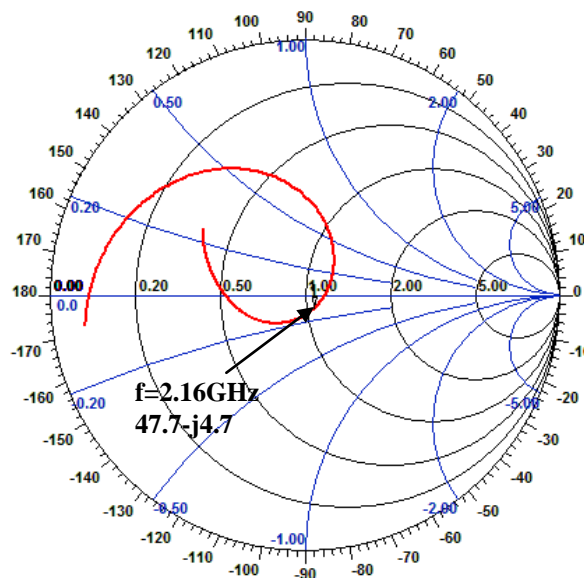


Fig.5.9 Smith chart for the folded monopole with optimum  $d_1$  ( $L_g = 35\text{mm}$ ,  $W_g = 18\text{mm}$ ,  $l_1 = 11\text{mm}$ ,  $w = 3\text{mm}$ ,  $l_2 = 10\text{mm}$ ,  $l_3 = 3\text{mm}$ ,  $d_1 = 6.5\text{mm}$ )

Smith chart showing the impedance variation is given in Fig.5.9. At the resonant frequency, input impedance became  $47.7 - j4.7\Omega$ . From the smith

chart it is clear that feed offset adds inductive reactance and impedance became less capacitive. This improves the matching. But large offset distance will introduce high asymmetry in the structure. So even though it shows good impedance bandwidth with offset distance, antenna radiation pattern is tilted.

**Surface current distribution**

The simulated surface current distribution for the resonant frequency, 2.16GHz is shown in Fig.5.10. The surface current density is maximum over the folded arm, which constitutes the resonance length. Due to the offset, there is a significant current flow along the edge of the ground plane which can cause a slight shift in the radiation pattern.

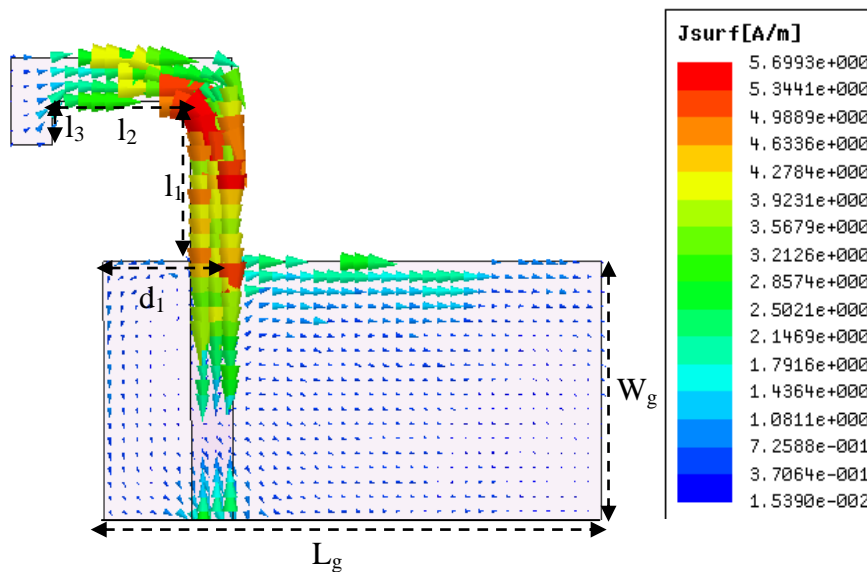
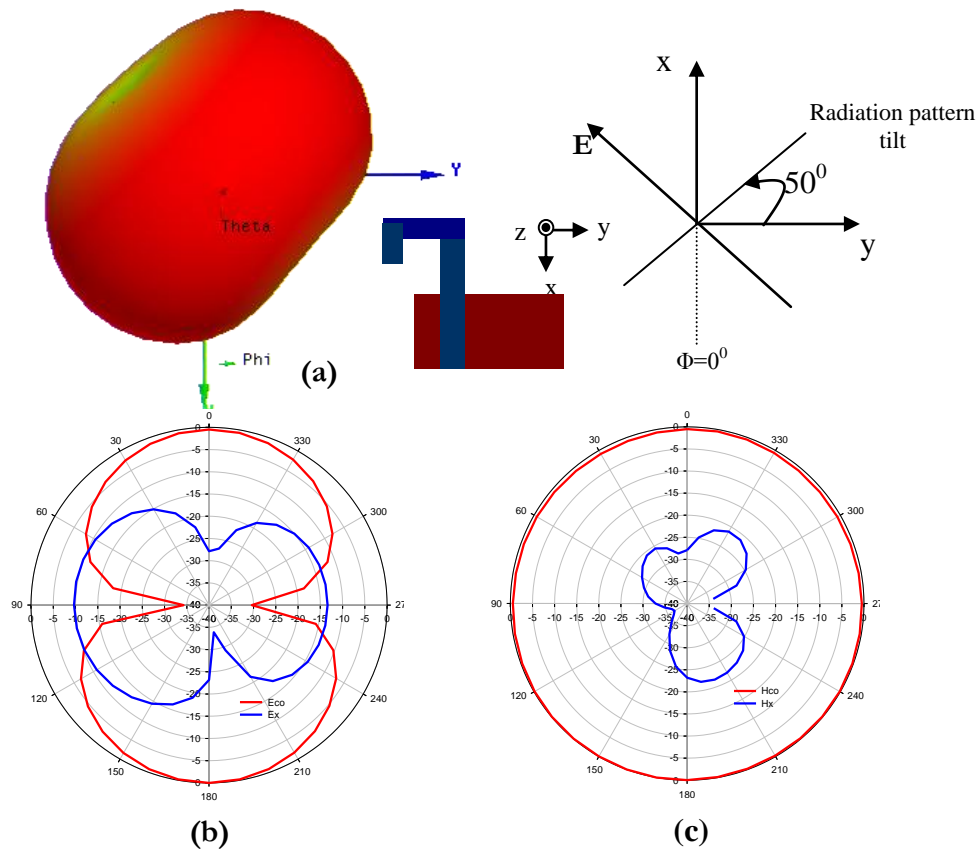


Fig.5.10. Simulated surface current distribution at the resonant frequency ( $L_g = 35\text{mm}$ ,  $W_g = 18\text{mm}$ ,  $w = 3\text{mm}$ ,  $l_1 = 11\text{mm}$ ,  $l_2 = 10\text{mm}$ ,  $l_3 = 3\text{mm}$ ,  $d_1 = 6.5\text{mm}$ )

**Radiation pattern**

The simulated 3D radiation pattern corresponding to  $d_1 = 0.08\lambda_d$  at the resonant frequency is given in Fig.5.11a. Radiation pattern is tilted by an angle of  $50^\circ$  in the azimuth plane as compared to the printed monopole. This

may be due to the radiation from the ground plane and asymmetric geometry of the present system. In the former case, due to symmetry in the configuration, fields from the ground plane edges on either side of the monopole strip are of same strength and opposite direction, which cancels at the farfield. The two dimensional radiation pattern measured at the resonant frequency along the two principal planes are given in Fig 5.11b&c.



**Fig.5.11. Radiation pattern at 2.16GHz for the folded monopole with optimum  $d_1$  ( $L_g = 35\text{mm}$ ,  $W_g = 18\text{mm}$ ,  $w = 3\text{mm}$ ,  $l_1 = 11\text{mm}$ ,  $l_2 = 10\text{mm}$ ,  $l_3 = 3\text{mm}$ ,  $d_1 = 6.5\text{mm}$ )**  
**(a) 3D pattern (b) E plane (c) H plane**

The radiation pattern is nearly omnidirectional with a figure of eight in the E plane. Cross polarization is better than -25dB along the bore sight.

Polarization of the antenna is linear and tilted by an angle of  $-45^\circ$  with respect to the y axis.

Antenna shows an average gain of 2.1dBi in the operating band with an efficiency of 93% at the resonant frequency. The increase in gain and efficiency are because of the better impedance match due to the feed offset.

### 5.2.5 Ground plane study

The main objective of this chapter (folding analysis) is to achieve compactness without much deterioration in the radiation performances. The present ground plane dimensions have been optimized for better impedance bandwidth in the case of dual band dual strip antenna. But in the present analysis of folded (top loaded) monopole, it is observed that folding increases the input impedance and impedance becomes highly capacitive. Impedance matching improves as the offset distance decreases. In this context, a detailed analysis of the finite ground plane on antenna performances is required to further down size the antenna and to optimize its dimensions for a competent design.

#### 5.2.5.1 Effect of ground plane width ' $W_g$ '

Finite ground plane effect has been studied for the folded monopole with offset spacing  $d_1=0.08\lambda_a$ . In this analysis width of the ground plane has been changed by keeping all the other parameters constant. The reflection characteristics are shown in the Fig.5.12. It is observed that impedance bandwidth decreases as ground plane width reduces. This behaviour is as expected and is similar to that observed in the case of dual band dual strip antenna explained in chapter 4. There is not much change in the resonant frequency. So from this analysis once again it is confirmed that ground plane width controls the bandwidth and there is hardly any impact on resonant frequency.

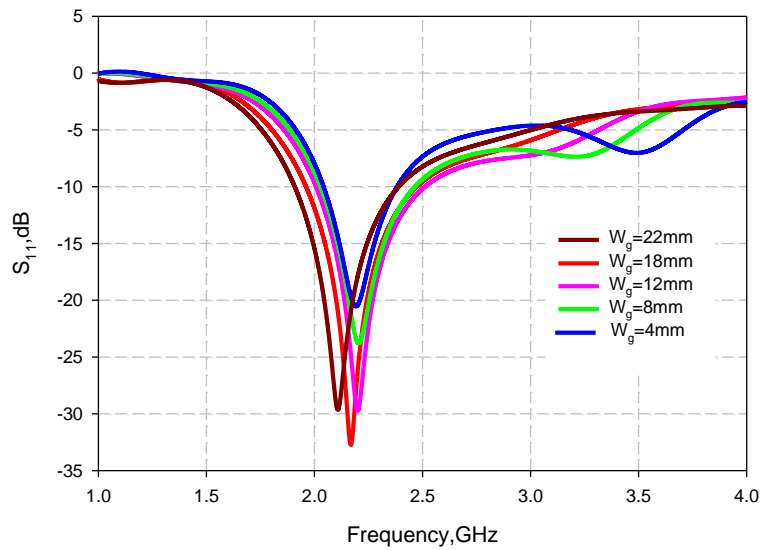


Fig.5.12 Reflection characteristics of folded monopole with various ground plane widths  $W_g$  ( $L_g = 35\text{mm}$ ,  $l_1 = 11\text{mm}$ ,  $l_2 = 10\text{mm}$ ,  $l_3 = 3\text{mm}$ ,  $w = 3\text{mm}$ ,  $d_1 = 6.5\text{mm}$ )

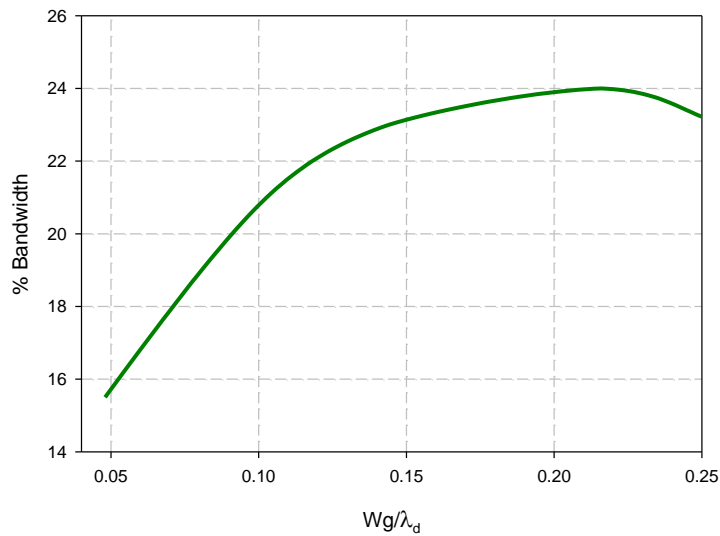


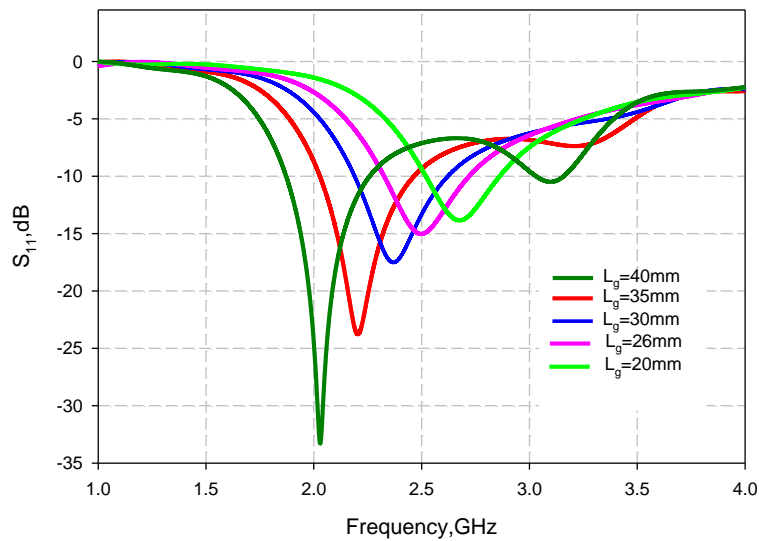
Fig.5.13 Variation of percentage bandwidth with various ground plane widths  $W_g$  ( $L_g = 35\text{mm}$ ,  $l_1 = 11\text{mm}$ ,  $l_2 = 10\text{mm}$ ,  $l_3 = 3\text{mm}$ ,  $w = 3\text{mm}$ ,  $d_1 = 6.5\text{mm}$ )

Fig.5.13 shows the variation of impedance bandwidth with respect to the ground plane width  $W_g$ . As  $W_g$  increases bandwidth also increases up to a width of  $W_g = 0.22\lambda_d$ , beyond that it decreases. For  $W_g = 0.22\lambda_d$  a maximum

of 24% bandwidth is recorded. But keeping compactness as the primary concern,  $W_g=0.1\lambda_d$  for which 21% bandwidth obtained is considered as optimum  $W_g$  for a compact folded design. Here  $\lambda_d$  is the wavelength in the substrate corresponding to the resonant frequency.

### 5.2.5.2 Effect of ground plane Length ' $L_g$ '

In this section effect of ground plane length on antenna performances are explained. Reflection characteristics are shown in Fig. 5.14. It is observed that as the ground plane length decreases, resonant frequency increases as shown in the figure. This is similar to the observations in the previous chapter for the case of printed monopole. There it was concluded that resonant frequency increases considerably if ground plane length  $L_g$  reduces below  $0.8\lambda_d$ .



**Fig.5.14. Reflection characteristics of folded monopole with various ground plane lengths  $L_g$  ( $W_g = 8\text{mm}$ ,  $l_1 = 11\text{mm}$ ,  $l_2 = 10\text{mm}$ ,  $l_3 = 3\text{mm}$ ,  $w = 3\text{mm}$ ,  $d_1 = 6.5\text{mm}$ )**

Another important observation is the reduction in bandwidth as ground plane length decreases. Variation of percentage bandwidth with different ground plane length is plotted in Fig.5.15. Antenna shows

maximum bandwidth of 20.5% for  $L_g=0.42\lambda_d$ , after that bandwidth reduces as shown in the figure. Here also for a compact antenna design,  $L_g=0.35\lambda_d$  is considered as optimum even though bandwidth is 4% less for this case.

As the ground plane length  $L_g$  increases, the second resonance which is due the L shaped path as mentioned in the previous chapter also decreases with good impedance match as shown in Fig.5.14.

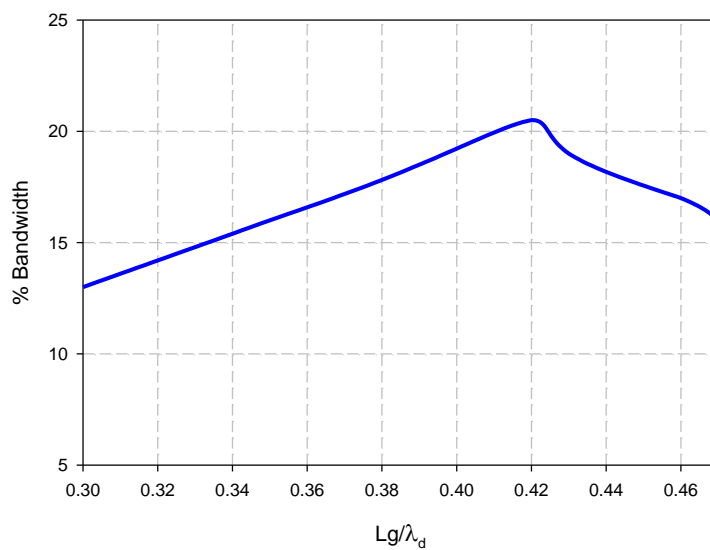


**Fig.5.15. Variation of percentage bandwidth with various ground plane lengths  $L_g$**   
( $W_g = 8\text{mm}$ ,  $l_1= 11\text{mm}$ ,  $l_2=10\text{mm}$ ,  $l_3=3\text{mm}$ ,  $w = 3\text{mm}$ ,  $d_1=6.5\text{mm}$ )

A detailed analysis has been carried out on folded monopole configuration with optimised parameters  $L_g=0.35\lambda_d$ ,  $W_g=0.1\lambda_d$  and  $d_1=0.08\lambda_d$ . The measured reflection characteristics is plotted along with FDTD simulated result in Fig. 5.16. Antenna resonates at 2.5GHz with 2:1 VSWR band extends from 2.32GHz to 2.71GHz.

The simulated surface current distribution for this case at the resonant frequency is given in Fig.5.17. A quarter wave variations corresponding to the resonant frequency is observed along the folded monopole strip as shown in the figure. Antenna shows linear polarization along  $-45^\circ$  with respect to y



axis. The measured transmission parameter along the bore sight, for the entire operating band is shown in Fig.5.18. This shows the polarisation is same in the entire band.

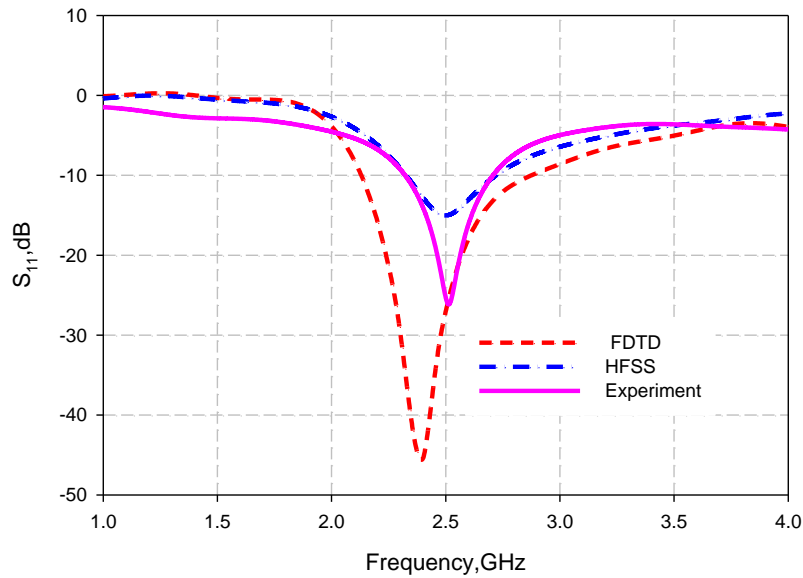


Fig.5.16. Reflection characteristics for the folded monopole with optimum dimensions ( $L_g=26\text{mm}$ ,  $W_g = 8\text{mm}$ ,  $l_1= 11\text{mm}$ ,  $l_2=10\text{mm}$ ,  $l_3=3\text{mm}$ ,  $w = 3\text{mm}$ ,  $d_1=6.5\text{mm}$ ,  $\epsilon_r=4.2$ ,  $h=1.6\text{mm}$ )

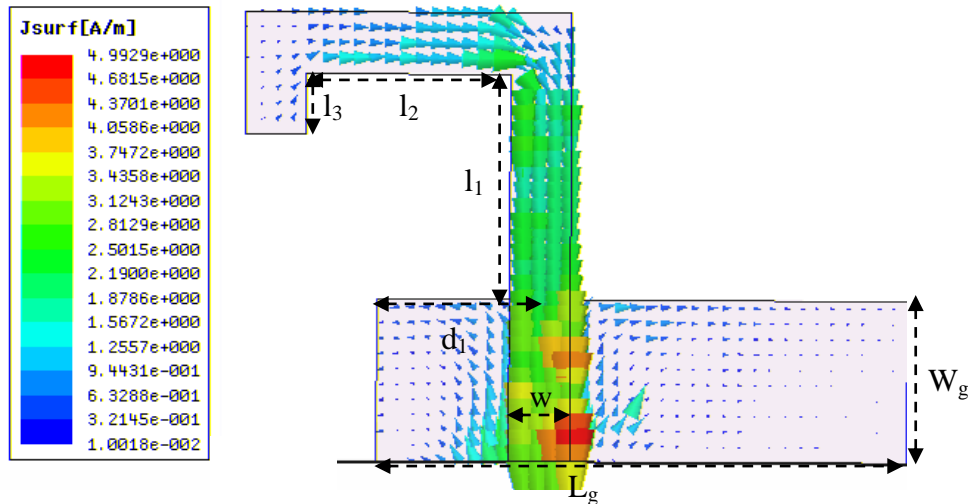


Fig.5.17. simulated surface current distribution at 2.5GHz ( $L_g=26\text{mm}$ ,  $W_g = 8\text{mm}$ ,  $l_1= 11\text{mm}$ ,  $l_2=10\text{mm}$ ,  $l_3=3\text{mm}$ ,  $w = 3\text{mm}$ ,  $d_1=6.5\text{mm}$ ,  $\epsilon_r=4.2$ ,  $h=1.6\text{mm}$ )

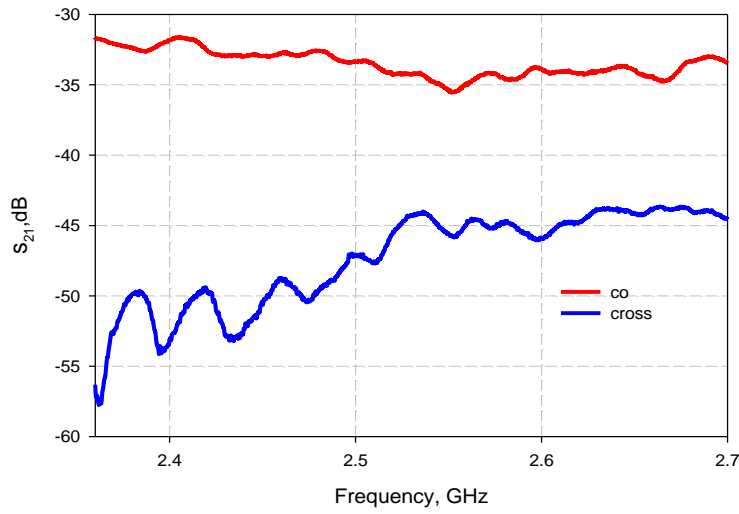


Fig.5.18. Measured co-polarised and cross-polarised power with frequency ( $L_g=26\text{mm}$ ,  $W_g = 8\text{mm}$ ,  $l_1= 11\text{mm}$ ,  $l_2=10\text{mm}$ ,  $l_3=3\text{mm}$ ,  $w = 3\text{mm}$ ,  $d_1=6.5\text{mm}$ )

**Radiation pattern**

The simulated 3D radiation pattern at the resonant frequency is shown in Fig.5.19.

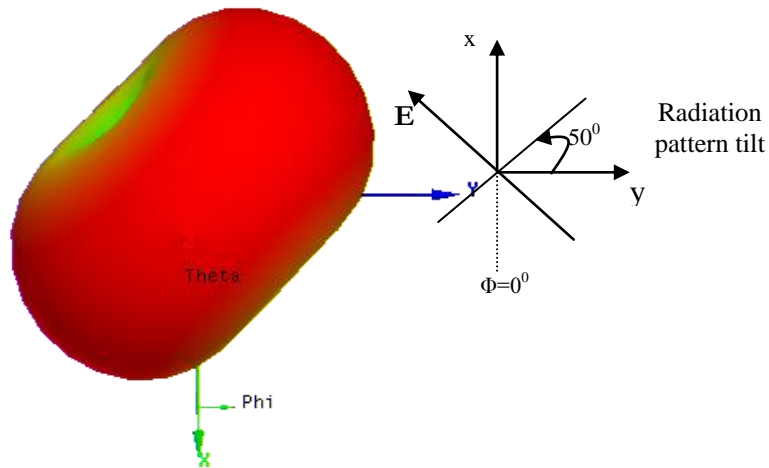


Fig.5.19 3D radiation pattern for the folded monopole with optimum dimensions ( $L_g=26\text{mm}$ ,  $W_g = 8\text{mm}$ ,  $l_1= 11\text{mm}$ ,  $l_2=10\text{mm}$ ,  $l_3=3\text{mm}$ ,  $w = 3\text{mm}$ ,  $d_1=6.5\text{mm}$ )

Radiation pattern is tilted by an angle of  $50^\circ$  in the azimuth plane as compared to printed monopole antenna. Tilt in the radiation pattern is because of the asymmetry in the configuration due the feed offset .

Average gain of the antenna measured in the band is 1.96dBi with an efficiency of 91% at the resonant frequency.

### 5.2.6 Effect of top loading

In the previous sections performance of the folded monopole antenna is compared with that of the printed monopole antenna. From the experimental and simulation results it is understood that folding the monopole towards the ground plane increases the coupling between the ground plane and the signal strip, which results in higher capacitive input impedance. A detailed study on feed offsetting and ground plane truncation has been carried out. It has been proved that feed offset can improve the impedance bandwidth. The compactness can be achieved by truncating the ground plane without much deterioration in antenna performances.

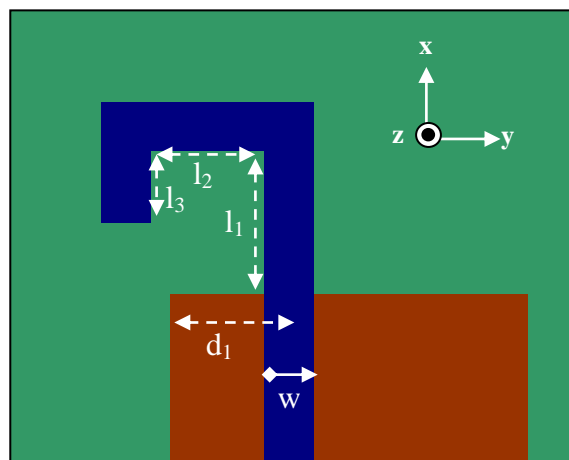


Fig.5.20. Folded monopole antenna  
( $L_g=26\text{mm}$ ,  $W_g = 8\text{mm}$ ,  $l_1= 11\text{mm}$ ,  $l_2=10\text{mm}$ ,  $l_3=3\text{mm}$ ,  $w = 3\text{mm}$ ,  
 $d_1=6.5\text{mm}$ )

In this section a detailed investigation has been carried out to study the effect of different folding options (top loading positions). The folded monopole configuration has three distinct design parameters like  $l_1$ ,  $l_2$  and  $l_3$

as shown in Fig.5.20. The study has been focused on the impact of these design parameters on antenna performances.

### 5.2.6.1 Variation of $l_1$

In this case, the parameter  $l_1$  is varied by keeping the total length ( $l_1 + l_2 + l_3$ ) of the folded antenna constant. This analysis has been carried out on the folded monopole antenna with offset distance  $d_1=0.08\lambda_d$  and ground plane dimensions  $L_g=0.35\lambda_d$  and  $W_g=0.1\lambda_d$ . Reflection characteristics obtained are plotted in Fig.5.21. It is clear from the figure that impedance bandwidth reduces as  $l_1$  decreases. As  $l_1$  decreases the top loaded L-shaped strip ( $l_2 + l_3$ ) becomes closer to the ground plane and this in turn increases the coupling between the ground plane and the top loaded arm. In the case of  $l_1=11\text{mm}$ , antenna resonates with 15.6% bandwidth where as for  $l_1=5\text{mm}$  bandwidth is reduced to 9.6% as shown in the figure. So it is concluded that as  $l_1$  increases antenna shows good impedance bandwidth. But increasing  $l_1$  further will affect the compactness.

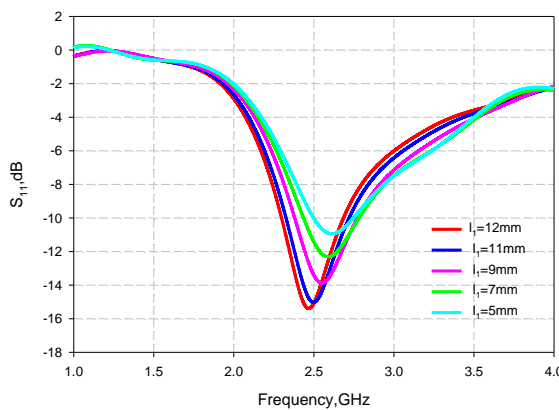


Fig.5.21. Reflection characteristics for different  $l_1$  ( $L_g=26\text{mm}$ ,  $W_g = 8\text{mm}$ ,  $l_1 + l_2 + l_3 = 24\text{mm}$ ,  $w = 3\text{mm}$ ,  $d_1=6.5\text{mm}$ )

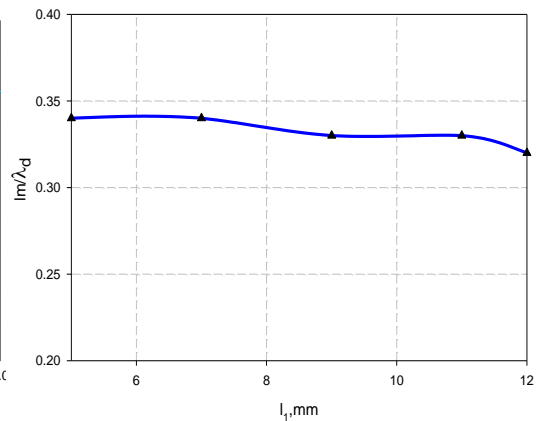


Fig.5.22. Total resonant length variation for different  $l_1$  ( $L_g=26\text{mm}$ ,  $W_g = 8\text{mm}$ ,  $l_1 + l_2 + l_3 = 24\text{mm}$ ,  $w = 3\text{mm}$ ,  $d_1=6.5\text{mm}$ )

Impact of  $l_1$  on total resonant length ( $l_m = l_1 + l_2 + l_3$ ) is shown in Fig.5.22. It is found that the total resonant length remains almost constant with  $l_1$  variation.

### 5.2.6.2. Variation of $l_2$

Impact of the horizontal strip  $l_2$  is analyzed in this section. Experiment has been conducted by varying  $l_2$  by keeping the total folded length constant at 24mm. Reflection characteristics corresponding to  $l_2$  variations are plotted in fig.5.23. Here also it is observed that as  $l_2$  increases, antenna shows better impedance bandwidth. Variation of total resonant length ( $l_m = l_1 + l_2 + l_3$ ) against  $l_2$  is plotted in Fig.5.24. Resonant length remains almost constant with respect to  $l_2$  variation as shown in the figure.

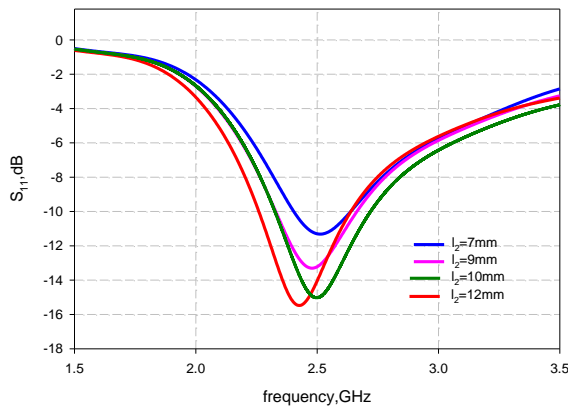


Fig.5.23. Reflection characteristics for different  $l_2$  ( $L_g=26\text{mm}$ ,  $W_g = 8\text{mm}$ ,  $l_1 + l_2 + l_3 = 24\text{mm}$ ,  $w = 3\text{mm}$ ,  $d_1=6.5\text{mm}$ )

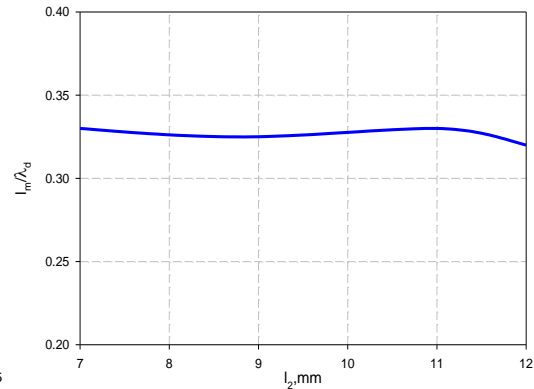
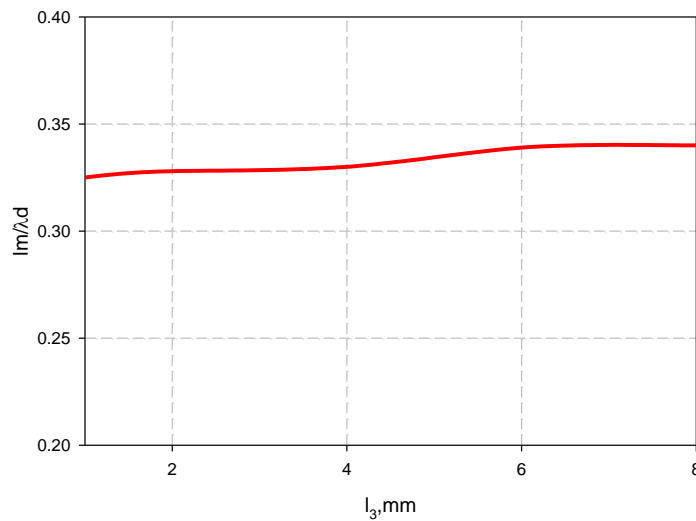


Fig.5.24. Total resonant length variation for different  $l_2$  ( $L_g=26\text{mm}$ ,  $W_g = 8\text{mm}$ ,  $l_1 + l_2 + l_3 = 24\text{mm}$ ,  $w = 3\text{mm}$ ,  $d_1=6.5\text{mm}$ )

### 5.2.6.3. Variation of $l_3$

Variation of total resonant length with respect to  $l_3$  is shown in Fig.5.25. Variation study has been conducted by keeping  $l_1=11\text{mm}$  and  $l_2, l_3$  varied as keeping  $l_1+l_2+l_3=24$ . The resonant length remains almost constant with  $l_3$ .

From the folding analysis carried out in this section, it is concluded that folding lengths ( $l_1, l_2, l_3$ ) have significant impact on impedance matching. Folding the strip with a constant total length ( $l_1+l_2+l_3$ ), affects impedance bandwidth more compared to the resonant frequency. Variation of resonant frequency is very less.



**Fig.5.25** Total resonant length variation for different  $l_3$   
( $L_g=26\text{mm}$ ,  $W_g = 8\text{mm}$ ,  $l_1 + l_2 + l_3=24\text{mm}$ ,  $w = 3\text{mm}$ ,  $d_1=6.5\text{mm}$ )

### ***Inferences***

The following conclusion were arrived after the exhaustive simulation and experimental analysis

- ♣ Folding a printed monopole towards the ground plane increases the input impedance. Impedance becomes capacitive and antenna losses the impedance matching.
- ♣ Radiation pattern shows a  $10^\circ$  tilt in the azimuth plane compared to a normal printed monopole
- ♣ Feed offsetting towards the edge of the ground plane improves the impedance bandwidth. But feed offsetting gives asymmetry in the configuration. Radiation pattern has been tilted by  $50^\circ$  in the azimuth plane compared to a normal printed monopole.

- ♣ Feed offsetting introduces another resonance similar to that of the offset-fed monopole mentioned in chapter 4. This is due to the meandered path including the ground plane.
- ♣ Ground plane width variation affects bandwidth
- ♣ As the ground plane length decreases, the “second resonance” shift towards the higher side.
- ♣ Folding position/top-loading position has significant impact on antenna performances.
- ♣ As  $l_1, l_2$  increases antenna shows better impedance bandwidth. But for keeping the compactness, a minimum level of compromise on performance is required.
- ♣ As in the case of dual strip antenna mentioned in chapter 4, a folded arm on the ground plane can excite second mode with compact geometry.

### 5.3 Double folded dual strip antenna

The main objective of this chapter is to achieve compactness by folding the dual strip antenna designed in chapter 4. The impacts of feed offset, ground plane truncation, top loading on impedance bandwidth and radiation characteristics are evaluated in the previous sections. It has been found that for a compact ground plane, the second resonance has been shifted to the higher side as in the case of printed dual strip antenna discussed in chapter 4. In this section another folded arm (which is obtained by folding the vertical ground strip mentioned in dual strip antenna) is introduced as an extension from the ground plane at a spacing ‘s’ as shown in the Fig.5.26.

The total length of the strip is taken same as that of the dual strip antenna designed for 1.8/2.4GHz and it is 29mm. This has been folded as shown in the Fig.5.26 with  $l_4=11\text{mm}$ ,  $l_5=11\text{mm}$  and  $l_6=7\text{mm}$ .  $l_4$  and  $l_5$  are

kept as same as  $l_1$  and  $l_2$  which are the optimized dimensions for the folded monopole. Initially the spacing 's' has been taken as 13mm same as that of the dual band dual strip antenna designed for 1.8/2.4GHz.

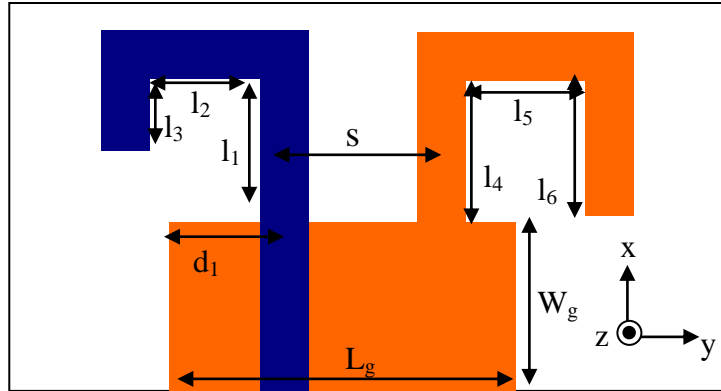


Fig.5.26 Geometry of folded dual strip antenna  
 $(L_g=26\text{mm}, W_g = 8\text{mm}, l_1= 11\text{mm}, l_2=10\text{mm}, l_3=3\text{mm},$   
 $w = 3\text{mm}, d_1=6.5\text{mm}, l_4= 11\text{mm}, l_5=10\text{mm}, l_6=8\text{mm}, s=13\text{mm})$

### 5.3.1 Reflection characteristics

The measured, simulated and FDTD computed reflection characteristics of the antenna are shown in Fig.5.27.

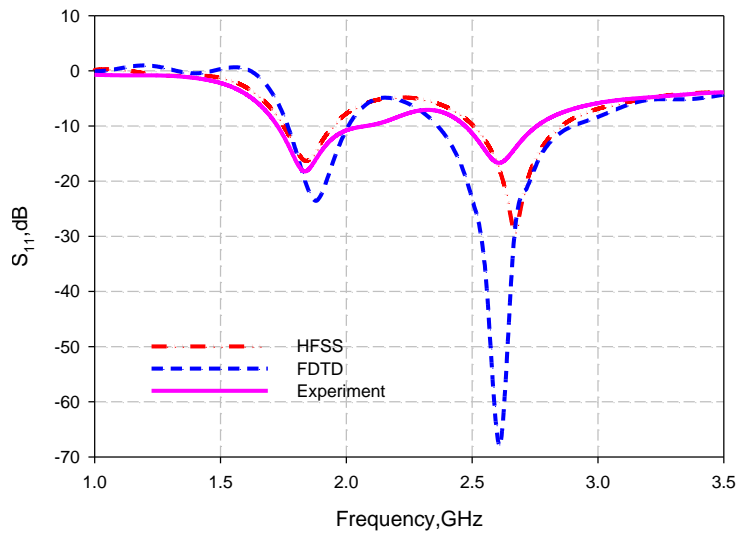


Fig.5.27 Reflection characteristics of the folded dual strip antenna  
 $(L_g=26\text{mm}, W_g = 8\text{mm}, d_1=6.5\text{mm}, l_1= 11\text{mm}, l_2=10\text{mm}, l_3=3\text{mm},$   
 $l_4= 11\text{mm}, l_5=10\text{mm}, l_6=8\text{mm}, w = 3\text{mm}, s=13\text{mm})$



Apart from the original resonance at 2.5GHz, a new resonance is obtained at 1.82GHz. The resonance at 2.5GHz is slightly shifted to 2.63GHz as shown in the figure. The 2:1 VSWR bandwidth obtained for the new resonance is 360MHz and for the higher resonance is 300MHz.

In Fig.5.28 reflections characteristics of folded monopole and folded dual strip antenna are compared. By introducing another folded arm, the folded monopole antenna's resonant frequency has been shifted from 2.5GHz to 2.63GHz and a new lower resonance is appeared at 1.82GHz. The shift in the higher resonance is due to the coupling between the folded monopole and the folded ground arm. Bandwidth corresponding to the higher resonance has been slightly reduced from 15% to 12%.

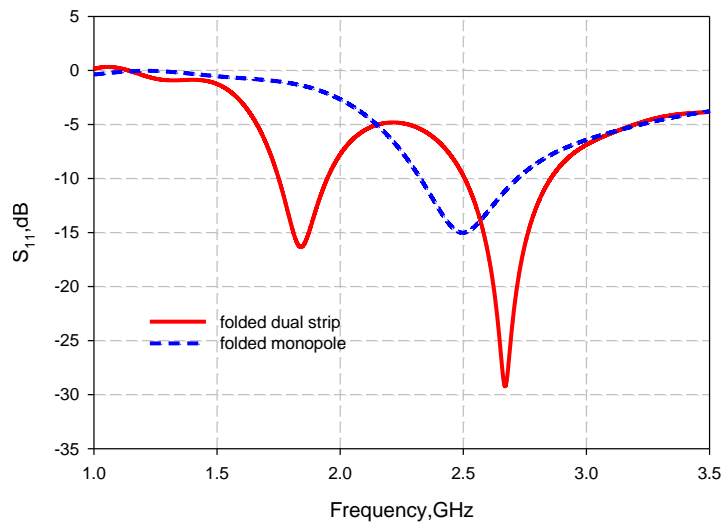


Fig.5.28. Reflection characteristics of folded monopole and folded dual strip antenna

### 5.3.2 Surface current distribution

The simulated surface current distributions for the two resonant frequencies are shown in Fig.5.29. Fig.5.29a shows the surface current distribution corresponding to 1.82GHz. The meandered current path a-b-c-d-e-f-g-h clearly shows that antenna acts as a half wave, asymmetrically fed

folded dipole. The half wave current variation is clearly visible in the figure. So the addition of the folded strip to the ground plane increases the meandered current path and hence lowers the resonant frequency without much change in the fundamental resonance of the folded monopole.

Where as in the case of second resonance (2.63GHz) the surface current distribution is as shown in Fig.5.29b. There is a quarter wave variation along a-b-c-d, corresponding to 2.63GHz as shown in the figure.

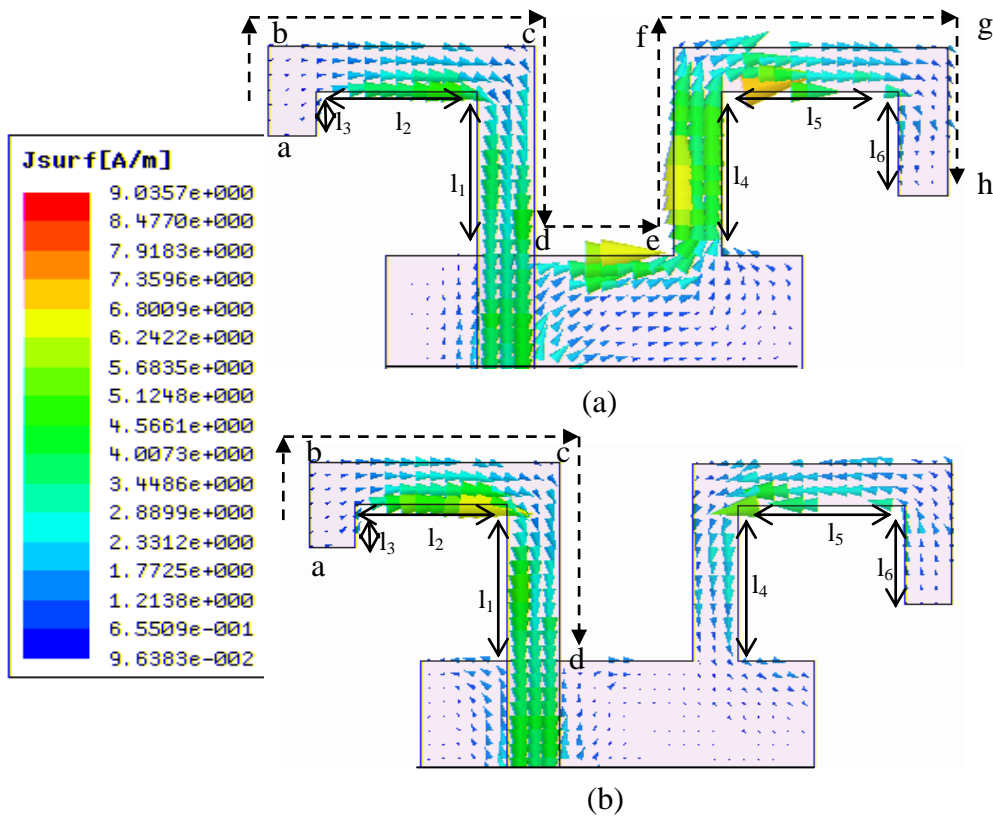


**Fig.5.29. Simulated surface current distribution of folded dual strip antenna**  
 $(L_g=26\text{mm}, W_g = 8\text{mm}, d_1=6.5\text{mm}, l_1= 11\text{mm}, l_2=10\text{mm}, l_3=3\text{mm},$   
 $l_4= 11\text{mm}, l_5=11\text{mm}, l_6=7\text{mm}, w = 3\text{mm}, s=13\text{mm})$   
**(a). 1.82GHz (b) 2.63GHz**

But the current along the ground arm ( $l_4+l_5+l_6$ ) is in the opposite direction with reduced strength. From the experimental and simulation

analysis it is observed that for the higher resonance, the folded ground arm affects both the radiation pattern and impedance matching.

### 5.3.3. Radiation pattern

The simulated radiation patterns for the two resonances are shown in Fig.5.30. The 3D pattern for 1.82GHz is shown in Fig.5.30a. The radiation pattern is equivalent to a dipole placed along the y-axis but with a tilt of  $10^\circ$  ( $\phi=190^\circ$ ) in the azimuth direction. In the case of 2.65GHz radiation plane is tilted by  $20^\circ$  in the azimuth plane compared to a printed monopole antenna as shown in Fig.5.30b.

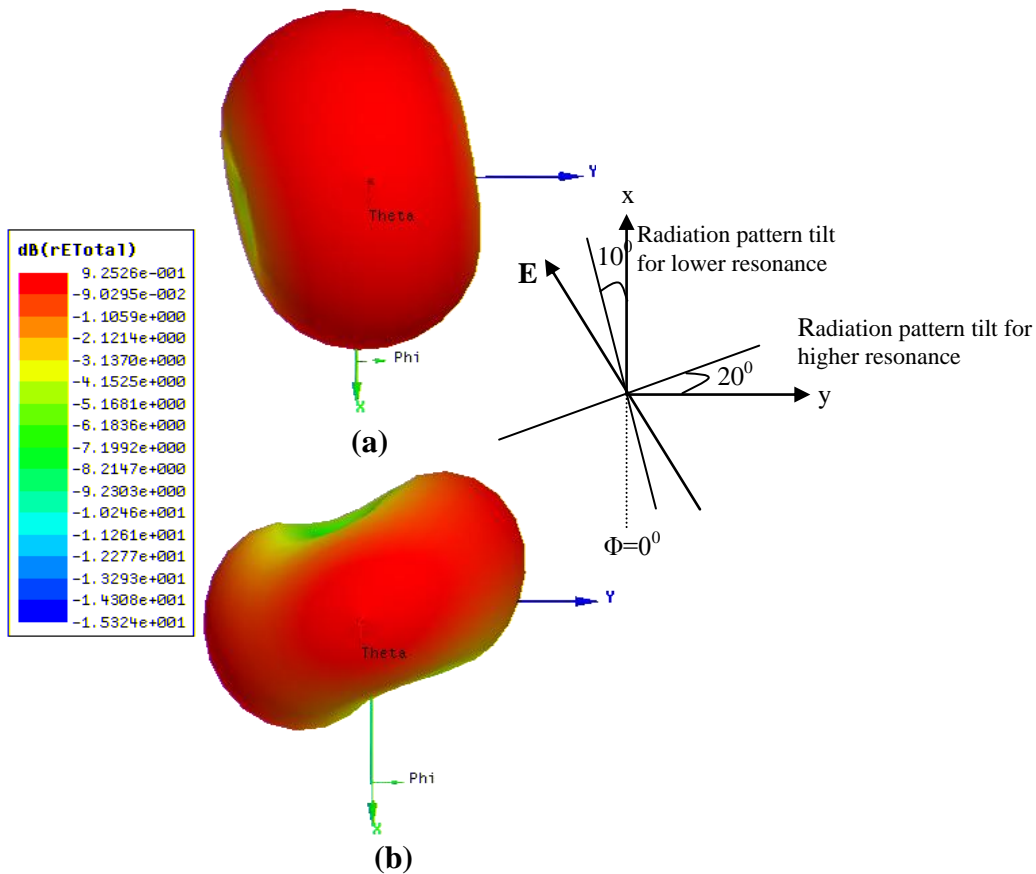
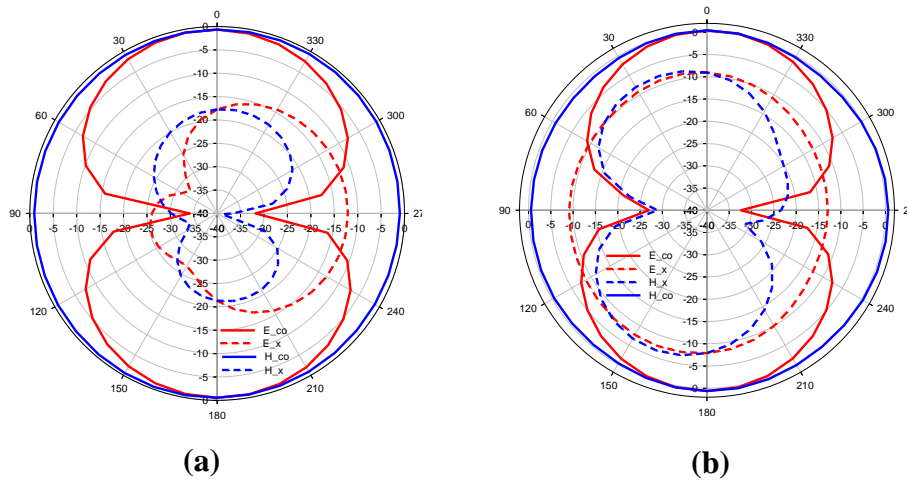
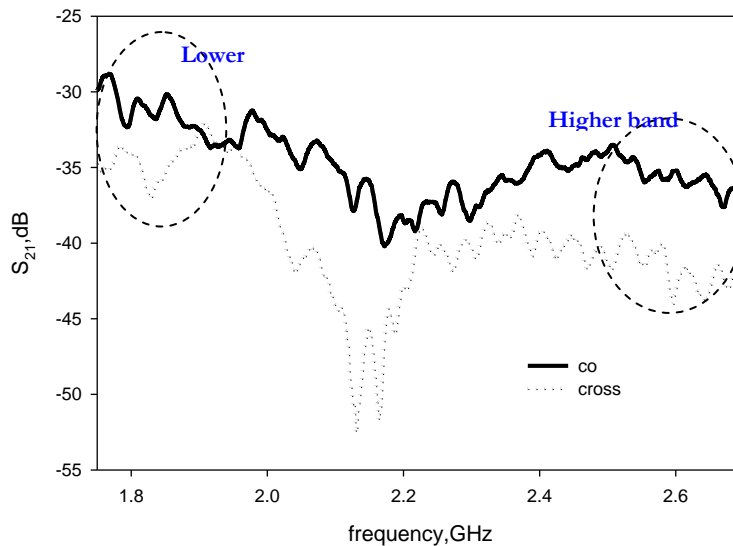


Fig.5.30 3D radiation pattern of the folded dual strip antenna  
 (a) 1.82GHz (b) 2.63GHz  
 ( $L_g=26\text{mm}$ ,  $W_g = 8\text{mm}$ ,  $d_1=6.5\text{mm}$ ,  $l_1= 11\text{mm}$ ,  $l_2=10\text{mm}$ ,  $l_3=3\text{mm}$ ,  
 $l_4= 11\text{mm}$ ,  $l_5=11\text{mm}$ ,  $l_6=7\text{mm}$ ,  $w = 3\text{mm}$ ,  $s=13\text{mm}$ )

The 2D radiation patterns along the two principal planes are given in Fig.5.31. Radiation pattern is figure of eight in the E plane with a half power beam width of  $83^\circ$  for 1.82 GHz and  $70^\circ$  for 2.63GHz respectively. H plane pattern is non directional for both the resonances. Antenna shows similar radiation performances in the entire band. Polarization of the antenna is measured along  $30^\circ$  with respect to X axis for both the resonances.



**Fig.5.31** 2D radiation pattern of the folded dual strip antenna  
 (a) 1.82GHz (b) 2.63GHz



**Fig.5.32** Measured power level ( $S_{21}$ )

The far field power level measured in the entire band is shown in Fig. 5.32. This shows the polarisation is same in the entire band. Antenna shows an average gain of 1.96dBi in the lower band and 2.1dBi in the higher band. The measured efficiency of the antenna is 86% and 88% respectively for the lower and higher resonant frequencies.

#### 5.3.4. Variation of spacing between the arms 's'

The impact of spacing between the folded arms has been analyzed in this section. The reflection characteristics obtained for different spacing 's' are plotted in Fig.5.33. As 's' increases, the lower resonance decreases due to the increase in the meandered resonant length. Another important observation is the reduction in impedance match with decrease of spacing. In the case of higher resonance which is explicitly due to the folded monopole strip, a slight increase in the resonant frequency and impedance match is observed with increase in spacing. As the spacing increases, the capacitive coupling between the folded ground strip and the folded signal strip decreases and hence improves the impedance match.

For very small values of s(s=0mm, s=3mm) performance of the antenna is different from the other cases. In this case for the higher resonance, antenna behaves like a halfwave dipole excited by a combination of microstrip line and bifilar line as clear from the surface current distribution shown in Fig.5.34b. For the lower resonance, the behaviour is same as expected but because of less spacing, coupling is high and antenna loses matching. Surface current distribution for this case is given in Fig.5.34a. Meandered current path is clear from the figure. Current strength is maximum at the vertical strips. This also contributes radiation and the resultant radiation pattern is different from that obtained in the case of folded dual strip antenna with s=13mm (Fig.5.30a). Radiation pattern for the lower resonance is given in Fig.5.35a. But the radiation pattern obtained

in the case of higher resonance is almost same as that of a horizontal half wave dipole and is shown in Fig.5.35b. Slight tilt in the pattern is due to the asymmetry in the antenna structure.

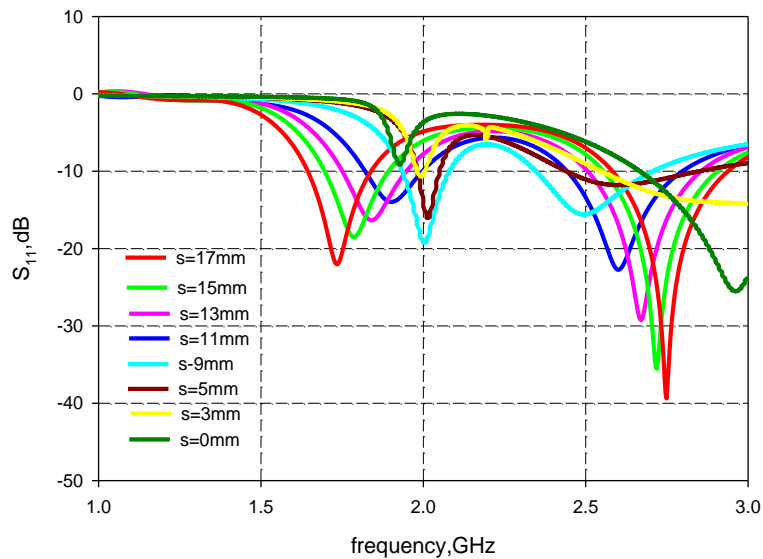


Fig.5.33. Variation of Spacing's'  
 $(L_g=26\text{mm}, W_g = 8\text{mm}, d_1=6.5\text{mm}, l_1= 11\text{mm}, l_2=10\text{mm}, l_3=3\text{mm},$   
 $l_4= 11\text{mm}, l_5=10\text{mm}, l_6=8\text{mm } w = 3\text{mm})$

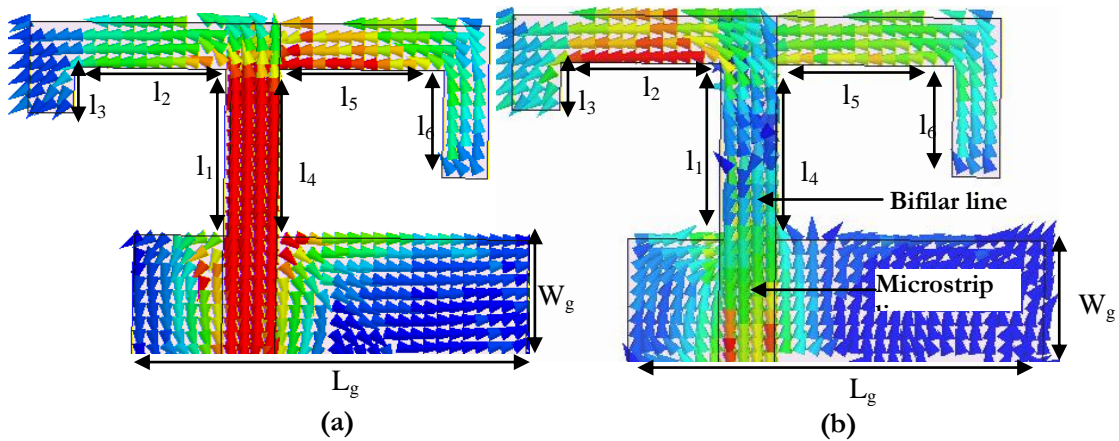
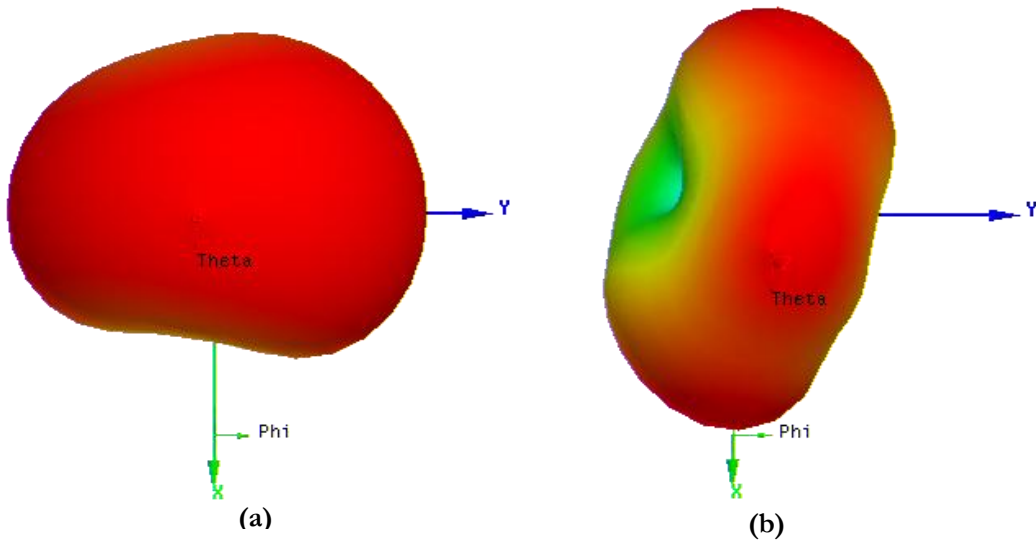
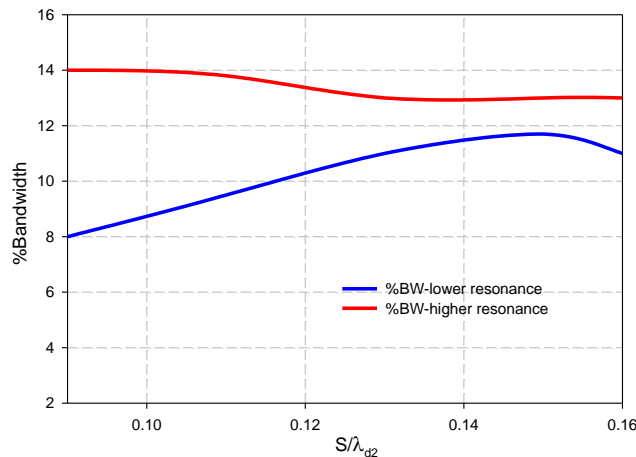


Fig.5.34 Surface current distribution for  $s=0\text{mm}$   
 (a) 1.92GHz (b) 2.97GHz  
 $(L_g=26\text{mm}, W_g = 8\text{mm}, d_1=6.5\text{mm}, l_1= 11\text{mm}, l_2=10\text{mm}, l_3=3\text{mm},$   
 $l_4= 11\text{mm}, l_5=10\text{mm}, l_6=8\text{mm } w = 3\text{mm},)$



**Fig.5.35 3D Radiation Pattern for  $s=0\text{mm}$**   
 (a) 1.92GHz (b) 2.97GHz  
 ( $L_g=26\text{mm}$ ,  $W_g = 8\text{mm}$ ,  $d_1=6.5\text{mm}$ ,  $l_1= 11\text{mm}$ ,  $l_2=10\text{mm}$ ,  
 $l_3=3\text{mm}$ ,  $l_4= 11\text{mm}$ ,  $l_5=10\text{mm}$ ,  $l_6=8\text{mm}$ ,  $w = 3\text{mm}$ )

Variation of percentage bandwidth for both the resonances with respect to spacing 's' is plotted in Fig.5.36. As 's' increases impedance bandwidth for the lower resonance increases up to  $s=0.15\lambda_{d2}$ , beyond that it decreases. Whereas for the higher resonance, for very small values of 's' good impedance bandwidth is observed. From the analysis it is concluded that for a compact dual band operation,  $s=0.13 \lambda_{d2}$  can be considered as optimum.



**Fig.5.36 Percentage bandwidth for different Spacing's'**  
 ( $L_g=26\text{mm}$ ,  $W_g = 8\text{mm}$ ,  $d_1=6.5\text{mm}$ ,  $l_1= 11\text{mm}$ ,  $l_2=10\text{mm}$ ,  
 $l_3=3\text{mm}$ ,  $l_4= 11\text{mm}$ ,  $l_5=10\text{mm}$ ,  $l_6=8\text{mm}$ ,  $w = 3\text{mm}$ )

### 5.3.5. Impact of folded arm lengths

The folded dual strip antenna shows two resonances. The higher resonance is due to the folded monopole strip and the lower resonance is due to the meandered current path as mentioned in Fig.5.29. From the current distribution and from the other parametric analysis it is clear that the resonant length is as explained above. Still for formulating the design equations, a detailed analysis has been carried out by varying the total length of the folded arms (folded monopole arm  $(l_1+l_2+l_3)$  and grounded arm  $(l_4+l_5+l_6)$ ).

Variation of resonant frequencies with respect to grounded arm length is plotted in Fig.5.37. In this case,  $l_6$  is varied by keeping  $l_4$  and  $l_5$  as constants and hence the total length varies. It is shown that as length increases, lower resonance decreases due to the increases in the resonant length. Higher resonance also decreases; but the variation is less compared to the lower resonance. Variation of resonant frequencies with respect to the variation in grounded arm length is shown in Fig.5.38.

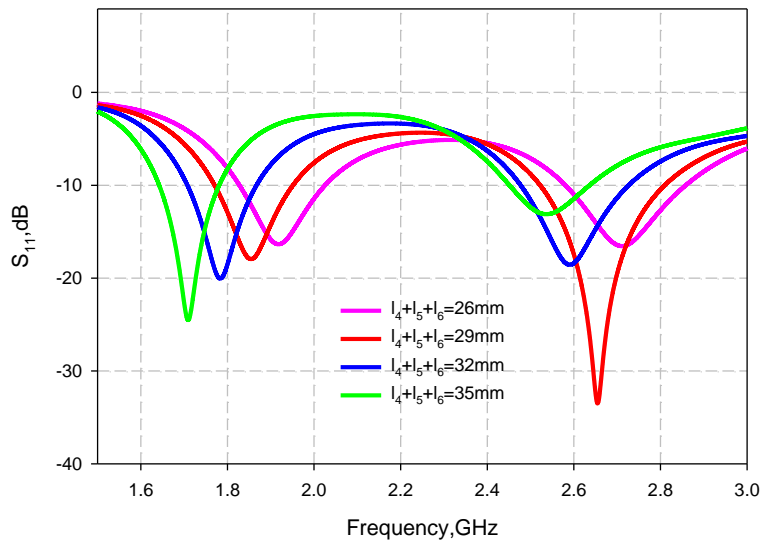
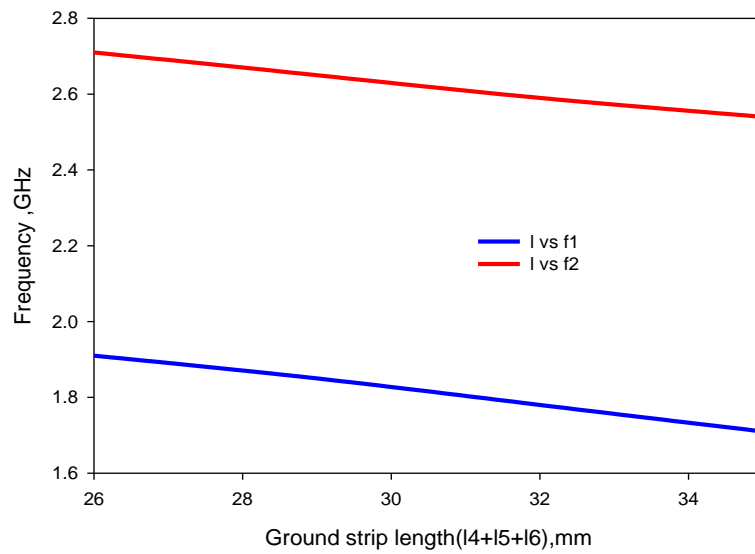
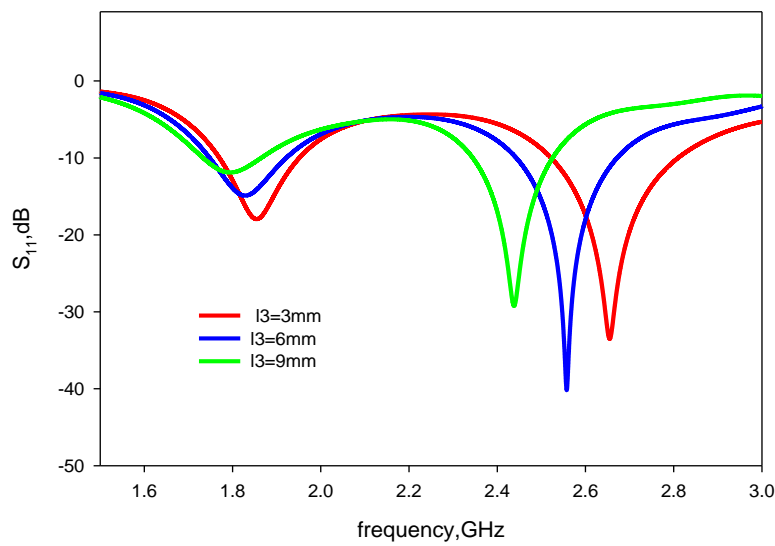


Fig.5.37. Reflection characteristics for different ground strip lengths ( $L_g=26\text{mm}$ ,  $W_g = 8\text{mm}$ ,  $d_1=6.5\text{mm}$ ,  $l_1= 11\text{mm}$ ,  $l_2=10\text{mm}$ ,  $l_3=3\text{mm}$ ,  $w = 3\text{mm}$ ,  $s=13\text{mm}$ )





**Fig.5.38. Variation of resonant frequencies with ground strip length**  
 ( $L_g=26\text{mm}$ ,  $W_g = 8\text{mm}$ ,  $d_1=6.5\text{mm}$ ,  $l_1= 11\text{mm}$ ,  $l_2=10\text{mm}$ ,  
 $l_3=3\text{mm}$ ,  $w = 3\text{mm}$ ,  $s=13\text{mm}$ )



**Fig.5.39. Reflection characteristics for different folded monopole lengths**  
 ( $l_1+l_2+l_3$ )  
 ( $L_g=26\text{mm}$ ,  $W_g = 8\text{mm}$ ,  $d_1=6.5\text{mm}$ ,  $l_4= 11\text{mm}$ ,  $l_5=10\text{mm}$ ,  
 $l_6=8\text{mm}$ ,  $w = 3\text{mm}$ ,  $s=13\text{mm}$ )

The study has been also conducted by varying the folded monopole total length ( $l_1+l_2+l_3$ ). Keeping  $l_1$  and  $l_2$  constant,  $l_3$  varied and hence the

total length is varied. Reflection characteristics obtained for various monopole strip lengths ( $l_1+l_2+l_3$ ) are plotted in Fig.5.39. As  $l_1+l_2+l_3$  increases, both the resonance decreases and the variation for lower resonance is similar to that observed in the case of ground strip length ( $l_4+l_5+l_6$ ).

### 5.3.6 Effect of dielectric constant ( $\epsilon_r$ )

The effect of dielectric constant on antenna performances has been studied by simulating the antenna on different substrate materials.  $\epsilon_r$  has been varied from 2.2 to 4.4. The  $50\Omega$  feed line has been redesigned for corresponding  $\epsilon_r$  values. Reflection characteristics are shown in Fig.5.40. As expected resonant frequencies decreases with increase in dielectric constant.

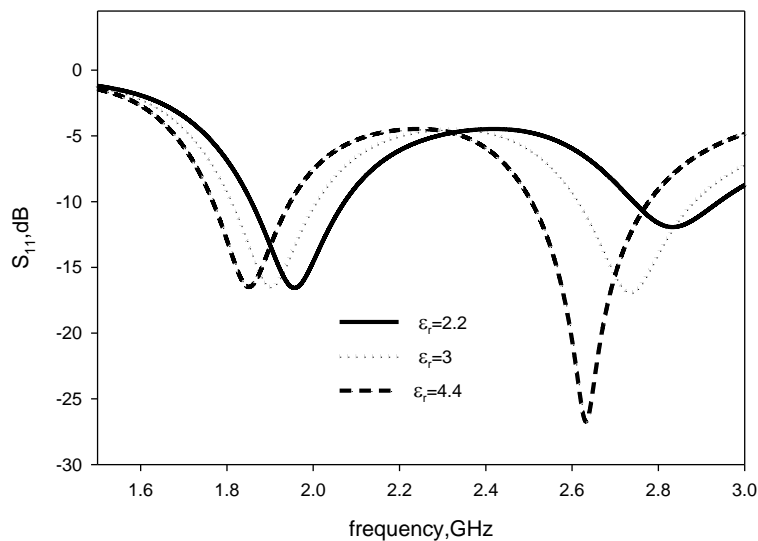
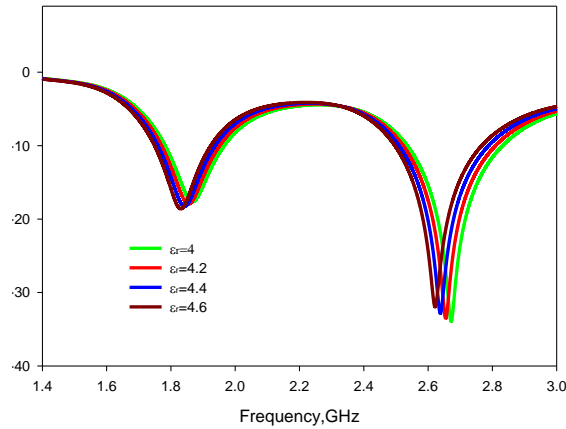


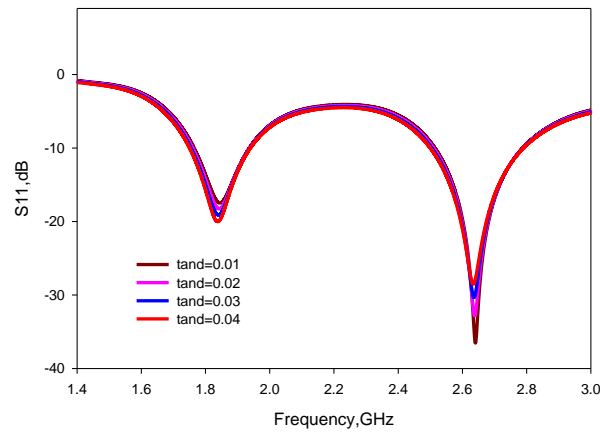
**Fig.5.40. Effect of dielectric constant**  
 ( $L_g=26\text{mm}$ ,  $W_g = 8\text{mm}$ ,  $d_1=6.5\text{mm}$ ,  $l_4= 11\text{mm}$ ,  $l_5=10\text{mm}$ ,  $l_6=8\text{mm}$ ,  
 $l_4=11\text{mm}$ ,  $l_5=10\text{mm}$ ,  $l_6=8\text{mm}$ ,  $s=13\text{mm}$ )

Sensitivity study has been carried out on FR4 substrate by varying dielectric constant from 4 to 4.6 and loss tangent from 0.01 to 0.04. The results are shown in Fig.4.43 b. For a 13% variation in dielectric constant,  $\pm 1.7\%$  variation is observed for lower resonant frequency and  $\pm 1.9\%$  is observed for higher resonant frequency. Variation on loss tangent affects the

impedance matching and bandwidth. As the  $\tan\delta$  increases bandwidth also increases for both the resonances.



(a)



(b)

**Fig.5.40b. Sensitivity study on FR4 substrate**

**(a) Dielectric constant variation (b) Loss tangent variation**

$(L_g=26\text{mm}, W_g=8\text{mm}, d_1=6.5\text{mm}, l_4=11\text{mm}, l_5=10\text{mm}, l_6=8\text{mm},$   
 $l_4=11\text{mm}, l_5=10\text{mm}, l_6=8\text{mm}, s=13\text{mm})$

### 5.3.7 Effect of substrate thickness (h)

The study has been conducted by varying the substrate thickness and the reflection characteristics are shown in Fig.5.41. As substrate thickness increases both the resonances decrease as in the case of dual strip antenna

discussed in chapter 4. The variation is more for the lower resonance compared to the higher resonance. This is because for the lower resonance, thickness ( $h$ ) is a part of resonant length as discussed in the case of dual strip antenna.

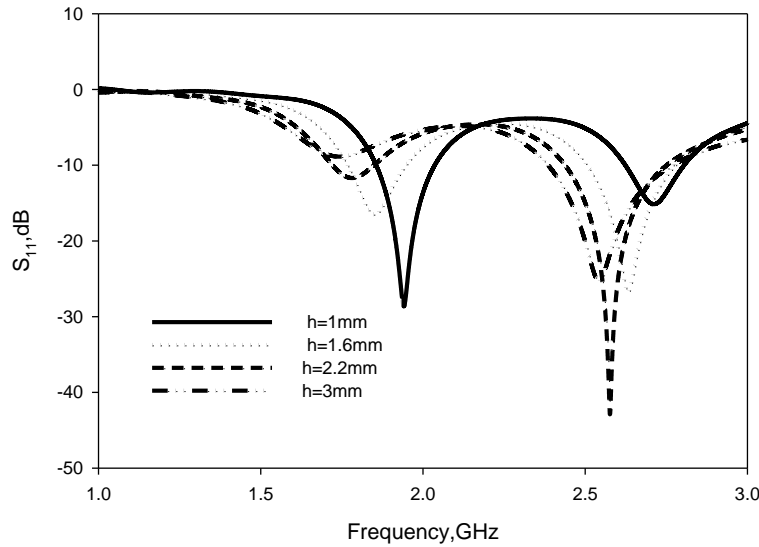


Fig.5.41. Effect of substrate thickness ( $h$ )  
 $(L_g=26\text{mm}, W_g = 8\text{mm}, d_1=6.5\text{mm}, l_4= 11\text{mm}, l_5=10\text{mm}, l_6=8\text{mm},$   
 $l_4= 11\text{mm}, l_5=10\text{mm}, l_6=8\text{mm} s=13\text{mm})$

#### 5.4 Design procedure for a compact dual band folded dual strip antenna

From the simulation and experimental analysis starting from the folded monopole to the folded dual strip antenna, a design procedure for the compact dual band folded dual strip antenna has been derived.

In this dual band folded dual strip antenna design, the second resonance  $f_2$  (higher) is the fundamental mode of the folded monopole and the lower resonance  $f_1$  is the new mode which is due to the meandered path generated by adding the folded arm ( $l_4+l_5+l_6$ ) on the ground plane. The ground plane dimensions ( $L_g, W_g$ ), folded monopole strip lengths ( $l_1, l_2$  and  $l_3$ ) and the feed offset ( $d_1$ ) have to be designed for the second

resonance ( $f_2$ ). The spacing's' and the ground strip lengths ( $l_4$ ,  $l_5$  and  $l_6$ ) have to be designed for the lower resonance ( $f_1$ ). The step by step design procedures are given below.

Step1:- Select a substrate material with dielectric constant  $\epsilon_r$  and height  $h$ .

Step2:- Find out the width of the 50Ω microstrip feed line on the above substrate using the standard formula [1].

Step3: Keep same widths for signal strip as well as ground strip for design simplicity.

Step4. Calculate the effective dielectric constant using the equation

$$\epsilon_{eff} = \frac{\epsilon_r + 1}{2} \dots\dots\dots (5.1)$$

where  $\epsilon_r$  is the relative dielectric constant of the substrate.

Step5:- Find out ground plane dimensions based on the given formulae

$$Lg = \frac{0.34c}{f_2 \sqrt{\epsilon_{eff}}} \dots\dots\dots (5.2)$$

$$Wg = \frac{0.12c}{f_2 \sqrt{\epsilon_{eff}}} \dots\dots\dots (5.3)$$

where  $c$  is the velocity of light and  $f_2$  is the higher resonant frequency.

Step6:- Find out the length of the folded monopole strip ( $l_1$ ,  $l_2$  and  $l_3$ ) corresponding to the higher frequency  $f_2$  based on the equation,

$$l_1 = \frac{0.134c}{f_2 \sqrt{\epsilon_{eff}}} - \frac{(h-1.6)}{1.2} \dots\dots\dots (5.4)$$

$$l_2 = \frac{0.14c}{f_2 \sqrt{\epsilon_{eff}}} - \frac{(h-1.6)}{2.4} \dots\dots\dots (5.5)$$

$$l_3 = \frac{0.09c}{f_2 \sqrt{\epsilon_{eff}}} - \frac{(h-1.6)}{2.4} \dots\dots\dots (5.6)$$

Step7:- find out the feed offset position from the ground plane edge  $d_1$  as

$$d_1 = \frac{0.076c}{f_2 \sqrt{\epsilon_{eff}}} \dots\dots\dots (5.7)$$

Step8: Find out the length of the grounded strip ( $l_4$ ,  $l_5$  and  $l_6$ ) for the lower resonance  $f_1$  as,

$$l_4 = \frac{0.106c}{f_1 \sqrt{\epsilon_{eff}}} - \frac{(h-1.6)}{2.4} \dots\dots\dots (5.8)$$

$$l_5 = \frac{0.13c}{f_1 \sqrt{\epsilon_{eff}}} - \frac{(h-1.6)}{2.4} \dots\dots\dots (5.9)$$

$$l_6 = \frac{0.1c}{f_1 \sqrt{\epsilon_{eff}}} - \frac{(h-1.6)}{2.4} \dots\dots\dots (5.10)$$

Step9:- Calculate the spacing between the strips based on the equation,

$$s = \frac{0.13c}{f_1 \sqrt{\epsilon_{eff}}} \dots\dots\dots (5.11)$$

The coefficients in these equations are derived using the exhaustive experimental and simulation studies.

This design equations are valid only for frequency ratio  $1 \leq f_2/f_1 < 2$  as in the case of dual strip antenna mentioned in chapter 4.

## **5.5 Design and development of folded dual strip antenna for modern communication bands**

The design equations have been validated by designing the folded dual strip antenna for various modern communication bands. Two different antennas have been designed, fabricated and tested, one for the DCS/PCS/WLAN applications covering both 1.8GHz and 2.4GHz bands and the other for GSM applications covering the 800GHz and 900GHz bands. The designed dimensions and experimental /simulation results are well explained in the following sections.

### **5.5.1 Design and development of dual band folded dual strip antenna for DCS/PCS/2.4GHz WLAN applications**

#### **5.5.1.1 Introduction**

Using the above mentioned design equations an antenna resonating at 1.8GHz and 2.4GHz is designed. Both of these bands are popular for mobile and WLAN applications. With the designed dimensions antenna has been modelled using FDTD technique. The fabricated antenna has been tested and the experimental results are compared with FDTD results and HFSS simulated results. The antenna resonating at 1.87GHz and 2.46GHz has 2:1 VSWR bandwidth of 17% and 9% respectively. The proposed antenna offers 53% area reduction compared to a standard rectangular microstrip antenna. Details of the antenna design and experimental results are presented below.

#### **5.5.1.2. Antenna Structure and Design**

Antenna has been fabricated on FR4 substrate of dielectric constant  $\epsilon_r=4.4$  and thickness  $h=1.6\text{mm}$ . As per the above design procedure, the dimensions are given in table 5.1. The design geometry is as shown in Fig. 5.42.

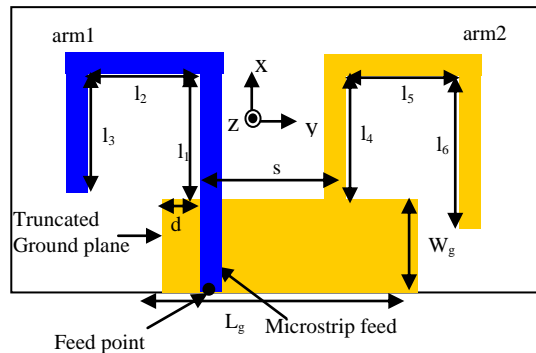


**Fig. 5.42 Geometry of the designed antenna for DCS/PCS/WLAN applications**  
 ( $L_g=26\text{mm}$ ,  $W_g = 8\text{mm}$ ,  $d_1=6.5\text{mm}$ ,  $l_1= 11\text{mm}$ ,  $l_2=10.75\text{mm}$ ,  $l_3=7\text{mm}$ ,  $l_4= 11\text{mm}$ ,  $l_5=10.75\text{mm}$ ,  $l_6=12\text{mm}$ ,  $w = 3\text{mm}$ ,  $s=9\text{mm}$ )

Microstrip feed line is designed for  $50\Omega$  characteristics impedance and the widths of both the strips are kept same as that of  $50\Omega$  microstrip line. Photographs of the proposed antenna are shown in Fig.5.43.

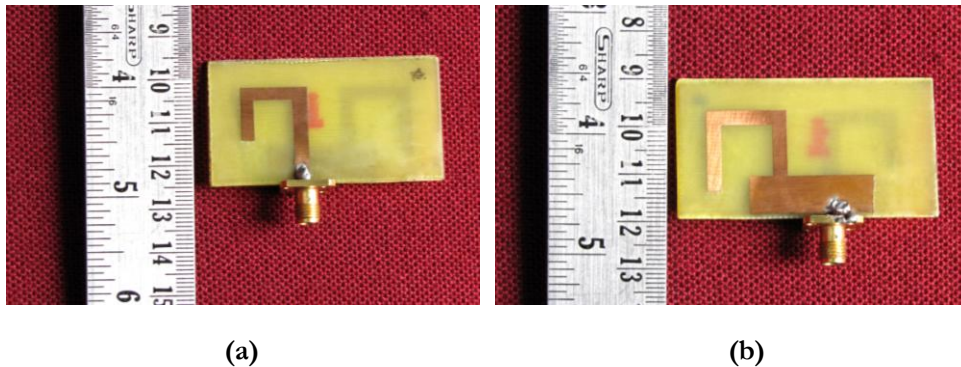


**Fig. 5.43 Photographs of the proposed antenna**  
 (a) Top view (b) Bottom view

### 5.5.1.3 Results and discussion

The measured and simulated return loss characteristics of the proposed dual frequency antenna are shown in Fig.5.44. Simulation was carried out using Ansoft HFSS. FDTD computed results are also compared with the experimental and simulation results. Antenna exhibits resonances at 1.87GHz and 2.46GHz with 2:1 VSWR bandwidths of 17.3% and 9.3% respectively. The lower resonant band extending from 1675MHz to 2000MHz (325MHz) is wide



enough to cover DCS and PCS bands. The higher resonant band from 2330 MHz to 2560MHz (230 MHz) covers the 2.4GHz WLAN.

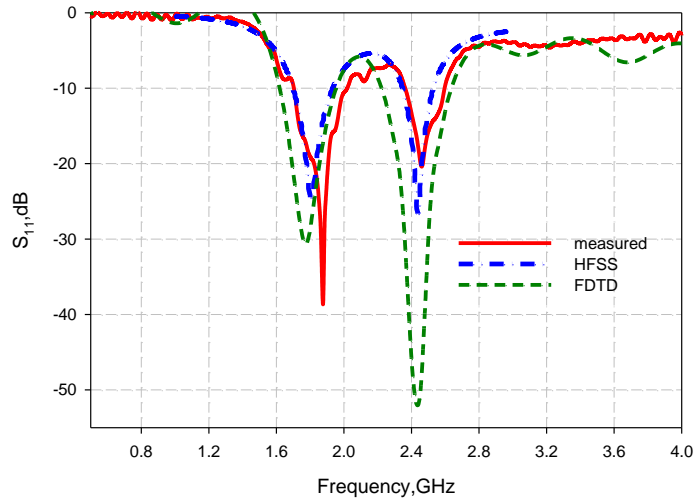


**Fig.5.44. Reflection characteristics of the designed antenna for DCS/PCS/WLAN applications**  
 $(L_g=26\text{mm}, W_g = 8\text{mm}, d_1=6.5\text{mm}, l_1= 11\text{mm}, l_2=10.75\text{mm}, l_3=7\text{mm}, l_4= 11\text{mm}, l_5=10.75\text{mm}, l_6=12\text{mm}, w = 3\text{mm}, s=9\text{mm})$

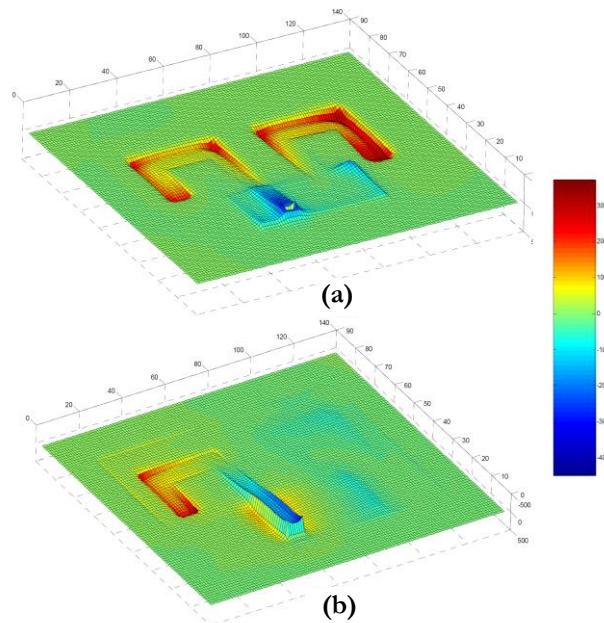


**Fig.5.45 Electric field ( $E_x$ ) one cell above the substrate**  
 (a) 1.87GHz (b) 2.46GHz  
 $(L_g=26\text{mm}, W_g = 8\text{mm}, d_1=6.5\text{mm}, l_1= 11\text{mm}, l_2=10.75\text{mm}, l_3=7\text{mm}, l_4= 11\text{mm}, l_5=10.75\text{mm}, l_6=12\text{mm}, w = 3\text{mm}, s=9\text{mm})$

FDTD computed electric field distributions at the resonant frequencies are shown in Fig.5.45. Ex component for 1.8GHz is similar to a halfwave dipole as shown in Fig.5.45a. Whereas for the higher resonance electric field distribution is same as that of a quarter wave monopole and is shown in Fig.5.45b. Field strength radiating from the ground strip is weak for this frequency.

The simulated current distributions of the antenna at the two resonant frequencies are presented in Fig.5.46. From the figure, it is well understood that current distribution of the antenna is similar to that of a dipole at 1.8GHz. Where as at 2.4GHz, arm1 of the antenna behaves as a quarter wave monopole, while arm2 affects the radiation pattern and impedance matching as mentioned earlier.

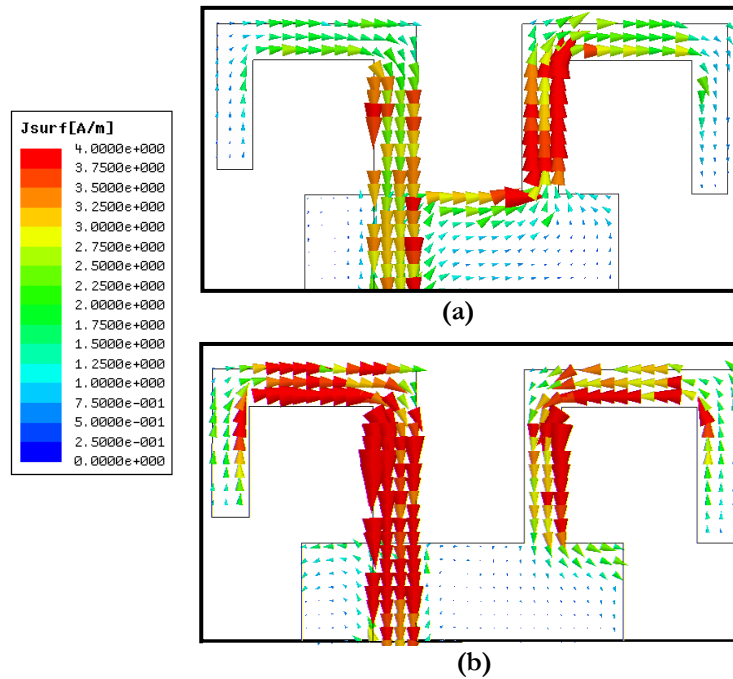


Fig.5.46 Simulated current distributions of the antenna at two resonant frequencies.  
 (a) 1.87GHz (b) 2.46GHz  
 ( $L_g=26\text{mm}$ ,  $W_g = 8\text{mm}$ ,  $d_1=6.5\text{mm}$ ,  $l_1= 11\text{mm}$ ,  $l_2=10.75\text{mm}$ ,  $l_3=7\text{mm}$ ,  
 $l_4= 11\text{mm}$ ,  $l_5=10.75\text{mm}$ ,  $l_6=12\text{mm}$ ,  $w = 3\text{mm}$ ,  $s=9\text{mm}$ )

The radiation pattern for the lower resonance is equivalent to a dipole placed along the y-axis but with a tilt of  $10^\circ$  ( $\phi=190^\circ$ ) in the azimuth

direction. For higher resonance the radiation plane is tilted by  $20^\circ$  in the azimuth plane compared to a printed monopole antenna. The measured normalized radiation patterns along the two principal planes at the center frequencies of the respective bands are shown in Fig.5.47. Radiation patterns are nearly omnidirectional. Radiation patterns at other frequencies in the respective bands are similar to those shown in Fig.5.47.

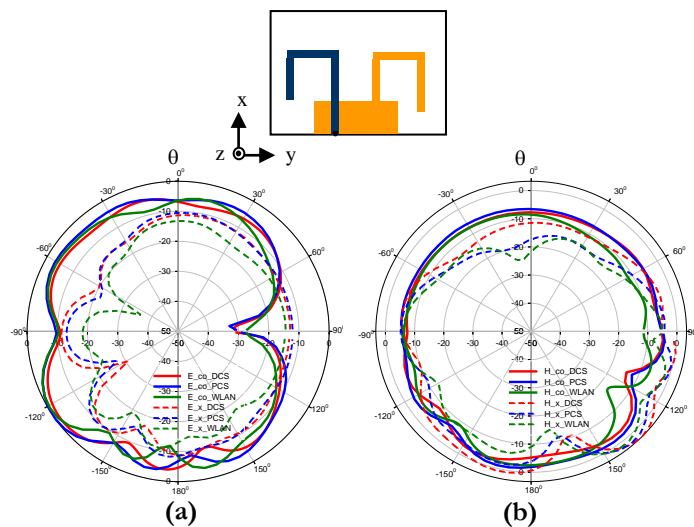


Fig.5.47 Radiation Patterns of the antenna in DCS, PCS and WLAN bands  
 (a). E plane (XZ plane) (b). H plane (YZ plane)  
 ( $L_g=26\text{mm}$ ,  $W_g = 8\text{mm}$ ,  $d_1=6.5\text{mm}$ ,  $l_1= 11\text{mm}$ ,  $l_2=10.75\text{mm}$ ,  $l_3=7\text{mm}$ ,  
 $l_4= 11\text{mm}$ ,  $l_5=10.75\text{mm}$ ,  $l_6=12\text{mm}$ ,  $w = 3\text{mm}$ ,  $s=9\text{mm}$ )

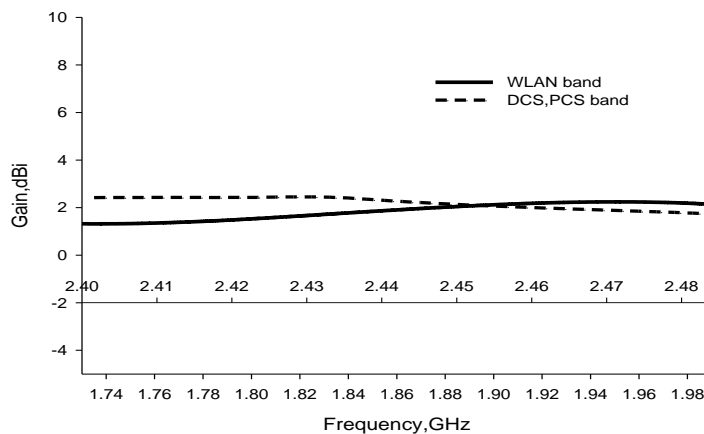


Fig. 5.48 Gain of the antenna in the desired bands  
 ( $L_g=26\text{mm}$ ,  $W_g = 8\text{mm}$ ,  $d_1=6.5\text{mm}$ ,  $l_1= 11\text{mm}$ ,  $l_2=10.75\text{mm}$ ,  $l_3=7\text{mm}$ ,  
 $l_4= 11\text{mm}$ ,  $l_5=10.75\text{mm}$ ,  $l_6=12\text{mm}$ ,  $w = 3\text{mm}$ ,  $s=9\text{mm}$ )

Polarization of the antenna is measured along  $30^\circ$  with respect to X axis for both the resonances. The measured antenna gain against frequency is shown in the Fig.5.48. Antenna has an average gain of 2.2dBi in the DCS band, 1.94dBi in the PCS band and 1.9dBi in the WLAN band.

Thus a compact dual band antenna for DCS/PCS/2.4 GHz WLAN applications has been designed and experimentally studied. The proposed antenna shows wide impedance band width, good radiation coverage and moderate gain, suggesting its usefulness in DCS/PCS/2.4GHz WLAN applications.

### 5.5.2. Design and development of dual band folded dual strip antenna for GSM applications

The design equations are confirmed by extending the proposed design to GSM 800/900 bands. Antenna has been fabricated on FR4 Epoxy substrate with dielectric constant 4.4 and thickness 1.6mm. Dimensions of the antenna for this case are mentioned in Table5.1. The return loss characteristics of the GSM 800/900 antenna is illustrated in Fig. 5.49. Here the two resonances (838MHz & 943MHz) merged to form a wideband with a 2:1 VSWR bandwidth of  $\sim 18\%$ . The band extends from 810MHz to 966MHz is wide enough to cover both GSM 800/900 bands.

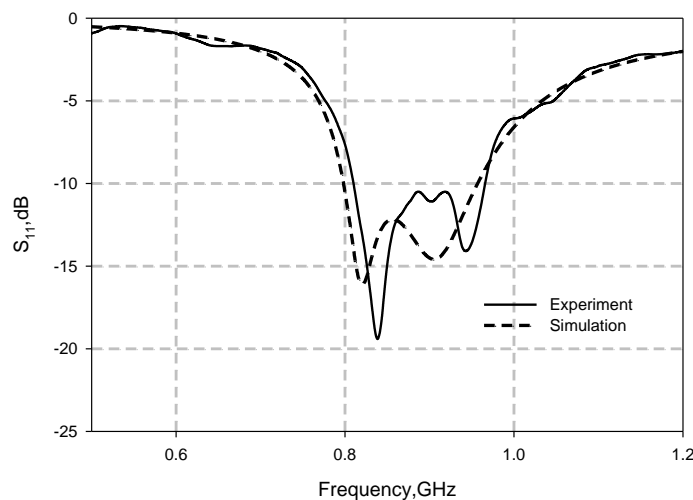


Fig.5.49 Return loss characteristics of the GSM 800/900 antenna

Design equations are validated on other commercially available substrates with different  $\epsilon_r$  and h. Specifications of the antennas with the simulation/experimental results are shown in Table 5.1.

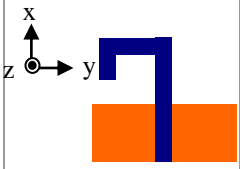
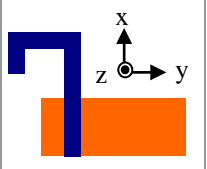
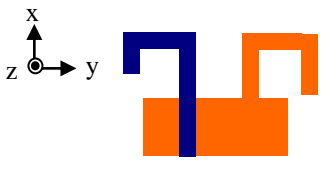
**Table 5.1 Design parameters on different substrates**

Substrate	Substrate Parameters		Antenna Parameters (mm)											Designed frequencies (GHz)		Results obtained (GHz)	
	$\epsilon_r$	h(mm)	W	$l_1$	$l_2$	$l_3$	$l_4$	$l_5$	$l_6$	Lg	Wg	$d_1$	s	$f_1$	$f_2$	$f_1$	$f_2$
FR4 Epoxy	4.4	1.6	3	11	10.75	7	11	10.75	12	26	8	6.5	13	1.8	2.4	1.87	2.46
FR4 Epoxy	4.4	1.6	3	30	29	18.7	29	25	26	70	25	13.5	21	0.8	0.9	0.838	0.943
Rogers RO3006	6.15	1.28	1.8	10.25	10.6	7.35	12	14	11	22.5	8	12	11	1.8	2.4	1.74	2.37
Rogers 6010LM	10.2	0.635	0.6	15	11.4	8.7	11.5	13	15	18	6.3	4	9	1.8	2.4	1.75	2.41

## 5.6 Conclusion

A compact dual band folded dual strip antenna has been derived from the microstrip fed dual strip antenna mentioned in chapter 4 by folding. The effect of folding on the antenna performances has been well studied. From the simulation and experimental analysis, folding dimensions and spacing between the folded arms are optimized. With the optimized parameters a compact dual band folded dual strip antenna has been derived. The design equations were developed and validated on different commercially available substrates for modern communication bands. Major conclusions from this chapter have been summarized in the following table 5.2. Three different configurations are compared in the table.

Table.5.2. comparison of three different folded configurations

Antenna	Microstrip fed Folded Monopole Antenna	Offset fed Folded Monopole Antenna	Compact Folded Dual Strip Antenna	
Configuration				
Antenna Parameters (mm)	$L_g = 35, W_g = 18, l_1 = 11, l_2 = 10, l_3 = 3, d_1 = 17.5$	$L_g = 26, W_g = 8, l_1 = 11, l_2 = 10, l_3 = 3, d_1 = 6.5$	$L_g = 26, W_g = 8, d_1 = 6.5, l_1 = 11, l_2 = 10.75, l_3 = 7, l_4 = 11, l_5 = 10.75, l_6 = 12, s = 9$	
Substrate parameters	$h = 1.6\text{mm}, \epsilon_r = 4.4$	$h = 1.6\text{mm}, \epsilon_r = 4.4$	$h = 1.6\text{mm}, \epsilon_r = 4.4$	
Resonant frequency(GHz)	$f = 2.31$	$f = 2.5$	$f_1 = 1.87$	$f_2 = 2.46$
Bandwidth	No matching	15.6%	17%	9%
Radiation pattern	Doughnut like pattern, tilted by $10^\circ$ in the azimuth plane compared to a printed monopole	Tilted by $50^\circ$ in the azimuth plane compared to a printed monopole	Tilted by $100^\circ$ in the azimuth plane compared to a printed monopole	Tilted by $20^\circ$ in the azimuth plane compared to a printed monopole
Beam width	$73^\circ$ in E-plane non directional in H-plane	$73^\circ$ in E-plane, Non directional in H-plane	$83^\circ$ in E-plane, non directional in H-plane	$70^\circ$ in E-plane, non directional in H-plane
Gain (dBi)	1.74	1.96	2.2	1.9
Efficiency (%)	80	91	89	86
Polarization	Linear, $-45^\circ$ with respect to y axis	Linear $-45^\circ$ with respect to y axis	Linear, $30^\circ$ with respect to x axis	Linear, $30^\circ$ with respect to x axis

.....□□.....

## *Chapter - 6*

# **CONCLUSION**

---

<i>Contents</i>	<b>6.1 Thesis Highlights</b>
	<b>6.2 Inferences from the analysis of microstrip-fed printed monopole antenna</b>
	<b>6.3 Inferences from compact dual band dual strip antenna</b>
	<b>6.4 Salient features of compact dual band folded dual strip antenna</b>
	<b>6.5 Comparison of compact folded dual strip antenna, dual strip antenna and printed monopole antenna</b>
	<b>6.6 Suggestions for future work</b>

---

This Chapter gives the highlights of the thesis along with major conclusions derived from the numerical and experimental analysis carried out in the previous chapters. A compact dual band planar antenna has been derived from a microstrip-fed printed monopole configuration. This chapter gives a summary of the design and inferences obtained from various analysis.

---

## 6.1 Thesis Highlights

This chapter brings the thesis to a close by summarizing the results obtained out of the numerical as well as experimental investigations conducted on microstrip-fed printed monopole antenna. Objective of the thesis was to develop a compact dual-band planar antenna suitable for compact wireless connectivity terminals such as mobile phones, wireless LAN etc.

Overviews of compact antennas, the challenges in compact antenna design, present state of art in compact antenna research and motivation of the present work are summarised in chapter 1. A thorough review of compact antennas, antennas for mobile/WLAN applications, wide band and multiband techniques have been carried out and presented in chapter 2.

The theoretical and experimental methodology for antenna characterization has been explained in the chapter 3. It also explains the major elements of FDTD which is used in the thesis for the theoretical analysis and design of dual strip antenna and folded dual strip antenna.

Theoretical and experimental investigation on the resonance and radiation mechanism of the dual band dual strip antenna was the key element of chapter 4. Evolution of a dual band antenna from microstrip fed printed monopole configuration was well explained with the help of experiment and simulation. Effect of various antenna dimensions on antenna performances has been analysed by experiment and simulations. Based on that design equations were derived. The design equations are validated for a dual band antenna for DCS and 2.4GHz WLAN applications in various commercially available substrates.

Further size reduction was achieved by folding the strips of the dual strip antenna. The folding analysis along with design procedure for a



compact folded dual strip antenna was presented in Chapter 5. Based on the design equations compact dual band folded dual strip antennas for various applications such as GSM, DCS and WLAN have been proposed.

## 6.2 Inferences from the analysis of microstrip-fed printed monopole antenna

The major findings after analysing the microstrip-fed printed monopole antenna are as follows

- A printed monopole having a length of  $0.25 \lambda_d$  with a ground plane dimensions  $\lambda_d \times 0.5 \lambda_d$  will give two resonances. One is primarily due to monopole strip and the other is due to the L shaped path which includes both the monopole strip and the ground plane length ( $d_2$ ).
- Impedance bandwidth for both the above resonances can be properly matched by offsetting the microstrip feed line. While offsetting the feed line there exist three resonant paths; first due to monopole strip, second due to the L shaped current path and the third one due to reflected L shaped path. Matching for the third resonance corresponding to reflected L shaped path is poor and it is at the higher end.
- Ground plane truncation has significant impact on resonant frequencies and bandwidth. Ground plane width has very little influence on resonant frequencies but strong impact on bandwidths. Maximum bandwidth is observed for a width  $W_g$  of  $0.5\lambda_d$ . Ground plane length  $L_g$  affects both the resonances and the variation is predominant for second resonance. This again confirms L shaped resonant path for second resonance. For small  $L_g$ , matching for second resonance is poor and the antenna exhibits good performance only in first mode.

- Since truncated ground plane has significant impact on resonant frequencies, a suitable modification on the ground plane to enhance the current path will result in two distinct resonances. These resonances can be fine-tuned to lower resonant bands without compromising the compactness.

### 6.3 Inferences from compact dual band dual strip antenna

A compact printed monopole antenna has been analyzed and ground plane has been modified by adding another strip as an extension from the ground plane. Conclusions derived from the above analysis are given below.

- Printed monopole antenna with compact ground plane ( $0.5\lambda_d \times 0.25\lambda_d$ ) shows only single resonance. The second resonance, due to the L shaped path has been shifted to the higher side due to reduction in ground plane dimension. Adding another strip to the ground plane lowers the second resonance due to the 'L' shaped path. Extension of another strip to the ground plane constitute a meandered current path on the antenna structure with 'I' shape on the signal strip and 'reflected L' shape on the ground plane. This configuration behaves like an asymmetrically fed dipole for the new resonance.
- The spacing between the strips is the crucial parameter which controls the matching and to some extent the resonant frequency. There is an optimum spacing for which antenna shows good impedance bandwidth for both the higher and lower bands.
- Variation in signal strip length ' $l_m$ ' affects both the resonant frequencies since it affects both the monopole resonant length (higher resonance) and the meandered length (lower resonance). Variation of ground strip length ' $l_g$ ' changes the lower resonance considerably. But the higher resonance remains almost unchanged.

- Increase in strip width increases the bandwidth. But for simple design, widths of the strips are kept same as  $50\Omega$  microstrip line width.
- Variation in ground plane length  $L_g$ , does not affect the lower resonance significantly. But it affects higher resonance and the variation is more for  $L_g < 0.8\lambda_d$
- Ground plane width  $W_g$  affects the impedance bandwidth for both the bands.
- In the case of lower resonance, the three important parameters which control the resonant frequency are monopole strip length ' $l_m$ ', ground strip length ' $l_g$ ' and spacing between the strips ' $s$ '. Even though the spacing ' $s$ ' is a part of the resonant length, more variation in resonant frequency is observed with respect to the signal strip lengths. The lower resonant frequency can be easily tuned by varying ' $l_g$ '. The impedance match can be improved by proper trimming of ' $s$ '.

#### **6.4 Salient features of compact dual band folded dual strip antenna**

For achieving further compactness dual strip antenna has been folded and analyzed. A detailed study has been carried out to find the impact of folding and after exhaustive analysis a design procedure for a compact dual band antenna has been derived. Important inferences are summarized below.

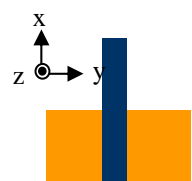
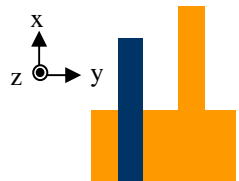
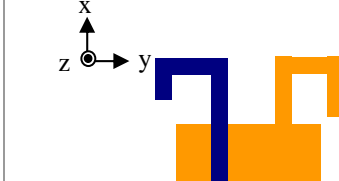
- Folding a printed monopole towards the ground plane increases the input impedance. Impedance becomes capacitive and antenna losses its impedance match.
- Feed offsetting introduces another resonance similar to that of the offset-fed monopole mentioned in chapter 4. This is due to the meandered path including the ground plane.

- Ground plane width controls the bandwidth. As the ground plane length decreases, the “second resonance” shifts towards the higher side.
- Folding position/top-loading position has significant impact on antenna performances. As  $l_1, l_2$  increases antenna shows better impedance bandwidth. But for compact applications, a compromise on size and performance is required.
- Addition of another folded arm to the ground plane brings the second resonance to the lower side. Thus the lower resonance, which is due to the meandered path including both the folded arms and the ground plane edge, is similar to that of an asymmetric dipole. Thus the folded dual band dual strip antenna works as an asymmetric fed dipole for the lower resonance and as a folded monopole for the higher resonance.
- The new design gives an area reduction of 53% compared to rectangular microstrip antenna operating at the same frequency.

### **6.5 Comparison of Compact folded dual strip antenna, dual strip antenna and printed monopole antenna**

Microstrip-fed printed monopole antenna has been modified by adding an additional strip to the ground plane so as to increase the resonant length due to the L-shaped path. The resultant dual band dual strip antenna has been analyzed and design equations were developed. Further compactness, folding study has been conducted on dual strip antenna by folding. A performance comparison of the printed monopole antenna, dual band dual strip antenna and dual band folded dual strip antenna are summarized in Table 6.1.

Table.6.1 Comparison of Microstrip-fed Printed Monopole, Dual strip Antenna and Folded Dual Strip Antenna

Antenna	Microstrip fed printed monopole antenna	Microstrip-fed dual band dual strip antenna		Microstrip-fed dual band folded dual strip antenna	
Design					
Antenna parameters (mm)	$L_g=38, W_g=19, l_m=19, l_g=29, d_1=d_2=19, w=3$	$L_g=35, W_g=18, l_m=24, l_g=29, d_1=13.5, s=13, w=3$		$L_g=26, W_g=8, d_1=6.5, l_1=11, l_2=10.75, l_3=7, l_4=11, l_5=10.75, l_6=12, s=9$	
Substrate parameters	$h=1.6\text{mm}, \epsilon_r=4.4$	$h=1.6\text{mm}, \epsilon_r=4.4$		$h=1.6\text{mm}, \epsilon_r=4.4$	
Frequency(GHz)	2.76	1.8	2.4	1.87	2.44
Bandwidth (%)	19	10.8	9.8	17	9
Radiation pattern	Doughnut like pattern, symmetric	Tilted by $45^\circ$ in the azimuth plane	Tilted by $45^\circ$ in the azimuth plane	Tilted by $100^\circ$ in the azimuth plane compared to a printed monopole	Tilted by $20^\circ$ in the azimuth plane compared to a printed monopole
Beam width	$80^\circ$ in E-plane Non-directional in H-plane	$83^\circ$ in E-plane, $120^\circ$ in H-plane	$83^\circ$ in E-plane, $120^\circ$ in H-plane	$83^\circ$ in E-plane, $330^\circ$ in H-plane	$70^\circ$ in E-plane, $315^\circ$ in H-plane
Gain(dBi)	2.24	2.3	3.6	2.2	1.9
Polarization	Linear along x	Linear, along x	Linear, along x	Linear, $30^\circ$ with respect to x axis	Linear, $30^\circ$ with respect to x axis

## 6.6 Suggestions for future work

In the present thesis dual resonance has been achieved on a printed monopole configuration by adding another strip to the ground plane. In this case the L-shaped resonant path has been modified to U shaped to give a lower resonance. It is also observed that a suitable modification on the

proposed dual band design by placing another strip besides the ground strip excites a third resonance with poor matching. By properly adjusting the spacing between the strips and ground plane dimensions, a better impedance match can be achieved yielding a triple band antenna. The reflected L shaped path can also be converted to another U shaped path by properly placing another strip on the other side so as to achieve a multiband design.

Future studies can be carried out to correct the tilt in the polarization and radiation pattern. The folded dual strip configuration reduces the tilt in the radiation pattern compared to the dual strip configuration. But still a tilt of  $20^\circ$  is there for the higher resonance compared to a printed monopole antenna.

In the case of dual strip antenna, for the higher resonance (monopole mode), the presence of the ground strip (lg) creates a null in the third quadrant. This null can be improved by suitably optimizing the spacing's'. The present study optimized the spacing 's' for a compact dual band design. The spacing and length of the ground strip can be optimized to achieve a directional pattern with a desired null in the third quadrant. This design can be considered for mobile phone antennas with reduced SAR.

In the present compact dual strip and folded dual strip designs, the widths of the strips (both monopole and ground strip) are kept as that of the  $50\Omega$  microstrip line to reduce the design complexity. Modification in the design with different strip widths is one area that may be looked into to enhance the antenna properties.

.....❧.....

## *Appendix -A*

# **A COMPACT DUAL BAND PLANAR BRANCHED MONOPOLE ANTENNA FOR DCS/2.4GHz WLAN APPLICATIONS**

---

<b>Contents</b>	<b>1. Introduction</b>
	<b>2. Antenna design</b>
	<b>3. Experimental results</b>
	<b>4. Conclusion</b>
	<b>5. References</b>

---

---

A compact dual band planar antenna for a digital communication system (DCS)/2.4-GHz WLAN application is presented. The two resonant modes of the proposed antenna are associated with various lengths of the monopoles, in which a longer arm contributes for the lower resonant frequency and a shorter arm for higher resonant frequency. The experimental results show that the designed antenna can provide excellent performance for DCS/2.4-GHz WLAN systems, including sufficiently wide frequency band, moderate gain, and nearly omnidirectional radiation coverage.

---

---

## **1. Introduction**

The rapid development of modern wireless communication urges on the need of dual band or multiband antennas. Planar monopole antennas have found wide spread application in wireless communication industry due to their attractive features like ease of fabrication, low cost, and nearly omnidirectional radiation characteristics. Recently, the design of dual band or multiband antennas has received the attention of antenna researchers. Numerous designs of dual frequency monopole antennas have been demonstrated, including the use of a combination of two parallel monopoles excited by a coplanar waveguide (CPW) feed line [1], microstrip excited triangular monopole with a trapezoidal slit [2], monopole antenna based on tapered meander line geometry [3], and parallel line loaded monopole antenna [4] etc. Most of the monopole antennas reported in the literature are mounted above a large ground plane which increases the complexity of the system. In this section, a novel design of dual frequency monopole antenna excited by microstrip feed line with a truncated optimum ground plane is proposed. The principle of dual frequency operation is to introduce various resonating lengths to a simple strip monopole antenna. Experimental results demonstrate that the impedance matching of the proposed antenna depends upon the ground plane dimensions and frequency tuning can be achieved by tuning the two resonant lengths. Parameters of the antenna are experimentally optimized and the radiation and reflection characteristics of a prototype suitable for digital communication system (DCS)/2.4-GHz WLAN application are presented. Details of the design and experimental results are also presented and discussed.

## **2. Antenna Design**

The following section describes the design procedure to modify a simple strip monopole antenna for dual band characteristics. Fig.A.1 shows three



different configurations of planar monopole antennas. Antenna1 is a  $\lambda_d/2$  strip monopole excited by a  $50\Omega$  microstrip line with a truncated optimum ground plane width of  $\lambda_d/2$ . Even though wide bandwidth is achieved with this configuration the antenna occupies an area of 85% compared to a standard rectangular patch resonating at the same frequency. The antenna1 is modified by meandering the strip monopole to a hook like radiating structure in order to achieve compactness. The antenna2 with ground plane width  $\lambda_d/4$  require a resonant length of  $0.62\lambda_d$  to obtain the resonant frequency at the desired value. Since the hook like radiating structure is a top loaded planar strip, the capacitive coupling between the horizontal strip and ground plane adds a capacitive reactance at the input impedance of the planar monopole which lowers the bandwidth of operation compared to that of antenna 1. However, Antenna 2 offers a size reduction of 76% compared to a standard rectangular patch resonating at the same frequency. Antenna 3 is a modified version of antenna 2 with an additional hook like radiating structure to obtain two different current paths resulting in dual band operation. The arm1 of the monopole must be loaded at a distance of  $\lambda_{d1}/4$  from the ground plane and arm2 must be loaded at a distance of  $\lambda_{d2}/4$  from the ground plane for obtaining good impedance matching and radiation characteristics. The designed antenna is printed on standard FR4 substrate of thickness 1.6 mm and relative permittivity 4.36. The strip monopole is excited by a  $50\Omega$  microstrip line with truncated ground plane of dimensions  $L_G \times W_G$ . The length and width of the truncated ground plane is optimized for maximum bandwidth without affecting the impedance matching. For the design convenience the strip width of the monopole is set as 3 mm, width of 50- microstrip line. The proposed dual frequency antenna owns two different resonant paths of lengths  $L_L = l_1 + l_2 + l_3 + l_4$  and  $L_H = l_1 + l_5 + l_6$ . Tuning the length  $L_L$  can fix the first resonance at 1.8 GHz while tuning the length  $L_H$  can fix the second resonance at 2.4 GHz.

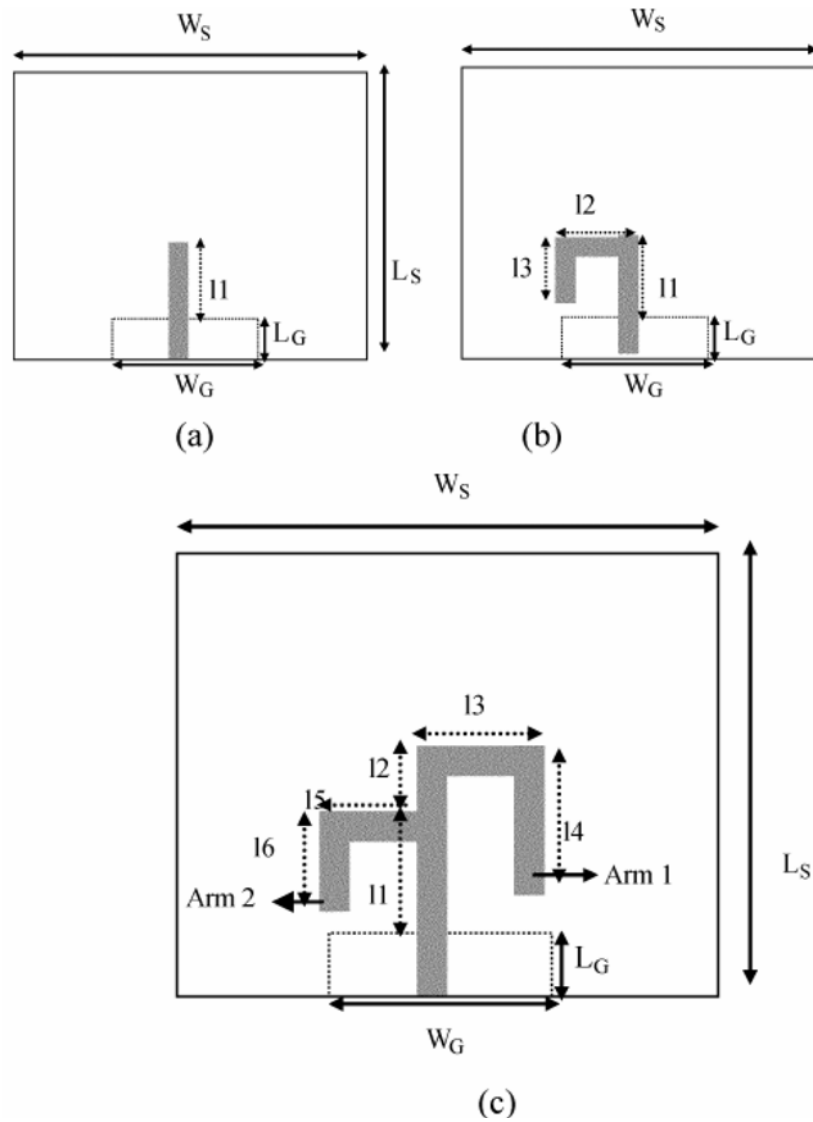


Fig.A.1. (a) Single frequency strip monopole antenna1.  $L_G = 3$  mm,  $W_G = 30$ mm,  $l_1 = 30$  mm,  $\epsilon_r = 4.36$ ,  $h = 1.6$ mm,  $L_S = 35$ mm,  $W_S = 30$  mm. (b) Compact hook shaped antenna2 for single band operation.  $L_G = 3$ mm,  $W_G = 15$  mm,  $l_1 = 15$ mm,  $l_2 = 10$ mm,  $l_3 = 12$ ,  $\epsilon_r = 4.36$ ,  $h = 1.6$  mm,  $L_S = 30$ mm,  $W_S = 30$ mm. (c) Geometry of the dual frequency planar Monopole antenna3  $L_G = 3$ mm,  $W_G = 15$ mm,  $l_1 = 15$ mm,  $l_2 = 5$  mm,  $l_3 = 13$ mm,  $l_4 = 16$  mm,  $l_5 = 10$  mm,  $l_6 = 12$  mm,  $\epsilon_r = 4.36$ ,  $h = 1.6$ mm,  $L_S = 30$ mm,  $W_S = 30$  mm.

### 3. Experimental Results

Typical proposed antennas were implemented and characterized using a HP8510C vector network analyzer. The antenna was simulated with the aid of IE3D in order to obtain the proper dimensions of the antenna. Fig.A.2 illustrates the reflection characteristics of various antenna configurations. Antenna1 resonating at 2.41 GHz offers a wide bandwidth of 500 MHz (2.20 GHz–2.70 GHz). But the dimensions of the antenna are comparable to that of standard rectangular patch antenna. Antenna2 resonating at 2.44 GHz offers 400-MHz bandwidth with an area reduction of 76% compared to that of conventional patch antenna. The Antenna 3 offers two distinct resonant modes at 1.725GHz and 2.45GHz, respectively. The lower impedance bandwidth due to the resonant length, determined by 2:1 VSWR is 505 MHz (1.375–1.88 GHz), which meets the requirement of DCS system. The upper resonance due to the length reaches 220 MHz (2.33–2.55 GHz), which covers the 2.4-GHz WLAN band.

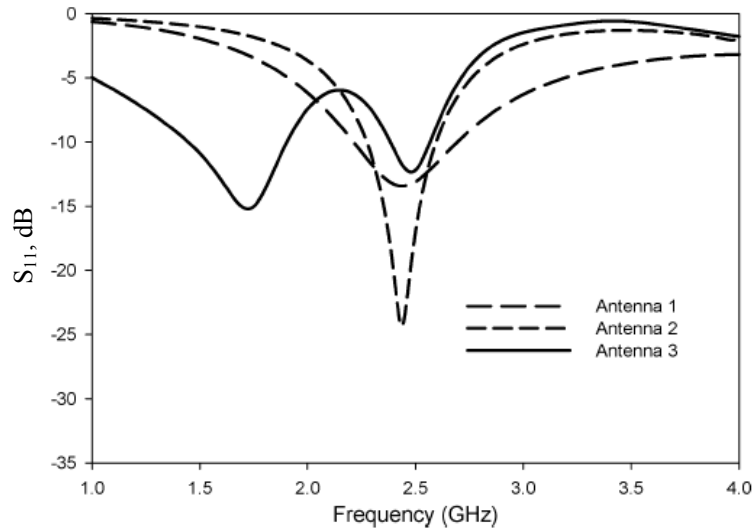


Fig.A.2. Variation of return loss with frequency for the proposed antennas

The characteristics of various antenna configurations are summarized in Table I. From the table it can be inferred that for Antenna 2 top loading a strip monopole decreases the bandwidth due to the capacitive coupling between the horizontal strip and ground plane but with a large reduction in overall size of the antenna. For antenna3 bandwidth enhancement is observed for the lower resonant frequency as the arm2 increases the inductive reactance. But for the higher resonance degradation in bandwidth is observed due to the increased capacitive coupling. The Antenna 3 with dual band characteristics offers an area reduction of 67% compared to conventional patch antenna.

TABLE I  
CHARACTERISTICS OF THE PROPOSED ANTENNAS

ANTENNA	Fr (GHz)	Band (GHz) Bandwidth (MHz)	Average Gain	Area reduction (compared to standard circular patch)
Antenna 1 (Single frequency)	2.4	2.20-2.70 500 20.8%	3.2dBi	15%
Antenna 2 (Single frequency)	2.44	2.28-2.68 400 16.4%	3dBi	76%
Antenna 3 (Dual frequency)	1.725 GHz 2.45 GHz	1.375-1.88 505 29% 2.33-2.55 220 8.9%	2.53dBi 2.1dBi	67%

The Fig. A.3 (a) and A.3 (b) gives the radiation patterns at 1.8 and 2.4 GHz respectively. The antenna is linearly polarized along the direction. The antenna gains are about 2.53dBi and 2.1dBi in DCS and WLAN bands, respectively. Gain variations are less than 1dBi within the band.

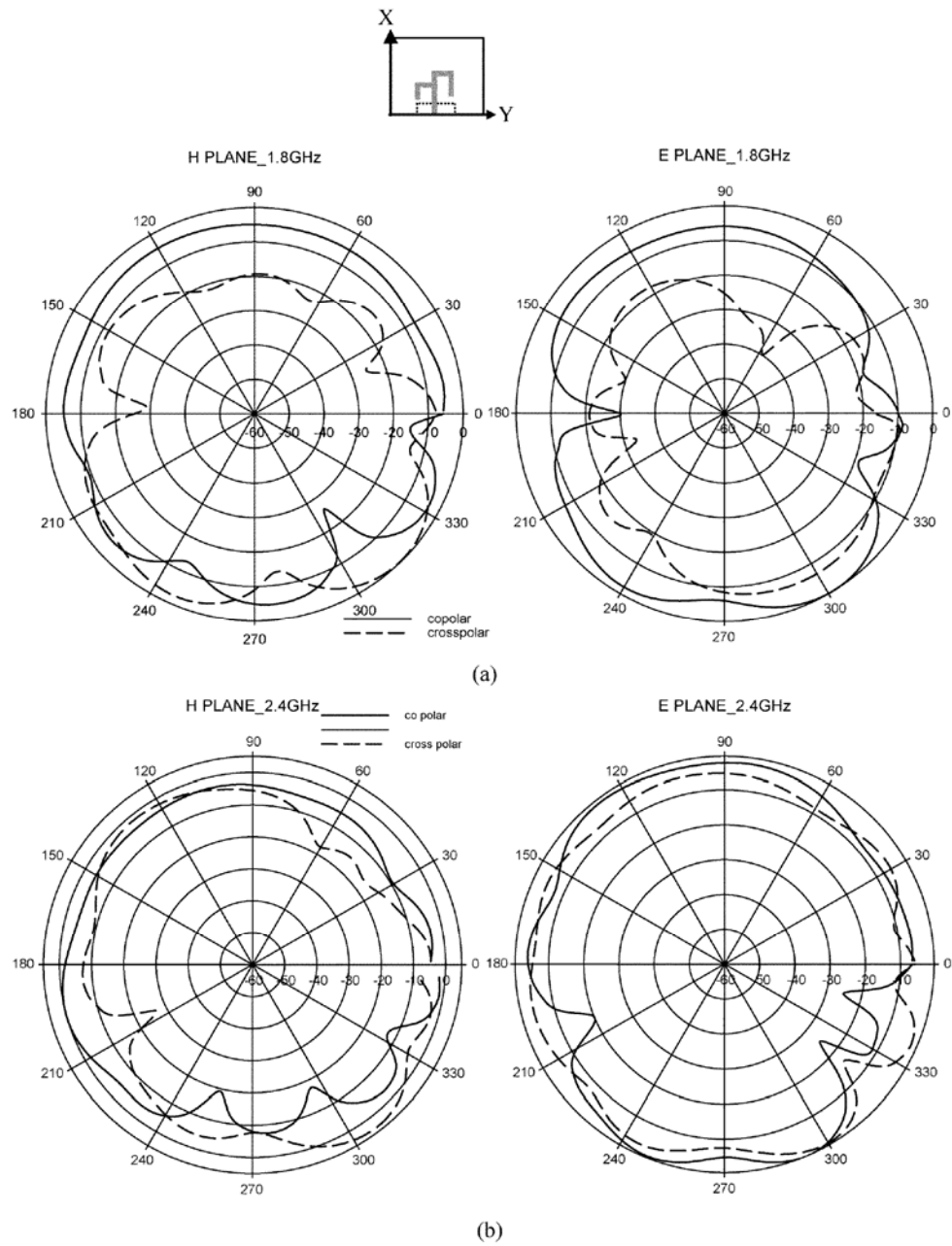


**Fig.A.3.** Radiation characteristics of the proposed antenna (a) 1.8GHz, (b) 2.4GHz  $L_G=3\text{mm}$ ,  $W_g=15\text{mm}$ ,  $l_1=15\text{mm}$ ,  $l_2=5\text{mm}$ ,  $l_3=13\text{mm}$ ,  $l_4=16\text{mm}$ ,  $l_5=10\text{mm}$ ,  $l_6=12\text{mm}$ ,  $sr=4.6$ ,  $h=1.6\text{mm}$

The design parameters of the antenna are  $l_1= 0.25 \lambda_{d2}$ ,  $l_1+l_2=0.25\lambda_{d1}$ ,  $l_3= 0.163\lambda_{d1}$ ,  $l_4= 0.2\lambda_{d1}$ ,  $l_5= 0.17 \lambda_{d2}$ ,  $l_6=0.2\lambda_{d2}$ ,  $L_G=0.0375 \lambda_{d1}$ ,  $W_G= 0.25\lambda_{d2}$ . The first resonant length depends on  $L_L =l_1 +l_2 +l_3 +l_4$  and second on  $L_H = l_1 +l_5 +l_6$ . The length  $l_1$  is common to both the resonant frequencies. For optimum bandwidth for the second resonance it is found that  $l_1= 0.25\lambda_{d2}$ . Similarly for the first resonance the criteria is  $l_1 +l_2= 0.25 \lambda_{d1}$ . Design equations are verified by conducting experiments at various frequency bands. Fig.A.4 presents the reflection characteristics of different prototypes of the antenna designed with the aid of design equations and operating dual modes in various standard wireless communication bands. Fairly good agreement is observed between designed and experimental results. Fig. A.5 (a) depicts the influence of  $\epsilon_r$  on two resonant frequencies of the two modes satisfying above design equations. The typical variation of resonant frequencies for different substrate heights is shown in Fig. A.5(b).

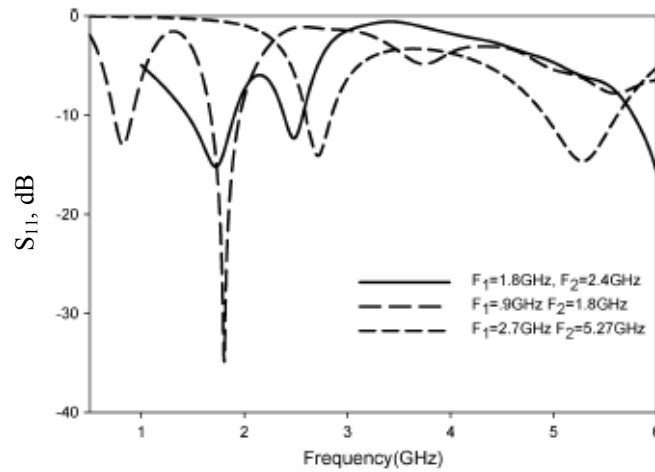
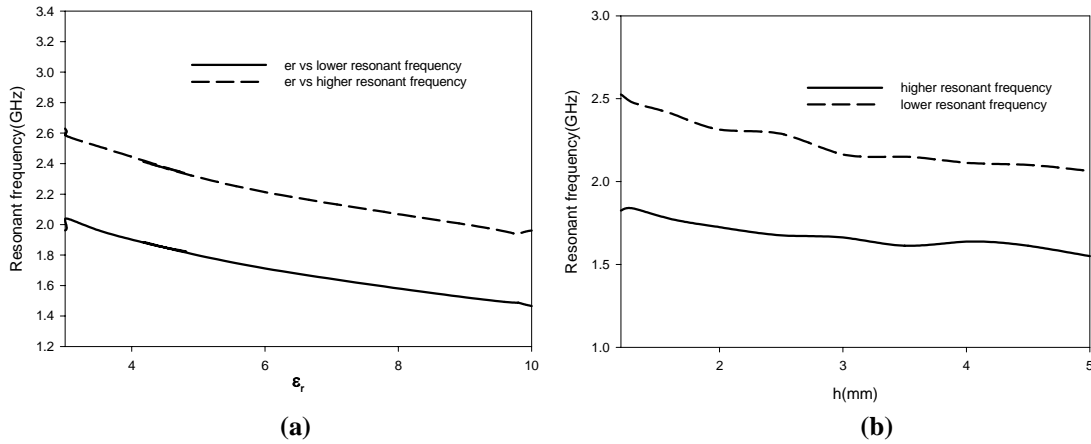


Fig.A.4. Reflection characteristics of the proposed antenna operating in various frequency bands



**Fig.A.5. (a) Variation of resonant frequencies with  $\epsilon_r$  of the substrate,  $h=1.6\text{mm}$   
(b) Variation of resonant frequencies with substrate thickness,  $\epsilon_r=4.36$**

#### **4. Conclusion**

A novel design of a dual frequency planar monopole antenna has been proposed. With two different resonant lengths the proposed antenna offers dual band operation with 67% area reduction compared to a conventional patch antenna. Sufficient bandwidth, moderate gain, and omnidirectional radiation characteristics of the proposed compact dual band antenna reflects its efficacy in mobile and wireless communication applications.

#### **5. References**

- [1]. H. D. Chen and H. T. Chen, A CPW fed dual frequency monopole antenna, *IEEE Trans. Antennas Propag.*, vol. 52, no. 4, pp. 978–982, Apr. 2004.
- [2]. H. M. Chen, Microstrip fed dual frequency printed triangular monopole antenna, *Electron. Lett.*, vol. 38, pp. 619–620, Jun. 2002.
- [3]. B. Sun, Q. Liu, and H. Xie, Compact monopole antenna for GSM/DCS operation of mobile phone handsets, *Electron. Lett.*, vol. 39, pp. 1562–1563, Oct. 2003.
- [4]. T. Sukiji, Y. Kumon, and M. Yamasaki, Double folded monopole antenna using parallel line or co axial cable, *Proc. Inst. Elect. Eng.*, vol. 149, pp. 17–22, Feb. 2002.

.....✉.....

## *Appendix -B*

# **COMPACT PLANAR MULTIBAND ANTENNA FOR GPS,DCS,2.4/5.8 GHz WLAN APPLICATIONS**

---

<b>Contents</b>	<b>1. Introduction</b>
	<b>2. Antenna design</b>
	<b>3. Results and discussion</b>
	<b>4. Conclusion</b>
	<b>5. References</b>

---

A compact single feed multiband planar antenna configuration suitable for GPS, DCS, 2.4/5.8GHz WLAN applications is presented. The antenna of dimensions 38mm x 3mm x 1.6mm offers good radiation and reflection characteristics in the above frequency bands. The antenna has a simple geometry and can be easily fed using a 50 $\Omega$  coaxial probe.

---



## **1. Introduction**

The rapid progress in personal and computer communication technologies demand integration of more than one communication systems into a single compact module. To comply with the above requirement compact high performance multiband planar antennas with good radiation characteristics are needed. A planar single feed dual L antenna of dimensions 30.5mm x 21.5mm x 13mm operating in GPS and PCS bands is proposed in [1]. The dual band antenna for the ISM band (2.4/5.8GHz) using a backed microstrip line proposed in [2] has an overall dimension of 30 x 20 mm<sup>2</sup> on FR4 substrate and offers a maximum gain of 4dBi. Dual frequency antenna configuration proposed in [3] uses triple stacked microstrip patch antennas with a slot in the middle patch, to achieve triple band operation. In this section a compact single feed planar antenna with three wide 2:1 VSWR operating bands around 1.8GHz, 2.4GHz and 5.8GHz respectively, covering four useful frequency bands namely GPS (1575.4MHz), DCS (1800MHz), 2.4GHz (2400-2485MHz) and 5.8GHz (5725-5825MHz) WLAN is presented.

## **2. Antenna design**

Geometry of the proposed antenna is shown in Fig. B.1. It is etched on FR4 substrate of relative permittivity,  $\epsilon_r = 4.7$  and thickness  $h = 1.6\text{mm}$ . The antenna has two arms of lengths  $l_1 = 38\text{mm}$ ,  $l_2 = 33\text{mm}$  and widths  $w_1 = w_2 = 1\text{mm}$  placed symmetrically on either side of a middle element of length  $l_3 = 17\text{mm}$  and width  $w_3 = 1\text{mm}$ . The feed point of the antenna is optimized to be at the middle of edge AB. Good impedance matching is achieved by embedding a reflector of dimensions  $L = 40\text{mm}$  and  $W = 25\text{mm}$  on the bottom side of the substrate at an offset  $d = 0.5\text{mm}$  from the edge AB as shown in Fig.B.1.

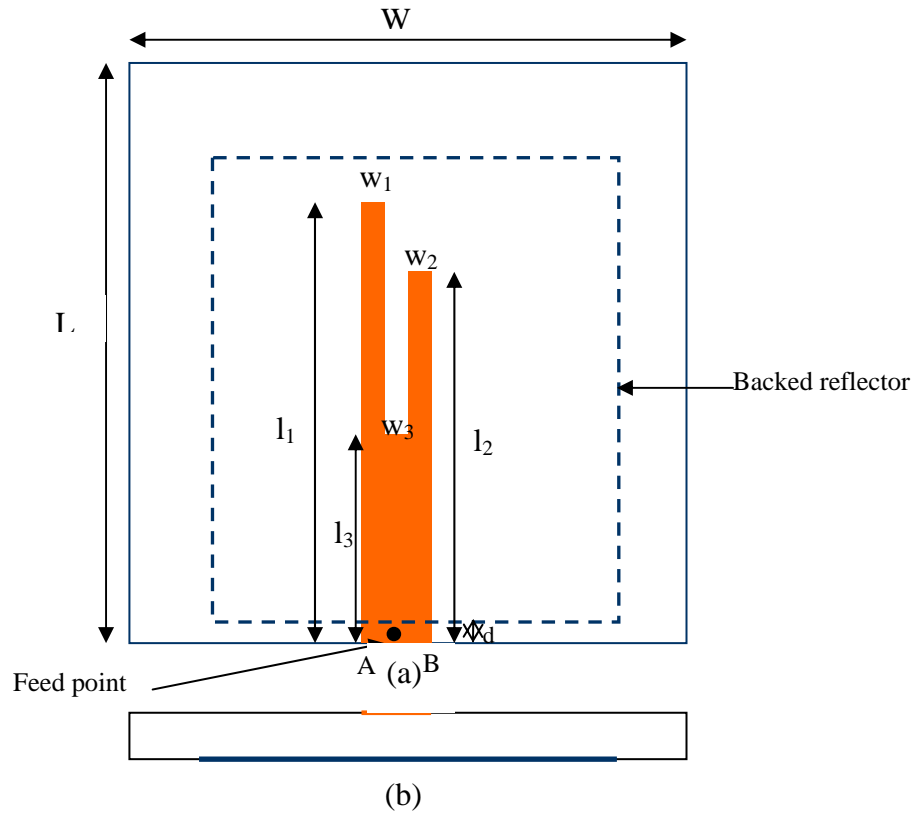


**Fig. B.1** Geometry of the proposed antenna (a) Top view (b) Side view  
 $L=40$  mm,  $l_1=38$ mm,  $l_2=33$ mm,  $l_3=17$ mm,  $W=25$  mm,  
 $w_1= w_2=w_3=1$ mm,  $h=1.6$  mm,  $d=0.5$ mm

From the experimental and simulation results, it is understood that the lower resonance can be tuned by varying the length  $l_1$  of arm 1. Resonance in the 2.4GHz band is influenced by the length  $l_1 + l_2 - 2 l_3$ . When length  $l_3$  of the middle element is increased, the second resonance shifts upwards whereas; it gets lowered when the length  $l_2$  is increased. Dimensions of the reflector affect both the resonance frequency and impedance matching in the 5.8GHz band. Another antenna with  $l_1=79.4$ mm,  $l_2=77.48$ mm and  $l_3=60.54$ mm, exhibits resonance at 940MHz, 1.85GHz and 5.2GHz respectively suitable for GSM/DCS/5.2GHz WLAN applications.

### 3. Results & Discussion

The measured return loss characteristic of the proposed antenna is shown in Fig. B.2. Three resonant bands are observed at frequencies 1.75 GHz, 2.45GHz and 5.76GHz with 2:1 VSWR bandwidths of 23%, 5% and 4.5% respectively. The lower resonant band with 406MHz (1466-1872) bandwidth is wide enough to cover the GPS/DCS bands. The higher resonant bands with 124MHz (2372-2496) and 260MHz (5630-5890) bandwidths cover the 2.4GHz and 5.8GHz WLAN bands respectively.

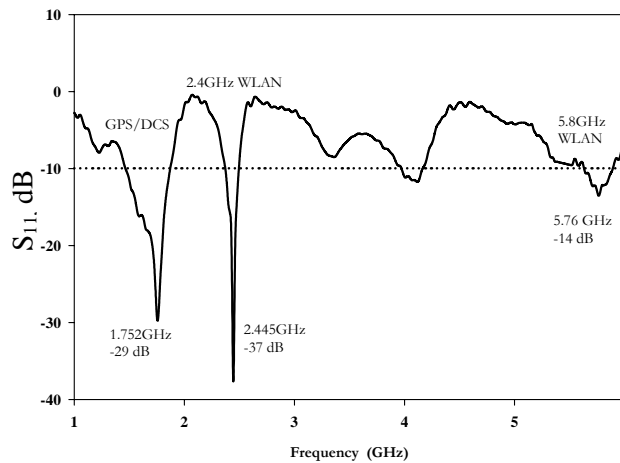


Fig. B.2. Return loss characteristics of the antenna

The normalized E-plane and H-plane radiation patterns measured at the centre frequencies of the respective bands are shown in Fig.B.3. The patterns are observed to be nearly omni directional in the H-plane, with a cross polar level better than -15dB in the bore-sight direction. The antenna exhibits similar radiation characteristics in all the desired bands.

The measured antenna gain against frequency is presented in Fig.B.4. The antenna offers a peak gain of 7.38dBi in the GPS band. The maximum gain observed in the DCS, 2.4GHz WLAN, 5.8GHz WLAN bands are 3.73dBi, 4.22dBi and 4.65dBi respectively. The radiation performance of the antenna in all the above bands is summarized in Table.B1. It is observed

that all bands except the 5.8GHz band are linearly polarized along Y direction. The 5.8GHz band is orthogonal to the other bands.

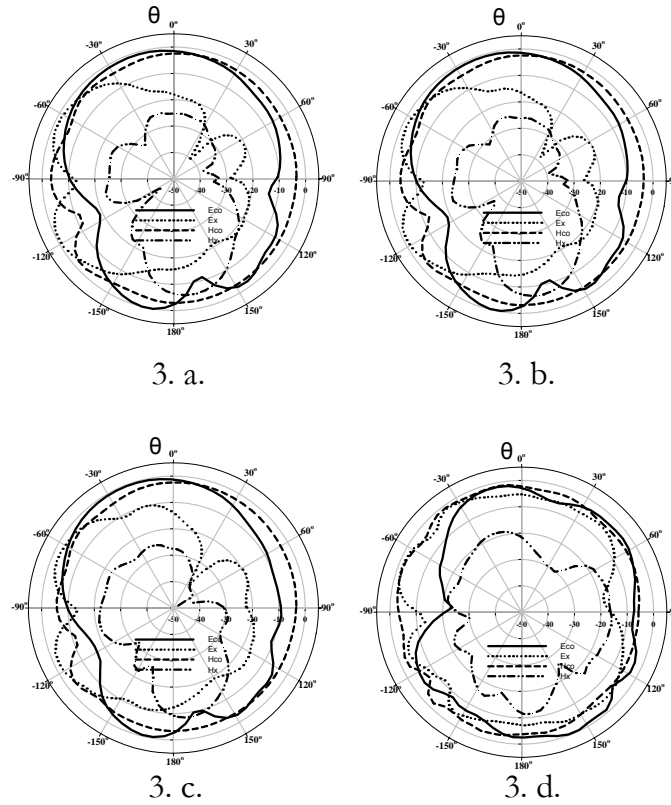


Fig. B.3. Radiation Patterns at the centre frequency of the desired bands  
 3.a GPS band 3.b. DCS band 3.c. 2.4GHz WLAN band 3.d.  
 5.8GHz WLAN band

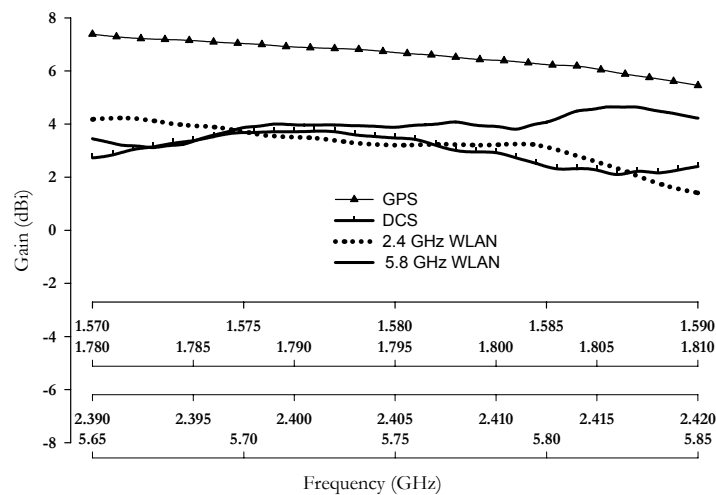


Fig. B.4. Gain of the antenna in the desired bands

Table B-1

Band (GHz) and application		Gain (dBi) max/min	Polarisation	Cross-polar level (dB)	Radiation pattern	
					H-plane	E-plane
1.46–1.87	GPS	7.38/5.45	Linear along y direction	–23	Omni-directional	HPBW = 90° at 1.75 GHz
	DCS	3.73/2.1				
2.37–2.49 2.4 GHz WLAN		4.22/1.31	Linear along y direction	–25	Omni-directional	HPBW = 80° at 2.45 GHz
5.63–5.89 5.8 GHz WLAN		4.65/3.12	Linear along x direction	–19	Omni-directional	HPBW = 126° at 5.76 GHz

#### 4. Conclusion

A Novel compact multiband antenna suitable for GPS, DCS, 2.4/5.8GHz WLAN application is designed and analysed. Antenna shows moderate gain and nearly omnidirectional radiation characteristics in the entire band.

#### 5. References

- [1]. Chen, Z., Ganjara, A.D., and Chen, X., A dual-L antenna with a novel tuning technique for dual frequency applications, *IEEE Trans. Antennas. Propag.*, 2002, 50, (3), pp. 402–403
- [2]. Choi, S.H., Park, J.K., Kim, S.K., and Kim, H.S., Design of dual-band antenna for the ISM band using a backed microstrip line, *Microw. Opt. Technol. Lett.*, 2004, 41, (6), pp. 457–460
- [3]. Ryu, H.-C., Ahn, H.-R., Lee, S.-H., and Park, W.S., Triple-stacked microstrip antenna for multiband system, *Electron. Lett.*, 2002, 38, (24), pp. 1496–1497

.....✂.....

## RESUME OF THE AUTHOR

### MANOJ JOSEPH

Research Scholar  
Centre for Research in ElectroMagnetics and Antennas  
Department of Electronics  
Cochin University of Science and Technology  
Tel: +91-484-2576418, Mob: +91-9950769409  
Email: josephmanoj@gmail.com

---

### Objective

To pursue research activities in the field of Printed antennas, Computational Electromagnetics, and Microwave imaging.

### Areas of Interest

Compact Planar Antennas, Printed monopoles, microwave material characterization, Microwave remote sensing, Radar image processing.

### Education

M.Sc Electronics  
Specialization: Microwave Electronics  
Cochin University of Science and Technology (2003)  
Score: CGPA 8.93, First class with Distinction

B.Sc Physics  
S.D.College, Alappuzha , Kerala university(2001)  
Score: 92.8% First class

### Awards Obtained

- Young Scientist Award of International Union of Radio Science (URSI) and had an official meeting with the President of India in 2005
- Research Fellowship by Kerala State Council for Science, Technology and Environment (KSCSTE) in 2003

### Research Experience

- Working as a Scientist/Engineer 'SC' in Regional Remote Sensing Centre, NRSC/ISRO, CAZRI Campus ,Jodhpur from 28<sup>th</sup> May 2007 onwards
- Worked as a Research scholar in Centre for Research in ElectroMagnetics and Antennas, Dept.of Electronics, Cochin University of Science And Technology from 1<sup>st</sup> January 2004 to 27<sup>th</sup> May 2007

**Publications:**

---

International Journal	: 10
International Conference	: 05
National Conference	: 03

**Computer Proficiency**

---

- C, C++, MATLAB, LabVIEW, Assembly Level Programming,
- Antenna Designing softwares like Ansoft HFSS, AnsoftDesigner, Zeland IE3D, Zeland FIDELITY, Microwave Office, Microstripes and CST Microwave Studio.
- Image processing and GIS packages like ERDAS imagine, ArcGIS,ENVI and Geomatica.

.....*✍*.....

## **LIST OF PUBLICATIONS OF THE AUTHOR**

### **International Journals**

- [1]. "Compact wideband antenna for 2.4 GHz WLAN applications", M. Joseph, B. Paul, R.K. Raj, and P. Mohanan, IEE Electronics Letters, Vol.40, No.20, 11th Nov. 2004,pp-1460-1461
- [2]. "Compact Dual-Band Antenna For DCS/2.4 GHz WLAN Applications" Manoj Joseph, Rohith K.Raj, M.N.Suma and P.Mohanan, Microwave and Optical Technology Letters, Vol.48, No.5, May 2006, pp-856-859
- [3]. "Microstrip-fed Dual band Folded Dipole Antenna for DCS/PCS/2.4GHz WLAN Applications" Manoj Joseph, Rohith K. Raj, Suma M. N, C. K. Aanandan, K. Vasudevan and P. Mohanan., International Journal for Wireless and Optical communications (IJWOC) Vol.4,No.1,January 2007,pp 43-51.
- [4]. "A New Compact Microstrip-fed Dual-band Coplanar Antenna for WLAN applications", Rohith K. Raj, Manoj Joseph, K.Vasudevan, C. K. Aanandan and P. Mohanan, IEEE Transactions on Antennas and Propagation .Vol.54 No.12, December 2006,pp 3755-3762
- [5]. "A Compact Dual Band Planar Branched Monopole Antenna for DCS/2.4GHz WLAN Applications" Suma M.N, Rohith K Raj, Manoj Joseph, Bybi P.C and P. Mohanan, IEEE Microwave and Wireless Components Letters, vol. 16, no.5, May 2006, pp 275-277
- [6]. "Compact planar multiband antenna for GPS, DCS, 2.4/5.8 GHz WLAN applications" R.K Raj, M. Joseph, B. Paul and P. Mohanan, IEE Electronics Letters, vol.41, no.6, 17th March 2005, pp-290-291.



- [7]. “Planar Branched Monopole Antenna for UWB Applications”, K. Francis Jacob, Suma M.N, Rohith K. Raj, Manoj Joseph and P. Mohanan, Microwave and Optical Technology Letters, Vol 49, No.1, January 2007, pp 45-47.
- [8]. “ Wide band Dumbell shaped Patch Antenna”, K. Francis Jacob, Suma M.N, Manoj Joseph and P. Mohanan, Microwave and Optical Technology Letters, USA Vol. 48, No. 11, November 2006, pp 2295-2296
- [9]. “Compact uniplanar antenna for WLAN applications”, Deepu, V, Rohith, K.R, Manoj, J, Suma, M.N, Vasudevan, K, Aanandan C.K, Mohanan, P, IEE Electronics Letters, vol.43, no.2, 18th January 2007, pp 70-72.
- [10]. “Compact asymmetrc coplanar strip fed monopole antenna for multiband applications” Deepu V, Rohith.K.Raj, Manoj Joseph, Suma M.N, and P.Mohanan, IEEE Transactions on Antennas and Propagation .Vol.55 No.8, August 2007, pp 2351-2357

### **International and National Conferences**

- [1]. “Planar multiband antenna”, Manoj Joseph, Rohith K. Raj, Binu Paul, P. Mohanan, IEEE APS 2005.
- [2]. “A Novel Compact wideband antenna”, Manoj Joseph, Rohith K. Raj, Binu Paul, C. K. Aanandan, K. Vasudevan and P. Mohanan, URSIGA2005.
- [3]. “Compact wideband antenna for Bluetooth applications”, Manoj Joseph, Rohith K. Raj, Binu Paul, K. Vasudevan, C. K. Aanandan ,P. Mohanan and K.G.Nair, National Symposium on Antennas and Propagation (APSYM-2004)

- [4]. "A New Compact Coplanar Antenna", Rohith K. Raj, Manoj Joseph, C. K. Aanandan, K. Vasudevan and P. Mohanan ,URSIGA2005.
- [5]. "A New compact printed antenna with coplanar configuration", Rohith K. Raj, Manoj Joseph, C. K. Aanandan, K. Vasudevan and P. Mohanan, IEEE APS 2005.
- [6]. "Compact Coplanar antenna for Active Antenna Applications", Rohith.K.Raj, Manoj Joseph, C.K.Aanandan, K.vasudevan, P.Mohanan, National Symposium on Antennas and Propagation (APSYM-2004)
- [7]. "Compact asymmetric coplanar strip fed multiband antenna for wireless applications", Deepu V, Rohith K.Raj, Manoj Joseph, Suma M.N ,C.K.Aanandan,K. Vasudevan and P.Mohanan ( APSYM-2006).
- [8]. "Compact Dual band antenna for WLAN applications" Deepu V, Rohith K.Raj, Manoj Joseph, Suma M.N , and P.Mohanan (IEEE APS-07,Honolulu,Hawaii,USA)

.....❧.....

## INDEX

### A

analyzer, 82, 83, 85, 86,88  
Anechoic Chamber, 82, 84, 89  
asymmetric dipole, 94, 104, 105, 125  
asymmetrically, 18  
AUT, 83, 84, 86

### B

baluns, 8, 13  
Bandwidth, 85  
bifilar line, 8, 14,127  
Bluetooth, 2, 11  
Boundary Conditions, 64, 88  
Broadband,1,2,4,5,8,9,10,11,12,14,16,17,  
21,24,28

### C

Compact, 24, 26  
coplanar waveguide, 6, 8, 13, 14  
coupling, 122, 123, 124, 126, 127, 133, 139  
Crema Soft', 85, 86

### D

DCS, 3- 6, 10, 12, 15, 21- 26, 91, 142, 144,  
146, 148, 152,187-189, 213- 218  
dielectric constant, 92, 114, 138, 140, 142,  
152, 183, 185, 187, 192  
dipole, 7, 8, 9, 13, 14, 18, 20, 22,  
23,105,116,125  
Double folding, 152  
dual band dual strip antenna, 195, 196,  
198, 200, 201  
DVB-H, 2, 11, 12

### E

efficiency, 81, 87, 89

### F

far field, 73, 74, 75, 80, 84, 86  
FDM, 58  
FDTD, 29, 30, 31, 32

feed offset, 91, 99, 100, 101, 103, 105, 107,  
108, 119, 122, 140, 141  
FEM, 57, 58, 59, 77, 79  
Finite ground plane, 91, 106, 129  
folded dual strip antenna, 195, 196, 197,  
199, 200, 201

### G

gain, 82, 84, 86  
Gaussian pulse, 68, 69, 71, 73  
GPS, 213, 214, 216, 217, 218  
GSM, 3, 4, 5, 6, 12, 22, 26

### H

halfwave dipole, 178, 190  
HFSS, 79, 88  
HP8510C, 82, 83, 88

### I

Internal antenna, 26

### K

Kraus, 89

### M

Maxwell, 18, 29, 59, 60, 63, 87  
metamaterials, 9  
microstrip antenna, 3, 4, 5, 9,21  
microstrip fed, 2, 3, 10, 14, 15, 16, 17  
Microstrip line, 8, 70, 73, 205  
Microwave substrates, 81  
Mohan, 22, 23, 24, 25, 26, 89  
MOM, 58  
monopole, 6, 7, 12, 14, 15, 16, 18, 20, 21, 22  
*Mur*, 65, 67, 88, 154

### N

Numerical dispersion, 63

## INDEX

### O

offset, 158, 159, 160, 162, 167, 168, 169, 172, 184, 186

### P

Pattern reconfigurable, 20  
PCS, 5, 6, 12, 26  
Photolithographic, 57, 80  
PIFA, 5, 10, 11, 20, 22, 25, 26  
Planar Monopole, 3, 18, 21, 22, 25, 29  
PML, 79  
Polarization, 157, 162, 177, 194  
printed antennas, 1, 2, 3, 30  
printed monopole, 2, 4, 9, 14, 15, 16, 21, 25, 195, 196, 197, 198, 199, 200, 201, 202  
*Propagation*, 21, 22, 24, 25, 26, 29, 30, 31, 32

### R

Radiation, 79  
Radiation boundary, 79  
radiation pattern, 152, 156, 157, 160, 161, 167, 176, 177, 178, 190  
References, 87, 218  
Resistive source model, 68  
Return loss, 72, 85

### S

SAR, 202  
Sheen, 19, 29  
Sine function, 71  
Smith chart, 159  
spacing, 151, 152, 162, 172, 173, 178, 180, 185, 186, 193  
Staircase transition, 70

### T

THRU calibration, 86  
Time domain, 87, 88  
top loading, 152, 168, 172  
truncated ground plane, 198

### U

UWB, 7, 9, 10, 12, 18, 25, 26, 29

### V

Vasudevan, 23, 24  
Vector Network Analyzer, 82  
VNA, 82, 85, 165, 174, 187, 188, 192  
VSWR, 85, 86

### W

Wen, 5, 12, 22, 26  
WLAN, 1, 2, 11, 19, 20, 21, 22, 23, 213, 214, 215, 216, 217, 218  
Wong, 3, 6, 21, 22

### Y

Yee, 18, 29, 68, 70, 87  
YIG, 82